

Development of a techno-economic energy system model considering the highly resolved conversion and multimodal transmission of energy carriers on a global scale

Zur Erlangung des akademischen Grades eines

**Doktors der Wirtschaftswissenschaften
(Dr. rer. pol.)**

von der KIT-Fakultät für Wirtschaftswissenschaften
des Karlsruher Instituts für Technologie (KIT)

genehmigte

DISSERTATION

von

Viktor Slednev, M.Sc.

Tag der mündlichen Prüfung:	06.02.2024
Referent:	Prof. Dr. Wolf Fichtner
Korreferent:	Prof. Dr. Valentin Bertsch

Kurzfassung

Im Rahmen dieser Dissertation wird ein Energiesystemmodell entwickelt, welches eine integrierte und hochaufgelöste Analyse der Gewinnung, Umwandlung, Speicherung, Nutzung und des multi-modalen Transports von Energieträgern im Rahmen einer techno-ökonomischen Einsatz- und Ausbauplanung ermöglicht. Die ausgabenminimale Deckung der europäischen Strom- and Wärmenachfrage bis 2050 steht dabei im Fokus einer geschlossenen linearen mehrperiodigen Optimierung globaler Energieflüsse unter Berücksichtigung des multi-modalen Straßen-, Schienen- und Schiffstransports sowie der elektrischen und gasbasierten Übertragungsnetzinfrastruktur. Ziel ist hierbei alternative Transformationspfade für die vollständigen Dekarbonisierung des Umwandlungssektors sowie des Endenergieverbrauchs modellendogen und unter Berücksichtigung der Sektorenkopplung zu bestimmen.

Ausgehend von der Struktur bestehender Transportnetzwerke sowie der Verteilung netzferner Primärenergiepotentiale wird im Rahmen der Arbeit ein datengetriebener Ansatz entwickelt um das Spannungsdreieck zwischen der Abbildung hoch aufgelöster Potentiale der Energieumwandlung auf lokaler Ebene, der gesamtenergetischen Bilanzierung auf aggregierter Ebene und dem dazwischen liegenden räumlichen und zeitlichen Ausgleich über mehrere Transportmodi und Energieträger hinweg aufzulösen. Hierfür werden Top-Down und Bottom Up Ansätze kombiniert und ausgehend von einer auf 100m aufgelösten einheitlichen Regionalisierung werden Prozesse zum Ausgleich der Energienachfrage und des Energieangebots, die jeweils auf derselben Wetterbasis simuliert werden, aggregiert und definiert.

Im Kontext der Optimierung einer sektorübergreifenden Dekarbonisierung des Energiesystems im erweiterten europäischen Raum sowie des angrenzenden Stromsektors in Zentralasien und der MENA Region, unter Berücksichtigung zusätzlicher Angebotspotentiale in Patagonien, konnte die Funktionalität des Ansatzes validiert werden. Die Ausweitung des erneuerbaren Stromangebots im Betrachtungsraum bildet dabei flankiert von Stromnetzausbaumaßnahmen die Grundlage für die Ausweitung der endenergetischen Stromnutzung, beispielsweise im Wärmesektor, sowie im Umwandlungssektor zur Erzeugung von Wasserstoff. Hierbei zeigt sich eine große technologische Bandbreite bei der Transformation des Energiesystems. So wird Wasserstoff über unterschiedliche Umwandlungs- und Transportrouten, sowohl aus erneuerbaren als auch aus fossilen Energieträgern, sowohl an Land als auch auf See, ausgebaut. Dies treibt stellenweise den Ausbau der elektrischen Transportnetze, darunter auch vermaschter DC-Netze für die endogene Verknüpfung einzelner Offshore-Windparks und senkt diesen an anderer Stelle wieder, wenn beispielsweise die elektrische Anbindung der Windparks ans Land durch die Einspeisung in umgewidmete Erdgasleitungen ersetzt wird.

Abstract

This dissertation develops an energy system model that enables an integrated and high-resolution analysis of the extraction, conversion, storage, use and multi-modal transportation of energy sources in the context of techno-economic deployment and expansion planning. The focus is on the minimum expenditure coverage of European electricity and heat demand by 2050 in a closed linear multi-period optimization of global energy flows, taking into account multi-modal road, rail and ship transport as well as the electrical and gas-based transmission network infrastructure. The aim is to determine transformation paths for the complete decarbonization of the transformation sector and final energy consumption endogenously and taking sector coupling into account.

Based on the structure of existing transport networks and the distribution of remote primary energy potentials, a data-driven approach is developed to resolve the tension triangle between the mapping of high-resolution potentials of energy conversion at the local level, the overall energy balancing at the aggregated level and the spatial and temporal balancing in between across multiple transport modes and energy carriers. For this purpose, top-down and bottom-up approaches are combined and, starting from a uniform regionalization with a resolution of 100m, processes for balancing energy demand and energy supply, which are simulated on the same weather basis, are aggregated and defined.

The functionality of the approach is validated in the context of optimizing the cross-sectoral decarbonization of the energy system in the extended European region and the neighboring electricity sector in Central Asia and the MENA region, taking into account additional supply potentials in Patagonia. The expansion of the renewable electricity supply in the area under consideration, flanked by electricity grid expansion measures, forms the basis for the expansion of electricity use, for example in the heating sector, as well as in the conversion sector for the production of hydrogen. The results illustrate, that there is a wide range of technologies involved in the transformation of the energy system. Hydrogen is being expanded via various conversion and transportation routes, both from renewable and fossil energy sources, both on land and at sea. This drives the expansion of the electrical transport networks, including meshed DC networks for the endogenous connection of individual offshore wind farms, and reduces it again elsewhere, for example when the electrical connection of wind farms to land is replaced by feeding into rededicated natural gas pipelines.

Table of Contents

Kurzfassung	i
Abstract.....	ii
Table of Contents.....	iii
List of Illustrations	v
List of Abbreviations	xii
1 Introduction.....	1
2 Development of an integrated energy system modeling approach.....	5
2.1 General modeling concept of PERSEUS-gECT	6
2.2 Classification of the modelling concept within the literature	11
2.3 Formal structure of the optimization model	13
2.3.1 Modeling the conversion, transmission and storage of commodities based on a general concept of process, units and producers	13
2.3.2 Reference energy system of PERSEUS-gECT.....	17
2.3.3 Definition of specific constraints.....	25
2.4 Data structure of PERSEUS-gECT	49
2.4.1 General approach for defining the nodal basis of energy conversion, distribution and demand based on the existing infrastructure as well as regional generation and demand potentials.....	49
2.4.2 Approach for defining resource availability constraints for the conversion of renewable energy carriers (existing & potential units and profiles).....	59
2.4.3 Approach for defining resource availability constraints for the conversion of non-renewable energy carriers (existing & potential units and profiles).....	96
2.4.4 Approach for regionalizing final and useful energy demand and profiles 100	
2.4.5 Approach for the definition of the transport network.....	108
3 Application of the PERSEUS-gECT for modeling the development of the European energy system until 2050 considering energy imports from MENA, Central Asia and Patagonia	121
3.1 Scenario definition and parametrization.....	121
3.1.1 Definition of the general scenario framework	121
3.1.2 Techno-economic assumptions for the parametrization of the case study and scenario specification	124
3.2 Results of the case study	126

3.2.1	Development of the energy system as a result of the emission balance	127
3.2.2	Development of the energy system as a result of mainly electricity related drivers.....	134
3.2.3	Development of the energy system as a result of mainly gas related drivers	156
4	Conclusion and limitations.....	168
4.1	General approach.....	168
4.2	Mathematic problem formulation	169
4.3	Data model.....	170
4.4	Case study	172
4.5	Limitations and Outlook.....	175
	References	178
	Annex	191

List of Illustrations

Figure 1.1:	Example of the interaction between different components of an energy system	2
Figure 2.1:	Structure of PERSEUS-gECT.	6
Figure 2.2:	Simple network example (left), complex network example(right).	9
Figure 2.3:	Overlay of the gas and electricity transmission grid, the challenge of matching supply areas.....	10
Figure 2.4:	General approach for the problem definition and parametrization in PERSEUS-gECT.	11
Figure 2.5:	Conversion process types in PERSEUS-gECT.....	14
Figure 2.6:	Modelled energy balance.....	18
Figure 2.7:	Approach for evaluating conversion paths from the primary to the final energy conversion.	20
Figure 2.8:	Classification of non-final demand processes.	21
Figure 2.9:	General scheme for a specification of EHG and OCP processes (a) and example for a process coupling for modelling the transshipment of commodities.....	22
Figure 2.10:	Classification of the final demand sector and the possible conversion processes.	23
Figure 2.11:	Current geographic boundaries of PERSEUS-gECT	24
Figure 2.12:	Illustration of the reference energy system of PERSEUS-gECT based on the main processes.....	26
Figure 2.13:	Parametrizing basic EHG processes.....	28
Figure 2.14:	Modelling a multi-modal, multi commodity fuel supply for EHG processes	31
Figure 2.15:	Possible coupling of processes for producing synthetic fuel oil based on a hydrogen driven Fischer Tropsch process.....	33
Figure 2.16:	General model of a storage.....	35
Figure 2.17:	Modelling of integrated primary energy conversion and storage processes	37
Figure 2.18:	Approach for modelling spatial flows.....	40
Figure 2.19:	Modelling of transport related energy carrier conversion and reconversion processes	42
Figure 2.20:	Coupling of processes for modelling HVDC flows in DCTT (left) and DCMT (right) systems	43

Figure 2.21:	Modelling of final demand fuel flexibilities and switching processes..	48
Figure 2.22:	Approach for defining a common regional basis for an assessment of demand and generation potentials and profiles	51
Figure 2.23:	General approach of an variable definition based on an overlay of supply areas of different transport systems and weather cells	53
Figure 2.24:	Comparison of different variable aggregation approaches for defining regional potentials and profiles.....	54
Figure 2.25:	Approach for the definition of variables for modelling the generation and grid connection of offshore windfarms in remote areas.....	55
Figure 2.26:	Coupling of offshore and onshore processes for modelling the interdependencies between land and sea-based conversion chains for a production, storage and transmission of energy carriers	57
Figure 2.27:	Distribution of onshore and offshore wind energy potentials (greenfield ad brownfield) in Europa (left) and the development of wind onshore capacities in Germany in a reference scenario.....	60
Figure 2.28:	Approach for the assessment of wind onshore potentials	62
Figure 2.29:	Placement of wind turbines with respect to wind ellipse distance restrictions.....	63
Figure 2.30:	Considered designated areas for wind offshore conversion in the North Sea and Baltic Sea	64
Figure 2.31:	Exemplary illustration of the distribution of the LCOE of wind onshore (left) and wind offshore (right) conversion in 2035 in Europe	66
Figure 2.32:	Approach for modelling wind energy conversion profiles	67
Figure 2.33:	Exemplary validation of the modelled wind generation profiles based on a comparison with ENSTO-E data for Germany in 2018.....	68
Figure 2.34:	Location of existing or planned turbines in the current WECS database of PERSEUS-gECT	69
Figure 2.35:	Aggregation of potential wind turbines to wind farms variables in remote areas, illustrated for the case of Kazakhstan.....	71
Figure 2.36:	Comparison of the distribution of planned and repowered wind onshore turbines and the remaining potential in Europe and selected areas based on the full load hours	72
Figure 2.37:	General approach for modelling solar energy conversion potentials..	75
Figure 2.38:	Approach for modelling PV and STC potentials.....	77
Figure 2.39:	Approach for a PV-BESS regionalization and SDP-based dispatch optimization for deriving PV-BESS potentials and dispatch restrictions	78
Figure 2.40:	Implications of a pure LCOE based allocation of PV, illustrated for the case of Germany	80

Figure 2.41:	Comparison of the distribution of existing and potential ground mounted and rooftop PV units in Europe and North Africa based on the full load hours	81
Figure 2.42:	Approach for calculating solar thermal (CPS, flat plate collector) and PV profiles.....	82
Figure 2.43:	Distribution of considered solar thermal potentials in Europa, MENA and Central Asia with respect to the energy yield of RTSWH units (left) and the LCOE of CSP units (right)	84
Figure 2.44:	Considered resource classes for biomass and waste based conversion processes	85
Figure 2.45:	Structure, capacity and distribution of biomass and waste driven existing EHG units.....	87
Figure 2.46:	Distribution of the considered grid connected (left) and off-grid SNG potential	88
Figure 2.47:	Distribution, number and capacity of hydro power units by type	90
Figure 2.48:	Allocation of considered hydro storages and the modelling of cascaded hydro power plants in PERSEUS-gECT	91
Figure 2.49:	Approach for a regional inflow approximating for run-of-river and poundage units.....	92
Figure 2.50:	Approach for estimating the GSHP potential and defining GSHP variables	94
Figure 2.51:	Distribution of considered geothermal, marine and CBM units and approach for a tidal profile modelling.....	95
Figure 2.52:	Distribution of modelled natural gas production units and their proven reserves	96
Figure 2.53:	Structure and capacity of existing conventional EHG units	97
Figure 2.54:	Approach for a capacity adequacy assessment in order to derive lower bounds for the expansion of dispatchable EHG units based on (Hartel et al. 2019).....	98
Figure 2.55:	Approach for modelling the regional potential of final energy and useful energy demand conversion units	100
Figure 2.56:	Approach for modelling low and high-temperature heating demand profiles.....	103
Figure 2.57:	Exemplary validation of the bottom-up demand modelling approach based on a comparison of the modelled daily natural gas demand in Germany in 2019 with data from the gas system operators	106
Figure 2.58:	Exemplary validation of the bottom-up demand modelling approach based on a comparison of the modelled hourly electricity demand in Germany, France and Norway in 2017 with ENTSO-E data.....	107

Figure 2.59:	Edges of the transport system and main data sources for all networks except district heating and point-to-point connection of offshore units (a) and the exemplary approach for a graph definition (b).....	109
Figure 2.60:	Considered gas and oil pipelines in PERSEUS-gECT and approach for defining the capacity in the gas model.....	110
Figure 2.61:	Considered ship, road and rail edges	111
Figure 2.62:	Definition of supply areas of the electricity transport grid	113
Figure 2.63:	Capacity of the considered AC-grid in the reference case in 2050 without endogenous expansion	114
Figure 2.64:	Potential and existing edges of the HVDC grid.....	115
Figure 2.65:	Average impact of dynamic line rating on the transmission capacity in the considered AC grid	116
Figure 2.66:	Approach of defining the layout of generic district heating networks	117
Figure 2.67:	Layout of district heating supply areas in selected German regions as a result of a generic district heating planning.....	118
Figure 2.68:	Distribution of the considered district heating grids in PERSEUS-gECT	119
Figure 3.1:	Evaluation of the temporal problem reduction based on a comparison of the sorted generation and demand curves for 2050	123
Figure 3.2:	Distribution and development of the final energy demand in the reference scenario.....	125
Figure 3.3:	Net position of national CO ₂ emissions in 2050 and comparison of the CO ₂ balance of Germany and UK against the background of the dispatch of all EHG units and the utilization of the electricity and gas transmission grid.	128
Figure 3.4:	Structure of the total CO ₂ emission balance in 2050.....	129
Figure 3.5:	Dispatch of direct air capture and hydrogen-to-jet units against the background of pipeline and shipping-based CO ₂ flows	130
Figure 3.6:	Development of final demand switching capacity and comparison of the allocation of heat pumps (blue scale) and combustion boilers (red scale), which are chosen for the final demand-switch.....	132
Figure 3.7:	Structure of the electricity generation in 2050	135
Figure 3.8:	Development of the electricity generation capacity of EHG units and their regional distribution.....	136
Figure 3.9:	Development of the endogenously installed electricity generation capacity of EHG units and their regional distribution	137
Figure 3.10:	Development of the flexibly dispatchable electricity generation capacity of EHG units and their regional distribution	138

Figure 3.11:	Development of the residual load and the contribution of intermittent renewables for the electricity demand balancing.....	139
Figure 3.12:	Cumulated wind onshore injection into the AC grid and the utilization of the AC grid in 2050.....	142
Figure 3.13:	WECS and PV electricity generation density (left) and capacity density (right).....	143
Figure 3.14:	Cumulated wind offshore generation and the utilization of the HVDC system in 2050.....	144
Figure 3.15:	Cumulated PV injection into the AC grid and the utilization of the AC grid in 2050.....	145
Figure 3.16:	Comparison of the allocation of rooftop PV-BESS units and ground-mounted utility scale BESS units.....	146
Figure 3.17:	Stacked electricity generation of EHG units, differentiated by main conversion class in 2050.....	148
Figure 3.18:	Cumulated electricity demand of electrolyzers in the AC grid and comparison with the wind offshore generation in 2050.....	150
Figure 3.19:	Comparison of the dispatch of electrolyzers (left), wind onshore units (middle) and nuclear power plants (right) with respect to the utilization of the hydrogen and AC grid in Eastern Europe in 2050 ...	152
Figure 3.20:	Comparison of AC line flows on edges of the reference grid and the expansion grid in 2050	153
Figure 3.21:	Comparison of the dispatch of the HVDC transmission system (left) and the HVDC expansion (right) in 2050	154
Figure 3.22:	Cumulated flows on lines of the electricity transmission system and identification of main transport corridors in the North Sea and Baltic Sea in 2050	155
Figure 3.23:	Comparison of the wind onshore and PV generation in the AC grid in 2050.....	155
Figure 3.24:	Structure of the hydrogen production and transport	157
Figure 3.25:	Interdependency between components of the hydrogen and electricity system in the North Sea. Right part: hydrogen production and hydrogen pipeline and shipping flows, upper left corner: wind onshore and flows in the AC grid and hydrogen pipelines, lower left: Wind offshore and flows in HVDC lines	158
Figure 3.26:	Comparison of the cumulate hydrogen pipeline flows with the shipping of LH2 and LOHC.....	160
Figure 3.27:	Comparison between the cumulated hydrogen pipeline and shipping flows (left) and the natural gas pipeline and shipping flows (right) ..	161

Figure 3.28:	Cumulated dispatch of methane based hydrogen production processes and comparison of the unit placement with the placement of possible CO2 sinks.....	163
Figure 3.29:	Comparison between the cumulate hydrogen pipeline flows in 2050 in blended or replacement NG pipelines (left) and blended (NG) or parallel new H2 pipelines (right)	164
Figure 3.30:	Process coupling examples involving Fischer Tropsch and steam reformation processes.....	166
Figure A.1:	Country info and complete CO2 emission balance in 2050	191
Figure A.2:	Classification of EHG processes	192
Figure A.3:	Default parameters for the definition of the land cover based suitability	193
Figure A.4:	Considered main resource classes for the assessment of the biomass potential and their data sources	194
Figure A.5:	Properties of the main considered biomass resource classes.....	195
Figure A.6:	Match between CLC classes and biomass resource classes	196
Figure A.7:	Match between Copernicus land cover classes and biomass resource classes	197
Figure A.8:	Comparison of the ERAA and ENTSOE run-of-river time series for Germany	198
Figure A.9:	Considered PHES Potential	198
Figure A.10:	Considered nodes per system in PERSEUS-gECT	199
Figure A.11:	Extract of the OSM based extra high voltage transmission grid in PERSEUS-gECT for Eurasia and Africa	200
Figure A.12:	Extract of the OSM based high voltage grid in PERSEUS-gECT for Eurasia and Africa	201
Figure A.13:	Selected potential DCMT and DCTT (direct offshore grid connection) HVDC sub-grid in the case study.....	202
Figure A.14:	Hourly timeseries of the DLR impact in the transmission grid in weather year 2019.....	202
Figure A.15:	Exemplary results of the transport system in 2050 of the first model run in the case study.....	203
Figure A.16:	Comparison of the simulated hourly time series of the reference electricity final demand in Europe of 2019 and 2050	203
Figure A.17:	Zoom on the CO2-emission balance of the largest positive and negative net-emission countries in 2050	204
Figure A.18:	Oil flows in 2050	205

Figure A.19:	Structure of the final demand switching for low temperature heat in 2050.....	206
Figure A.20:	Structure of the low temperature supply from non-primarily EHG related processes in 2050.....	206
Figure A.21:	Distribution of transport related CO2 emissions excluding ports and storages	207
Figure A.22:	Analysis of the residual load development in the reference TYNDP 2022 Distributed Energy Scenario for multiple weather years.....	208
Figure A.23:	Installed wind onshore, wind offshore and photovoltaic capacity per country in 2050	209
Figure A.24:	Cumulated wind onshore generation and flows in the AC grid in 2050-focus on Europe.....	210
Figure A.25:	Comparison of the potential and realized power generation from solar and wind based energy conversion systems (including PV-BESS).....	210
Figure A.26:	Comparison of the dispatch of electricity generation units in the complete energy system (top) and in Germany (bottom) in 2050 per time slice	211
Figure A.27:	Comparison of the cumulated dispatch of electrolyzers (bottom right), wind offshore units (top, right), wind onshore units (bottom left) and nuclear power plants (top left) in the English Channel region in 2050	212
Figure A.288:	Cumulated electricity flow in the German grid and neighboring regions in 2050.....	213
Figure A.29:	Volume of hydrogen storages and cumulated hydrogen flows in the gas grid in 2050	213

List of Abbreviations

AEL	Alkaline Electrolysis
BESS	Battery Energy Storage System
CB	Combustion Boiler
CC	Combined Cycle
CCU	Carbon Capture and Use
CCUS	Carbon Capture Use and Storage
CCS	Carbon Capture and Storage
DAC	Direct Air Capture
DAC	Demand Side Management
ENTSO-E	European Network of Transmission System Operators for Electricity
ENTSO-G	European Network of Transmission System Operators for Gas
FT	Fischer Tropsch
GT	Gas Turbine
HP	Heat Pump
LNG	Liquified Natural Gas
LOHC	Liquid organic energy carrier
PtL	Power-to-Liquid
PEM	Proton Exchange Membrane (Electrolysis)
PV	Photovoltaic
SFO	Synthetic Fuel Oil
SNG	Synthetic Natural Gas
SOEC	Solid Oxid Fuel Cell
ST	Steam Turbine
TYNDP	Ten-Year Network Development Plan

UCTE Union for the Co-ordination of Transmission of Electricity

WECS Wind Energy Conversion System

1 Introduction

With the long-term strategy to reach climate neutrality by 2050, which was submitted by the EU in March 2020 to the United Nations Framework Convention on Climate Change UNFCCC, the European Union formulated the goal to reduce the greenhouse gas emissions to net zero¹. With this goal the EU is among many other regions and countries who have joined the “Climate Ambition Alliance: Net Zero 2050”, which started in 2020². In order to align with the Paris Agreement to limit the global temperature increase below 2°C, however, a fundamental restructuring of the energy system is needed. Energy system models may provide a valuable insight to decision makers how this goal may be reached and are therefore increasingly applied in this research field (DeAngelo et al. 2021). In this context, mainly national energy system models such as MESSAGE, TIMES or OSeMOSYS, are chosen from the broad range of available energy system models, which were developed since the 1950s (Kueppers et al. 2021; Lopion et al. 2018). The common idea underlying many of these approaches is the modelling of the energy system through a directed flow of energy from the source to the sink. Apart from the academic research, a hierarchical multi-method approach is more common for addressing the issue of achieving net zero, such as applied by the European electricity and gas transmission network operators (ENTSO-E, ENTSOG). In the combined long-term planning of the gas and electricity transmission systems, the European network operators thus start from initial national estimates of the demand and capacity development, followed by a development of trajectories and an expansion of the transmission capacities (ENTSO-E – ENTSOG 2020). Facing the challenge of modelling a complex system, in which multiple competing and complementary strategies might be applied for reaching net-zero CO₂ emissions, both approaches have their pros and cons. While national energy system models are highly suitable for modelling the development of complex energy conversion chains in simplified single node models with a reduced temporal resolution, the approach of the transmission system operators might address the complex interdependencies between distributed generators and loads in the grid, once their capacity and location is known. As the suitability of each decarbonization strategy depends on the spatial, temporal, technological and sectoral relation between existing and potential energy conversion, storage and transmission options, a combination of both approaches is desirable. Based on the next figure, which illustrates a few conversion, storage and transmission processes, the interdependency between some “popular” emission reduction strategies is discussed next, aiming at addressing some open research questions. It is assumed, that the heating and electricity demand of a residential consumer (lower right corner) with a battery electrical vehicle should be covered based on the energy conversion from wind and solar (only PV) or methane and hydrogen. Additionally, it is considered that there

¹ This goal is also the “heart” of the European Green Deal EU (2023).

² Currently this alliance has 136 national states and 22 regions as members (https://climateinitiativesplatform.org/index.php/Climate_Ambition_Alliance:_Net_Zero_2050, last checked: 18.12.2023).

is the option to convert, store and transport these derived energy carriers at or between different sites in order to achieve the restriction of generating net zero emissions. The objective function minimizes the total system cost for the load coverage.

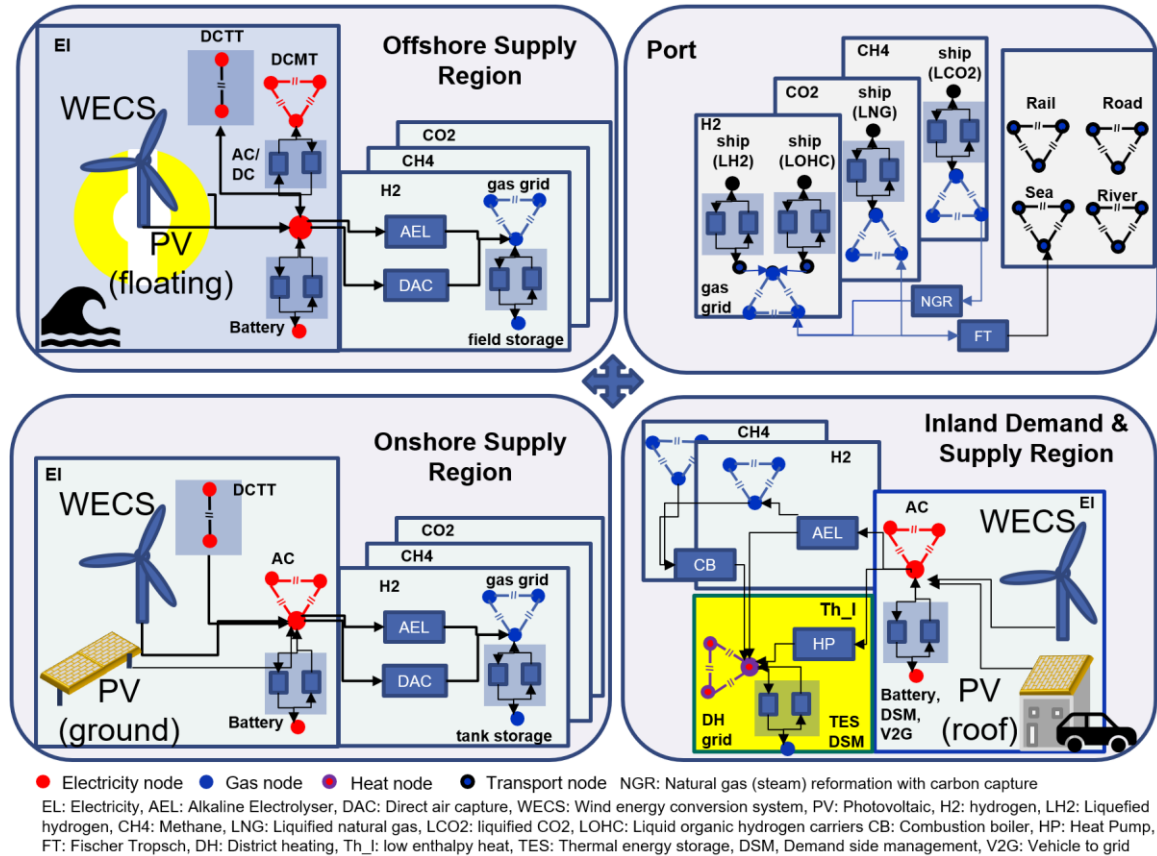


Figure 1.1: Example of the interaction between different components of an energy system

Multiple trade-offs arise in case a direct electrification of the demand is chosen. The dimensioning of the local electricity and heat conversion (WECS, PV, HP) and storage (Battery, V2G) technologies and their flexibilities (DSM for el and th), for example, should be weighed against the onshore and offshore electricity grid, storage and generation. The central question under investigation in this context is the placement (next to the load or apart) and the shares of renewable technologies. Taking into account the transmission systems, the impact of the load increase (HP) of a decentral consumer in the electricity grid in most cases deviates from the location of the decrease of methane or hydrogen in the gas grid, as the supply areas of both systems are non-overlapping. On the other hand, if the indirect electrification route is considered, such that electrolyzers might be built, the previously mentioned problem also arises for decentral generators if the hydrogen production is fed into the gas grid. Depending on the structure of the distribution grid, the same renewable generation might disappear in one electricity transmission grid node and appear as a hydrogen injection multiple kilometers away in the gas grid. With the possibility to reduce the need for an electricity grid expansion through a shift of the energy transmission into the gas system, the impact for the expansion of renewables and the transmission system

depends on the placement of the electrolyzers in the gas and electricity grid. If the electrolyzers are placed next to consumers, which might be not the most probable scenario for residential consumers but is widely discussed for large industrial consumers, the need for a grid expansion increases. In the context of placing electrolyzers next to generation centers, the tradeoff between the existing natural gas system and the potentially required additions within the gas system needs to be evaluated. In this case not only the viable transportation mode must be examined in more detail, namely whether to opt for a transport via ship or pipe in the first place, but also the type of the energy carrier for shipping (e.g. LH₂, LOHC, NH₃) and the type of pipeline flow (blending, replacement, parallel addition) in the second case must be evaluated. Furthermore, it must be considered, that depending on the placement of the electrolyzers in the offshore grid (offshore or at the landing), also the structure of this electricity system will change. A further effect of the indirect electrification strategy is that the energy system will most probably require an intercontinental spatial (ideally global) definition of system boundaries, as favorable areas may lie on different continents and are now in competition to the regional (e.g. Northwest Europe) and local balancing of supply and demand. If finally the option of carbon capture and storage and the utilization of methane as an energy carrier is taken into account, the solution might shift from an electrification path to reach net zero CO₂ emissions, to a fossil driven scenario. In this scenario the so called “blue” hydrogen is produced after a steam methane reformation with subsequent carbon capture and storage and requires transportation. In this context, a trade-off must be considered between hydrogen production in natural gas producing countries or in importing countries on the one hand and on the other hand the import by ship or pipe, such that LNG or pipeline natural gas is replaced. For example, in natural gas importing countries, the trade-off between a blue hydrogen production at LNG import locations with a potential short distance pipeline or shipping based CO₂ transport to storages and a location next to load centers must be weighted. When importing hydrogen by ship or pipe, the expansion of the hydrogen network is concurring with the CO₂ pipeline network expansion. Additionally, if a Fischer Tropsch based conversion from hydrogen to a synthetic fuel oil is taken into account, a further temporal CO₂ sink option is included, which has potential effects on the allocation of NGR and DAC units. From the point of view of the usage of excess heat potentials, the Fischer Tropsch processes additionally could be used to provide high temperature excess heat for the LOHC unloading or the DAC processes and the AEL unit might be used for covering low temperature heat demands. In all cases a locational planning across multiple processes and sectors is needed. With the availability of DAC processes also the share of the remaining natural gas in the final demand coverage becomes a variable to consider, as potential renewable excess generation might be used to run the processes and to reduce the size of the electricity and hydrogen grid expansion while converting some part of the current structure of the fossil-based energy system. As each single path in the above examples is rather extreme in a certain sense, a balanced energy system that achieves net-zero at low cost, would most probably include a combination of all discussed options, such that each component will be ideally dimensioned with respect to the regional conditions and preceding and subsiding processes.

The prerequisite for an evaluation of these interdependences is a spatially and temporally highly resolved modelling of the generation and demand potentials and profiles. In order to allow a

flexible reallocation of energy carrier specific supplies and demands between the nodes of the energy system model, these potentials and profiles furthermore need to be defined with a corresponding high resolution below the nodes of the possible transmission system. Currently a combination of a cross sectoral energy flow modelling for linking multiple conversion processes, with a highly temporal and spatial consideration of existing and potential conversion, storage and transmission technologies is not available.

In order to close this research gap and provide a profound decision support for the energy system planning, in the following an approach is presented, which allows to evaluate these open research questions on a global scale. After a brief description of the general approach and a classification within the existing literature in chapter 2, a detailed description of the developed integrated energy system modeling approach is provided. The suitability of the approach for the modelling of large scale, complex energy systems is afterwards demonstrated in a case study in chapter 3. In the last chapter 4 the results are summarized and a conclusion with respect to the limitations is drawn.

Considering that the developed approach covers a broad range of research fields in the energy system modelling, the literature review for the single components of the developed model is provided directly next to the description of the components in chapter 2. At the same place also the developed energy system model, in the following referred to as PERSEUS-gECT³, and its tool chain for the problem structuring, parametrization and solution, is classified within the literature. The model description in chapter 2 is divided in a description of the general modelling approach in chapter 2.1 and its placement into the literature of energy system models in chapter 2.2, followed by the definition of the formal model structure in chapter 2.3 and the data structure in chapter 2.4. In this context the definition of the reference energy system and of the structure of the mathematic optimization problem is included in chapter 2.3, while the approach for the parametrization of the energy model is provided in 2.4. In the following case study in chapter 3 it is shown that the developed approach is able to bridge the granularity gap between an energy system transformation on an intercontinental scale and a cross-sectoral optimization of complex conversion chains on a nodal scale. Although it is shown that the developed approach provides a plausible answer to each of the previously raised questions, there is still room for further developments. The last chapter therefore includes a detailed discussion of the limitations and the future work.

³ PERSEUS (**P**rogram **P**ackage for **E**mission **R**eduction **S**trategies in **E**nergy **U**se and **S**upply)-gECT (**g**lobal **E**nergy **C**onversion and **T**ransport).

2 Development of an integrated energy system modeling approach

The general purpose of PERSEUS-gECT is to provide a framework for a multi-period techno-economic expansion and dispatch planning of the supra-European energy system considering the conversion, transmission and storage of multiple energy carriers and related commodities. A spatial and temporal highly resolved modeling of regional conversion restrictions, ranging from the primary to the final energy conversion of existing and future processes, constitutes the basis of the developed framework. With a focus on developing a consistent hourly modeling approach of all weather-dependent supply and demand processes, such as the intermittent renewable resource availability of wind and solar on the one hand and thermal heating and cooling processes on the other hand, the aim of PERSEUS-gECT is to provide a decision support for planning the energy system while taking into account the complex spatial and temporal interdependencies due to varying weather and climate conditions.

From the perspective of a central planner with deterministic perfect foresight the developed approach should provide a decision support for finding an optimal configuration of the energy system such that all expenses for covering an exogenously given demand for certain energy carriers, which might be either the input or output of a final energy conversion process, are minimized. Starting from the configuration of the existing energy system, an optimal spatial and temporal balancing for multiple energy carriers should be determined based on an endogenous expansion of processes for their conversion, transmission and storage with respect to technical and political restrictions, such as the emission reduction targets for CO₂. In this context an approach for defining the nodal basis of energy conversion, distribution and demand based on the existing infrastructure as well as regional generation and demand potentials is developed. Next to the challenge of parametrizing such a complex system with respect to the actual installed and future technologies, another main challenge lies in an adequate definition of decision variables and nodes, while considering the high degree of freedom for linking multiple conversion processes for multiple energy carriers within a multi-modal transmission model.

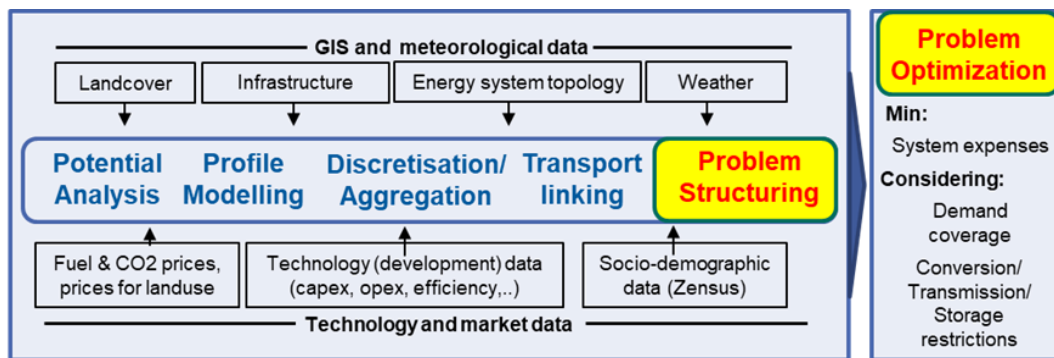


Figure 2.1: Structure of PERSEUS-gECT.

As illustrated in figure 2.1, the framework of PERSEUS-gECT therefore consists of an approach for defining the data structure of the model in the first step and setting up an appropriate large-scale linear optimization model in the second step.

In the following chapter 2.1 the overall modeling concept of PERSEUS-gECT is described first, followed by a short literature classification of the approach in 2.2. Thereafter, its two components consisting of the formal structure of the mathematical optimization model on the one hand and the underlying data structure on the other hand are defined in chapter 2.3 and chapter 2.4.

2.1 General modeling concept of PERSEUS-gECT

The main purpose of PERSEUS-gECT is to bridge the gap between modeling approaches which aim to optimize the energy balance of a system such that multiple energy carriers and transformation processes between the primary energy supply and useful energy demand might be endogenously adjusted for multiple sectors on the one hand and models which focus on a specific sector and a detailed representation varying regional resource and demand constraints and the balancing system on the other hand. In the first case, the decision support often focusses either on modeling the transformation on a large scale, like the national level, or contrary, on a small regional scale, such as the municipality level. In consequence, the spatial balancing of supply and demand is either overestimated or underestimated. In the second case, the focus on the transmission system often comes with the trade-off of an exogenously fixed allocation of demand and supply potential to the nodes of the systems under consideration. Thus, the challenge lies in bridging the granularity gap between a regionally accurate assessment of supply and demand potentials and profiles, and a global multi-sectoral, multi-energy balancing with respect to transmission and storage restrictions.

From a modeling point of view the challenge is to define an appropriate data and model structure, in order to combine an efficient data handling with a minimal problem size for modeling the relevant dynamics of the energy systems. One possible structure for an efficient modeling of such a multi-sectoral, multi-energy system is to apply the concept of a directed graph for

modeling the energy and commodity flow, conversion and storage. Within the PERSEUS model family, which is based on the energy flow model EFOM, this is realized by classifying the nodes of the graph as producers ($pn \in PROD$), which are linked by edges $(pn, pn', ec) \in \Omega$ directing the flow of commodities, such as energy and materials ($ec \in EC$), between producers. Concerning the data structure, a hierarchical approach is realized, with an aggregation of producers to sectors or subregions and later on to regions on the highest aggregation level. Below the producer level, multiple units ($pu \in UNIT$) define the capacity of a certain conversion or storage technology. These units serve as an endogenous capacity bound for underlying conversion processes ($pp \in PROC$), defining the set of alternative operation configurations of a unit with regards to the predefined input-to-output ratio for the conversion of commodities. In this context, a producer may be classified as an abstract entity, comprising related activities, which convert, store, demand or supply energy or materials within a certain sector or subregion, assuming a lossless and unrestricted transmission of commodities between the internal processes. The energy flow graph is ultimately determined by integrating both the source and sink node to the set of producers and defining the exogenous demand for a commodity through fixed flows directed towards the sink. Driven by the need to meet an exogenously given demand, an optimal configuration of the graph is obtained by adjusting the unit capacities. This adjustment aims to minimize the system expenses related to both capacity investments and the operation of processes or flows at a certain activity level. In this context the temporal dimension is structured such that $tp \in TP$ defines the realization points for capacity changes on a period basis, often representing a period of years. Considering varying supply and demand conditions within a period, changes of the process and flow levels are realized on a sub-period scale of time steps $ts \in TS$, often representing weighted hours of certain days within a year. Thus, the nodal balance equations, which span the energy graph, balance the level of flow variables f , conversion process variables x and storage variables s , in a way that the amount of a commodity flowing in, being produced and stored during a preceding time step in a node must equal the sum of outflows, demands and the storage level at the end of the time step¹:

$$\begin{aligned} \sum_{pn' \in \Omega_{pn', pn, ec}} f_{pn', pn, ec, tp, ts} \alpha_{pn', pn, ec, tp}^{flow} + \sum_{pp \in PROC_{pn, ec}} x_{pp, tp, ts} \alpha_{pp, pn, ec, tp}^{out} + \\ \sum_{pp \in STORPROC_{pn, ec}} s_{pp, tp, ts-1} \alpha_{pp, pn, ec, tp}^{stor} = \\ \sum_{pn' \in \Omega_{pn, pn', ec}} f_{pn, pn', tp, ts} + \sum_{pp \in PROC_{pn, ec}} x_{pp, tp, ts} \alpha_{pp, pn, ec, tp}^{in} + \\ \sum_{pp \in STORPROC_{pn, ec}} s_{pp, tp, ts} \end{aligned} \quad (2.1)$$

$$\forall pn \in PROD, \forall ec \in EC, \forall tp \in TP, \forall ts \in TS | ts > 1$$

, where $STORPROC \subset PROC$ defines a subset of processes which store commodities. In this context, the level of the associated storage variable $s_{pp, tp, ts}$ defines the amount of energy or material which is stored in a producer node at the end of the time step. By multiplying the

¹ A detailed discussion of approaches for modeling storage restrictions in different models of the PERSEUS family is omitted at this point. One possible approach to solve the storage restriction for the first time-step is to apply a coupling to the storage level of the last time-step, instead of the non-existing previous one.

variables with a specific coefficient α , conversion, storage and flow efficiencies are modeled. Besides the outflow and storage variable of the specific time step, which is not further adjusted, this approach allows to define flow losses ($\alpha_{pn',pn,ec,tp}^{flow}$), storage losses due to a self-discharge ($\alpha_{pp,pn,ec,tp}^{stor}$) and to fix the ratio between and within the conversion of input commodities ($\alpha_{pp,pn,ec,tp}^{in}$) to output commodities ($\alpha_{pp,pn,ec,tp}^{out}$). Contrary to flows, which are defined based on a specific edge $(pn, pn', ec) \in \Omega$, process variables may convert multiple input commodities to multiple output commodities and are not indexed based on a specific producer node. However, a strict hierarchical order is applied based on the domain definition $pp \in PROC_{pn}$ such that each variable is uniquely assigned to one producer. Next to the nodal balance equation, the endogenous capacity restriction of processes, storages and flows based on a unit variable is a main part of most PERSEUS models, among many other specific constraints. While all variables may have a specific lower and upper bound, it is important to note that the relation of processes/flows to units is of the type N:1, meaning that a single unit may restrict multiple processes/flows. As illustrated in the following figure 2.2, the clear advantage of such an approach is the possibility to define complex cascading energy and material conversion processes for each producer and to balance the flows between producers based on a plain data structure and a single equation type.

The main drawback of such an approach on the other hand is the strong assumption of a lossless and unrestricted transmission of commodities between the internal processes. In case multiple transmission systems are considered for the flow of multiple commodities, the number of producers usually grows rapidly with each additional commodity and network added to the system, as the topology of the different networks usually doesn't match. The simple case of a graph with three regions, and one producer with two conversion processes per region, each producing commodity c from a and b may illustrate this drawback. Without intraregional network constraints the nodal balancing constraint results in nine equations with six process and nine flow variables, assuming a positive inflow and outflow of each commodity between each region (figure 2.2.a). In case a network with limited capacity is considered for one of the input commodities, for example for commodity b, in a way that the two conversion processes are connected to different nodes of the network, the problem size increases significantly (figure 2.2.b).

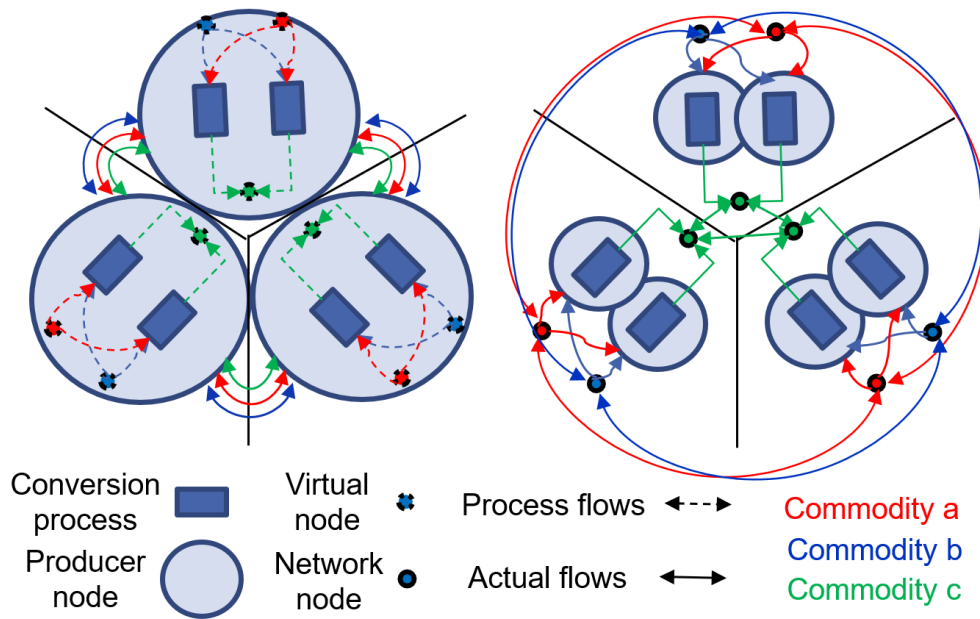


Figure 2.2: Simple network example (left), complex network example (right).

Besides of two additional flows per region, for adding the network, the producer node in each region has to be split in six nodes adding six additional flows per region in order to avoid a shortcut in the flow of the introduced network. In total 15 additional equations and 18 flow variables are added additionally to the six flow variables which are initially introduced. In a small-scale energy system considering the transport of multiple networks, such as models on a municipality scale, the increase of the problem size might be acceptable. With an increasing size of the energy system, the advantage of such an approach, however, significantly decreases. This is a challenge in particular for sector coupling processes, considering that in large scale energy systems with transmission grid restrictions, most processes are not directly connected to the nodes of a transport system, but indirectly through a distribution grid. The standard case of decentral consumers with the options to cover their space heating demand based on an electrically driven heat pump or a gas fired boiler illustrates the challenge, taking into consideration the different topologies of the gas and electricity transport infrastructure. When assuming non-overlapping supply areas for the same commodity below the transmission grid level, the challenge arises, that consumers may be situated within the supply area of the same gas node but connected to different electricity nodes.

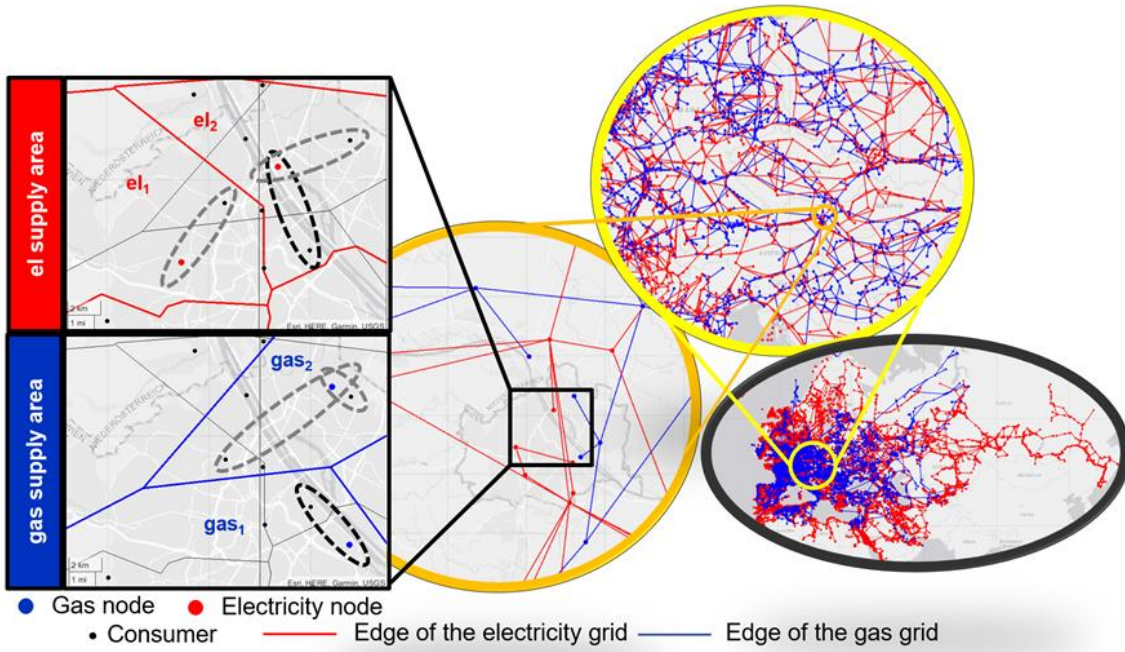


Figure 2.3: Overlay of the gas and electricity transmission grid, the challenge of matching supply areas

In PERSEUS-gECT this problem is addressed by generalizing the concept of producers, processes and units in a way that the definition of a producer is reduced to an entity, that relates processes and units with a common geographic property² and function. In the previous example that described the balancing of two processes in three regions, the possibility to assign a process to different nodes obviously solves the challenge, which arises with the introduction of intraregional network constraints, as no additional variables or constraints are needed besides the two introduced additional flows per region. By relaxing the assumption of a non-restricted commodity flow between all processes associated to a producer, the concept of a producer might be extended in a way that $pn \in PROD$ defines the relation between a set of processes which cover the same spatial area or are allocated at the same point and a set of nodes, which are linked by these processes. In this context, the concept of a balancing node is reduced such that $n \in N$ only defines an entity without internal restrictions for the flow of energy or material. With a less restrictive definition of a process, including the possibility to link different nodes, the need to differentiate between flows and conversion processes can be omitted. Instead, a generalized definition of a process is chosen. Next to the already known functionality of converting commodities within a node and time step, a conversion of commodities between different nodes of the same time step (flow) and between same nodes of different time steps (storage) as well as a combination of both (flow with storage), is included. A process $x_{pp,tp,ts}$ thus defines a directed flow of energy and material starting from potential different nodes in time step ts and ending in potential different nodes of time step $ts' \geq ts$, which includes and extends the former

² This might be an exact geographical location (latitude, longitude) or a polygon defining a certain area.

definition of flows and storages. Furthermore, a less restrictive definition of a unit is chosen, allowing a N:N relation between processes and units, such that a process may be restricted by multiple units.

A major drawback of the developed approach is the need to break the clear structure of an energy flow graph on the one hand and the clear hierarchy of regions/subregions/processes/flows on the other hand. With increasing degree of freedom for the definition of nodes and processes, the challenge of parametrizing a clear data structure increases. Therefore, a focus of PERSEUS-gECT lies in the definition of producers, relating possible processes with possible nodes, starting from the graph of existing and potential transport systems for multiple energy and material commodities on the one hand and regional demand/supply potentials on the other hand. As illustrated in the following figure 2.4, the main idea for defining the model structure lies in overlaying of a spatial highly resolved potential analysis with the topology of the transport infrastructure. This integration enables the discretization/aggregation of decision variables and their interconnection between the nodes within the transport graph.

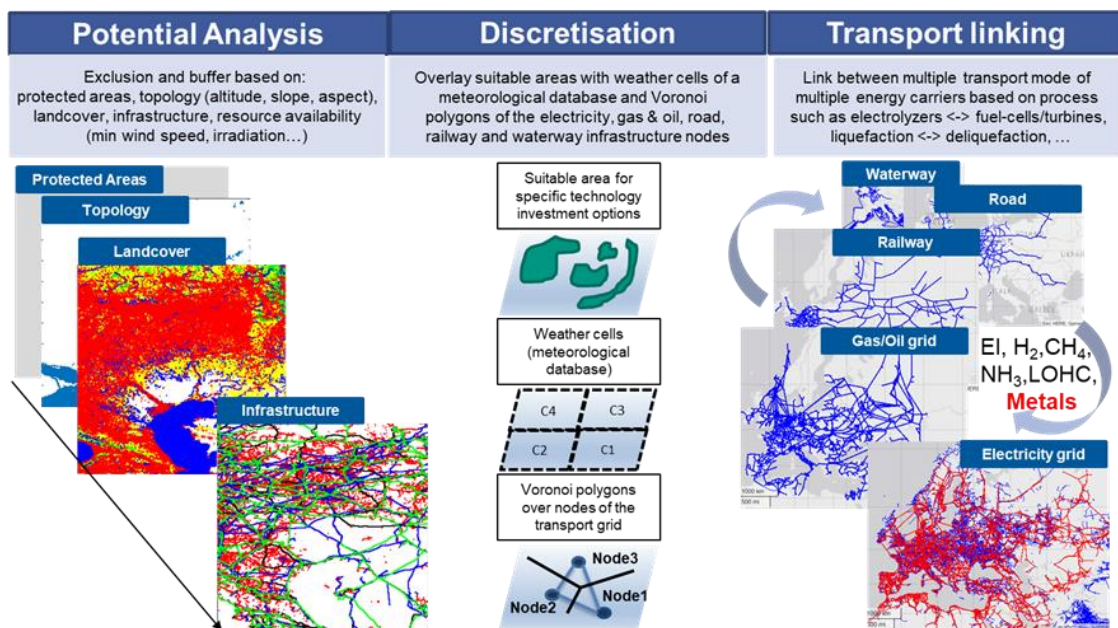


Figure 2.4: General approach for the problem definition and parametrization in PERSEUS-gECT.

2.2 Classification of the modelling concept within the literature

A detailed overview of the literature for certain aspects of the developed modeling approach can be found in the specific sub chapters. The goal of the following brief overview is to give an insight of how the developed approach in general might be classified within the existing literature. In general PERSEUS-gECT can be classified within the broad category of energy system

optimization models, which aim to provide insight on the development of the energy system from a regional to a global scale. In recent years many open source models, of which PyPSA (Brown et al. 2018) is maybe the most prominent and widely used, have been developed with the scope of providing easy assessable and transferable methods for the parametrization and optimization of energy systems based on open source data. Besides of the multiple branches of PyPSA, such as PyPSA-EUR and PyPSA-Earth, (Parzen et al. 2023) mentions several other models such as OSeMOSYS Global, Genesys, LUT, LEAP in this context. The publication classifies these models according to their representation of the transmission system (power flow (PF), transport model (TP), linearized optimal power flow (LOPF), security constrained linearized optimal power flow SCLOPF), the consideration of unit commitment (UC) constraints, the sector coupling and a pathway optimization, and for the authors very important, the sector free and openness of the model. Within this classification PyPSA complies with all criteria while the majority of the other before mentioned methods are applicable for modelling the sector coupling while taking into account unit commitment constraints and a certain representation of the transmission system. An interesting observation is the allocation of the TIMES and MARKAL within this framework, with the ability to combine a linearized optimal power flow and unit commitment constraints, with its initial strength of modelling complex sector coupled systems within a single node model. This might represent an interesting link to the developed own approach, as PERSEUS-gECT evolves from the same model family of energy flow graph based representations of the energy system (Rosen 2008). The comparison to this type of national energy planning tools is therefore more suitable, which are referenced by (Krishnan et al. 2016) as co-optimization tools for the power system generation and expansion planning. A comprehensive overview of on the needed inputs and a comparison of existing methods which also includes an older version of the original PERSEUS model may be found in (Liu et al. 2013). In the current setting a comparison of PERSEUS-gECT with classical linear optimization models, which model the development of the electricity and heating system such as the REMix(Gils et al. 2019), might be more suitable than the comparison to open source based approaches as done by (Parzen et al. 2023). Instead of developing generic models which might solve small problem instances with the described properties with the mentioned constraint of SCLOPF and UC problems, the comparison with large scale multi commodity energy system models might be more suitable. Following the classification of (Dranka et al. 2021) with the differentiation of co-optimization models along the categories in short and long-term planning in six different problem fields focusing on (i) energy and reserve markets, (ii) electricity and gas networks, (iii) micro grid, (iv) water nexus, (v) multi energy carrier and (vi) generation and transmission network expansion planning (GEP & TEP), the number of approaches with a comparable problem spectrum to PERSEUS-gECT is limited. Neglecting a modelling of micro grid and of the water nexus, the currently developed approach tries to combine the long-term planning in the remaining categories with a high spatial and technological resolution. While the number of approaches with a detailed modelling in the categories (i), (ii) and (vi) is very large, the amount decreases in case the transport of multiple energy carriers is integrated. The National Long-Term Energy and Transportation Planning (NETPLAN) software developed for modelling the energy and transport infrastructure in the US is one example for this kind of exiting approaches. Approaches, which combine the expansion of a multi-energy carrier

transport system with a combined multi energy generation and demand planning on the one hand and the transmission expansion planning of the electricity and gas network on the other hand, are rather rare. In most cases, in which a generation and/or transmission network is optimized with a high technological and spatial resolution, only one sector is considered. For the (electricity) generation planning, for example, numerous examples can be found, with a good overview provided by (Sadeghi et al. 2017). (Hemmati et al. 2013b) on the other hand provide a good literature overview for the transmission network expansion planning problem. Concerning the combination of both problems, the overview of (Hemmati et al. 2013a; Latorre et al. 2003) and more recently (Li et al. 2021) could be mentioned, which focus on a co-optimization in the power system. In this context, PERSEUS-gECT could be placed in the triangle of the before mentioned literature streams. Starting from a detailed modelling of the combined GEP and TNEP (a), the high granularity of the recently trending open source and open data-based type of approaches (b) is combined with the detailed cross-sectoral modelling approach of classical national energy planning tools (c).

2.3 Formal structure of the optimization model

The formal structure of the techno-economic multi-commodity and multi-period energy system expansion and dispatch optimization model PERSEUS-gECT is based on a rather general definition of processes, units and producers for a spatial and temporal balancing of an exogenously given demand of certain energy carriers with the goal of minimizing the system expenses. Therefore, the general concept for modeling the conversion, transmission and storage of commodities is defined in a first step in chapter 2.3.1. Following the rather abstract definition of the problem structure, the actual reference energy system is defined in chapter 2.3.2, which is modeled in PERSEUS-gECT based on processes, units and producers. With the definition of the actual conversion, transmission and storage systems, the constraints for their balancing and expansion might be specified. The specification of the general constraint set introduced in 2.3.1 is thus part of the last chapter 2.3.3.

2.3.1 Modeling the conversion, transmission and storage of commodities based on a general concept of process, units and producers

Given a set of nodes $n \in N$ and a set of time steps $ts \in TS$ of a time period $tp \in TP$, the basic structure of the model is defined based on the concept of processes $pp \in PROC$ for the conversion, transmission and storage of one or more commodities $ec \in EC$ between these nodes and time steps. In this context the variable $x_{pp,tp,ts}$ defines a certain conversion activity starting in time step $ts \in TS$ of time period $tp \in TP$. Each process activity might convert multiple input commodities from multiple nodes to multiple output commodities at multiple nodes and time steps $ts' \geq ts \in TS$. The nodal balancing equation thus depends on the domain definition of a process and the conversion ratios:

$$\sum_{ts' \in TS} \sum_{pp \in PROC_{n,ec}} x_{pp,tp,ts'} \alpha_{pp,n,ec,tp,ts'}^{out} = \sum_{pp \in PROC_{n,ec}} x_{pp,tp,ts} \alpha_{pp,n,ec,tp,ts}^{in} + b_{n,c,tp,ts}^{dem} \quad (2.2)$$

$$\forall n \in N, \forall ec \in EC, \forall tp \in TP, \forall ts \in TS$$

Eq. 2.2 follows the convention of defining the exogenous nodal demand $b_{n,ec,tp,ts}^{dem}$ for a certain commodity $ec \in EC_n$ in each time step as a positive right-hand side (rhs) parameter. Furthermore, the conversion outputs of current or previous ($ts' \leq ts \in TS$) process activities associated with a certain node-commodity pair $pp \in PROC_{n,ec}$ define the inflow into a node depending on the positive coefficient $\alpha_{pp,n,ec,tp,ts'}^{out}$. Vice versa, conversion inflows of current process activities are allocated on the right-hand side depending on the coefficient $\alpha_{pp,n,ec,tp,ts}^{in}$ while exogenous inflows of commodities into a node are defined based on a negative rhs parameter $b_{n,c,tp,ts}^{dem}$. While most stationary storage processes are linked with $ts' = ts - 1$, corresponding to an inflow of a commodity starting from the same node in a preceding time step, longer time lags ($tl \geq 1$) are possible in case of spatial flows, considering that the transport of a commodity over long distances might take days or weeks, depending on the chosen system. For modeling the storage state in cases where the time lag is greater than the current time step, the current time step is usually linked to the end of the year such that $ts' = |TS| + (ts - tl)$. Due to this start problem, the restriction that only previous storage states are considered ($ts' \leq ts$) is actually missing in the nodal balance and shifted to $\alpha_{pp,n,ec,tp,ts'}^{out}$. In the following figure, the different process types and their balancing are illustrated:

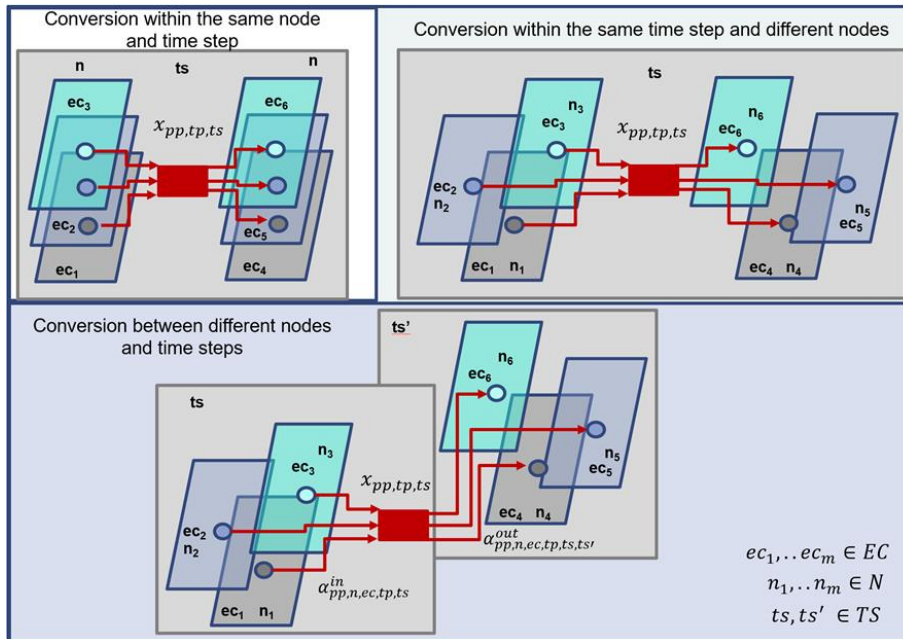


Figure 2.5: Conversion process types in PERSEUS-gECT.

By rearranging the coefficients in a way that the matrix $A_{tp,ts}^{inout}$ includes all input and output coefficients of processes with $ts' = ts$, while $A_{tp,ts-tl,ts}^{inout}$ includes the output coefficients of all

conversion processes with a time-lag tl of period $tp \in TP$, the nodal balance equation for each period $tp \in TP$ might be expressed as follows³:

$$\begin{bmatrix} A_{tp,ts-tl} & & \\ \vdots & \ddots & \\ A_{tp,ts-tl,ts} & \dots & A_{tp,ts} \end{bmatrix} \begin{matrix} x_{tp,ts-tl} \\ \vdots \\ x_{tp,ts} \end{matrix} = \begin{matrix} b_{tp,ts-tl} \\ \vdots \\ b_{tp,ts} \end{matrix} \quad (2.3)$$

, where $x_{tp,ts}$ includes all process activities of a time step. In this context the rhs Parameter $b_{tp,ts}$ is a vector of length $NC = \sum_{n \in N} |C_n|$, where C_n defines the set of commodities which are balanced at node n .

Considering that processes might be assigned to multiple nodes of the graph and to multiple commodities, which makes a unique assignment to a certain region or sector difficult, their regional and sectoral classification is based on the assignment $pp \in PROC_{pn}$ to a certain producer $pn \in PROD$. A producer thus defines a virtual node to which processes with the same geographical, sectoral and functional classification are connected. Besides of processes, each producer also includes a set of units $pu \in Unit_{pn}$ in order to model the capacity of certain technologies.

For fixed capacities, the restriction of process levels might directly be applied based on a lower $lb_{pp,tp,ts}$ and upper bound $ub_{pp,tp,ts}$ parameter of the conversion activity in time step ts .

$$lb_{pp,tp,ts} \leq x_{pp,tp,ts} \leq ub_{pp,tp,ts} \quad (2.4)$$

In case of an endogenous capacity expansion, one or multiple process activities $x_{pp,tp,ts}$ might be restricted by the capacity of one or multiple process units $y_{pu,tp'} = [y_{pu,tp'}^{exp} y_{pu,tp'}^{dis} y_{pu,tp'}^{lev}]^T$. In most cases, it is sufficient to work with a single expansion variable $y_{pu,tp'}^{exp}$, which is defined at the commissioning period $tp' \leq tp$, in order to restrict the process activities of the current period $tp \in TP$. For processes with an endogenous decommissioning before the end of lifetime, however, the level of a process unit $y_{pu,tp}^{lev}$ is defined based on the level in the previous period plus the expansion $y_{pu,tp'}^{exp}$ minus the dismantling $y_{pu,tp}^{dis}$ during the current period:

$$y_{pu,tp}^{lev} = y_{pu,tp-1}^{lev} + y_{pu,tp'}^{exp} - y_{pu,tp}^{dis} \quad (2.5)$$

In general, the subset of conversion processes $PROC_{pn}$ and units $Unit_{pn}$ associated with a producer $pn \in PROD$ might be coupled by $k = 1:K$ capacity constraint relations, such that the variable capacity constraint relation has the following form:

$$\sum_{pp \in PROC_{pn}} x_{pp,tp,ts} \alpha_{pp,k,tp,ts}^{cap} \leq \sum_{tp' \leq tp} \sum_{pu \in Unit_{pn}} y_{pu,tp'} \beta_{pu,k,tp',tp,ts}^{cap} + b_{pn,k,tp,ts}^{cap} \quad (2.6)$$

$$\forall tp \in TP, \forall ts \in TS, pn \in PROD, k = 1:K$$

³ For a better readability the superscript for matrix A and rhs Parameter b are neglected. Furthermore, time-lags which cause a start problem definition ($ts - tl \leq 0$) are neglected.

Considering that all equality constraints such as the nodal balancing equation 3.1 or the process unit level definition in 3.4 might be reformulated to inequality constraints, the problem structure defined in 3.8 already shows the overall structure of the optimization problem. As already mentioned, PERSEUS-gECT is formulated as a linear optimization model, that minimizes all relevant expenses for the operation and expansion of the system:

$$\min ZF = \sum_{tp \in TP} \left[\begin{array}{c} \sum_{ts \in TS} \sum_{pp \in PROC} x_{pp,tp,ts} c_{pp,tp,ts}^{var} \\ \sum_{ts \in TS} \sum_{n \in N} \sum_{ec \in EC} \sum_{pp \in PROC} x_{pp,tp,ts} c_{n,ec,tp,ts}^{fuel} \alpha_{pp,n,ec,tp,ts}^{in} \\ \sum_{pu \in Unit} y_{pu,tp} (c_{pu,tp}^{fix} + c_{pu,tp}^{inv}) \end{array} \right] \quad (2.10)$$

In this context $c_{pa,tp,ts}^{var}$ includes the discounted variable cost of a process activity in time step ts and period tp which might include variable operations and maintenance cost, port fees, while $c_{n,ec,tp,ts}^{fuel}$ includes the discounted commodity specific expenses. Process unit variables on the other hand are multiplied with the discounted fixed cost for the operation of a specific capacity $c_{pu,tp}^{fix}$ and the parameter $c_{pu,tp}^{inv}$ which includes discounted expenses for the expansion or dismantling of a unit capacity.

2.3.2 Reference energy system of PERSEUS-gECT

PERSEUS-gECT follows a data driven approach for modeling the energy and material balance within a certain region and time horizon. Depending on the specific scenario, period and regional context, a sequence of multiple processes is used to model either a partial or complete energy balance. This encompasses various stages ranging from the extraction of primary energy carriers to the final energy conversion, ensuring the fulfillment of sector-specific useful energy demand. This includes the transport, storage and conversion of multiple primary and secondary energy carriers and further commodities. An overview of the actual balance of commodities along the energy conversion chain is illustrated in the following table 3.6:

EC	IMP	EXP	PPRD	TRA	STOR	Transformation				Final demand		
						TI_EHG	TO_EHG	TI_OCP	TO_OCP	TI_FD	TO_FD	
comb_fuel												
comb_solids												
fossil_solids	1				(b)	1					1	
biomass			1			1		1			(a)	
waste			1			1				1		
metals				1	1	1				1		
other_solids						1						
comb_gas												
CH4_gases												
CH4			1	1	1	1		1	1	1		
NG			1									
SNG										1		
L(S)NG				1	1			1	1			
C(S)NG				1				1	1			
biogases						1		1	1		(a)	
MG						1						
H2				1	1	1		1	1	1		
LH2				1	1			1	1			
CH2				1				1	1			
NH3				1	1			1	1			
other_gas												
comb_liquids												
Oil & Oil prod												
oil	1			1	1	1					1	
fossil_oil	1											
SFO										1		
liquid_biofuels						1					(a)	
MeOH				1	1			1	1			
LOHC				1	1			1	1			
other_liquids												
other_nonres												
nuclear	1							1				
wind			1					1				
solar			1		(c)			1				
hydro			1		1			1				
geo			1					1				
marine			1					1				
other_res												
electricity				1	1	1	1	1	1	1	1	1
heat				(d)	1	1	1	1	1	1	1	1
CO2				1	1			1	1	1		1

IMP: import, EXP: export, PPRD: primal production, TRA: transport, STOR: storage, TI/TO: transformation input/output, EHG: electricity and heat generation, OCP: other conversion process, FD: final demand

(a) final demand of bioenergy is regionally balanced in advance and therefore excluded from the optimization

(b) storage processes only used for modelling the final demand flexibility, no explicit storages for fossil solids considered

(c) used for modelling integrated electricity and heat storages, such as for concentrated solar power plants and photovoltaic-battery systems

(d) topology and capacity of district heating networks is defined in advance, during the optimization transport restrictions are neglected

Figure 2.6: Modelled energy balance

Driven by the final energy and non-energy demand ($ec^{FD} \in EC$) of transformation processes using fossil solids, biomass, methane, hydrogen, oil, electricity or heat as an input in order to balance a sectoral useful energy demand such as space heating, the aforementioned energy carriers are either imported, internally extracted or produced considering transmission and storage restrictions. Besides of some modifications, the structure of the illustrated reference energy systems in general follows the approach of Eurostat for structuring the energy balance within a system⁶. Concerning the availability of primary energy carriers, PERSEUS-gECT models the primary production of natural gas and renewables based on field specific natural gas data and a spatial highly resolved techno-economical potential analysis for renewable energy sources. In case of fossil solids, oil and uranium, the primary production is neglected. Instead, the inflow of

⁶ <https://ec.europa.eu/eurostat/documents/38154/4956218/ENERGY-BALANCE-GUIDE.pdf/>

these primary energy carriers into the system is modeled based on a simple import flow from a global slack node. In addition to the generation of heat and electricity, the conversion to secondary carbon and non-carbon-based combustible fuels, such as hydrogen and its derivatives is modeled. Considering CO₂ emission restrictions, PERSEUS-gECT enables an endogenous adjustment of production, transmission, storage and demand capacities for most energy carriers such that the multi-modal flow of energy might be optimized from the source to the sink. In this context the model considers a national and global balancing of CO₂ emissions from each conversion, transmission and storage processes within the system, such that the combustion of fossil, biogenic or synthetic carbon-based energy carriers injects CO₂ to a national atmosphere node or into a node of the transmission and storage system for CO₂ while the production of the non-fossil energy carriers demands CO₂. As a consequence, there is no need to differentiate transformation outputs depending on the transformation inputs, such as renewable or non-renewable electricity, heat, hydrogen, methane or fuel oil in order to establish emission reduction targets. Assuming that the characteristics for the transmission, storage and final demand conversion for biomethane, synthetic natural gas from power (Sabatier) and natural gas are comparable, in PERSEUS-gECT only the processes for their primary conversion are differentiated. Analogously to methane, the same simplified approach is applied to fuel oil products, independent of their biogenic, synthetic or fossil source. Considering that transmission, storage and conversion processes are defined based on their transformation inputs and outputs, the general approach to avoid an exponential increase in the number of processes is to model only the flow of some base commodities which are differentiated with respect to transmission, storage and conversion restriction. In addition to the differentiation of heat and low temperature heat driven by the demand side, methane, hydrogen, CO₂ and electricity are differentiated in order to model different transport modes. Besides of a gaseous pipeline transport, the previously mentioned gases might be compressed or liquified for a transportation by rail, road and waterway. For the electricity transport the possibility to choose between the AC and DC transmission system necessitates a differentiation of the commodity. In addition to the already mentioned supply or demand driven commodities, the transport, storage and use in the transformation sector of secondary energy carriers, such as liquid organic hydrogen carriers (LOHC), ammonia (NH₃) and reactive metals (RM) is considered in order to model the alternative hydrogen-based conversion and reconversion paths. Although these commodities are also produced and demanded in the chemical or steel industry, their final demand is neglected in the current model state and the energy to produce these commodities for a non-energetic use is included in the demand of the mentioned final demand energy carriers such as electricity or hydrogen.

As illustrated in the following figure 3.7, the goal of this approach is to evaluate alternative conversion paths for a spatial and temporal balancing of supply and demand considering the topology of multiple transport and storage systems on the one hand and regional demand and supply availabilities and potentials on the other hand.

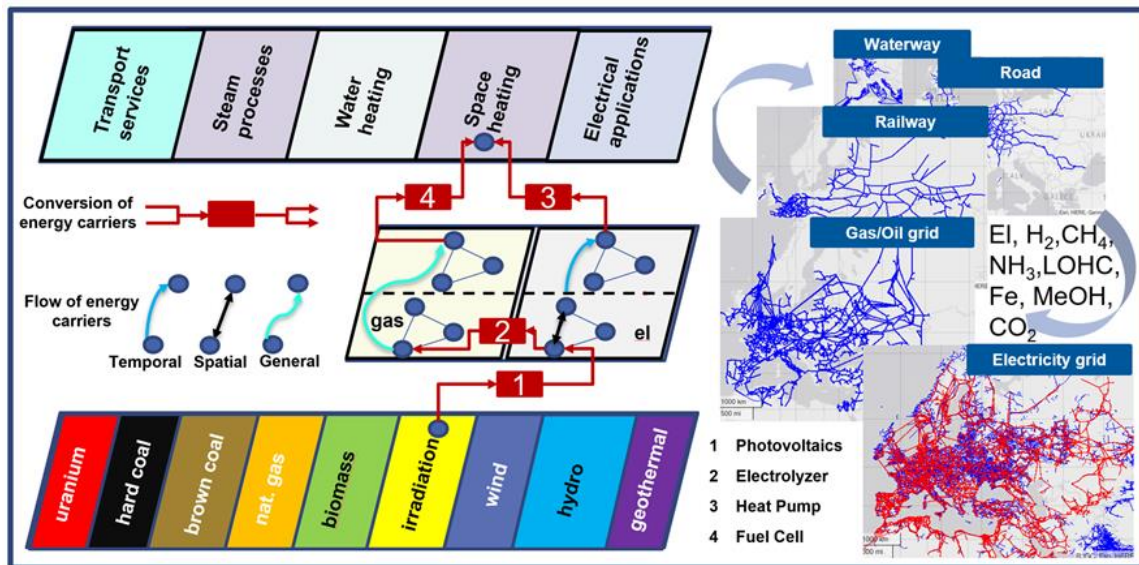


Figure 2.7: Approach for evaluating conversion paths from the primary to the final energy conversion.

In this context the nodes of the transport and storage system are linked by processes, defining a potential spatial and/or temporal transformation of one or multiple commodities and may have a variable capacity defined by units. With a unique assignment of each process and unit to a producer, defining a regional entity, which represents a specific geographic point, line or area with an associated set of related nodes, a mapping of regional availabilities and potentials to processes and units is enabled. The flexibility to convert energy carriers between the nodes of multiple transport systems of usually non-overlapping topology with a minimal amount of variable, however, has the drawback that processes and units cannot be directly associated to a specific node or energy carrier or even function. Keeping this ambiguity in mind, processes and units might be classified based on a combination of their main function, input and output commodities, sector, technology and eventually their commissioning year and aggregation status. From a functional point of view a differentiation between the electricity and heat generation (EHG) and other commodity production (OCP) of the transformation sector and final demand conversion (FD) is possible. Due to the focus on transmission and storage restrictions, the spatial and temporal transformation is further differentiated in primary storage (STOR) or transmission (TRANS) related conversions, with import flows included in the last mentioned. This also includes processes for modeling a multi-modal switch of the same commodity between nodes, while transmission or storage related conversions between different commodities such as liquification/regasification or compression/decompression is included in OCP. Finally, it should be kept in mind that although each process and unit might be assigned to a unique subset with $pp = \{pp^{EHG}, pp^{OCP}, pp^{STOR}, pp^{TRANS}, pp^{FD}\} \in PROC$ and $pu = \{pu^{EHG}, pu^{OCP}, pu^{STOR}, pu^{TRANS}, pu^{FD}\} \in UNIT$, the scope of the processes and units is not exclusively restricted to the main definition of the subset. OCP processes for producing biogases or synthetic fuels, for example, might also coproduce heat which might be used in district

heating. The reasoning for the classification is to allow an intuitive structuring of the model input and output data.

Following the convention to classify EHG conversions based on the main input fuel, OCP conversions based on the main output commodity and spatial/temporal flows based on the storage/transmission system, following main classes of processes and units might be differentiated:

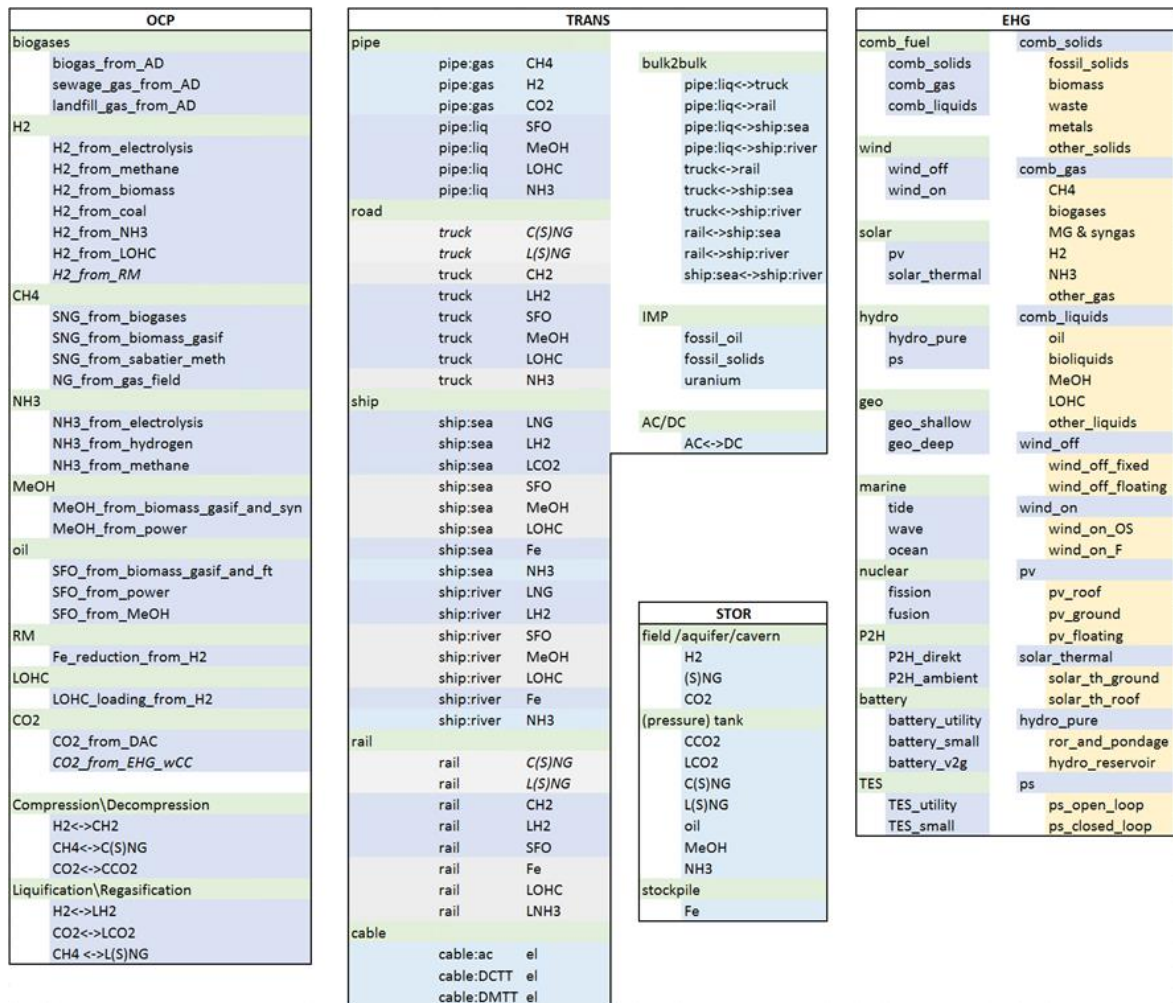


Figure 2.8: Classification of non-final demand processes.

Due to the convention to model electricity storages, such as battery and hydro storages, as generators within the electricity system, processes which model the storage of electricity or heat are included in the EHG set and not in the STOR set. Furthermore, it should be noted that most processes for modeling the separation of CO2 are included in the EHG set as part of a pre- or post-combustion separation of CO2 from carbon-based fuels, while direct air capture (DAC) processes are included in the OCP set. Considering the output, EHG processes and units might be classified according to a combined (CHP) or exclusive generation of electricity (EOP) and heat (HOP). Vice versa, the OCP set might be further differentiated based on the input commodities.

In order to model the transshipment of a commodity between two transport systems, the complexity ranges from a simple unloading process of iron from rail to ship, to the injection of shipped LNG into the gas grid, necessitating a combination of OCP, STOR and TRANS conversions. This might involve the unloading of LNG from a ship into a land-based LNG storage infrastructure and a regasification of LNG to NG. A possible realization of such as process chain, which is assigned to a producer, is shown in figure 2.9b, including processes for a liquification and regasification, port fees for loading and unloading, and storage variables for modeling the volume, inflow, outflow and boil-off. Finally, processes and units might be differentiated with respect to the general and technical specification, as shown in figure 2.9a.

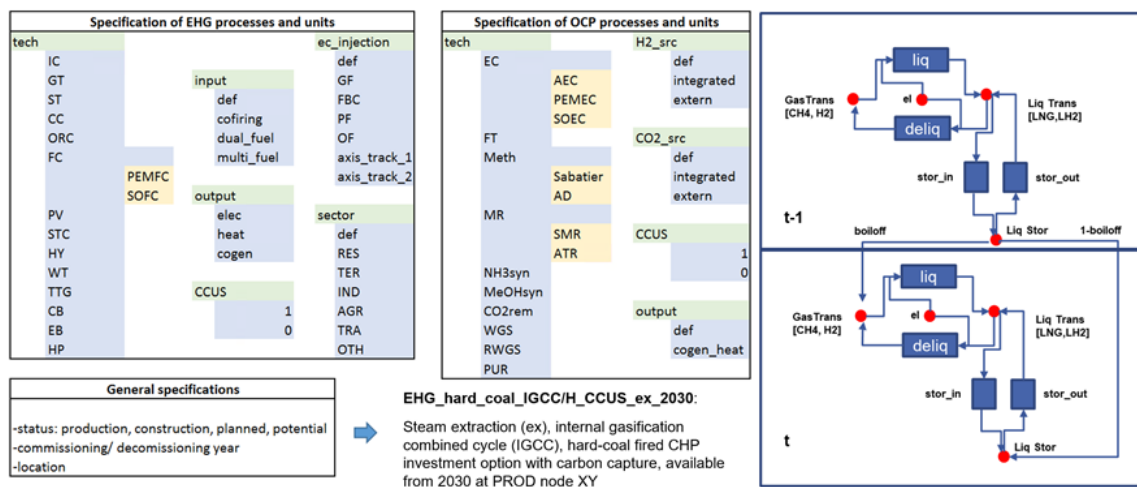


Figure 2.9: General scheme for a specification of EHG and OCP processes (a) and example for a process coupling for modelling the transshipment of commodities.

Depending on the specification of the system boundaries, upstream processes might be implicitly included within a process or modeled as separate processes, with a higher degree of freedom for dimensioning the different unit capacities and technologies. For example, a power-to-liquid plant might be characterized by a single process with electricity as single input and Fischer-Tropsch fuels as output, implicitly including the electricity consumption of the electrolyser (EC) and direct air capture unit (DAC), or reduced to a Fischer-Tropsch process (FT) which takes hydrogen and CO₂ from a grid. In the first case the configuration of the FT, EC and DAC technologies is fixed and production takes place at the same location and time, while in the second case the hydrogen and CO₂ supply might be endogenously adjusted, with the possibility to use hydrogen and CO₂ which might be converted by other technologies, during previous time steps in other regions.

On the demand side, the processes for converting final demand commodities ec^{FD} might be differentiated on a sectoral and process level. Following a classification analog to the TYNDP 2022, this includes a sectoral differentiation of the industrial (IND), residential (RES), tertiary (TER), transport (TRA), agriculture (AGR) and energy sector (NRG_E). In this context NRG_E and TRA only include the demand of processes which are not explicitly modeled as EHG, OCP, TRANS

and STOR conversions (e.g., excluding liquification and regasification plants), while distribution and storage losses are endogenously considered in the modeling TRANS, STOR and EHG processes. On a sub-sectoral level, PERSEUS-gECT considers a further differentiation of the residential and industrial sector, such that single (HHs), double (HHd) and multifamily (HHm) households are considered on the one hand and various industry sectors such as iron and steel and chemical and petrochemical on the other hand. On the processes level the differentiation is mainly driven by the classification of direct electricity application and various heating and cooling applications. The technology classes for converting energy carriers to space heat or hot water, such as heat pumps, fuel cells and boilers, obviously overlap with some considered in the EHG transformation sector and may only vary on the techno-economical parameters, allowing a differentiation of heat pumps in single family buildings and in the district heating network for example. Besides the possibility to model weather dependent heating and cooling demand profiles, which are consistent to the intermittent renewable supply profiles, the sectoral and process-based differentiation, which is shown in figure 2.10, is driven by the possibility to model demand flexibilities and fuel switching potentials with a high spatial and temporal resolution.

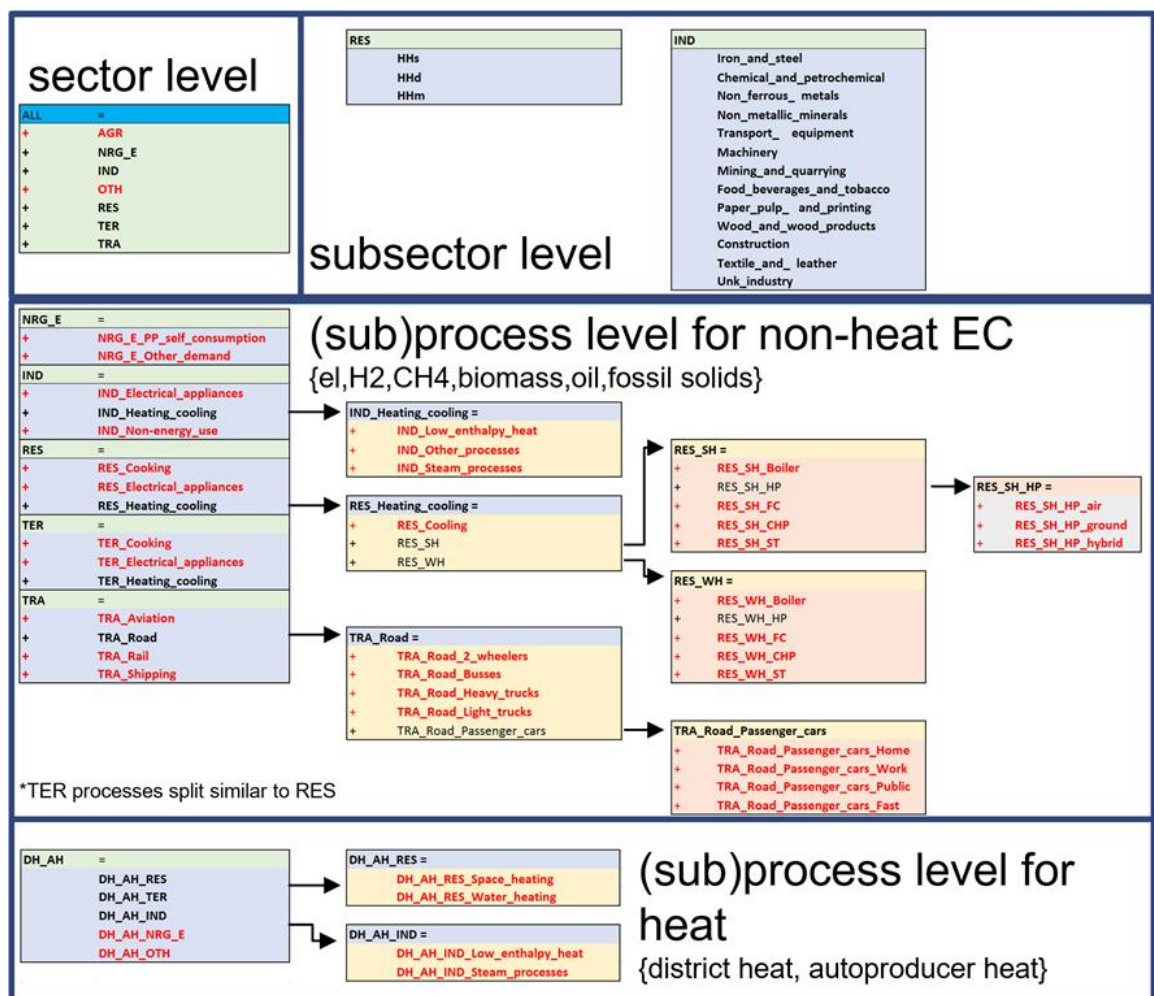


Figure 2.10: Classification of the final demand sector and the possible conversion processes.

In the current state PERSEUS-gECT focuses on an endogenous modeling of heating processes on the demand side and relies on a scenario based external definition of other conversion technologies and their drivers. For a decarbonization of the final demand the model thus may change the carbon intensity of a fuel by replacing fossil liquids and gases by low carbon synthetic or biogenic liquids and gases or by switching from gas fired boilers to heat pumps. Investments in the insulation of a building, which might reduce the space heating demand or in alternative drives in the transport sector, such as electric driven airplanes, ships or trucks, however, are not considered.

Concerning the system boundaries, the current focus of PERSEUS-gECT is to model the European energy system in 5-year periods until 2050, considering supply potentials and transmission restrictions in neighboring regions, including the electricity demand in all regions with a considered electricity grid. As illustrated in the following figure 2.11, showing all nodes of the system on the left and the location of producers with EHG processes on the right, the spatial coverage of PERSEUS-gECT includes Europe, Middle East and Northern Africa (MENA), Central Asia and Patagonia.

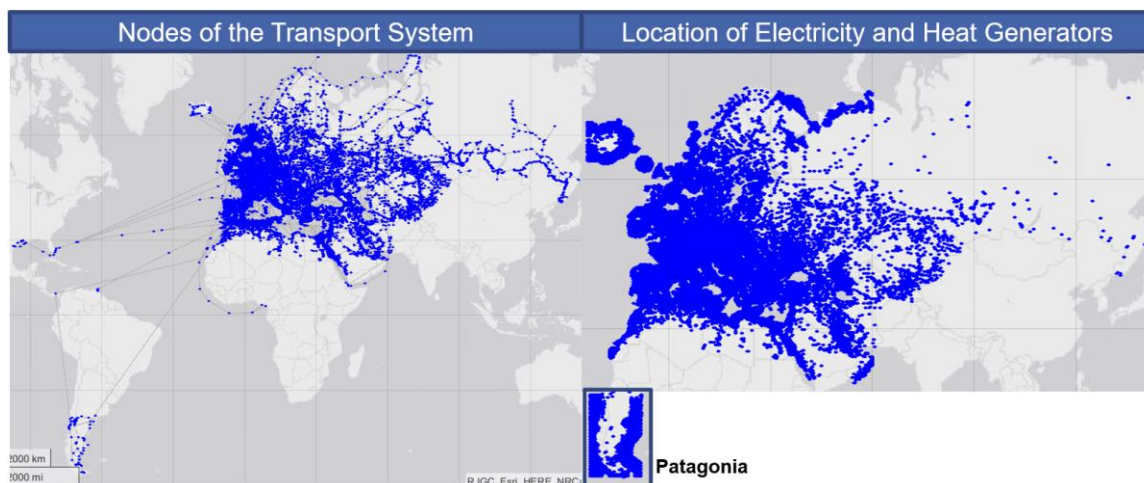


Figure 2.11: Current geographic boundaries of PERSEUS-gECT

While the conversion of primary energy is modeled in all regions, a complete energy balancing, considering the demand of all mentioned final energy carriers, is restricted to the European region, including Turkey, Georgia and Ukraine. Besides of Patagonia, which is only modeled on the supply side without the consideration of an electricity grid, a representation of the electrical network, including a modeling of the power demand, is considered in all regions. In order to model gas flows from terminals in Nigeria, Venezuela and the USA, PERSEUS-gECT additionally includes a representation of the relevant LNG infrastructure of these countries.

2.3.3 Definition of specific constraints

Following the description of the problem structure in chapter 2.3.1, the modeling of previously defined EHG, OCP, STOR, TRANS and FD processes and units for the conversion, transmission and storage of combustible fuels, heat, electricity and CO₂ should be described next. In this context the general and specific constraint sets which restrict the dispatch and expansion of processes are defined, while the approach for the actual variable definition and model parametrizing, is subsequently described in chapter 2.4.

Before going into a detail description of the specific constraints, first an overview of the interdependencies between the main EHG and OCP should be given. As illustrated in the following figure 2.12, the backbone of the modeled energy system is based on a balance of the electricity and heating system, as most processes either generate primarily electricity (ehg2el) and/or heat (ehg2th) from primary or secondary energy carriers. Alternatively, electricity and/or high-temperature heat is used as an input in order to produce synthetic combustible fuels (e.g., prod: H₂, prod: SNG), with a co-generation of excess-heat in many cases. Besides of multiple wind and solar conversion processes, the EHG set includes various EOP, HOP and CHP based thermal combustion processes and is linked to either the atmospheric CO₂ node or the CO₂ transmission and storage system in case of a carbon-based fuel. In addition to biomass and methane-based conversion routes, which cover multiple processes from the conversion of primary energy potentials to final energy demands, PERSEUS-gECT focuses on modeling the conversion of hydrogen from electricity, biomass or methane and the production of further derivatives such as NH₃, LOHC, MeOH, Fe, SFO and SNG.

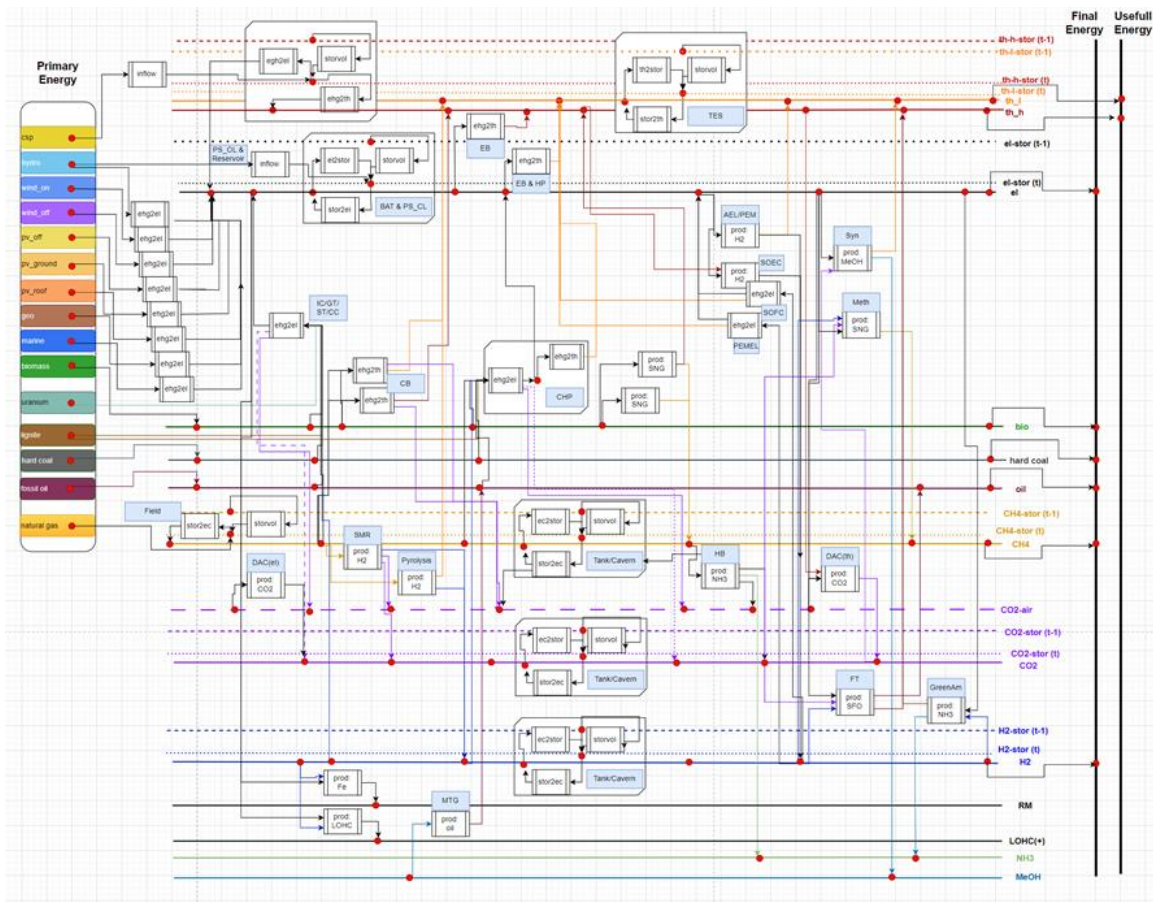


Figure 2.12: Illustration of the reference energy system of PERSEUS-gECT based on the main processes

Constraints for modeling EHG processes and units

In PERSEUS-gECT the modeling of a combined or separated production of electricity and heat may require a combination of multiple process and units, depending on the degree of freedom to change the nodes and share of input or output commodities within a period or the capacity between periods. In the simplest case of a renewable EOP with a fixed capacity, the generation is modeled based on a single non-negative process variable $0 \leq x_{pp,tp,ts} \leq ub_{pp,tp,ts}$. By using a specific profile upper bound in each time step, the input balancing might be neglected and the process appears only once on the left-hand-side of the electricity nodal balance equation with $\alpha_{pp,n,ec,tp,ts,ts}^{out} = 1$. This simplified approach is applied to model the run-of-river, marine and geothermal electricity generation, as these are the only renewable technologies without an endogenous capacity expansion, besides of pump-storage⁷ and hydro-reservoir. Next to the mentioned hydro storages, concentrated solar power (CSP) and photovoltaic-battery systems are also modeled with a storage function and should be described at a later point. In general, the modeling of the input balancing is only considered for (combined) thermal power and heat

⁷ Actually, the possibility for an expansion of closed loop pump storages is included, based on a potential analysis from the literature. In the default settings this option is however neglected.

plants as well as for power-to-heat applications such as heat-pumps (HP) or electrical boilers (EB), while most renewables are currently modeled based on regional profiles and potentials. In the current stage, this also applies to biomass, where each EHG, OCP and FD process is modeled based on a regional individual resource potential, as transport restrictions and regional resource competition of the multiple transformation and final demand conversion processes are ignored. The balancing of the fuel demand from a market (hard-coal, lignite, uranium) or a transport network node (oil, methane, hydrogen) is therefore only modeled for combustible fuels fired internal combustion (IC) engines, steam-turbines (ST), gas-turbines (GT), combined cycle (CC), combustion boilers and fuels cells (PEMEL, SOFC), in addition to the grid balancing of electricity driven EHG application. Concerning the time-step specific availability of fluctuating renewable electricity resources, like processes $PROC^{fRES}$ such as wind (onshore, offshore) or pv (ground, roof, offshore), the general capacity constraint (eq. 2.6) is specified as follows:

$$x_{pp,tp,ts}^{ehg2el} \leq \sum_{tp' \leq tp} \sum_{pu \in Unit_{pn}} y_{pu,tp'}^{exp} \beta_{pu,pp,tp',ts}^{profile} \beta_{pu,pp,tp',tp,ts}^{degrad} + \sum_{u \in Unit_{pn}} y_{pu,tp}^{fix} \beta_{pu,pp,tp,ts}^{profile} \quad (2.11)$$

$$\forall tp \in TP, \forall ts \in TS, \forall pp \in PROC_{pn}^{fRES}, \forall pn \in PROD$$

where $\beta_{pu,pp,tp',ts}^{profile}$ is the normed profile of a unit capacity expansion $y_{pu,tp'}^{exp}$ in the current or previous period or of the fixed $y_{pu,tp}^{fix}$ capacity of the current period, which restricts a process $pp \in PROC_{pn}^{fRES}$. $\beta_{pu,pp,tp',tp,ts}^{degrad}$ is the profile degradation between the commissioning year and the current period. In the most simple case of a unique process-to-unit tuple (pp,pu) and no fixed capacities, the profile restriction reduces to following simple expression:

$$x_{pp,tp,ts}^{ehg2el} \leq \sum_{tp' \leq tp} y_{pu,tp'}^{exp} \beta_{pu,pp,tp',ts}^{profile} \beta_{pu,pp,tp',tp,ts}^{degrad} \quad (2.12)$$

$$\forall tp \in TP, \forall ts \in TS, \forall pp \in PROC_{pu}, \forall pu \in UNIT_{pp}$$

However, it should be noticed that such a simple relation is only valid for large scale wind or solar farm projects with all units lying within the same weather cell and connected to the same electricity grid node⁸. Concerning the capacity potential restriction, following constraint is applied to model k=1:K potential spatial resource competition constraints between units of the same technology or between technologies:

$$\sum_{tp' \leq tp} \sum_{pu \in Unit_{pn}} y_{pu,tp'}^{exp} \beta_{pu,k,tp',ts}^{space} + y_{pu,tp}^{fix} \beta_{pu,k,tp}^{space} \leq POT_{pn,k}^{space} \quad (2.13)$$

$$\forall tp \in TP, \forall pp \in PROC_{pn}, \forall pn \in PROD$$

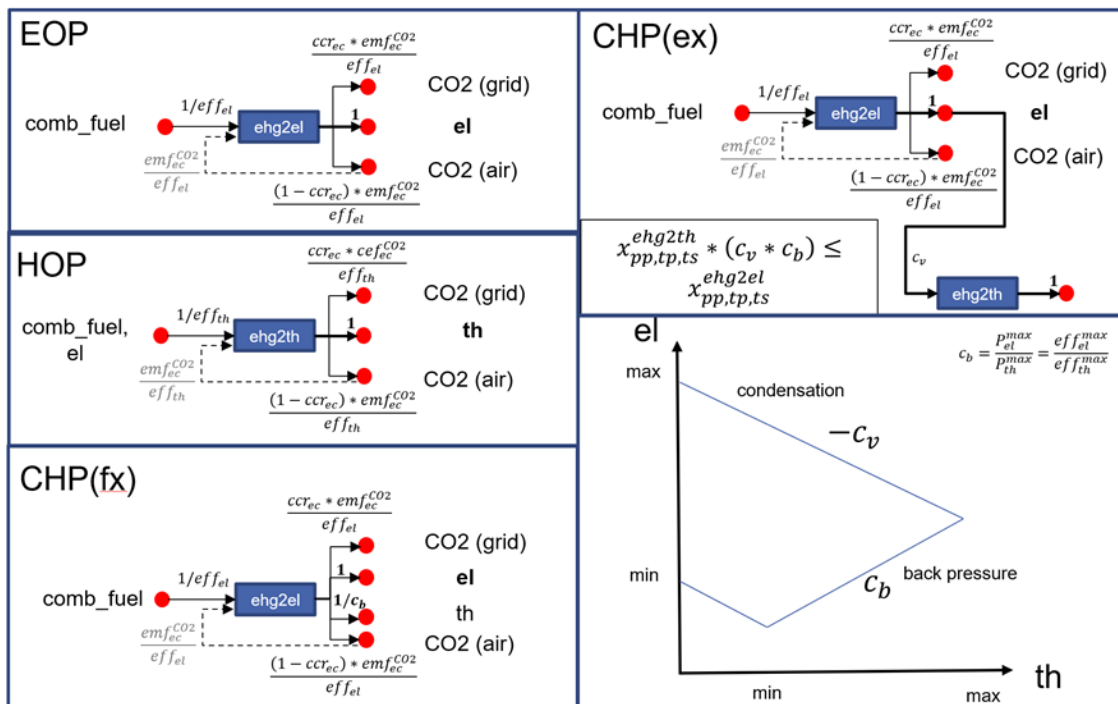
As no endogenous dismantling is modeled for renewable units with a spatial resource potential, the dismantling variable is missing here⁹. Analog to the nodal balancing of run-of-river, marine

⁸ The approach to handle multiple wind turbines or PV modules with diverging technical configuration and actual resource availability conditions (wind speed, irradiation) considering existing assets and various investment options (greenfield/brownfield/planned) and grid connection options, is discussed at a later point (chapter 2.4).

⁹ A detailed description of spatial constraints for renewables is discussed at a later point (chapter 2.3.3).

and geothermal electricity generation, the electricity nodal balance coefficient of wind and pv based processes without an internal storage function is simply one ($\alpha_{pp,n,ec,tp,ts,ts}^{out} = 1$) and the input coefficient is zero. Considering the highly regional technical specification and resource dependency of bioenergy (mass, gas, liquids) and waste fueled electricity and heat combustion generators and boilers, PERSEUS-gECT focuses on modeling dispatch and reinvestment decisions with the option of an additional carbon capture for these EHG processes and units. After additionally excluding the locally exogenously fixed final demand consumption of the residential, tertiary and industrial sector, the remaining biomass potential is primarily considered as a source for OCP processes for the production of biomethane (from biogas upgrading after anerobic digestion of biomass or from biomass gasification) in case of a locally available gas grid node. A greenfield expansion of biomass fueled EHG units is thus only considered in areas without a gas grid connection option and only on basis of the remaining potential after excluding the demand of fixed, existing or potentially reinvested EHG and FD processes.

Before going into the detailed modeling of a multi-commodity fuel inflow from multiple nodes, first the general approach for modeling EOP, HOP and CHP processes, which is illustrated in the following figure 2.13, should be described next.



eff= efficiency, emf=CO2 emission factor, ccr=carbon capture rate, cb= back pressure coefficient, cv= power loss factor, el= electricity, th: thermal heat, EOP= electricity only plant, HOP= heat only plant, CHP=combined heat power, with fixed (fx) (back pressure turbine) or variable (ex) (steam extraction) power-to-heat ration, p_{el}^{max} maximum electrical generation [MW], p_{th}^{max} maximum thermal generation [MW]

Figure 2.13: Parametrizing basic EHG processes

In line with the special case of the already described wind and solar based EOP, the nodal balance output coefficient ($\alpha_{pp,n,el,tp,ts,ts}^{out}$) of all EOP processes is set to 1 and the inflows and other

outputs (CO₂) are defined in reference to the electricity generation. For processes with an input balancing, such as natural gas fired gas turbines, this means that the input coefficient $\alpha_{pp,n,CH_4,tp,ts}^{in}$ is defined based on the electrical efficiency ($1/eff_{el}$). Depending on the carbon emission factor of the fuel mix, for which the process is defined¹⁰ and the carbon capture rate of a potential CCS technology, CO₂ is either injected into a transmission and storage grid node or into the air. Depending on the system boundaries of the bioenergy fueled EHG process, the withdrawing of CO₂ from the air might be included within the same process, which either results in a net-zero emission for processes without a direct air capture or to negative emissions depending on the capture rate. This applies to biomass as well as to biogas-fired generators, as long as the preprocessing steps, like the anaerobic digestion of biomass to biogas are modeled within the system boundaries and not in a separate process. HOP processes are modeled analogous to EOP processes depending on the thermal efficiency ($1/eff_{th}$) and the temperature range of the technology, with the simplification to classify the output either as low-temperature (th_l) or high-temperature (th_h) heat, if it is below or above 100 degree Celcius. It should be noted that both heat products might be either injected into a district hot water or steam grid node or used onside as an input for further processes. Concerning the combined generation of electricity and heat (CHP), a differentiation between processes with a fixed and variable power-to-heat ratio is made. Back-pressure steam turbines or fuel cells with a heat usage are thus modeled as fixed CHP (fx) processes with the convention to define the electricity output as the reference commodity ($\alpha_{pp,n,el,tp,ts,ts}^{out} = 1$) and the thermal output in relation to the maximum electricity generation based on a power coefficient (c_b), which is often referred to as the back-pressure coefficient¹¹. In PERSEUS-gECT c_b is assumed to be fixed and is defined as the quotient of the maximum electrical power (P_{el}^{max}) and the maximum thermal heat output (P_{th}^{max}), which equals the quotient of the electricity efficiency and thermal efficiency, with both efficiencies assumed to be constant:

$$c_b = \frac{P_{el}^{max}}{P_{th}^{max}} = \frac{eff_{el}^{max}}{eff_{th}^{max}} \quad (2.14)$$

In a pure linear system, without a minimum thermal or electrical output, the generation of both commodities therefore lies on the lower line from the zero point to the point of the maximum thermal and electrical generation, shown in fig.2.13. In the current stage PERSEUS-gECT is run as a pure linear model, thus the definition of a minimum capacity and of further start-up or shutdown constraints, which is theoretically possible, is currently ignored during the construction phase of the model.

¹⁰ In all cases without a co-firing, such as biomass with coal, a process is defined for a single fuel input, such as hard coal or methane.

¹¹ For the sake of simplicity, the process classification refers to the reference output, which is electricity in case of fixed CHP processes, with the consequence that the process variable is still referenced as $x_{pp,tp,ts}^{ehg2el}$ although heat is also co-produced.

The modeling of steam extraction turbines, which may dynamically adjust the share of the heat and electricity output fractions, is based on the coupling of two processes. First, an electricity generation process converts the input commodities with a maximum electrical efficiency. Subsequently, the electricity output is considered as input for a heat generation process, with a conversion rate of c_v , which defines the power loss factor to the extent that an additional heat generation reduces the net electricity output P_{el}^{net} at a constant fuel demand:

$$c_v = \frac{P_{el}^{net} - P_{el}^{max}}{P_{th}^{max}} = \frac{P_{el}^{net} - x_{pp,tp,ts}^{ehg2el}}{x_{pp,tp,ts}^{ehg2th}} \quad (2.15)$$

The power loss factor c_v restricts the possible combination of heat and power outputs. In case electricity is plotted on the x-axis and heat on the y-axis as done in the previous figure 3.13, the turbine operation at pure back pressure mode defines a lower bound:

$$P_{el}^{net} \geq P_{th}^{max} c_b = x_{pp,tp,ts}^{ehg2th} c_b \quad (2.16)$$

Finally, both bounds (2.15 & 2.16) might be combined into a single constraint, which restricts the operation of the two electricity and heat generating processes in addition to the nodal balance equation:

$$x_{pp,tp,ts}^{ehg2el} \geq x_{pp,tp,ts}^{ehg2th} (c_v + c_b) \quad (2.17)$$

The modeling of EHG processes with multiple possible commodity inflows from multiple nodes should be discussed next. Consider a large-scale conventional power plant site with multiple gas turbines for burning natural gas which is located at the coast and has the possibility of a gas supply from a pipeline with a node allocated a few kilometers away or of a direct access via an LNG-ship on the site. One possibility to model such a conversion is to duplicate the process and to connect the first process directly to the gas grid (ignoring the short distance stup pipe flow from the power plant location to the grid node) and to connected second process to an on-side gas grid node. To this on-side gas grid node also the regasification unit, which converts LNG into NG, is connected. Alternatively, the stup pipe flow might be modeled and the GTs are all connected to the same internal node without duplication. With an increasing number of gas turbines clearly the second modeling approach should be preferred considering that in this case only one additional flow needs to be modeled. As illustrated in the following figure 2.14, the number of options increases dramatically in case hydrogen is considered as an investment option. Examples might be an investment into multiple H2-ready CHP processes, which might be suited for burning hydrogen as well as natural gas, or the retrofit of the existing turbines such that they can only burn hydrogen.

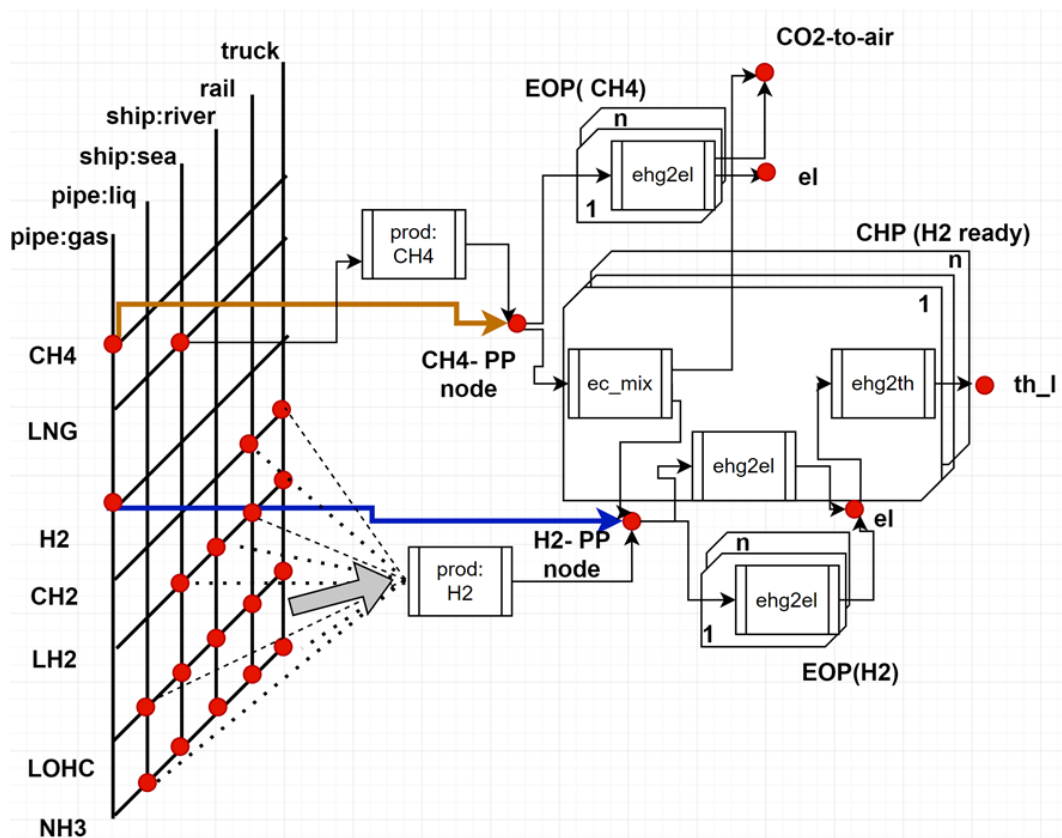


Figure 2.14: Modelling a multi-modal, multi commodity fuel supply for EHG processes

In addition to the option to choose between a gas grid supply of hydrogen or the ship delivery of liquified hydrogen (LH2), PERSEUS-gECT might include the possibility of multiple other transport options of hydrogen or its derivatives to the plant. In the example in total 17 alternatives for the ship, rail, truck and pipeline supply of hydrogen in different states (H2, CH2, LH2) or of its derivatives (NH3, LOHC) are illustrated. Obviously, it makes sense to define an internal H2 node for the plant side to which all conversion processes (LH2 regasification, NH3 cracking, etc.) from the multiple transport systems are connected instead of duplicating all possible (EHG) processes-to-input combinations. For EHG processes capable of transitioning between various fuels, like a hydrogen-ready CHP initially operating on methane, a fuel mixing process called "ec_mix" is employed. This process enables modeling a single process or process chain without the necessity of duplication based on the input fuel variations. The goal of the mixing process is to create an output fuel out of one or more input fuels with a defined energy content and emission factor. In the current example the CHP process chain is actually defined as a hydrogen consuming conversion. Consequently, the mixing process converts methane to a hydrogen equivalent, by adjusting the energy content and balancing the CO2 content with the CO2-air node.

Finally, the modeling of retrofit investment options should be discussed next, which is a replacement of existing natural gas fired GTs by hydrogen fired GTs with an adjusted lifetime and efficiency in the current example, but may also include a lifetime increasing retrofit of a nuclear power plant or the conversion of a coal fired steam turbine to the combustion of reactive metals,

such as iron. In all cases it must be assured that the activity level of an existing process is decreased according to the capacity of the new retrofitted process, which replaces the old one. Assuming a unique process to unit assignment for this kind of process, the capacity restriction of the old process has to be adjusted (2.18) in addition to the definition of a capacity restriction of the new process (2.19). This is implemented by subtracting the unit capacity of the retrofitted unit from the capacity of the old unit, adjusted by a factor which takes possible efficiency changes into account:

$$x_{pp,tp,ts}^{ehg2x_old} \leq y_{pu,tp}^{fix_old} - \sum_{tp' \leq tp} \beta_{pu,tp'}^{retrofit_exp} y_{pu,tp'} \quad \forall tp \in TP, \forall ts \in TS, \forall pp \in PROC_{pu}, \forall pu^{retrofit} \in UNIT_{pp} \quad (2.18)$$

$$x_{pp,tp,ts}^{ehg2x_new} \leq \sum_{tp' \leq tp} y_{pu,tp'}^{exp} \quad \forall tp \in TP, \forall ts \in TS, \forall pp \in PROC_{pu}, \forall pu^{retrofit} \in UNIT_{pp} \quad (2.19)$$

It should be noted that the modeling of EHG processes allows to split the inflow or outflow of a commodity on multiple nodes with a pre-defined share. Such an approach might be interpreted as a coupling with a synchronized dispatch of multiple processes which convert commodities between these nodes. Currently, such an approach is only considered in the modeling of final demand processes and therefore will be described later in a more detailed way.

The modeling of EHG processes with a storage function, such as hydro storages and CSP processes with a heat storage, is described within the chapter which focuses on storage processes.

Constraints for modeling OCP processes and units

In PERSEUS-gECT most OCP processes are logically allocated in the transformation sector and mainly convert secondary energy carriers (e.g., electricity and heat) into other secondary energy carriers (e.g., liquid or gaseous fuels and heat) or their intermediate products. With a focus on the conversion of hydrogen from electricity, biomass or methane and the production of further derivatives such as NH₃, LOHC, MeOH, Fe, SFO and SNG, modeling the coupling between OCP and the preceding EHG and subsequent TRANS processes is the main challenge. For the process parametrization, the convention sets the nodal balance output coefficient ($\alpha_{pp,n,ec,tp,ts,ts}^{out}$) of the main output commodity to 1 and defines the coefficient for further output commodities and for the inputs ($\alpha_{pp,n,ec,tp,ts}^{out}$) relative to the main output. Although OCP conversions might include a time lag, currently a production within the same time slice is the default case for most options. Considering that OCP processes usually link nodes of different transmission systems, such as the gas and electricity system, which in reality might be in the same neighborhood but not at the same spot, their spatial allocation imposes some challenge. To some extent OCP processes thus lead to a certain spatial flow of commodities. As illustrated in the following example of the Fischer-Tropsch based production of synthetic fuel oil, the modeling of such a process ranges from a standalone application depending of the available transport infrastructure for the input and output commodities, to the cascaded optimization of multiple OCP processes for an onsite conversion of intermediate products. In the latter case, the optimized usage of the

thermal heat by-product from the FT processes for the production of CO₂ or H₂ leads to multiple process chain layouts, depending on the opportunity to the grid supply.

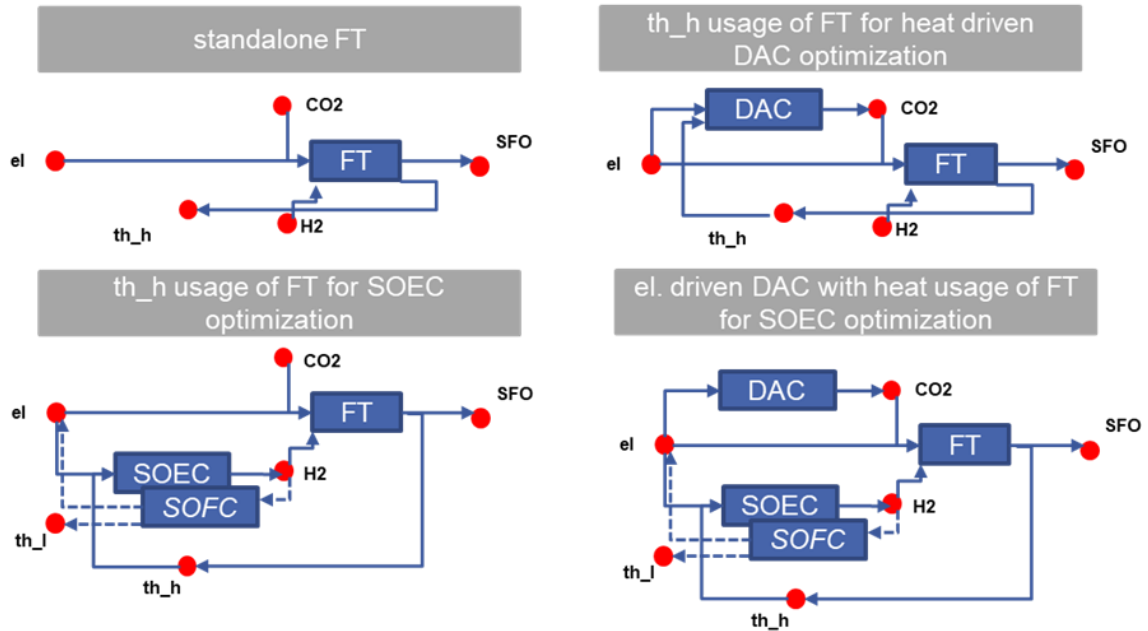


Figure 2.15: Possible coupling of processes for producing synthetic fuel oil based on a hydrogen driven Fischer Tropsch process

In general, each OCP process variable is simply restricted by a corresponding unit variable, considering that in most cases the investment into new technologies is modeled and that the efficient handling of existing processes or of replacement decisions is not relevant.

$$\forall tp \in TP, \forall ts \in TS, \forall pp \in PROC_{pu}, \forall pu \in UNIT_{pp} \quad x_{pp,tp,ts}^{prod:ec} \leq \sum_{tp' \leq tp} y_{pu,tp'}^{exp} \quad (2.20)$$

Constraints for modeling STOR processes and units

The concept of storages in PERSEUS-gECT is used to model a wide range of temporal conversion activities with the goal of balancing energy and material flows between time steps. Besides the modeling of classical stationary storage applications, such as battery, cavern or tank storages, this includes the modeling of flexibilities of the demand or supply side, such as load shifting from a controlled charging of electric vehicles or primary extraction flexibilities. Also, the modeling of period resolved balancing constraints, which limit for example the yearly CO₂ emission budget, is modeled based on storage processes. In general, the modeling of the operation and expansion of a storage might involve multiple processes and unit variables and defines a conversion of

multiple commodities from multiple to nodes to multiple other commodities¹² at multiple other nodes a later point of time. In this context the main purpose of a storage is to balance the net-position of nodal inflows and outflows of a commodity between different time steps. The basis of each storage modeling is the nodal balance of a process which represents the storages volume $x_{pp,tp,ts}^{storvol}$. In time step $ts \in TS$, for which this process is defined, the storage volume is a demand process which consumes commodity $ec \in EC$ from a storage node $n \in N^{STOR}$, with $\alpha_{pp,n,ec,tp,ts}^{in} = 1$. Vice versa, storage volume processes from preceding time steps $x_{pp,tp,ts'}^{storvol}$, with $ts' = \begin{cases} ts - tl & \text{if } ts - ts' \geq 1 \\ |TS| + ts - tl & \text{else} \end{cases}$ act as generators which inject a specific commodity ec , adjusted by the storage volume efficiency¹³ $\alpha_{pp,n,ec,tp,ts',ts}^{stor_eff}$ into the storage node. Considering that all other processes $x_{pp,tp,ts}^{non_storvol}$ besides of $x_{pp,tp,ts}^{storvol}$ convert energy and material only within a time step, the already defined general nodal balance equation for storage nodes might be specified as follows:

$$\begin{aligned} & \sum_{ts' \in TS} \sum_{pp \in PROC_{n,ec}} x_{pp,tp,ts'}^{storvol} \alpha_{pp,n,ec,tp,ts',ts}^{stor_eff} + \sum_{pp \in PROC_{n,ce}} x_{pp,tp,ts}^{non_storvol} \alpha_{pp,n,ec,tp,ts,ts}^{out} \\ & = \sum_{pp \in PROC_{n,ec}} x_{pp,tp,ts}^{storvol} + \sum_{pp \in PROC_{n,c}} x_{pp,tp,ts}^{non_storvol} \alpha_{pp,n,ec,tp,ts}^{in} + b_{n,ec,tp,ts}^{dem} \end{aligned} \quad (2.21)$$

$\forall n \in N^{STOR}, \forall ec \in EC, \forall tp \in TP, \forall ts \in TS$

For commodities which require negligible energy for loading or unloading, such as in case of the tank-based storage of commodities which are liquid at atmosphere pressure and space temperature (Oil, MeOH) or stockpile-based storage of solids commodities at the same conditions (Fe), the differentiation between storage and transmission nodes might be neglected. In this case the remaining inflows and outflows into the storage node include all other EHG, OCP, FD or TRANS processes. Differentiation of storage and transport nodes and specific charging and discharging processes for linking these nodes and inflow processes is required, in order to model storages with a charging or discharging efficiency below one. The following figure illustrates only storage related processes, and describes the parametrization of the nodal balance coefficients, with the convention defining $\alpha_{pp,n,ec,tp,ts,ts}^{out} = 1$ and $\alpha_{pp,n,ec,tp,ts,ts}^{in} = 1/eff$:

¹² If natural gas (NG) is stored in a pressurized tank through an electricity driven compressor, the input commodities are electricity and NG at pipeline pressure and the output is compressed NG (CNG).

¹³ The self-discharge of battery storages or the insulation losses of a TES are typical examples of processes with a loss of the storage volume over the temporal horizon. For these technologies a storage volume efficiency $\alpha_{pp,n,ec,tp,ts',ts}^{stor_eff}$ below one is defined.

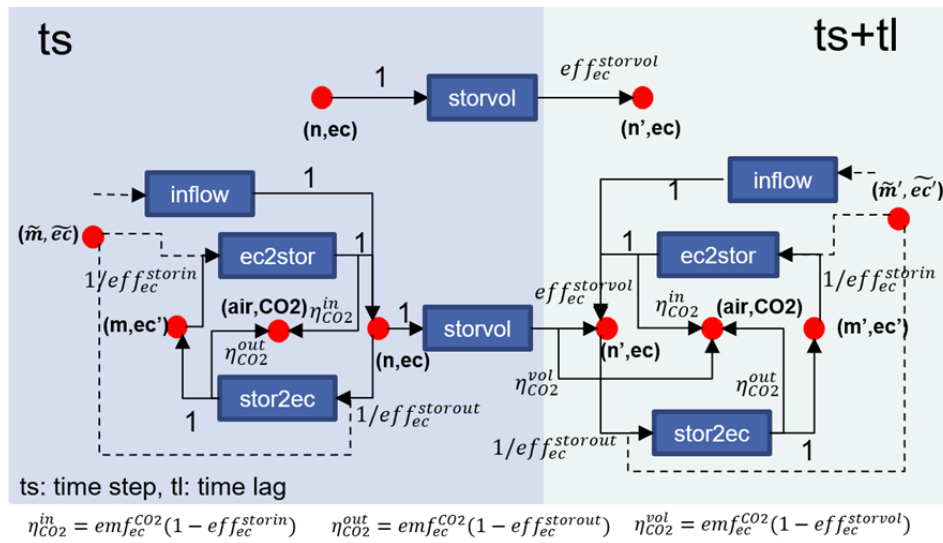


Figure 2.16: General model of a storage

In general, multiple strict positive charging $x_{pp,tp,ts}^{ec2stor}$ and discharging $x_{pp,tp,ts}^{stor2ec}$ and inflow $x_{pp,tp,ts}^{inflow}$ processes might be connected to the same storage node, with the convention to balance the first two mentioned on the input and output side while inflow processes might not be necessarily balanced on their input side. In this context, inflow processes are often used to model primary energy availability and are therefore restricted by a lower and upper bound profile.

Concerning the efficiency of charging and discharging processes, basically three different cases, depending on the energy source for the storage operation, need to be differentiated: (i) storages running exclusively based on the stored commodity, (ii) storages which operate independently of the stored commodity, (iii) storages which use partially the stored commodity as well as external energy sources for operation. In PERSEUS-gECT many storages use an external electricity or heat source in combination with the stored energy carrier if possible (iii) and the input-coefficients of $x_{pp,tp,ts}^{ec2stor}$ and $x_{pp,tp,ts}^{stor2ec}$ are adjusted accordingly. Besides of electricity and heat storages, which are a special case of scenario (i), isolated stationary storages (e.g., offshore gas cavern) or mobile storages (e.g., LNG shipping) are further examples for the first category while CO₂ storages are obviously purely driven by external energy carriers (ii). In case the charging or discharging processes are driven by carbon-based energy carriers, the CO₂ emission into the air needs to be balanced¹⁴. Based on the notation $\alpha_{pp,n,ec,tp,ts',ts}^{storout} = 1/\eta_{pp,n,ec,tp}^{stor_out}$ following specification of the storage nodal balance equation is possible:

¹⁴ The special case of a gas-boiloff from LH₂ or LNG will be described at a later point.

$$\begin{aligned}
 & \sum_{ts' \in TS} \sum_{pp \in PROC_{n,ec}} x_{pp,tp,ts'}^{storvol} \alpha_{pp,n,ec,tp,ts',ts}^{stor_eff} + \sum_{pp \in PROC_{n,ce}} x_{pp,tp,ts}^{inflow} \\
 & + \sum_{pp \in PROC_{n,ce}} x_{pp,tp,ts}^{ec2stor} + \sum_{pp \in PROC_{n,ce}} x_{pp,tp,ts}^{non_stor} \alpha_{pp,n,ec,tp,ts,ts}^{out} \\
 & = \sum_{pp \in PROC_{n,ec}} x_{pp,tp,ts}^{storvol} + \sum_{pp \in PROC_{n,ce}} x_{pp,tp,ts}^{stor2ec} \alpha_{pp,n,ec,tp,ts',ts}^{storout} \\
 & \quad \sum_{pp \in PROC_{n,c}} x_{pp,tp,ts}^{non_stor} \alpha_{pp,n,ec,tp,ts}^{in} + b_{n,ec,tp,ts}^{dem} \\
 & \quad \forall n \in N^{STOR}, \forall ec \in EC, \forall tp \in TP, \forall ts \in TS
 \end{aligned} \tag{2.22}$$

As usual, all storage processes $x_{pp,tp,ts}^{stor} = \{x_{pp,tp,ts}^{storvol}, x_{pp,tp,ts}^{inflow}, x_{pp,tp,ts}^{ec2stor}, x_{pp,tp,ts}^{stor2ec}\}$ with an exogenously fixed capacity are bound from above and below $lb_{pp,tp,ts}^{stor} \leq x_{pp,tp,ts}^{stor} \leq ub_{pp,tp,ts}^{stor}$. For simple volume constrained storages, without efficiency losses for loading or unloading, an endogenous capacity expansion in most cases might need be to defined based on modeling an expansion volume unit per processes, with a unique process to unit relation:

$$\begin{aligned}
 & x_{pp,tp,ts'}^{storvol} \leq \sum_{tp' \leq tp} y_{pu,tp'}^{exp} \\
 & \forall tp \in TP, \forall ts \in TS, \forall pp \in PROC_{pu}, \forall pu \in UNIT_{pp}
 \end{aligned} \tag{2.23}$$

In PERSEUS-gECT this simplified approach is used for modeling the storage of LOHC, oil, MeOH, NH₃, Fe and low temperature heat (th_l). While a definition of loading/unloading processes might be omitted, the restriction of the loading/unloading capacity needs to be assured through additional constraints. Without loss of generality, in the following the case of a storages process with a time lag of 1 and a unit expansion in the current period is described. Assuming that $c_rate_{pu,tp} = y^{vol_cap} / y^{stor2ec_cap}$ defines the ratio of the storage volume and the unloading capacity, while $io_rate_{pu,tp} = y^{ec2stor_cap} / y^{stor2ec_cap}$ defines the ratio of loading to unloading capacity, the investment into a technology with fixed ratio of volume to loading to unloading capacity might be expressed as follows:

$$\begin{aligned}
 & x_{pp,tp,ts}^{ec2stor} = x_{pp,tp,ts-1}^{storvol} \alpha_{pp,n,ec,tp,ts-1,ts}^{stor_eff} - x_{pp,tp,ts-1}^{storvol} \leq y_{pu,tp}^{exp} / c_rate_{pu,tp} \\
 & \quad \forall tp \in TP, \forall ts \in TS, \forall pp \in PROC_{pu}, \forall pu \in UNIT_{pp}
 \end{aligned} \tag{2.24}$$

$$\begin{aligned}
 & x_{pp,tp,ts}^{stor2ec} = -x_{pp,tp,ts-1}^{storvol} \alpha_{pp,n,ec,tp,ts-1,ts}^{stor_eff} + x_{pp,tp,ts-1}^{storvol} \leq y_{pu,tp}^{exp} io_rate_{pu,tp} / c_rate_{pu,tp} \\
 & \quad \forall tp \in TP, \forall ts \in TS, \forall pp \in PROC_{pu}, \forall pu \in UNIT_{pp}
 \end{aligned} \tag{2.25}$$

For storages which are characterized by their storage volume, the charging and discharging in consequence might be either directly bound by the storage volume capacity unit $y_{pu,tp}^{exp}$ which restricts restricting the corresponding storage volume process or indirectly by restricting the change in the storage volume variable. Further technologies, with a unit definition based on the storage volume, but with separate loading and unloading processes are tank, field or cavern-based storages for CO₂, H₂ or CH₄. The need for modelling separate loading and unloading processes results from efficiency losses or the consumption of auxiliary energy carriers for the loading/unloading. In this case the unit variable is directly linked to the loading or unloading process, which for instance might be a compressor that is running either on the energy carrier which should be compressed or based on an electricity consumption from the grid, such that $x_{pp,tp,ts}^{ec2stor}$ in this case additionally requires a balance with an electricity node. For EHG related processes, such as battery storages or hydro storages, the storage characterization based on the generation

capacity is more common. In case of an investment into a technology with fixed input to output capacity to volume ratio, the unit variable is therefore related to the generation capacity. Consequently, following relation between a process and a unit might be defined, considering only unit expansions within the current period:

$$x_{pp,tp,ts}^{storvol} \leq y_{pu,tp}^{exp} c_{rate_{pu,tp}}, \quad x_{pp,tp,ts}^{ec2stor} \leq y_{pu,tp}^{exp}, \quad x_{pp,tp,ts}^{stor2ec} \leq y_{pu,tp}^{exp} io_{rate_{pu,tp}} \quad (2.26)$$

$$\forall tp \in TP, \forall ts \in TS, \forall pp \in PROC_{pu}, \forall pu \in UNIT_{pp}$$

While storages of the LNG infrastructure and potential LH2 replacement or expansion options are described in more detail in a later point, it should be noted that the modeling of retrofit measure, for example the conversion of a gas-cavern storage from natural gas to hydrogen, follows the same logic as defined in the previous chapter of EHG.

The modeling of solar-based storages, either in combination of CSP with a high temperature TES or of rooftop photovoltaic with a battery system (PVBAT), is a special case of combined STOR and EHG processes. In both cases the storage is modeled as an integrated part of the EHG process chain and the primary energy inflow is adjusted accordingly. As illustrated in the following figure, the thermal heat generation from a solar irradiation is modeled as an upper bound for an inflow process into a TES. A conversion unit is connected to this storage, which either allows a direct utilization of the heat for an onsite off-grid application or the injection into a direct heating network or the generation of electricity. On the other hand, PV-Battery systems are modeled in a way that the storage is exclusively used for buffering the potential PV generation. Therefore, the potential electricity generation from a PV unit is split on the one hand to a process for directly charging the storage and on the other hand to a process for grid injection. The process to capacity restriction is adjusted accordingly.

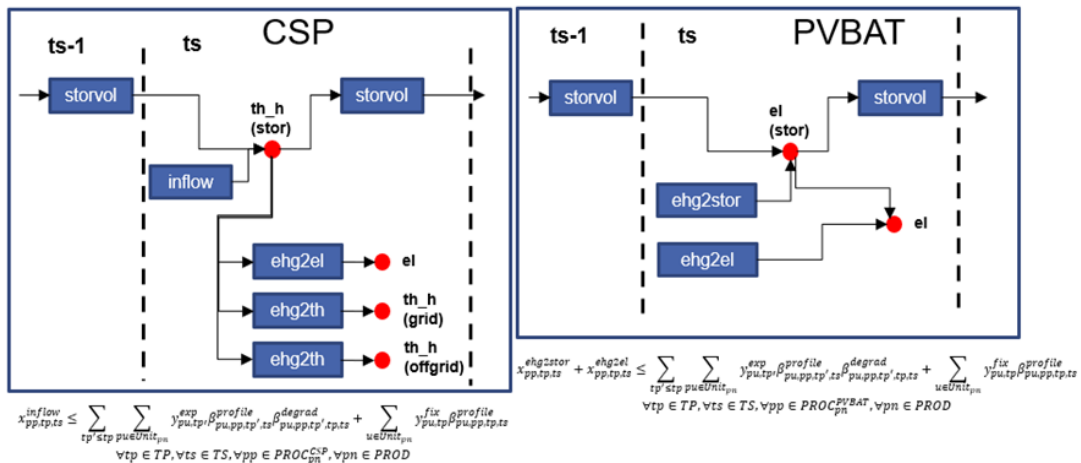


Figure 2.17: Modelling of integrated primary energy conversion and storage processes

The modeling of DSM processes largely follows the approach described in (Ruppert et al. 2019) and requires only a $x_{pp,tp,ts}^{storvol}$ and $x_{pp,tp,ts}^{ec2stor}$ process. By adjusting the lower and upper bounds for

the storage volume level and gradient, the load shifting potential, in terms of shifted volume or minimal/maximal load increase or reduction within a time step might be modeled. In this case $x_{pp,tp,ts}^{ec2stor}$ is used to model the inflow from a transport grid to a storage node and is therefore defined independent of the time dependent gradient of $x_{pp,tp,ts}^{storvol}$. This means that a load profile, for example the EV uncontrolled charging demand, is not directly defined as a rhs parameter $b_{n,ec,tp,ts}^{dem}$ of an electricity grid node $n \in N^{el_grid}$ but shifted to a storage node, which is connected to the electricity grid through a positive variable $x_{pp,tp,ts}^{ec2stor}$:

$$\begin{aligned} \sum_{pp \in PROC_{n,ec}} x_{pp,tp,ts-1}^{storvol} \alpha_{pp,n,ec,tp,ts-1,ts}^{stor_eff} + \sum_{pp \in PROC_{n,ce}} x_{pp,tp,ts}^{ec2stor} \\ = \sum_{pp \in PROC_{n,ec}} x_{pp,tp,ts}^{storvol} + b_{n,ec,tp,ts}^{dem} \end{aligned} \quad (2.27)$$

$$\forall n \in N^{STOR}, \forall ec \in EC, \forall tp \in TP, \forall ts \in TS$$

In the current example, the bounds on $x_{pp,tp,ts}^{storvol}$ are consequently adjusted with respect to the minimal and maximal state of charge (SOC) for the EV demand. Moreover, the maximal load increase and reduction within a time step might be defined based on the already introduced constraint restricting the storage volume gradient:

$$\begin{aligned} x_{pp,tp,ts-1}^{storvol} \alpha_{pp,n,ec,tp,ts-1,ts}^{stor_eff} - x_{pp,tp,ts-1}^{storvol} \leq MaxLoadReduction_{pp,tp,ts} \\ -x_{pp,tp,ts-1}^{storvol} \alpha_{pp,n,ec,tp,ts-1,ts}^{stor_eff} + x_{pp,tp,ts-1}^{storvol} \leq MaxLoadIncrease_{pp,tp,ts} \end{aligned} \quad (2.28)$$

$$\forall tp \in TP, \forall ts \in TS, \forall pp \in PROC_{pu}$$

Finally, the function of the national atmospheric CO2 storage will be described. As already mentioned, all combustion processes of the EHG, OCP, TRANS, STOR or FD sector $x_{pp,tp,ts}^{CO2_comb}$ which emit CO2 with a specific factor depending on the utilized fuel $\alpha_{pp,n,ec,tp,ts}^{CO2_emf}$ and the carbon capture rate $\alpha_{pp,n,ec,tp,ts}^{CO2_ccr}$ are injecting their CO2 to a virtual national atmospheric CO2 balancing node. On the other hand, processes which consume CO2 from the air, such as DAC or primary biomass conversion (AD) processes, are connected to the same national node. In case a balancing of national CO2 emissions is neglected, the storage volume variable $x_{pp,tp,ts}^{storvol}$ is used for balancing emissions between different time steps. Depending on the CO2 budget, which might be defined as an upper bound on the storage variable in the last time step of a period, national emission targets might be established. In order to establish a CO2 trading, each national balancing node is connected to a global slack node n0 through a directed flow variable $x_{pp,tp,ts}^{CO2_trade}$, such that CO2 might be injected and withdrawn from the slack node.

$$\begin{aligned} \sum_{pp \in PROC_{n,CO2}} x_{pp,tp,ts-1}^{storvol} + \sum_{n' \in N_n^{geo}} \sum_{ec \in EC} \sum_{pp \in PROC_n} x_{pp,tp,ts}^{CO2_comb} \alpha_{pp,n,ec,tp,ts}^{CO2_emf} (1 - \alpha_{pp,n,ec,tp,ts}^{CO2_ccr}) \\ + \sum_{pp \in PROC_{n,n0,CO2}} x_{pp,tp,ts}^{CO2_trade} \\ = \sum_{pp \in PROC_{n,ec}} x_{pp,tp,ts}^{storvol} + \sum_{n' \in N_n^{geo}} \sum_{pp \in PROC_n} x_{pp,tp,ts}^{DAC} + \sum_{pp \in PROC_{n0,n,CO2}} x_{pp,tp,ts}^{CO2_trade} \end{aligned} \quad (2.29)$$

$$\sum_{n' \in N_n^{geo}} \sum_{ec \in EC} \sum_{pp \in PROC_n} x_{pp,tp,ts}^{CO2_comb} \alpha_{pp,n,ec,tp,ts}^{CO2_emf} + b_{n,ec,tp,ts}^{dem}$$

$$\forall n \in N^{country}, \forall tp \in TP, \forall ts \in TS$$

In general, PERSEUS-gECT allows to define national emission targets as well as CO2 prices, which are attached to the flow variables which connect the slack node and the national nodes. In case

of a pure CO₂ pricing without national budgets, an additional CO₂ storage at the slack node is defined and the national CO₂ balancing storage volume variables are deleted.

Constraints for modeling TRANS processes and units

In general transmission processes and units include conversion activities with the primary goal of connecting two different nodes of the same commodity. In most cases the conversion process is defined as a positive variable, resulting in a directed flow between two nodes. Depending on the nodal balance input coefficient ($\alpha_{pp,n,ec,tp,ts}^{in}$) the process $x_{pp,tp,ts}^{dir_flow}$ demands commodity $ec \in EC$ in time step ts and node $n \in N$ and generates the same commodity, reduced by potential transmission losses, at node $m \in N$ in time step $ts' \geq ts$, depending on the nodal balance process output coefficient ($\alpha_{pp,m,ec,tp,ts'}^{out}$). For simple directed flows within the same transmission system, α^{in} is therefore defined as 1 and α^{out} is set to the efficiency of the transmission system for a flow of commodity ec over the edge (n,m) . In general, transmission processes might be parametrized in a way that the energy for the transport of an energy carrier between two nodes might be provided by another energy carrier. The shipping of liquified hydrogen through a diesel fueled vessel, for example, might be modeled as a process which consumes diesel and hydrogen in one node and produces liquified hydrogen in another. In the current stage, however, PERSEUS-gECT only considers transport options of energy carriers which are driven by the respective energy carrier for simplicity reasons. Therefore, the losses of a directed flow process include the energy demand of the commodity transmission and potential further losses, such as boil of losses, as long as they cannot be utilized within the processes. In case of a transmission of a carbon-based energy carrier, the CO₂ emission into the air is thus balanced by a flow to the national CO₂ atmosphere node and depends on the emission factor of the energy carrier and the efficiency of the transmission system. As indicated in the following figure, PERSEUS-gECT furthermore allows an analog modeling of intermodal flows, with a loading/unloading process which converts commodities between different transmission systems, such as truck-to-rail, including the possibility to consider loading/unloading times and fees. The simplified approach of modeling the spatial and intermodal transmission of a commodity based a directed flow with potential losses and a time lag is chosen for almost all commodities and transmission systems. Only the for the DC-approach based modeling of the AC power flow with quadratic loss approximation a less simplified model of the physical flow constraints is chosen. In the latter case the transmission process consists of an undirected flow variable ($\alpha^{in} = \alpha^{out} = 1$), which might take positive and negative values as well as a positive loss variable into account, which equally distributes the corresponding flow losses to the start and end node of an edge.

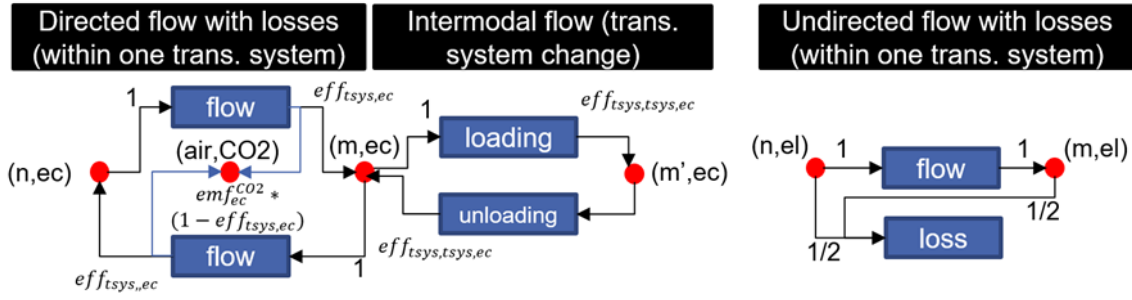


Figure 2.18: Approach for modelling spatial flows

Before the approach for the modeling of the electricity grid based on undirected flows will be described in more detail, first the modeling of the directed flows should be described. In general, the modeling of the ship, road, rail, pipeline or DC-cable transport of a commodity is rather trivial, as the flow processes and units are basically determined by the edges of the transport-infrastructure. Considering a unique definition of a flow processes $PROC_{n,m,ec}$ and units $Unit_{n,m,ec}$ based on the edges $(n, m, ec) \in (\Omega^{pipe}, \Omega^{road}, \Omega^{ship}, \Omega^{rail}, \Omega^{cable})$ of the modeled system and commodity, in most cases it is sufficient to include the capacity restriction of the processes in addition to the nodal balance equation in order to describe the transport system. This is either an upper bound for existing processes or a simple variable bound:

$$\sum_{pp \in PROC_{n,m,ec}} x_{pp,tp,ts}^{flow} \leq \sum_{tp' \leq tp} \sum_{pu \in Unit_{n,m,ec}} y_{pu,tp'}^{\exp} \quad (2.30)$$

$$\forall tp \in TP, \forall ts \in TS, \forall (n, m, ec) \in \Omega^{pipe}, \Omega^{road}, \Omega^{ship}, \Omega^{rail}, \Omega^{cable}$$

In this context it should be noted that PERSEUS-gECT allows a definition of multiple ($k=1:K$) flows for the same commodity over the edges of the same transport system. Depending on the specification of the transmission link set Ω , alternative notations of such an edge (n,m) , commodity (ec) , transmission option (k) tuple are chosen in the following. With $(n, m, k, ec) \in \Omega^{pipe:gas} \subseteq \Omega^{pipe}$ for example, k different transmission options between the nodes n and m for the pipeline transport of gases ($ec = \{H_2, CH_4, CO_2\}$) are specified, while $(n, m, k) \in \Omega^{pipe:H_2}$ restricts the set of connections to hydrogen pipelines. In case only one transmission option per edge of a specified system is considered, k might be neglected and following short notation might be chosen: $(n, m) \in \Omega^{tsys:EC}$. The transport of MeOH over the edges of the rail system: $(n, m) \in \Omega^{rail:MeOH}$ is an example for such a notation, as only one MeOH flow option is considered for one rail edge. While such a simple transport modeling approach is straight forward for the rail, road or ship transport of liquid or solid energy carriers, it should be noted that it implies a strong simplification for the modeling of gas flows. In the current state, the pipeline-based gas-flow is simply modeled as a capacity constrained transportation problem, considering the existing and planned natural gas pipeline infrastructure and the possibility to blend the natural gas flow with hydrogen in addition to the option of retrofitting natural gas pipelines to hydrogen or to build parallel hydrogen pipelines. Additionally, the option to build a CO₂ grid in parallel to the existing natural gas grid pipelines is considered. Thus, the challenge of adjusting the gas compression in a way that the grid injections and demands might be balanced, and considering a pressure drop within a pipe, is ignored and instead a constant loss factor per km of a directed pipeline flow is

assumed as an approximation. In PERSEUS-gECT $k = \{1,2,3\}$ alternatives for the linking of two nodes (n,m) of the same gas transmission system for a commodity $ec = \{CH_4, H_2, CO_2\}$, representing existing (1), replacement (2) and additional (3) edge option are considered. If $PROC_{n,m,k,ec}$ and $Unit_{n,m,k,ec}$ define the corresponding set of processes and units, following capacity restrictions might be differentiated:

$$\begin{aligned} & \sum_{pp \in PROC_{n,m,1,CH_4}} x_{pp,tp,ts}^{flow} + \sum_{pp \in PROC_{n,m,1,H_2}} \alpha_{pp,1,tp,ts}^{cap} x_{pp,tp,ts}^{flow} \\ & \leq \sum_{pu \in Unit_{n,m,1,CH_4}} y_{pu,tp}^{fix} - \sum_{pu \in Unit_{n,m,2,H_2}} \beta_{pu,2,tp,ts}^{cap} y_{pu,tp}^{lev} \end{aligned} \quad (2.31)$$

$\forall tp \in TP, \forall ts \in TS, \forall (n, m, k, ec) \in \Omega^{pipe:gas}, ec = \{CH_4, H_2\}$

$$\sum_{pp \in PROC_{n,m,k,ec}} x_{pp,tp,ts}^{flow} \leq \sum_{pu \in Unit_{n,m,k,ec}} y_{pu,tp}^{fix} \quad (2.32)$$

$\forall tp \in TP, \forall ts \in TS, \forall (n, m, k, ec) \in \Omega^{pipe:gas}, ec = \{CH_4, H_2\}, k = 1$

$$\sum_{pp \in PROC_{n,m,k}} x_{pp,tp,ts}^{flow} \leq \sum_{pu \in Unit_{n,m,k}} y_{pu,tp}^{lev} \quad (2.33)$$

$\forall tp \in TP, \forall ts \in TS, \forall (n, m, k) \in \Omega^{pipe:H_2}, k = 2$

$$\sum_{pp \in PROC_{n,m,k,ec}} x_{pp,tp,ts}^{flow} \leq \sum_{tp' \leq tp} \sum_{pu \in Unit_{n,m,k,ec}} y_{pu,tp'}^{exp} \quad (2.34)$$

$\forall tp \in TP, \forall ts \in TS, \forall (n, m, k, ec) \in \Omega^{pipe:gas}, ec = \{CO_2, H_2\}, k = 3$

Taking into account the different commodity properties, such as the energy density or flow rate based on $\alpha_{pp,1,tp,ts}^{cap}$, $\beta_{pu,2,tp,ts}^{cap}$, the first constraint assures that the flow of methane in an existing pipe plus the flow of blended hydrogen is smaller than the pipe capacity minus the capacity level of the replacement option, which converts the pipeline into a hydrogen only pipe. The following constraints individually restrict the different commodity flows over existing (2.21), replaced (2.21), and additional (2.21), pipelines. As the number of unit variables should be kept small, it must be noted that $y_{pu,tp}^{fix}$ is actually a parameter and $y_{pu,tp}^{lev} = y_{pu,tp-1}^{lev} + y_{pu,tp}^{exp} - y_{pu,tp}^{dis}$ is only defined for replacement options, while all the additional pipeline investment options for hydrogen and CO2 are modeled only based on an expansion variable $y_{pu,tp}^{exp}$.

In addition to the pipeline flow of gaseous commodities, the transport related conversion and reconversion processes of these commodities will be described next. Regasification and liquification, compression and decompression processes as well as the H2 unloading of secondary energy carriers such as LOHC and NH3 are actually a combination of OCP and storage processes. The main reason to invest into these technologies, however, is to convert and reconvert commodities, such that a potentially favorable transmission system might be used. As illustrated in the following figure, almost all processes for the conversion and reconversion of fuels for the transport are modeled as electricity grid connected applications, which allows to use electricity for the operation instead of the transported fuel. Additionally, the recovery of hydrogen from LOHC and NH3 is modeled as a mainly thermal driven process, which allows a combination with processes which either create high temperature heat as a main output (boiler) or as a byproduct (Fischer-Tropsch). The modeling of gas-driven compressors is an exception in this context, as the processes run only based on the fuel which should be converted.

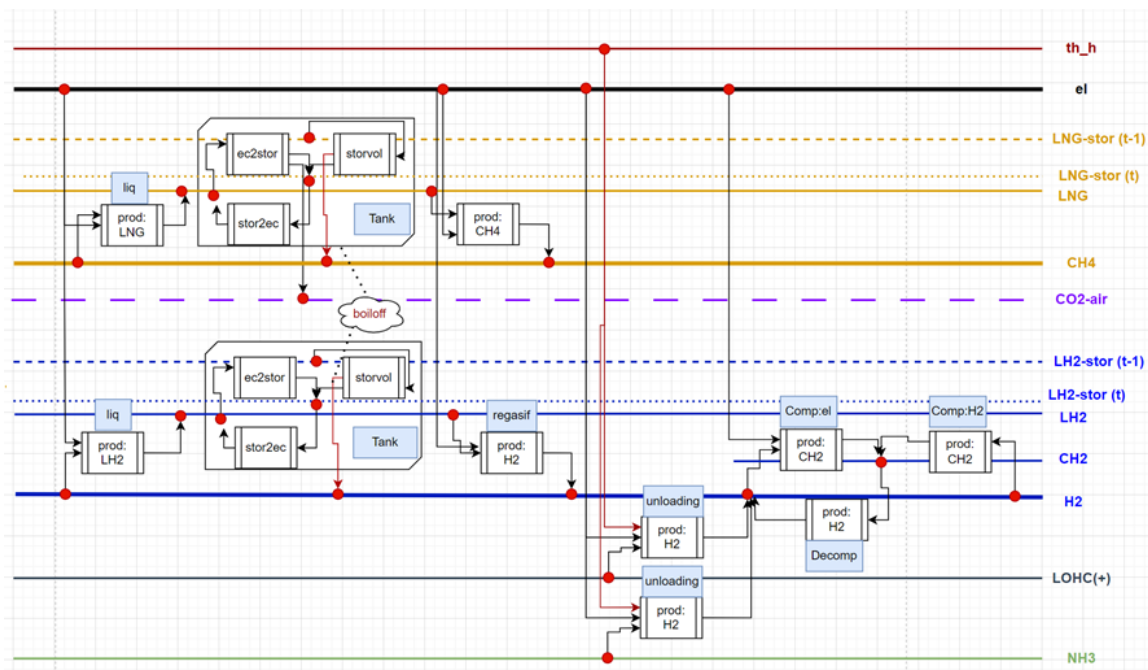


Figure 2.19: Modelling of transport related energy carrier conversion and reconversion processes

It should be noted that storages are an essential part of the transport infrastructure as loading and unloading time and varying capacities of the coupled systems need to be buffered. Figure 2.19 therefore illustrates the interaction of liquification, storage and regasification processes for the LNG and LH2 port-infrastructure. The capacity dimensioning between these units might be fixed or endogenously adjusted and contrary to the gas-pipeline infrastructure, a blending of methane and hydrogen, or of their liquified products, is not possible. Therefore, the retrofit of the existing LNG-infrastructure to LH2 is modeled as a pure replacement option and in case a parallel operation of both infrastructures is needed, the model may decide to build parallel LH2 liquification, storage and regasification units next to the existing LNG based.

The modeling of electrical transmission grid constraints in PERSEUS-gECT is based on a simple transport model of the DC grid and the linearized relaxation of the high and extra-high voltage AC-power flow, based on the DC-OPF approach. In the first case, a simple directed flow is used to model the transmission between nodes of the electricity system. Depending on the considered degree of freedom for an endogenous adjustment of the AC/DC and DC/AC converter capacity and the DC-transmission system, this may include one or multiple processes. In case of a two-terminal DC system (DCTT), a point-to-point transmission with equally dimensioned converter and transmission capacity is assumed. Therefore, only one process variable per direction, which already includes all losses for the AC/DC conversion, the DC-DC transmission and DC/AC reconversion and one unit variable, which restricts these processes, is needed. In multi-terminal DC systems (DCMT), a variable capacity adjustment of the conversion and transmission capacity is considered. The investment expenses for the converter and the transmission capacity are thus assigned to two individual units. Similarly, conversion and transmission processes and their losses, are split in separate variables. As illustrated in the following figure, the modeling of DCTT

systems reduces the number of constraints and variables, while a flexible design of a meshed DC-overlay grid is possible for DCMT systems:

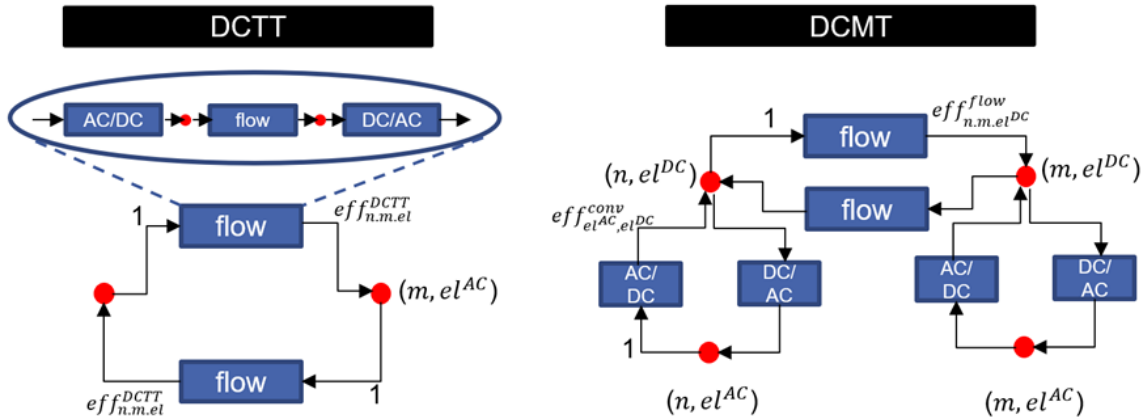


Figure 2.20: Coupling of processes for modelling HVDC flows in DCTT (left) and DCMT (right) systems

In PERSEUS-gECT all power generators and loads are connected to nodes of the AC-system. Thus, an adequate modeling of the transmission constraints is of great importance. In literature, many different formulations for a linearized modeling of Kirchhoff's current law (KCL) and voltage law (KVL), which define the physical load flow in a network, may be found (Hörsch et al. 2018; Neumann and Brown 2020). In general, the approaches might be differentiated with respect to the relaxation of the KVL constraint and the applied formulation, for relating active power generation or load to flow and/or phase angle variables. Often PTDF-based, angle-based or cycle-based formulations and their combination (e.g. angle-flow) are used. In PERSEUS-gECT an angle-flow based approach is chosen and KCL, which requires an energy conservation such that power inflows into a node equal the power outflows in each time step, is simply modeled as a part of the usual nodal balance equation:

$$\begin{aligned}
 & \sum_{pp \in PROC_{(m,n,k) \in \Omega^{AC}}} x_{pp,tp,ts}^{flow} + \sum_{ts' \in TP} \sum_{pp \in PROC_{n,ec}} x_{pp,tp,ts'} \alpha_{pp,n,ec,tp,ts',ts}^{out} \\
 = & \sum_{pp \in PROC_{(m,n) \in \Omega^{AC}}} x_{pp,tp,ts}^{loss} + \sum_{pp \in PROC_{n,ec}} x_{pp,tp,ts} \alpha_{pp,n,ec,tp,ts}^{in} + b_{n,ec,tp,ts}^{dem} \\
 & \forall n \in N, \forall tp \in TP, \forall ts \in TS, ec = el^{AC}
 \end{aligned} \tag{2.35}$$

In this context the set of processes $PROC_{m,n,k}$ is specified for the k possible branches of an edge (m,n) which connects the busses (nodes) of the transmission network for $el^{AC} \subseteq el \in EC$, while $(m,n,k) \in \Omega^{AC}$ defines the set of branches and $(m,n) \in \Omega^{AC}$ defines the set of edges. Per convention, a positive flow variable $x_{pp,tp,ts}^{flow}$ refers to a power inflow flow from node m to node n and vice versa to an outflow for negative values. The positive loss variable $x_{pp,tp,ts}^{loss}$ is used as an approximation for the quadratic flow losses, summed over the k branches linking the nodes m and n and should be defined at a later point.

For KVL, also known as Kirchhoff's second law, which defines that the sum of voltages around any cycle in the network is zero (Hörsch et al. 2018), multiple approximations of the actual nonlinear

power flow equations are possible. A common angle-flow based formulation of the DC-approach (Schweppe 2000), reduces KVL to a simple coupling of the phase-angle difference ($\theta_{n,c,tp,ts} - \theta_{m,c,tp,ts}$) of an edge to the branch flows $x_{pp,tp,ts}^{flow}$ over this edge. In this context the flow $x_{pp,tp,ts}^{flow}$ over each branch ($pp \in PROC_{(m,n,k) \in \Omega^{AC}}$) is weighted with the corresponding branch reactance $\alpha_{pp,el^{AC},tp,ts}^{reactance}$ (reciprocal of the branch susceptance) and in case of static branches KVL is assured based on following equation:

$$\sum_{pp \in PROC_{n,m,k}} x_{pp,tp,ts}^{flow} \alpha_{pp,ec,tp,ts}^{reactance} = \theta_{n,ec,tp,ts} - \theta_{m,ec,tp,ts} \quad (2.36)$$

$$\forall tp \in TP, \forall ts \in TS, \forall (n, m, k) \in \Omega^{AC}, ec = el^{AC}$$

The previous equation might seem uncommon due to the process-based indexing of the flow variable and reactance parameter instead of a bus-based notation. Basically, this is just a special case of constraint (3.8) and a generalization of the standard DC-based KVL notation:

$$x_{n,m,k,tp,ts}^{flow} \alpha_{n,m,k,tp,ts}^{reactance} = \theta_{n,tp,ts} - \theta_{m,tp,ts} = \Delta\theta_{n,m,tp,ts} \quad (2.37)$$

$$\forall tp \in TP, \forall ts \in TS, \forall (n, m, k) \in \Omega^{AC}$$

The quadratic loss approximation for static branches follows the approach of Dos Santos and Diniz (2010), to linearize the loss approximation, defined as the conductance weighted squared phase-angle difference: $x_{n,m,k,tp,ts}^{loss} = \alpha_{n,m,k,tp,ts}^{conductance} (\Delta\theta_{n,m,tp,ts})^2$, with a pricewise linear function at $\tilde{k} \in \tilde{K}$ points. In the common node-based notation, with $g_{n,m,k} = \alpha_{n,m,k,tp,ts}^{conductance}$, this results in adding \tilde{k} constraints for each branch $(n, m, k) \in \Omega^{AC}$ of the AC-transmission grid:

$$x_{n,m,k,tp,ts}^{loss} \geq -g_{n,m,k} (\Delta\theta_{n,m,tp,ts}^{\tilde{k}})^2 + 2g_{n,m,k} * \Delta\theta_{n,m,tp,ts}^{\tilde{k}} * |\Delta\theta_{n,m,tp,ts}| \quad (2.38)$$

$$\forall tp \in TP, \forall ts \in TS, \forall (n, m, k) \in \Omega^{AC}, \forall \tilde{k} \in \tilde{K}$$

Assuming that the same points ($\Delta\theta_{n,m,tp,ts}^{\tilde{k}} \geq 0$) for approximation are chosen on parallel branches and these points might be reformulated based on eq (2.27) such that $\Delta\theta_{n,m,tp,ts}^{\tilde{k}} = \Delta\theta_{n,m,k,tp,ts}^{\tilde{k}} = x_{n,m,k,tp,ts}^{flow,\tilde{k}} \alpha_{n,m,k,tp,ts}^{reactance}$ hold true, the number of loss variables might be reduced to one per edge and reformulated to the process-based notation following constraints for defining the static line loss in PERSEUS-gECT are added:

$$\sum_{pp \in PROC_{(n,m) \in \Omega^{AC}}} x_{pp,tp,ts}^{loss} \geq \sum_{pp \in PROC_{n,m,k}} (\alpha_{pp,tp,ts}^{\tilde{k},I} |x_{pp,tp,ts}^{flow}| + \alpha_{pp,tp,ts}^{\tilde{k},II}) \quad (2.39)$$

$$\alpha_{pp,tp,ts}^{\tilde{k},I} = 2x_{pp,tp,ts}^{flow,\tilde{k}} (\alpha_{pp,tp,ts}^{reactance})^2 \alpha_{pp,tp,ts}^{conductance}$$

$$\alpha_{pp,tp,ts}^{\tilde{k},II} = -(x_{pp,tp,ts}^{flow,\tilde{k}} \alpha_{pp,tp,ts}^{reactance})^2 \alpha_{pp,tp,ts}^{conductance}$$

$$\forall tp \in TP, \forall ts \in TS, \forall (n, m, k) \in \Omega^{AC}, \forall \tilde{k} \in \tilde{K}$$

In order to assert an operation within the thermal branch limits, a simple lower and upper bound might be defined for flows over static branches with $-Th_lim_{pp,tp,ts} \leq x_{pp,tp,ts}^{flow} \leq Th_lim_{pp,tp,ts}$. For variable branches, a straight forward approach is to specify the general

variable capacity constraint in a way that the free flow variable $x_{pp,tp,ts}^{flow}$ is limited by the binary branch unit $y_{pu,tp}^{lev}$ ¹⁵ from below and above:

$$|\sum_{pp \in PROC_{n,m,k}} x_{pp,tp,ts}^{flow} - \sum_{pu \in Unit_{n,m,k}} y_{pu,tp}^{lev} Th_{lim_{pu,tp,ts}}| \leq \sum_{pu \in Unit_{n,m,k}} y_{pu,tp}^{lev} Th_{lim_{pu,tp,ts}} \quad \forall tp \in TP, \forall ts \in TS, \forall (n, m, k) \in \Omega^{AC} \quad (2.40)$$

The drawback of such an approach is that the extension of the previously defined KVL and loss approximation restrictions for variable branches usually requires a BigM-based approach, in order to avoid an invalid restriction of $\Delta\theta_{n,m,tp,ts}$ in case a branch is not chosen. In standard notation form this approach might be expressed as follows:

$$|x_{n,m,k,tp,ts}^{flow} \alpha_{n,m,k,tp,ts}^{reactance} - \Delta\theta_{n,m,tp,ts}| \leq y_{n,m,k,tp,ts}^{lev} BigM_{n,m,tp,ts}^{KVL} \quad \forall tp \in TP, \forall ts \in TS, \forall (n, m, k) \in \Omega^{AC} \quad (2.41)$$

$$| -x_{n,m,k,tp,ts}^{loss} - g_{n,m,k} (\Delta\theta_{n,m,tp,ts}^{\tilde{k}})^2 + 2g_{n,m,k} * \Delta\theta_{n,m,tp,ts}^{\tilde{k}} * \Delta\theta_{n,m,tp,ts} | \leq y_{n,m,k,tp,ts}^{lev} BigM_{n,m,tp,ts}^{Loss} \quad \forall tp \in TP, \forall ts \in TS, \forall (n, m, k) \in \Omega^{AC}, \forall \tilde{k} \in \tilde{K} \quad (2.42)$$

Due to the challenge to select BigM parameters which should be large enough on the one hand such that the solution space is not restricted, but small enough on the other hand, in order for the problem to be numerically stable, in PERSEUS-gECT an alternative approach is applied. Assuming that at least one branch should be chosen for the set of active edges within a period (no edge might be deleted), $1 \leq k' \leq K$ alternative expansion stages for each edge are defined such that in each stage the parameters of the active branches are aggregated to define an equivalent model of the considered parallel branches within a single flow variable. Basically, a standard aggregation of parallel branches is performed and the equivalent line includes at least one branch in the first stage and all possible branches in the last stage. In the following, $(n, m, k') \in \Omega^{AC}$ denotes the set of equivalent branch expansion stages and $\alpha', Th_{lim}', \dots$ the adjusted parameters. In consequence a SOS1 type constraint has to be included, to ensure that for each edge (n,m) only one binary branch unit $y_{pu,tp}^{lev}$ with $pu \in Unit_{(m,n,k') \in \Omega^{AC}}$ has the value of 1 in each time period:

$$\sum_{pu \in Unit_{n,m,k'}} y_{pu,tp}^{lev} = 1 \quad \forall tp \in TP, \forall (n, m) \in \Omega^{AC} \quad (2.43)$$

Or expressed in the more common nodal notation:

$$\sum_{k \in (n,m,k') \in \Omega^{AC}} y_{n,m,k',tp}^{lev} = 1 \quad \forall tp \in TP, \forall (n, m) \in \Omega^{AC} \quad (2.44)$$

¹⁵ $y_{pu,tp}^{lev} = y_{pu,tp-1}^{lev} + y_{pu,tp}^{exp} - y_{pu,tp}^{dis}$

Assuming that each edge of the AC transmission grid might be extended, in the following the previously defined equations are slightly adjusted. For the variable branch limit the adjustment is quite trivial as only the parameters and sets are slightly changed:

$$|\sum_{pp \in PROC_{n,m,k'}} x_{pp,tp,ts}^{flow}| \leq \sum_{pu \in Unit_{n,m,k'}} y_{pu,tp}^{lev} Th_lim'_{pu,tp,ts} \quad \forall tp \in TP, \forall ts \in TS, \forall (n, m, k') \in \Omega^{AC} \quad (2.45)$$

Considering that the previous constraint in combination with the SOS1-type constraint defines that only one process flow variable per edge has non zero values, the adjustment of the KVL includes just a simple summation of all process options of an edge (own notation and common notation):

$$\sum_{pp \in PROC_{n,m,k'}} x_{pp,tp,ts}^{flow} \alpha'_{pp,ec,tp,ts}{}^{reactance} = \theta_{n,ec,tp,ts} - \theta_{m,ec,tp,ts} \quad \forall tp \in TP, \forall ts \in TS, \forall (n, m) \in \Omega^{AC}, ec = el^{AC} \quad (2.46)$$

$$\sum_{k \in (n,m,k') \in \Omega^{AC}} x_{n,m,k',tp,ts}^{flow} \alpha'_{n,m,k',tp,ts}{}^{reactance} = \theta_{n,tp,ts} - \theta_{m,tp,ts} = \Delta\theta_{n,m,tp,ts} \quad \forall tp \in TP, \forall ts \in TS, \forall (n, m) \in \Omega^{AC} \quad (2.47)$$

For the adjustment of the loss approximation a simple multiplication of the rhs parameter with the binary unit variable is needed.

$$\begin{aligned} \sum_{pp \in PROC_{(n,m) \in \Omega^{AC}}} x_{pp,tp,ts}^{loss} &\geq \sum_{pp \in PROC_{n,m,k'}} (\alpha_{pp,tp,ts}^{\tilde{k},I} |x_{pp,tp,ts}^{flow}|) + \sum_{pu \in Unit_{(n,m,k') \in \Omega^{AC}}} \alpha_{pu,tp,ts}^{\tilde{k},II} y_{pu,tp}^{lev} \\ \alpha_{pp,tp,ts}^{\tilde{k},I} &= 2x_{pp,tp,ts}^{flow,\tilde{k}} (\alpha_{pp,tp,ts}^{reactance})^2 \alpha_{pp,tp,ts}^{conductance} \\ \sum_{pu \in Unit_{(n,m,k') \in \Omega^{AC}}} \alpha_{pu,tp,ts}^{\tilde{k},II} &= -\sum_{pp \in PROC_{n,m,k'}} (x_{pp,tp,ts}^{flow,\tilde{k}} \alpha_{pp,tp,ts}^{reactance})^2 \alpha_{pp,tp,ts}^{conductance} \\ &\forall tp \in TP, \forall ts \in TS, \forall (n, m, k) \in \Omega^{AC}, \forall \tilde{k} \in \tilde{K} \end{aligned} \quad (2.48)$$

$$x_{n,m,tp,ts}^{loss} \geq -g'_{n,m,k'} (\Delta\theta'_{n,m,tp,ts}{}^{\tilde{k}})^2 y_{n,m,k',tp}^{lev} + 2g'_{n,m,k'} * \Delta\theta'_{n,m,tp,ts}{}^{\tilde{k}} * |\Delta\theta_{n,m,tp,ts}| \quad \forall tp \in TP, \forall ts \in TS, \forall (n, m, k') \in \Omega^{AC}, \forall \tilde{k} \in \tilde{K} \quad (2.49)$$

General constraints for modeling FD processes and units

With a focus on the energetic use of commodities, final demand processes which are not related to the generation of electricity and heat for applications such as space, water or process heating, including all non-energetic usage of commodities, are currently modeled as fixed rhs parameters. For the decarbonization of fixed final demand processes, currently only the option to replace a fossil fuel through an equivalent synthetic fuel is considered. Due to the heterogeneity of these fixed final demand processes, their coupling with carbon capture technologies or flexibilization through DSM is also neglected. Instead OCP and STOR processes in the proceeding transformation or transport sectors are used for the same goal. The investment into DAC or oil tanks is an example for such an indirect decarbonization and flexibilization of a fixed oil demand, besides the already mentioned replacement of fossil oil through low carbon synthetic oil. Contrary, EHG related final demand conversions are modeled as endogenous processes for the

coverage of a local heating or electricity usage demand of a specific sector and application and compete with the grid connected district heat or electricity supply from the EHG sector. Due to the convention in PERSEUS-gECT to define all processes for the modeling of EOP or of district heating connected CHP or HOP as a part of the EHG set, the set of FD processes mainly consists of residential, commercial or industrial boilers which are driven by electricity or combustible fuels. Furthermore, (small scale) heat pumps and fuel cells, which are not connected to the district heating grid, are part of the FD set. In the current step the development of district heating grids as well as the final demand usage of biomass is modeled in a preprocessing step and their heating demand is therefore fixed during the actual optimization run. On the final demand side, PERSEUS-gECT thus focuses on modeling the competition of fuel switching alternatives, such as the combustion of low carbon fuels instead of fossil fuels in boilers, with electrification alternatives, such as heat pumps or electrical boilers. As illustrated in the following figure, the final demand of each commodity is split in a fixed part, which is a rhs parameter in the balance of the corresponding transmission or demand node and a flexible part. The flexible part, which is either a high or low temperature heat demand or a specific electrical application, such as the EV charging, is connected to a virtual storage node, for modeling the demand side management (as described previously). The useful heat or electricity demand of the flexible part is therefore the rhs parameter of the virtual storage node, which drives the optimization.

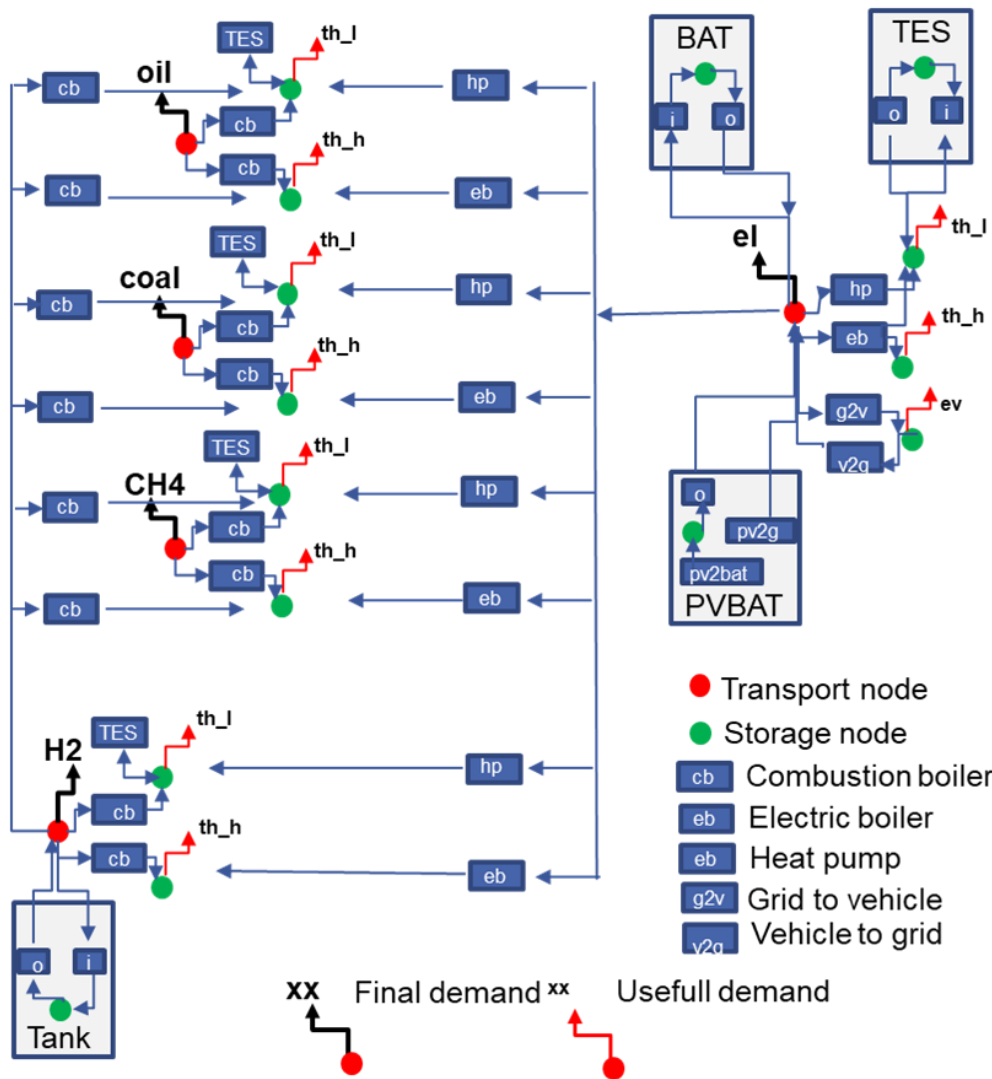


Figure 2.21: Modelling of final demand fuel flexibilities and switching processes

In the basic scenario, the final demand processes are largely existing combustion or electrical boilers, which connect the grid nodes with the fixed final demands to the virtual storage nodes, with the flexible useful demands. By investing into heat pumps, electrical boilers or hydrogen ready combustion boilers, new final demand processes might be created for replacing the initial coal, methane or oil-fired processes. In the extreme scenario, the non-fixed final demand for a specific commodity is completely substituted and the energy flow to a virtual storage, which was initially used for balancing the heat flexibility of an oil node for example, is completely covered by a heat pump process, which is connected to the electricity grid. In this context PERSEUS-gECT allows the modeling of multiple flexibilities, such as DSM, TES, battery storages, tank storages, PV-battery systems and grid-to-vehicle discharging, which might be used to increase the flexibility of final demand processes either on the input or the output side. From the mathematical point of view, FD processes are modeled analog to EHG or STOR processes, but with the

previously described characteristics for the definition of nodal balance input and output coefficients concerning the grid connection.

2.4 Data structure of PERSEUS-gECT

2.4.1 General approach for defining the nodal basis of energy conversion, distribution and demand based on the existing infrastructure as well as regional generation and demand potentials

In (Slednev et al. 2017b) an approach for regionalizing input data for generation and transmission expansion planning models (GEP and TNEP) was developed. The goal was to combine resource availability constraints of existing generation and transmission assets with greenfield potentials and to regionalize sectoral demand data, such that GEP and TNEP models with a variable grid topology might be parametrized with respect to spatial and temporal highly resolved demand and generation profiles. Later, this approach was extended in (Slednev et al. 2018) with a focus on the renewable expansion planning and the aim to define an adequate set of variables, considering varying generation profiles and potentials of competing technologies below the transmission grid level. Applied to the analysis of the European high and extra high voltage transmission grid planning, the approach was shown to be well suited for the parametrization of optimal power flow problems either in the AC or DC formulation (Ruppert et al. 2019; Slednev et al. 2021). While the consideration of sector coupled heat (heat-pump), transport (electric vehicle) and gas (electrolysers) demands and their flexibilities was already possible, the clear focus on the power sector and the generation side had the drawback of a limited suitability for an integrated modeling of the multi-modal transport of energy and material from the primary to the final conversion. Based on the own previous work in PERSEUS-gECT, a data driven approach for the definition and parametrization of nodes and connected or linked variables of a sector-coupled multi commodity GEP and TNEP model is developed. Besides of a spatial and sectoral extension of the data structure beyond the boundaries of the European power system, especially the former choice of the electricity grid topology as the main structuring element is adjusted. Instead of indexing all processes from the primary to the final conversion of energy and materials based on the nodes of a specific transport system for a specific commodity, and as previously done with the electricity bus based indexing approach, the general idea of PERSEUS-gECT is to define the regional basis based on an overlay of all possible transport systems. The goal of the developed approach is therefore to enable a highly resolved global assessment of energy resource potentials and (to a minor extent¹⁶) of the sectoral demands for specific applications on the one hand and on the other hand to define conversion variables which allow to

¹⁶ Due to the heterogeneity and regional varying availability of demand data, the approach is to model the sectoral demand of different regions with different degree of detail.

model possible conversion paths for balancing the energy demand and supply over multiple steps for the spatial, temporal and commodity-based transformation, with a good balance between problem size and accuracy.

In the first step, a highly resolved analysis of the exploited and remaining spatial potential (yearly power or energy) of energy generation and demand technologies and their intra-annual dispatch constraints (e.g., hourly profiles) is performed. In this context many approaches may be found in the literature, which is dominated by numerous publications focusing on the potential analysis of renewable energies, especially for the fluctuating wind and solar energy with a focus on wind onshore and PV. Concerning the modeling of regional demand processes, the focus in the literature lies on the regionalization of a (often national) sectoral demand for a specific energy carrier, while the bulk of bottom-up based approaches focus on specific consumers or applications and is not intended for modeling a whole sectoral demand for a country. Likewise, the approach of PERSEUS-gECT focuses on a bottom-up based modeling of renewable energies generation profiles and their potential, while demand profiles and quantities from a national or lower administrative area (NUTS 3) are mainly regionalized based on a specific key, while heating processes, which depend on the ambient temperature, are modeled bottom up. The default spatial resolution for the regional potential analysis in this context is 1ha (100m²) to which lower resolved potential areas, such as building shapes or the shapes of existing PV modules are aggregated. Alternatively, the exact locations (point with latitude, longitude) of a unit (e.g., for wind turbines) is considered. Before describing the different regional modeling approaches of the different generation and demand technologies in more detail in the next chapters, the general approach for deriving regional potentials and profiles should be described in the following¹⁷.

¹⁷ Conventional EHG units, including hydro generators, are treated in a separate way and should be described at a later point.

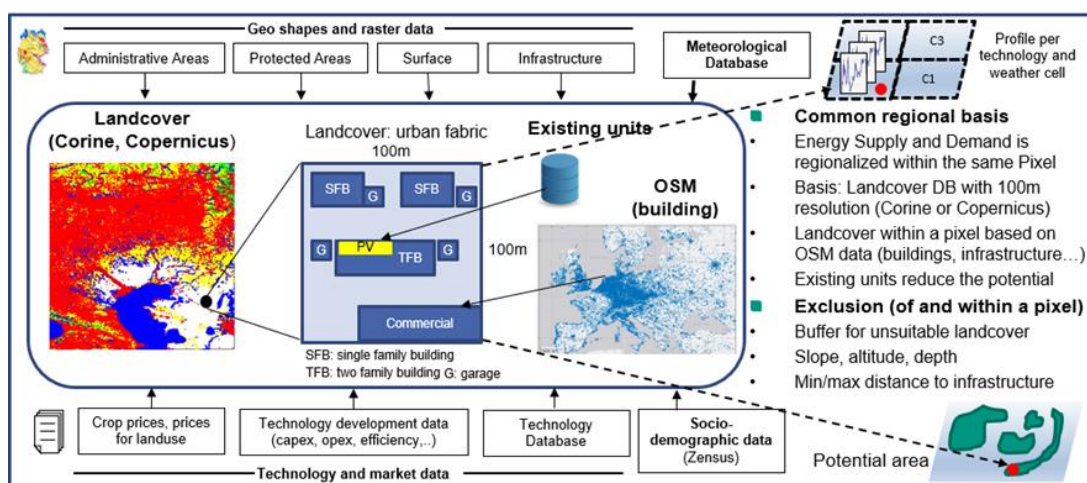


Figure 2.22: Approach for defining a common regional basis for an assessment of demand and generation potentials and profiles

As illustrated in the previous figure, a pixel with 100m resolution is chosen as a common regionalization basis for conversion technologies which either supply or demand energy. For a consistent global definition of the regional basis, currently the Copernicus landcover database (Marcel Buchhorn et al. 2020) is chosen. For Europe, a more detailed landcover classification of the single pixel based on the corine land cover (CLC) database (European Environment Agency 2019) is added. Within each pixel, mainly open street map data¹⁸ (OSM) are used for a further specification of the land use, especially for the identification and classification of buildings. The bottom up modeled spatial information, such as the number, type and area of buildings within a pixel is combined with top-down statistical socio-demographic data such as the number of households or building and their occupants, age, roof and space area etc. from an administrative region (e.g., NUTS3, NUTS2¹⁹, GAUL1, GAUL0²⁰). In combination with data on existing energy infrastructure assets such as PV modules (area, point) and wind turbines (point) from an own database and after the exclusion of unsuitable areas due technical or regulatory land use restrictions of a technology (slope, depth, distance to next building or grid), a common sectoral classification of energy demands and supply potentials exists. This means that within a pixel with 100m resolution, for example, the information about the PV potential on single family buildings with a garage is linked with the space heating demand of these buildings and the home charging demand of electric vehicles. If not further specified for the conversion technologies, the previously mentioned suitability concerning the land use is determined based on the copernicus or corine database with a 100m resolution, while topographical exclusion criteria are based on (Earth Resources Observation and Science Center, U.S. Geological Survey, U.S. Department of the Interior

¹⁸ OpenStreetMap contributors (2017).

¹⁹ Open Data Science Europe Metadata Catalog (2022).

²⁰ Global administrative boundaries - Data Europa EU (2023).

1997) gridded geographic information with a 30 seconds resolution for onshore GTOPO30²¹ or 1 minute resolution for offshore ETOPO1²² technologies. On a global scale, the exclusion of protected areas is based on the WPDA database²³ while NATURA2000 regions are additionally considered for Europe. If weather dependent variables such as minimal or maximal wind speed or solar irradiation are considered for the definition of exclusion areas, in general the average value from a certain range of historical reanalysed years (1990-2020 in most cases, 1985-2022 for special cases) based on the ERA 5²⁴ data set is used for the 30 km resolved weather cell. As most datasets for the definition of suitable or unsuitable areas are not natively resolved at a 1 ha level, the less resolved data sets are either interpolated or duplicated based on the underlying 100m resolved copernicus grid, which is the already mentioned basis of the regionalization framework.

In order to avoid a computational expansive modeling of supply and demand profiles for each technology within each pixel, one profile for each unit configuration within each cell of the regular gridded weather database, with 30 km spatial and 1 hour temporal resolution, is computed, assuming constant weather conditions within the cells. Considering the large amount of possible technical unit configurations, such as orientation (azimuth and aspect) of PV modules without tracking or the various hub-height to turbine combinations of wind energy conversion units, the first step of the potential analysis only includes unprocessed weather data such as temperature, wind speed and solar irradiation from a practical point of view. Afterwards, the computation of the final profiles is only performed if at least one pixel within a weather cell requires a specific demand or generation profile due to a potential or existing technical configuration.

Once the potential and profile of a conversion technology is known on a pixel basis, a pre-processing of the allocation planning and the choice of a preferred technology might be necessary. This is the case when the mutual competition for resources or the mutual exclusion of technologies limits the possibility to define a unit or process variable based on a simple aggregation of potentials and profiles of multiple pixels. The binary placement of wind turbines with respect to elliptic distance restrictions based on the main wind direction is such an example, considering that an endogenous modeling would require 100 special ordered sets of type 1 (SOS1) constraints in order to model the placement of one turbine technology within 1 km². The optimization of the district heating system is another example. After having defined which wind turbine should be ideally placed in which pixel or the district heating potential of each sector in the pixel, an adequate aggregation needs to be defined, to reduce the number of variables in the problem.

The general approach for the definition of variables for primary or final conversion technologies based on the aggregation of the 100m resolved potentials and profiles in PERSEUS-gECT follows the approach developed in (Slednev et al. 2018). In order to aggregate variables with similar

²¹ Earth Resources Observation and Science Center, U.S. Geological Survey, U.S. Department of the Interior (1997).

²² Amante, C. and B. W. Eakins (2009).

²³ UNEP-WCMC and International Union for Conservation of Nature (2021).

²⁴ Hersbach et al. (2020).

restrictions, first suitable areas and points for existing or potential investment technologies are overlaid with the weather cells of a meteorological database. These polygons are afterwards overlaid with the supply areas of transmission grid nodes, which are needed for balancing the conversion technology. The resulting polygons, which are characterized by equal input or output conditions (availability) for a technology, are subsequently overlaid in case of competing inputs or outputs between technologies. As illustrated in the following example, this means that electricity only primary and final conversions such as renewables or electrical vehicles are aggregated exclusively with regard to the supply area of the electricity transmission grid node, while hydrogen fueled FCEV (trucks or cars) are aggregated within the supply area of gas nodes. On the other hand, heat pumps or gas (CH₄ or H₂) fueled boilers for residential space heating are competing for the same output but have different input nodes. Therefore, an overlay of the gas and electricity supply areas is needed, resulting in an aggregation of pixels to variables for the generation of residential space heat with a unique allocation to gas, electricity and weather nodes.

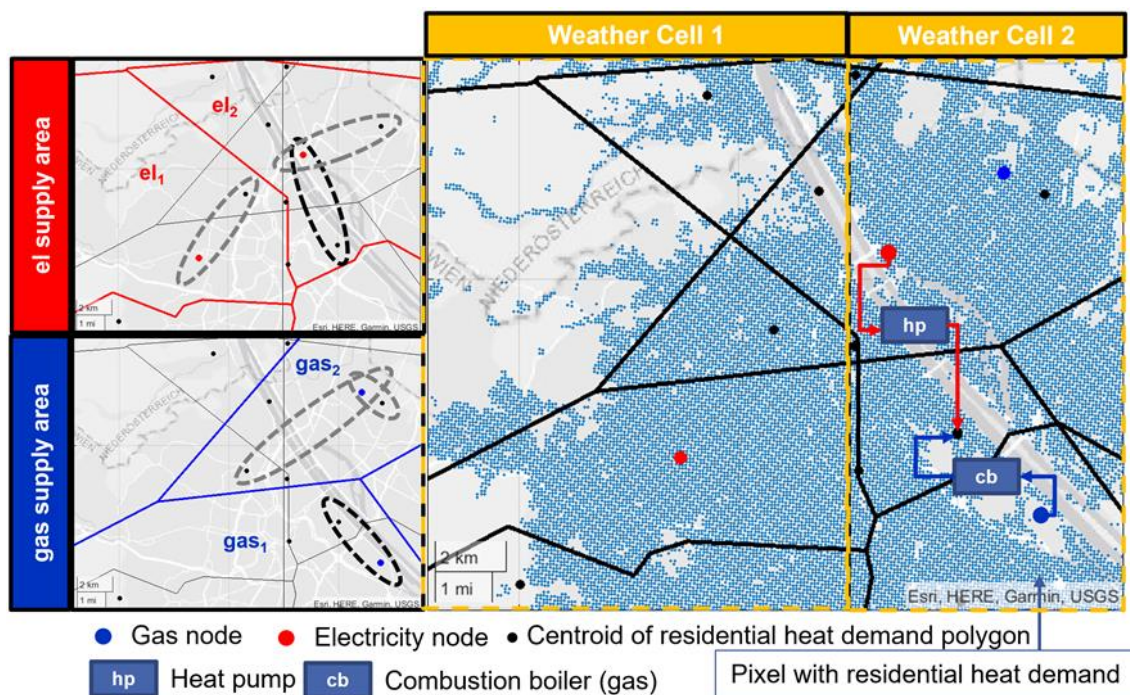


Figure 2.23: General approach of a variable definition based on an overlay of supply areas of different transport systems and weather cells

Depending on the considered conversion technologies and their local competition on the input or output side, this approach might lead to a significant increase of the problem size compared to more simplified approaches which focus only on one transport system (electricity) and are able to index the variables accordingly. The drawback of the flexibility to choose between alternative energy conversion paths is thus the definition of multiple balancing nodes in addition to the nodes of the transport or storage infrastructure and the definition of multiple variables of

the same technology class within the supply area of one node. For technologies with a weather dependent resource availability (wind and solar conversion), conversion efficiency (COP of heat pump) or useful energy demand (space heat for boilers and heat pumps), this means that at least one variable per unique technology configuration needs to be defined within each weather cell and supply area of a transport system, assuming the best case that they can be uniquely assigned to an existing node. The aggregation of wind-onshore turbines with the same conversion properties (same power curve, hub height) within the supply area of one electricity transmission grid node is such an example. In the worst case, however, an overlay of multiple competing transport systems necessitates the definition of multiple additional balancing nodes and variables, such as in the case of competing heating technologies which might be either driven by electricity or by solids (coal), liquids (oil), gaseous (CH₄, H₂) combustible fuels. Instead of defining multiple new nodes and variables for the modeling of such a case, an aggregation of nodes and variables might be performed in order to keep the problem size traceable. Each aggregation strategy however, comes at the cost of a reduced accuracy as information and flexibilities are lost.

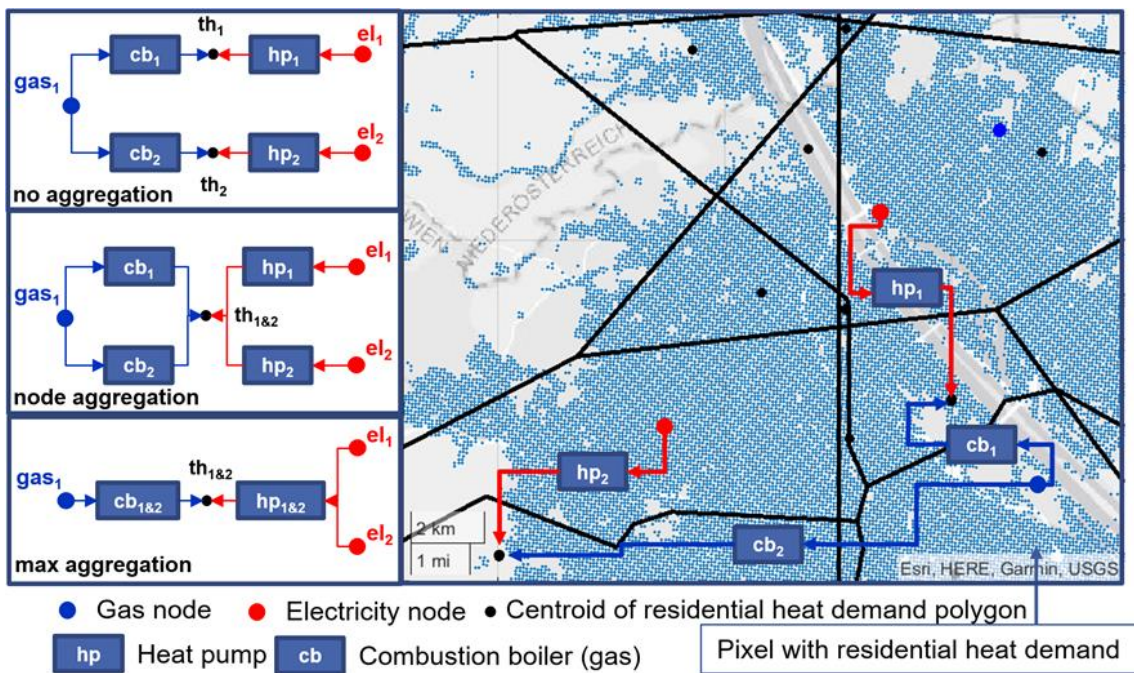


Figure 2.24: Comparison of different variable aggregation approaches for defining regional potentials and profiles

Depending on the considered technology and scenario, in PERSEUS-gECT different configurations of the same technology (e.g., multiple hub sizes of the same wind turbine), within different weather cells and or supply/areas (node aggregation) and different sectors (residential and commercial) might be aggregated.

So far, the focus was on the definition of primary and final energy conversion technologies (mainly FD and renewable EHG processes and units) which might be directly connected to the corresponding infrastructure. While this is always the case for FD processes, in PERSEUS-gECT, EHG processes in general as well as OCP, STOR and TRANS processes might be allocated in isolated areas, without the availability of the corresponding transport infrastructure. Usually, this applies to potentials of renewables such as wind onshore/ offshore or PV/CSP in remote areas. Before describing the general approach for the aggregation of isolated potentials, in a next step the definition of the nodal basis of offshore installations will be described, which is a special case concerning the structuring of isolated units. Considering the general lack of an existing transport infrastructure for the connection of offshore wind turbines in remote areas on the one hand and an existing or planned offshore gas and electricity infrastructure on the other hand, an approach is needed which allows a combined greenfield and brownfield expansion planning of EHG, OCP, STOR and TRANS units. In PERSEUS-gECT this is realized by a segmentation of existing and potential wind offshore turbines into disjunct sets of a certain size. Each set, which is either an existing or planned wind farm or may be interpreted as a potential wind farm, is uniquely assigned to an existing, planned or potential offshore converter, which bundles the generation prior to a further conversion and or transportation. The capacity of each set is either project dependent or limited to 2 GW in case of an offshore expansion. The general idea is to bundle the generation of neighboring wind-turbines, which are ideally laying within the same weather cell and a comparable water depth prior to a further processing.

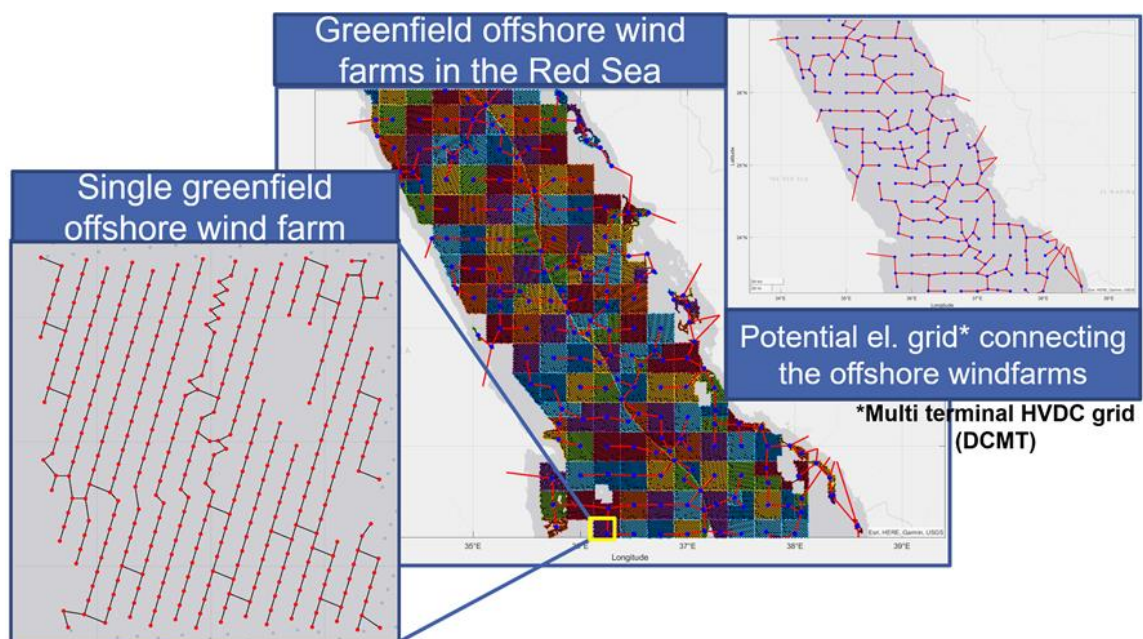


Figure 2.25: Approach for the definition of variables for modelling the generation and grid connection of offshore windfarms in remote areas

As floating PV units in PERSEUS-gECT are attached to single offshore wind turbines, the bundling approach for these turbines also defines the aggregation of offshore PV²⁵. Until now, an approach for the definition of offshore EHG variables based on the aggregation of wind and PV potentials was presented. The actual balancing of these variables, by defining an isolated or grid connected electricity node for the power injection, should be discussed next. The default approach is to consider a point-to-point electricity transmission to the next onshore landing point. Depending on the availability of alternative transport or conversion options, this might be either realized by explicitly modeling a DCTT transmission, involving the definition of an offshore converter node and of a corresponding directed flow or by a direct onshore balancing of the potential injection. In the latter case, which obviously reduces the problem size as well as the model flexibility, EHG process and units are parametrized such that transmission and conversion losses as well as operational and investment expenses for the DCTT transmission are implicitly considered. Besides the trivial case of existing or planned DCTT connections, there are multiple cases which may require more advanced approaches for structuring the offshore conversion than a simple aggregation at the next onshore substation. In the following figure this is illustrated for the North Sea region and southern Patagonia²⁶. In the southern corner of South America, the modeling of an onshore electricity and gas system is neglected in PERSEUS-gECT. The connection of offshore converters to the next onshore landing point, which is usually a port, therefore requires the definition of additional nodes and processes. Primarily, an isolated electricity node at the landing point needs to be defined, such that the electricity generation might be balanced. In the next step, further process chains and nodes for the production of energy carriers which might be efficiently shipped, such as liquified hydrogen, reactive metals or synthetic fuels, need to be defined due to the lack of modeled final demand at the landing point. One alternative to an implicitly modeled point-to-point connection to the next landing point lies in the multi-terminal-based interconnection of multiple offshore generation parks by HVDC cables. This allows to collect the generation from multiple generation sites and to link possible points for a further processing of the electricity, such as the port landing points in the current example. In this case an explicit modeling of the DCTT systems, which competes with the DCMT solution, is needed and the offshore generation is connected to an offshore converter node.

²⁵ A detailed description of floating PV is provided in the designed chapter 3.3.2

²⁶ For reasons of clarity, the implicit or explicit point-to-point connection of offshore generator to the onshore landing point is not visualized in both cases.

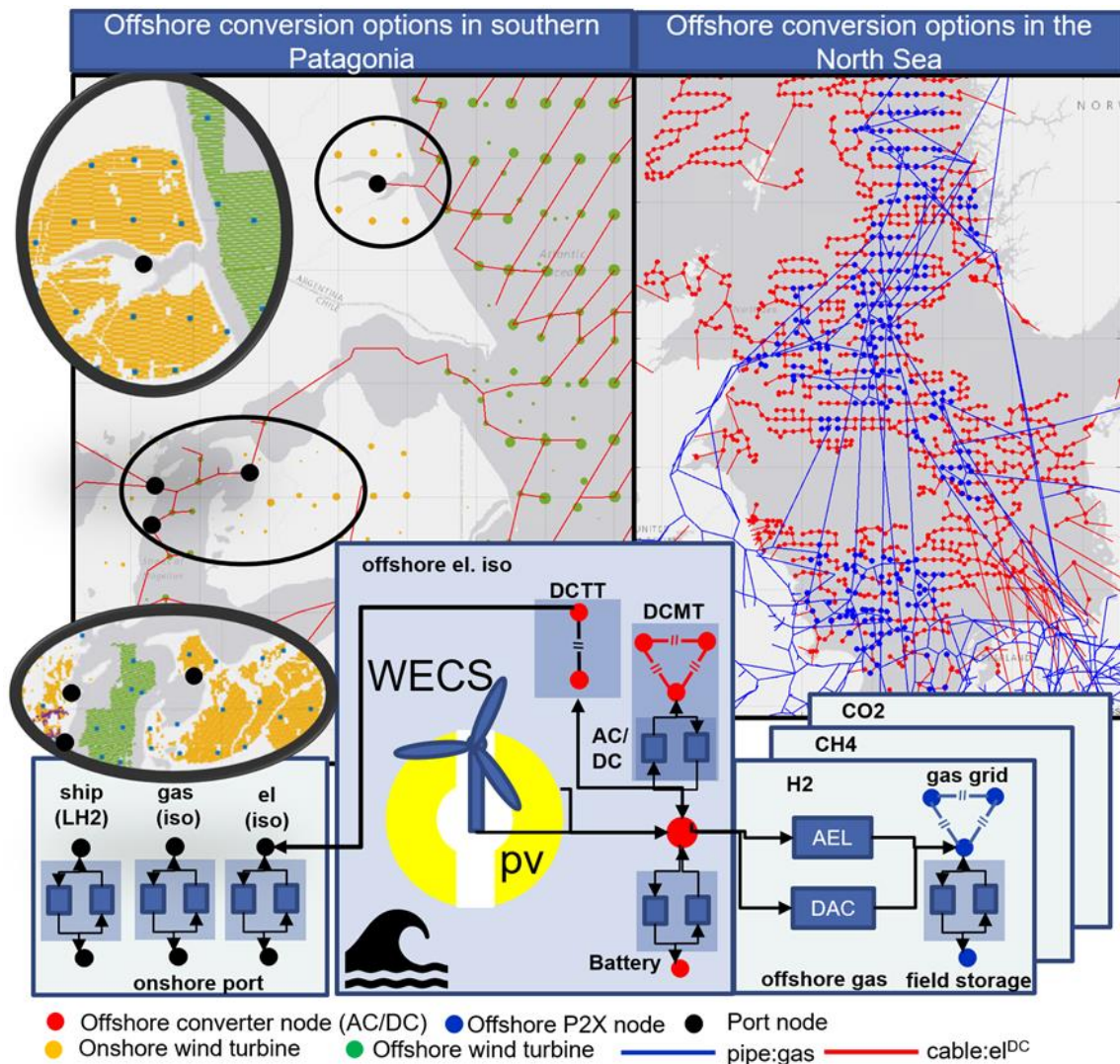


Figure 2.26: Coupling of offshore and onshore processes for modelling the interdependencies between land and sea-based conversion chains for a production, storage and transmission of energy carriers

While the lack of infrastructure is the driver of alternative conversion paths in some remote areas, the competition of the gas and electricity infrastructure might be another reason, such as in the North Sea. Instead of transferring electricity over large distances, a direct conversion of the energy might be an alternative in case on an existing or potential offshore gas infrastructure. In the current example, the availability of operating or depleted natural gas fields and their corresponding pipeline infrastructure in the neighborhood of potential offshore wind and PV generators may provide more favorable offshore conversion options. On the one hand, a completely off grid operation of primary energy conversion, storage and demand processes might be possible with the investment into wind and solar conversion technologies, which drive a direct air capture unit and a compressor to store CO₂ in a depleted gas field. Depending on the investment cost, a local temporal balancing of resource fluctuations might be favorable, taking into account the tradeoff between electricity grid expansion, renewable expansion and storage expansion for the optimal configuration of a DAC. On the other hand, the offshore electricity generation might

be directly shifted into the gas transport system in order to balance an onshore gas demand. This might include the connection of the electrolyzers and the wind/PV farms to an isolated electricity node and a complete shift of the natural gas infrastructure to transport hydrogen. Between these two extremes, the definition of local conversion hubs, which bundle the electricity generation and usage, might be useful, combining a spatial and local balancing of EHG, OCP, STOR and TRANS processes. From a structural point of view this means that offshore electricity generation and conversion technologies might be connected to isolated or grid connected offshore electricity and gas conversion, transmission or storage nodes. Therefore, each offshore wind and PV farm which is not directly connected to the onshore landing node is primarily connected to an isolated virtual electricity (AC) node. In case that the optimization might decide to invest into DCTT or DCMT systems, this node serves as the AC-bus of an offshore converter node. If not, it serves for the balancing of power-to-X processes. Additionally, an adjacent battery storage node is defined in order to model the tradeoff between spatial and temporal balancing on the electricity side. Conversion technologies which produce H₂ (AEL/PEM/SOEC), CO₂ (DAC) or SNG (combination of the first two plus methanation), are located next to the corresponding EHG unit, depending on the availability of a gas infrastructure (storage or pipeline). At specific hubs, which might be allocated at natural or artificial islands, finally additional conversion steps for the production, storage and shipping of energy carriers (SFO/LOHC/NH₃/Fe/MeOH) are defined.

The approach for aggregating isolated onshore EHG processes and the definition of further conversion steps is modeled analogous to the offshore case. The only difference is that in the current state the definition of resource potentials is restricted to a certain area around the nodes of the existing transport system. This means that wind, solar or biomass potentials might be defined in remote areas without the connection to an electricity or district heat grid within a certain threshold, as long as they are in a certain neighborhood to a node of the road, rail, waterway or pipeline infrastructure. PERSEUS-gECT thus focuses on the expansion of the existing electricity or gas grid topology. The expansion of onshore DCMT and DCTT systems is included as an alternative to the default AC based expansion to increase the capacity of the electric transmission system. However, it is restricted to selected projects without the degree of freedom to connect all isolated onshore electricity generation potentials, as it is the case in the offshore scenario. This means that in the aggregation step from the 100m resolved potentials to decision variables, each node of the non-electricity system is defined as a potential isolated electricity node $N_{el_iso}^{non_el} = \{N_{el_iso}^{gas:pipe}, N_{el_iso}^{liq:pipe}, N_{el_iso}^{ship:port}, N_{el_iso}^{rail:station}, N_{el_iso}^{road:hub}\}$ and each node of the non-gas system is defined as a potential gas node $N_{gas_iso}^{non_gas} = \{N_{gas_iso}^{cable:substation}, N_{gas_iso}^{liq:pipe}, N_{gas_iso}^{ship:port}, N_{gas_iso}^{rail:station}, N_{gas_iso}^{road:hub}\}$. If the aggregation of a primary EHG conversion potential (wind/solar/biomass etc.) is not possible within the supply area of the onshore electricity grid, instead one node from $N_{el_iso}^{non_el}$ is chosen as a basis. In case that this node is not part of the gas infrastructure, for example $n \in N_{el_iso}^{ship:port}$ an isolated gas node is created at the same location $n \in N_{gas_iso}^{ship:port}$. Finally, conversion processes for the production of hydrogen and derivated fuels as well as for their storage and potential conversion for transport (compression, liquification, etc.) are defined depending on the available local infrastructure. At specific hubs, which are in

general all ports but also major junctions of the rail and road infrastructure, processes for a multi modal energy and material flow are defined as well as further processing processes (e.g., Fischer Tropsch). For linking transport systems or connecting conventional EHG generator or other processes to certain nodes, depending on the specific process inputs and outputs, in general a specific distance limit is defined. The actual parametrization, however, is process and scenario specific and will be described at a later point.

2.4.2 Approach for defining resource availability constraints for the conversion of renewable energy carriers (existing & potential units and profiles)

In general, the definition of wind and solar potentials follows a bottom-up approach based on the exclusion of unsuitable landcover and topography areas with a certain buffer at a maximal spatial resolution of 100m. Afterwards the resulting greenfield potentials are reduced by the excluding areas for units which are either existing, in construction, approved, planned or announced. For bioenergy and waste, top down and bottom-up based approaches are combined depending on the considered primary energy source. For hydro, geothermal, marine and other PERSEUS-gECT focuses on parametrizing and especially regionalizing existing or planned generators and neglects greenfield potentials. In consequence the capacity of these generators is fixed and only the processes are modeled as variables, while the units are modeled as parameters. Concerning the modeling of intra-annual resource availability constraints PERSEUS-gECT focuses on a consistent parametrization of wind and solar energy conversion processes based on hourly ERA 5 reanalysis weather data. While complex fluid (heat, wind) or cell (PV) dynamics are ignored in this context and a rather simple modeling approach of the technical conversion process is chosen, the focus is laid on the consideration of the multiple existing and potential technology configurations. This includes the modeling of PV modules with multiple azimuth and aspect orientations or turbines at multiple hub heights and with multiple power curves within each relevant weather cell. For run-of river, seasonal hydro storages or open loop pump storages an own hydrological simulation of the inflows and dispatch boundaries is neglected. If possible, the processes are parametrized based on, publicly available national or zonal data. In all other cases a simplified assumption of a yearly fixed upper bound (equivalent to a fixed generation with curtailment) or completely flexible dispatch is made.

Overall, the definition of greenfield potentials for wind, solar and biomass energy conversion units and the computation of single profiles for the fluctuating renewables follows a rather straight forward approach known from the literature. The major challenge and focus of this work, however, lies in the combination of greenfield and brownfield potentials. As illustrated in the following figure, which is actually an own result of the potential analysis, a significant part of the deployment of the renewable potential in mature markets, such as Germany, is determined due to existing generators or concrete plans of companies or known tenders.

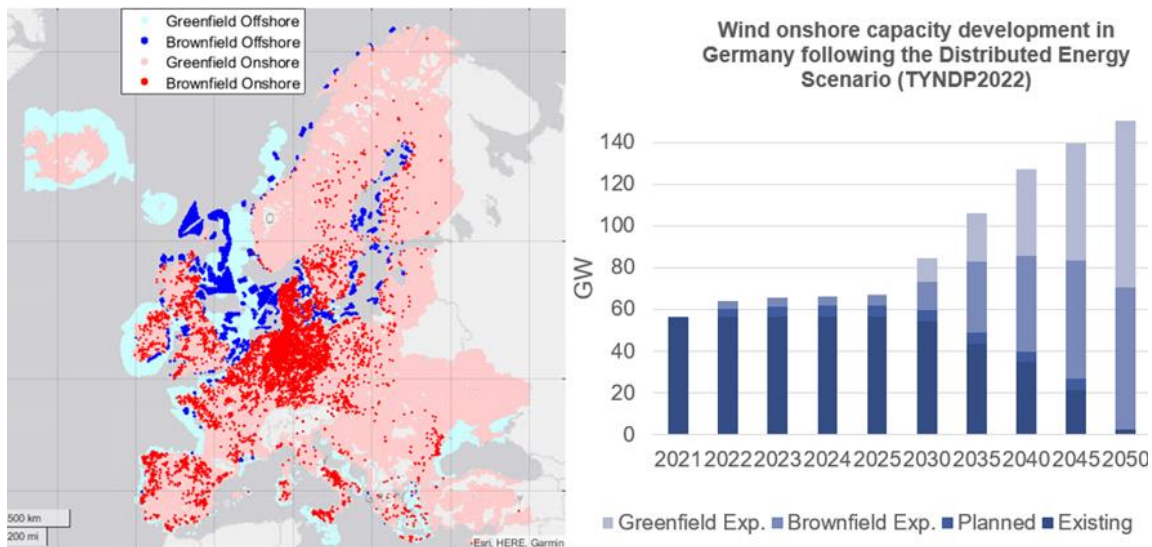


Figure 2.27: Distribution of onshore and offshore wind energy potentials (greenfield and brownfield) in Europe (left) and the development of wind onshore capacities in Germany in a reference scenario

Considering that the development of renewables in a multi period investment planning is path dependent and that major decarbonization milestones in Europe should be achieved within the next decade, underlines the importance of an adequate parametrization of the starting capacity, even for the planning of the 2050 energy system. After the description of the approach for defining greenfield potentials, therefore, the calibration of the database for known generators and the approach for combining greenfield and brownfield expansion will be described next. Finally, the approach for defining generation profiles, if applicable, is briefly described. It should be noticed that the focus of this work does not lie in the development of advanced approaches for a detailed modeling of renewable expansion potentials and generation profiles and the following levelized cost of electricity based (LCOE) economic analysis for a certain region and specific technology configuration (e.g., one wind turbine type at one hub height). Instead, the trade-off between exploiting grid-connected or off grid greenfield and brownfield renewable potentials should be modeled on a global scale within a multi period optimization. Thus, the focus lies on modeling the high heterogeneity of existing generators in combination with the increasing potentials for brownfield investment along the modeling horizon and the consideration of the technological development. The latter one is not restricted to a simple economy of scale-based approach of cost reduction but results in varying spatial capacity densities and generation profiles. In this context an approach is developed to combine a sectoral and spatial detailed allocation planning of renewables, which might be partially determined by sectoral targets for a uniform exploitation of regional resource potentials, with the parametrization and aggregation needs for modelling the renewable expansion and dispatch within a cross-sectoral and intercontinental balancing of energy supply and demand. The trade-off between local accuracy for the modelling of a specific technology within a year and global consistency, taking into account the cross and inter sectoral competition between technologies along the temporal and spatial dimension, is resolved by defining the variable aggregation based on a heuristic scenario driven expansion

planning prior to the actual optimization. Complex technological interdependencies on a local scale, such as the primary penetration of heat-pumps in properly insulated single family buildings in combination with the potential to combine PV battery systems in this sector with the flexibility of a controlled or bi-directional charging of electric vehicles might be addressed in this preprocessing step. Afterwards regional potentials and profiles might be aggregated with respect to this locally reasonable estimation of the system development such that a reduced number of final and primary energy conversion processes is defined between the input or output nodes of the multi-commodity transmission system. The goal is to define the variables in a way that the solution of the prior renewable expansion planning might be endogenously adjusted within the actual PERSEUS-gECT optimization run. All steps, starting from the greenfield potential analysis (i), the calibration of the existing set of renewable generators (ii), the profile generation (iii) as well as the heuristic expansion planning (v) based on an eventual preceding binary unit placement (iv) to define the techno-economic potential, are consequently a means to an end. An adequate variable definition and parametrization of an energy system model which takes transport restrictions for multiple commodities within multiple networks into account shall be achieved. In the following flow chart, the single steps are illustrated. Obviously, not all steps apply to all technologies. For renewables without a potential analysis, such as hydro, geothermal or marine, only the steps (ii), and to a certain extent (iii) and (v) are relevant. The analysis of bioenergy potential additionally takes (i) into account with a focus of using residues from the agricultural, forest or industry as a source for solid or gaseous bioenergy conversion processes. Contrary to the previously mentioned renewables, the computation of varying sub-period resource availability constraints for solar and wind energy conversion processes are modelled bottom up at an hourly basis and additionally a more detailed expansion planning is performed, including a binary heuristic turbine placement in the case of wind energy.

Wind (Onshore & Offshore)

In general, the first steps for the definition of the greenfield onshore and offshore potential for wind energy conversion systems (WECS) are quite basic and also apply for the definition of solar energy potentials. As illustrated for the case of defining suitable wind-onshore greenfield areas in Lower Austria, exclusion layers with the resolution of 100 meter are defined based on a set of unsuitable sites and subtracted from an administrative layer of a certain region.

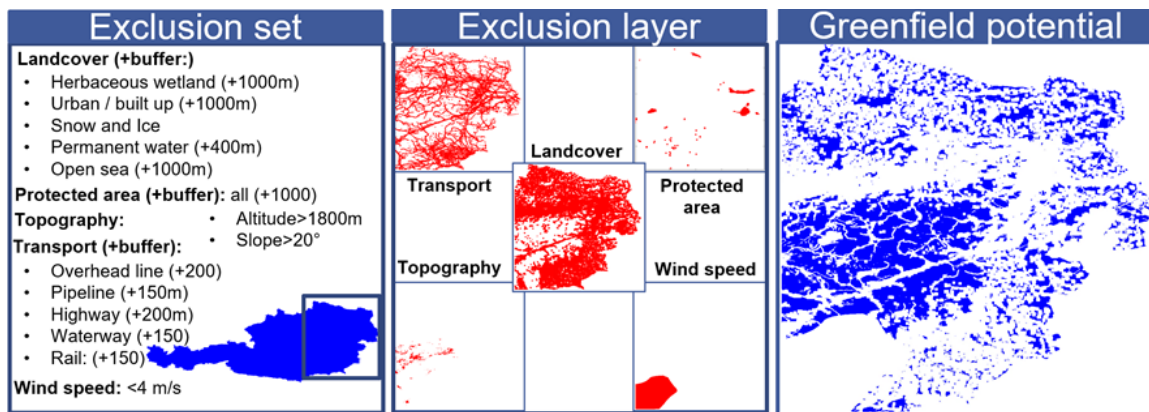


Figure 2.28: Approach for the assessment of wind onshore potentials

This approach is quite common in the literature, although the exclusion set and the defined minimal distances may vary within given ranges (McKenna et al. 2022). In the current example, the relevant classes of the less detailed Copernicus land cover classification are shown, as these values are globally available. Due to the higher degree of detail, however, in Europe landcover suitability based on CLC data are taken. The sources for the definition of the regionalization basis are, as already mentioned, OSM, ERA5, WPDA, Natura2000 and GTOPO30 data besides of Corine and Copernicus land cover data, that are interpolated to a 100 m resolution if the original resolution is higher. The processing of the data is implemented in MATLAB, and once all data are mapped on the same 100m resolution, the computation of exclusion or inclusion operations or the distance buffering can be efficiently performed based on simple matrix operations such as multiplication or addition. The computation of this first step for assessing the wind and solar greenfield potentials might be completed within a day for the currently covered regions, which includes Eurasia and North Africa above a latitude of 20° and South America. Once preprocessed, the later variation of exclusion areas and buffers, however, is less time expensive and might be done on a minute scale.

Following (McKenna et al. 2014) and the own previous work (Slednev et al. 2017b), the suitable areas for wind onshore and also wind offshore were subsequently weighted with a suitability factor and the best suitable turbine was determined for a specific land cover. In this context, the optimal choice was based on the calculated LCOE of the wind turbine and the capacity density, defined as the ratio of the wind farms power to the ground area. The latter factor was also used to approximate the space needed by a turbine. While such an approach is quite common in the literature (McKenna et al. 2022) and is even applied for an energy system analysis on municipality level (Weinand et al. 2019), the drawback of considering wake losses only based on the capacity factor is quite obvious in areas with complex suitability conditions. The most accurate solution of using a combinatorial optimization of the park layout with an explicit calculation of the wake losses however is currently limited to the level of single wind parks, considering that the extension to national or even continental dimensions is computationally challenging (McKenna et al. 2022). To bridge this gap, one possibility is to apply rotor diameter-based distance heuristics for the placement of single wind turbines. The basic idea of this approach is to

assume that the wake losses outside a wind ellipse, defined by a multiple of the rotor diameter (D) parallel and orthogonal (e.g., $8D/5D$) to the main wind direction, are acceptable with respect to the trade-off with the capacity density (McKenna et al. 2022). For taking this distance restriction between turbine into account often a heuristic for the turbine placement is applied, as done by (Jager et al. 2015) for determining the wind power potential in the federal state of Baden-Württemberg in Germany. Due to the focus on evaluating the placement of multiple wind turbines at multiple hub heights within multiple years on a global scale, in the current state of PERSEUS-gECT a rather simple placement heuristic has been chosen. Once the potential areas for the greenfield investment are defined, an optimal turbine for each investment period is selected from a set of candidate turbines for a certain area, with respect to the location of existing turbines and local weather conditions. In the first step to determine the optimal turbine, each candidate turbine is arranged in a regular grid within a weather cell with a predefined spacing between the turbines in x (longitude) and y (latitude) direction. As illustrated in the following figure for the case of an $8D/5D$ distance rule, the grid of potential wind turbines is subsequently rotated in the wind direction of the weather cell and overlaid with the potential area, which is discretized at a 100m resolution. Starting with a positioning in the upper left corner the grid is afterwards shifted in x and y direction, such that a maximal number of turbines might be placed.

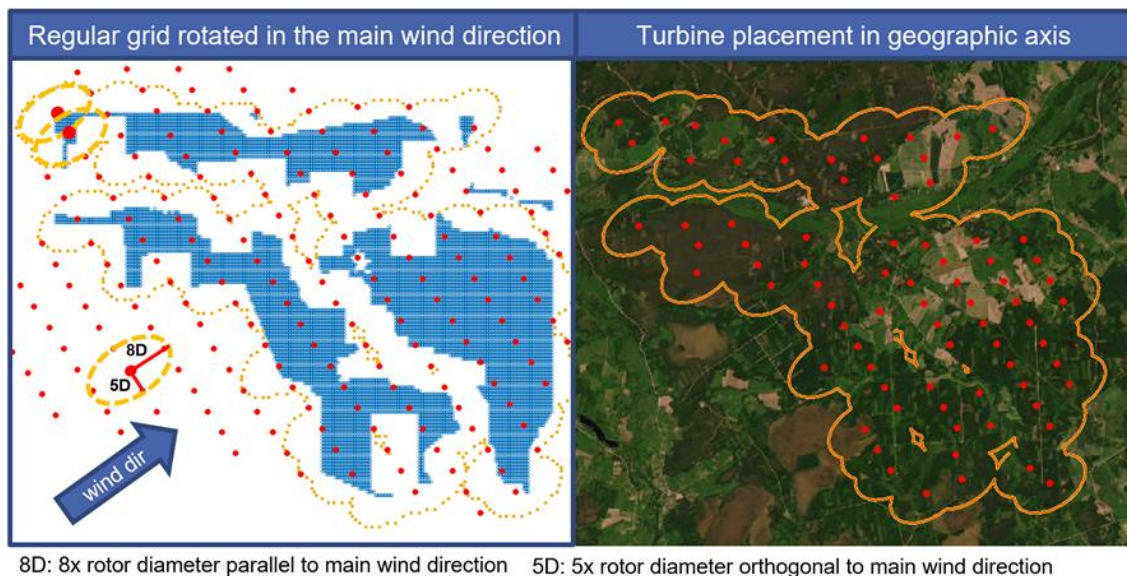


Figure 2.29: Placement of wind turbines with respect to wind ellipse distance restrictions

Finally, single turbines are successively placed on the boundaries of the wind ellipse, until all potential positions are excluded. Currently this simple placing heuristic is performed for 10 different onshore and 16 offshore wind turbines and at 5 hub heights (120,140,160,180,200) and the best turbine configuration for each investment period is defined based on a metric considering the computed LCOE, the resulting capacity density and the capacity factor of the specific technology. The weights of the performance factors and the distance restrictions are further regionally adjusted, taking into account a tighter turbine packing and a focus on higher density

factors in countries with scarce suitable onshore and offshore areas like Belgium and a focus on minimal wake losses and LCOE in countries like Argentina, Kazakhstan or Russia, where space and the rent for land is a less limiting factor. Existing wind turbines are initially excluded from this placement heuristic. Once the end of the technical lifetime is reached, however, a similar placement approach is performed for the evaluation of the repowering potential, taking into account the significant increase in rotor diameters of new turbines, which limits the potential to replace all turbines within an old wind park at the exact same location.

So far mainly the potential assessment for wind-onshore was described. Generally, wind offshore potentials are modelled quite similarly, starting with the definition of exclusion areas, the matching with the existing units and finally, the placement of turbines. However, some characteristics regarding the suitability of turbines and the area need to be taken into account when modelling wind offshore potentials. Due to the long planning horizons for developing offshore projects, the large project sizes and the needed grid infrastructure, a significant part of the wind offshore potential in the Northern Sea and the Baltic Sea lies within designated areas which are defined through the maritime spatial planning on national level or explicit projects from the industry. As illustrated in the following figure, which is based on national maritime spatial plans or explicitly designated areas for projects and tenders provided by national authorities (e.g., BSH, the Crown Estate, etc.) or international organizations such as HELCOM²⁷ or EMODnet²⁸, the suitable areas in the Northern Sea and the Baltic Sea are thus quite predetermined.

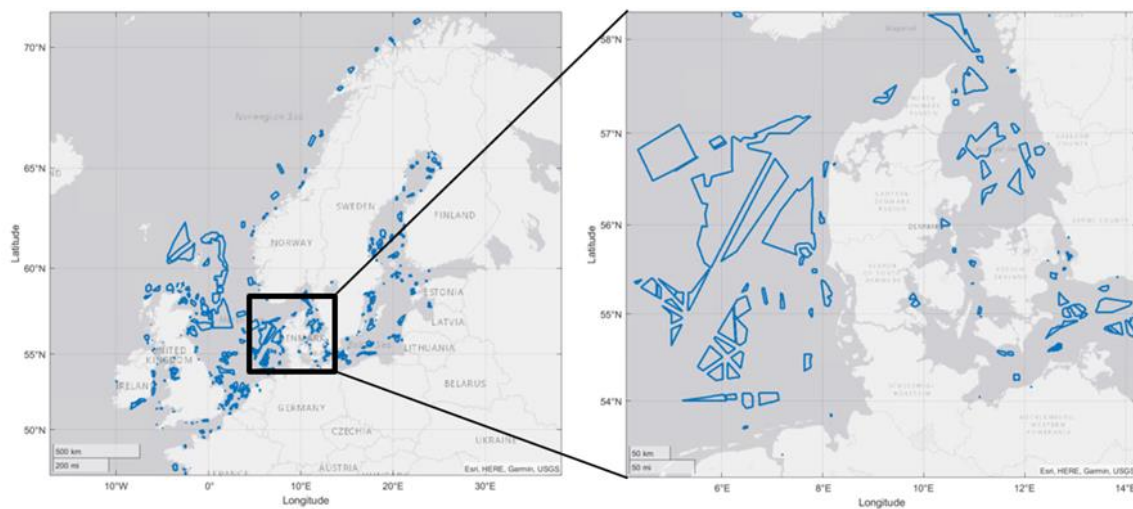


Figure 2.30: Considered designated areas for wind offshore conversion in the North Sea and Baltic Sea

²⁷ <https://helcom.fi/baltic-sea-trends/data-maps/>

²⁸ <https://emodnet.ec.europa.eu/en>

As maritime spatial plans might be adjusted, additional remaining greenfield potentials²⁹ are computed by excluding additional military areas³⁰ and the main shipping routes, which are determined from vessel density maps if not explicitly given. In the base scenario, near shore (<5400m) potentials and profiles are also computed but used only in case of known projects for determining the layout of the announced wind farm. Besides the definition of the suitable areas, the actual need to adjust the LCOE calculation depending on the water depth and distance to shore makes the offshore turbine placement computationally more challenging than in the on-shore scenario, although the same heuristic is applied. The reason is that for onshore wind the techno-economic specification of a turbine configuration³¹ is assumed to be independent of the location, with the exception of the binary exclusion of turbines based on the specific wind conditions (IEC classification). For the techno-economic parametrization of 10 wind turbine types at 5 hub-heights within a weather cell, 50 generation profiles³² need to be computed, and, based on the capacity factor, the LCOE is computed 50 times in each investment year. For wind offshore, however, the baseline cost depends on the water depth and CAPEX and fixed OPEX depends on the distance to the next port for installation and maintenance.³³ Actually constant cost for fixing floating wind offshore is assumed and applied in the deeper sea (>60m), while a water depth dependent cost function for monopile (<30m) and jacket (30m-60m) foundations is considered in shallow waters. As a consequence, the LCOE is computed for each suitable point in a weather cell for the heuristic turbine placement, resulting in maximum 7.2M computation steps, considering the cell resolution of 30 km, a 100m pixel resolution and 16 potential offshore turbines with 5 hub heights per investment period³⁴. The resulting LCOE of the chosen turbines is shown in the following figure for an investment in 2035 in Europe:

²⁹ After the general exclusion of unsuitable areas, such as all non-water bodies, protected areas, buffer around infrastructure, sand mining grounds etc. and the exclusion of existing wind parks and designated offshore energy areas.

³⁰ For wind onshore, the exclusion of military areas is also possible, but not considered in the default options. For wind-offshore these areas however are quite significant and therefore excluded in the base scenario.

³¹ For example, a Enercon E-160 EP5 turbine with 120m hub height in the investment year 2025.

³² Actually, the profiles are computed for the last 30 years in Europa, or 20 years (rest of the world) and an average value is taken.

³³The grid connection cost is modelled independently, due to the endogenous consideration of multiple grid connection options, therefore the balance of plant cost includes only the expenses for wind-park internal cabling.

³⁴ Fortunately, the profile calculation is independent of the water depth and distance to shore and doesn't increase.

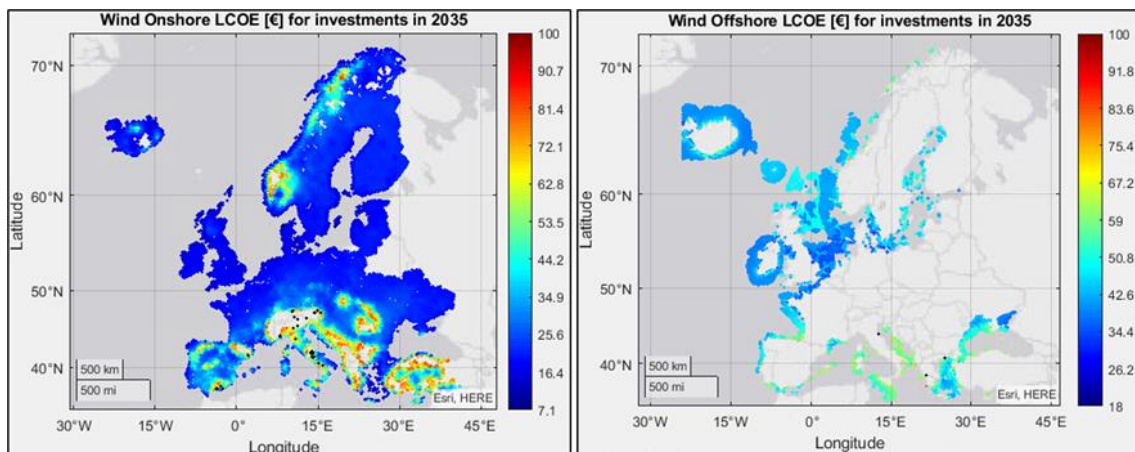


Figure 2.31: Exemplary illustration of the distribution of the LCOE of wind onshore (left) and wind offshore (right) conversion in 2035 in Europe

The techno-economic parametrization of wind onshore and offshore turbines, is based on existing approaches and the cost-component development is adjusted accordingly to fit the scenario, which means that the components are recalibrated to match the development for a reference turbine at a reference location. In the practical implementation, the cost component models “turbine_cost.py” and “dtu_wind_cm_main.py” from the tools TOPFARM2 of the DTU were taken, combined and recalibrated based on own assumptions in order to meet the cost development following the technology catalogue of the Danish Energy Agency. As the turbine placement algorithm is MATLAB-based, the initial python-based models are not utilized but an own implementation in MATLAB is implemented considering that 78667 weather cells are optimized only in the offshore case, such that the component models need to be executed $5.6e^{11}$ times in order to compute the LCOE for each investment period.

Concerning the modeling of the generation profile, a look-up function based on the performance curve of a turbine, which describes the power output at a certain wind speed, is used to translate wind speed into power. While there are multiple approaches in the literature to estimate the power curve of a wind turbine, as shown by (Carrillo et al. 2013), in PERSEUS-gECT a database³⁵ of more than 850 known power curves from various manufacturers is used as a basis for deriving profiles of existing turbines while a tool for generating generic power curves, developed by (Saint-Drenan et al. 2020), is used for modelling unknown power curves. Due to the fact that the utilized ERA 5 reanalysis weather database provides the wind speed at 10 and 100 heights³⁶, an adjustment to the wind speed at hub height and a correction of the air density is performed in a preceding step. As illustrated in the following figure, a simple logarithmic wind speed correction following (McKenna et al. 2014) is applied for adjusting the wind speed to the hub height and combining with the air density at hub height. The latter is calculated based on the hub-

³⁵ Various commercial and non-commercial sources were used for this database.

³⁶ ERA 5 provides the wind speed in an eastward component and a northward component.

height adjusted pressure and temperature as described by (Dupré et al. 2019) and the normalized wind speed is computed such that the potential maximal generation might be looked up (Eurek et al. 2017). In the last step, the normalized wind power profile is calculated by subtracting all possible losses, such as wake losses, electrical losses etc.

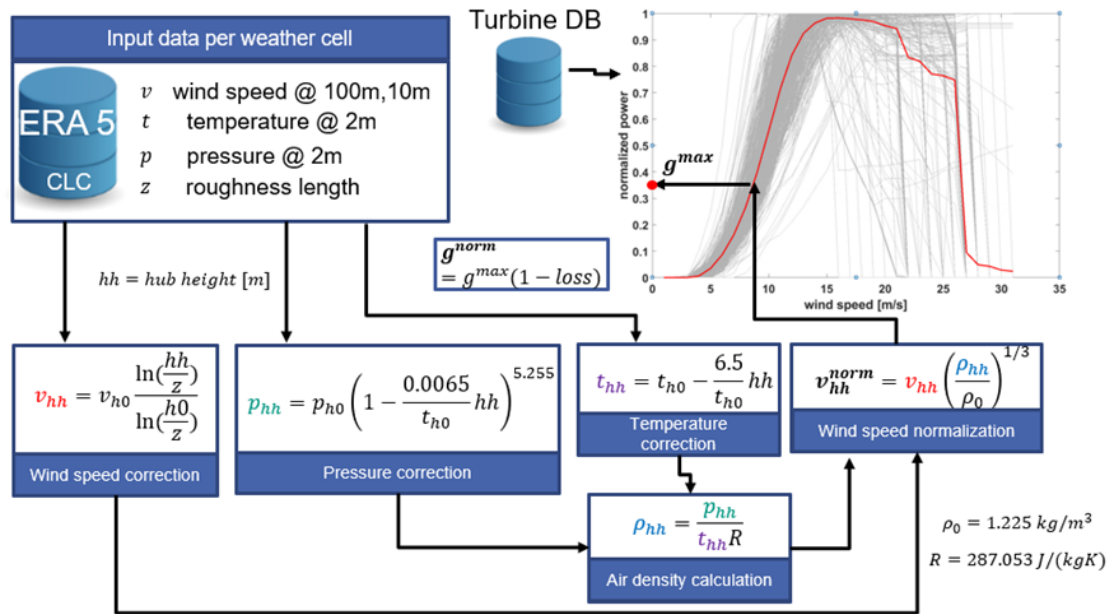


Figure 2.32: Approach for modelling wind energy conversion profiles

The focus of the bottom-up modelling was explicitly set on the analysis of fundamental drivers, and not on the development of an exact back-casting or short-term forecasting approach for the wind generation within a specific wind park or market, for which statistical methods are much better suited. Especially the impact of the technology development, which is mainly based on the hub-height and power curve development, and the regional allocation of existing, repowered and greenfield turbines in a year should be modelled. Although in the default case an actual wake modelling such as in (González-Longatt et al. 2012) is omitted and simply a loss factor of 0.85 following (Mainzer 2019) is assumed, which takes into account all losses except of the degradation, the general characteristic of the historic wind power time series still could be modelled quite accurately as shown in the following figure:

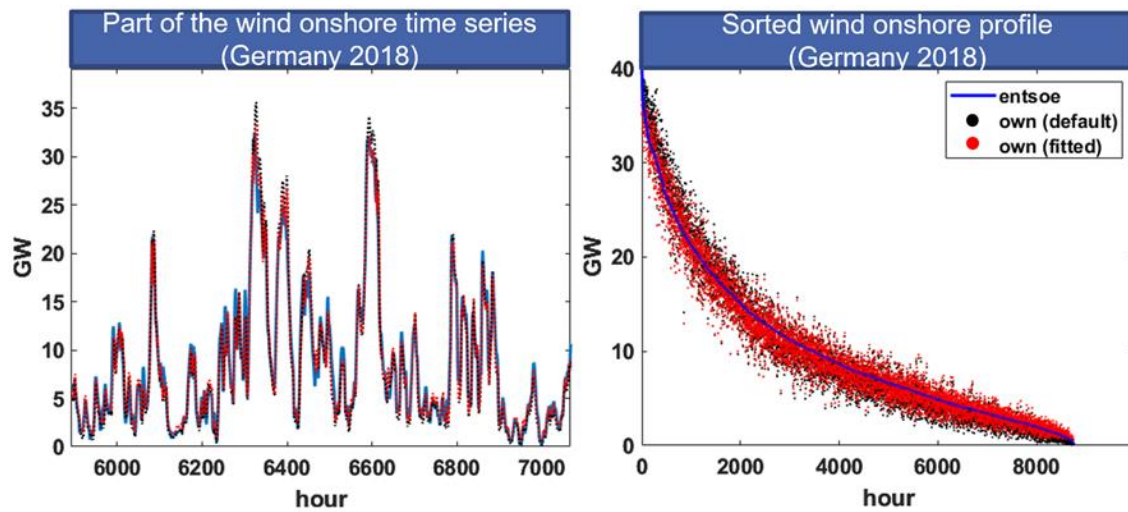


Figure 2.33: Exemplary validation of the modelled wind generation profiles based on a comparison with ENSTO-E data for Germany in 2018

The shown performance of the historic profile generation modelling is based on the aggregation of single turbine simulations from a database that includes 134.239 onshore and 21.315 offshore turbines of multiple states (operational, constructional, approved, announced, shelved, dismantled) which are mainly located in Europe. The individual degradation since the commissioning data in this context was set to 0.64% per year following (Mathew et al. 2022). The database is created from various sources such as the national authorities (e.g., MaSTR, No), commercial providers (e.g., the.windpower.net, PLATTS) and public databases (e.g., OSM, GEM, OPDS, MastR, etc.), and missing parameters are calibrated based on an approach described in (Slednev et al. 2018).

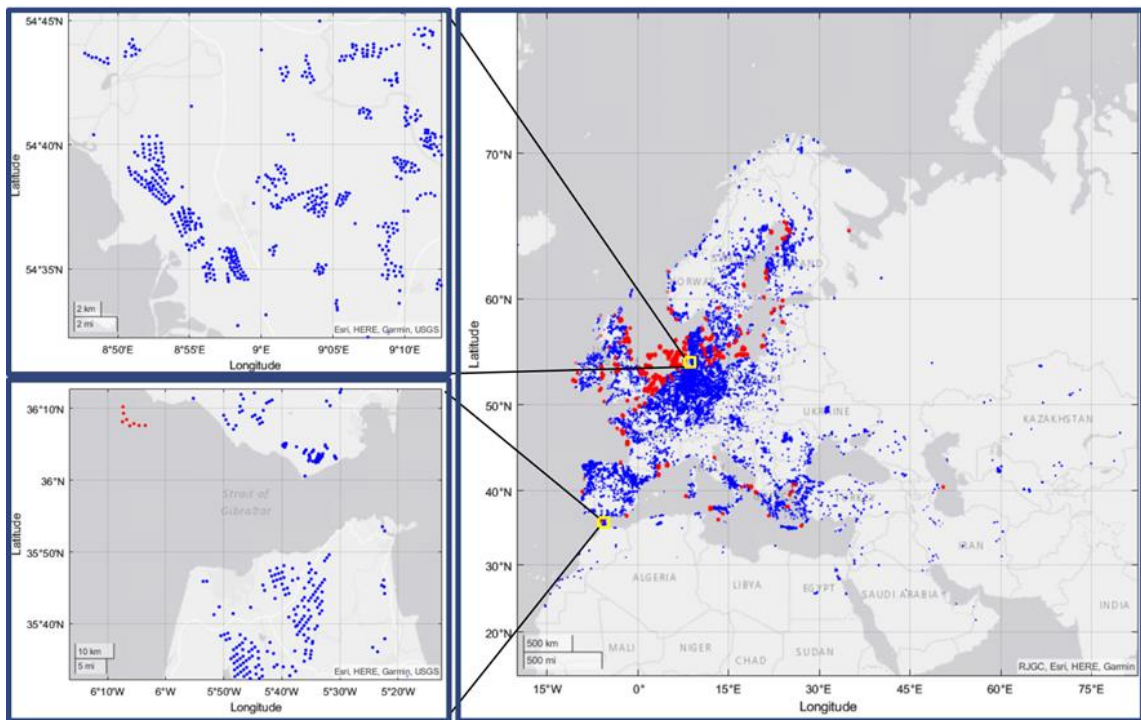


Figure 2.34: Location of existing or planned turbines in the current WECS database of PERSEUS-gECT

One challenging part in the calibration step of the database of existing turbines and the matching with greenfield potentials is to complete the data gaps of missing commissioning years or even missing turbines, such that the bottom-up sum within a year doesn't just match with the national installed capacity of a year but is consistent over the entire market ramp-up of the technology, dating back to the early 2000. For further reference, national data from Eurostat, IRENA, IEA and EIA are used, depending on the country.

In the last step of the definition of the wind onshore and offshore variables, the existing and potential turbines are aggregated to the nodes of the electricity transmission grid or to isolated electricity nodes located next to the nodes of other transmission systems (gas- and oil pipeline, rail, road, waterway==port) or to potential offshore wind farm nodes. In addition to the general aggregation approach, which was previously described, a further aggregation might be needed in order to keep the problem size manageable. In this context the aggregation of fixed capacities and their profiles at the level of grid connected or isolated electricity nodes is important in order to avoid an individual and rather heterogenic historic wind turbine technology configuration. Especially when taking into account that even within one wind park often turbines are installed from different manufacturers at different hub-heights and from different years, as well as from different market participants. Assuming that known turbines (operating, commission, approved or in a late planning state) are not decommissioned before the end of their technical lifetime, their capacity might be fixed and aggregated accordingly. The profile of the corresponding process in each period is thus the capacity weighted sum of all profiles of fixed turbines which are currently active. As a consequence, profiles from different power curves at different hub-heights

with different degradation stages and from different weather cells might be aggregated within the supply area of one electricity node. In the default settings, repowering decisions are equally fixed based on the selection of the best technology for the specific site in the decommissioning year of the original turbine. The aggregation of the remaining potential is more challenging due to varying optimal wind park layouts in the different investment periods³⁷ (due to the increase of the rotor diameter, hub-height etc.) on the one hand and specific regional characteristics on the other hand. With a closed meshed electricity network in Western Europe, the aggregation of onshore turbines with varying profiles is a less critical point compared to the handling of the same problem in isolated regions such as in Kazakhstan or for wind offshore. On the contrary, the development of the renewable expansion might be much better modelled in PERSEUS-gECT in scarcely populated regions considering that a pure techno-economic allocation might be assumed as the main driver for the investment, while in densely populated markets like Germany, a fair or more equal distribution is pursued due to primarily non-economic reasons such as the level of acceptance of the local population or burden charging issues. In PERSEUS-gECT this issue is addressed by running a yearly heuristic capacity expansion planning prior to the actual optimization with a local specification of constraints and the distribution logic. Thereafter, the allocated ($\hat{y}_{pu,tp}^{\text{exp } -a}$) and not allocated ($\hat{y}_{pu,tp}^{\text{exp } -na}$) remaining potential, meaning after the exclusion of fixed capacities ($y_{pu,tp}^{\text{fix}}$), is defined as the upper bound for two different unit variables ($y_{pu,tp}^{\text{exp } -a}$, $y_{pu,tp}^{\text{exp } -na}$) such that a process ($x_{pu,tp,ts}^{\text{ehg2el}}$) is limited once by the fixed capacity within a year and the expansion of two unit variables in the current and previous periods (specification of eq. 3.11).

$$\begin{aligned}
 x_{pp,tp,ts}^{\text{ehg2el}} \leq & \sum_{tp' \leq tp} \sum_{pu \in \text{Unit}_{pn}} y_{pu,tp'}^{\text{exp } -a} \beta_{pu,pp,tp',ts}^{\text{profile_exp } -a} \beta_{pu,pp,tp',tp,ts}^{\text{degrad}} + \\
 & \sum_{tp' \leq tp} \sum_{pu \in \text{Unit}_{pn}} y_{pu,tp'}^{\text{exp } -na} \beta_{pu,pp,tp',ts}^{\text{profile_exp } -b} \beta_{pu,pp,tp',tp,ts}^{\text{degrad}} + \\
 & \sum_{u \in \text{Unit}_{pn}} y_{pu,tp}^{\text{fix}} \beta_{pu,pp,tp,ts}^{\text{profile_fix}} \\
 \forall tp \in TP, \forall ts \in TS, \forall pp \in PROC_{pn}^{\text{RES}}, \forall pn \in PROD
 \end{aligned} \tag{2.50}$$

One reason for splitting the potential in different variables is that a certain part of the pre-allocation planning might be used to define regional sector specific lower or upper bound for the capacity expansion, which will be discussed in more detail later in the case of solar power. The second reason is that favorable and non-favorable potential within a supply area of an electricity node might be differentiated. In the case of the modelling of wind energy resource constraints, the pre-allocation planning is in general more relevant for the definition of onshore variables. While the aggregation to offshore wind farms and their grid connection was already previously discussed, the case of wind onshore should be discussed based on the example of Kazakhstan. Unlike in the case of Germany, where each potential turbine might be assigned to the next transmission grid, a limited potential is not the main challenge in the case of Kazakhstan, at least based on the underlying distribution grid and where national or local authorities define targets for the wind energy expansion even in regions with a low resource availability. As illustrated in

³⁷ Main drivers for varying park layouts are the increase of the rotor diameter and hub-height.

the following figure, the definition of the variables with respect to potential transmission constraints is more relevant.

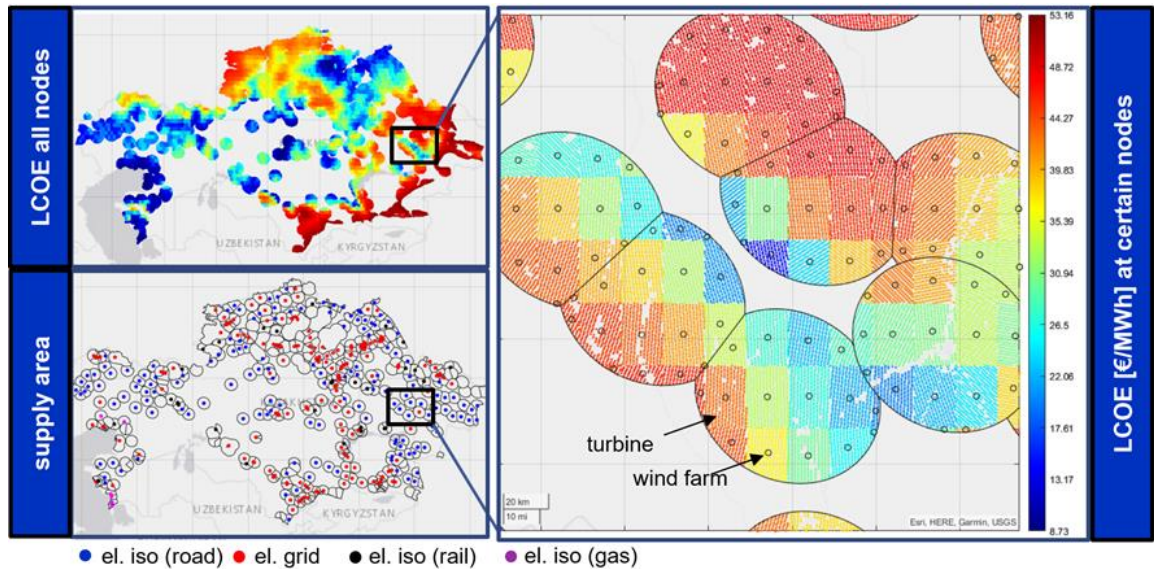


Figure 2.35: Aggregation of potential wind turbines to wind farms variables in remote areas, illustrated for the case of Kazakhstan

Therefore, a radial potential with a 40 km threshold around the nodes of the potential transmission systems is defined in the default settings. After the first round of the turbine allocation planning, which results in the placement of over 680k possible wind turbines from over 117 mio possible spots, the turbines within a weather cell might be aggregated to 5637 wind farms per investment period. In a second step an additional expansion planning might be performed and if needed the variables are aggregated to two expansion variables for the 410 relevant nodes in the country. Depending on the region and focus of the case study, different aggregation strategies might be applied. In this context a pre-analysis of the potentials, for example based on the TYNDP2022 scenario, gives an indication of the remaining potential and the potential number of variables which might be included in the model. In case the planned and repowered turbines are assumed to be fixed, the profile of 88621 turbines, mainly located in Western Europe, with a capacity of over 411 GW in 2050 might be aggregated without any loss of accuracy to the nodes of the electricity transmission system. As shown in the upper left corner of the following figure, this results in fixing the capacity in locations with the highest potential full load hours in that region.

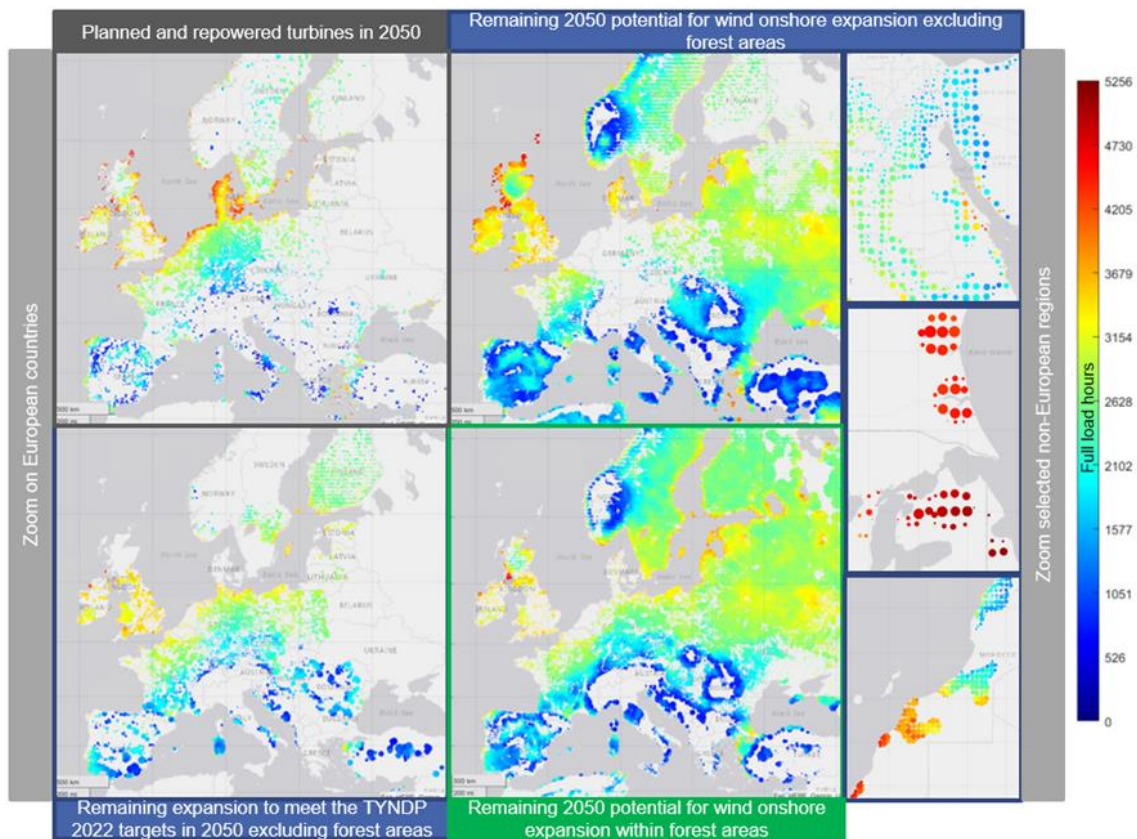


Figure 2.36: Comparison of the distribution of planned and repowered wind onshore turbines and the remaining potential in Europe and selected areas based on the full load hours

Based on a previous layout optimization, in the next step of the example, turbines are chosen on a yearly basis to meet the interpolated capacity targets of the decentral generation scenario of the TYNDP 2022. During this step, there is an equal emphasis on minimum LCOE, maximum generation and maximum capacity density, with the aim of avoiding an expansion in location which are covered by a forest. The resulting aggregation to 7142 units with an equal electricity node, weather cell and expansion period covering 5 years is shown in the lower left corner with a total capacity of around 630 GW. Afterwards the potential for open space located turbines in some parts of Western Europe is nearly exploited in the current example, as shown in the upper right corner³⁸. In other parts of the model region, however, a remaining large potential of 16416 GW for open field placed wind onshore turbines requires a modelling of 43844 units in case of considering weather cells and electricity nodes as an aggregation basis. Depending on the region, a clustering of potentials from different weather cells or even an aggregation of all units beneath an electricity node might be useful in order to balance the trade-off between model

³⁸ In the current example, an additional forest-based expansion of 17 GW aggregated to 233 units in Austria and the Benelux would be needed to meet the targets, assuming default distance restrictions, of which the 8D/5D turbine spacing and 1km distance buffer to villages are the strongest.

accuracy and size. In the previous example parts of Egypt, Morocco and Chile/Argentina are chosen to illustrate the different requirements for the aggregation. Finally, variables might be defined to model the remaining capacity expansion in forests, which would add 32,783 unit variables per time period with a capacity of 6,847 GW.

Solar (PV & thermal)

The approach for defining solar thermal and photovoltaic (PV) potentials and profiles is quite similar to the case of wind energy. For the definition of the ground mounted PV and concentrated solar power (CSP) technical potentials, an analog approach to the first step of the wind onshore potential analysis is chosen. Once unsuitable areas are excluded, a suitability factor depending on the land use is taken to define the share of the potential suitable land, upon which the solar modules or collectors might be placed. The suitability factor thus takes the competition with alternative land usage needs into account. Analogous to the capacity density based approach for wind, afterwards the available space is converted to a power capacity, although in this case the geographical space determines the module or collector area and thus the capacity, with the consequence that an allocation planning for single units might be omitted. Floating PV is modelled just like ground mounted installations with the difference of a slightly higher efficiency due to the water cooling and a potential which is determined by wind offshore turbines, based on the simple assumption that the floating units are installed in a ring pattern around the offshore turbines. For rooftop PV and solar thermal collectors, the definition of the suitable area is more challenging, considering that the landcover classification of urban buildup (Copernicus) or urban fabric (Corine) is rather unspecific for identifying the actual suitable rooftop area. Therefore, a bottom-up approximation of the rooftop area based on OSM building shapes and classifications and a top-down approach based on national building statistics is combined to determine the greenfield potential. The top-down approximation of the available roof area per building type and roof type in this context follows the rather simple approach of (Mainzer et al. 2014) which is also applied by (Weinand et al. 2019) for the potential assessment at municipality level. Although initially proposed for PV, it is assumed that solar thermal collectors might be placed on the same suitable area. For a part of the rooftop PV potential, an integrated modelling with a battery energy storage system is (PV-BESS) considered and in combination with the regionalization of the sectoral electricity demand the potential for these systems is modelled based on a dimensioning between the yearly electricity load and the PV and battery capacity based on (Kaschub et al. 2016). Besides of the individual expansion of PV and batteries, PERSEUS-gECT considers different degrees of freedom for the modelling of an integrated PV-BESS dispatch, based on a combined expansion. It ranges from a fixed battery and PV dispatch profile based on a prior stochastic self-consumption optimization on the low voltage level as shown in (Perau et al. 2021), to a completely independent dispatch of the systems, as applied in (Ruppert et al. 2019) and (Slednev et al. 2021). In the default settings, PV-BESS flexibility is modelled based on a coupled process, where the battery charging is restricted to the PV generation and the charging and discharging variables might be partially bound by limits derived from a prior decentral stochastic optimization.

Overall, the modelling of solar energy potentials and of the electric or thermal profile relies on the adaptation of existing approaches and instead of applying the most accurate method for a small area, the focus is placed on computing (sectoral) potentials and profiles on a 100 m scale for various module or collector orientations. The actual strength of PERSEUS-gECT in the context of the solar energy modelling lies in the combination of technical potentials and the exploited potential on a high spatial resolution and the flexible aggregation to variables which are not predetermined by a specific transmission system but allow an endogenous local or even off grid balancing of a sectoral supply and demand. In general, the literature on the assessment of solar energy potentials in various applications is very large ((Khan and Arsalan 2016),(Weinand et al. 2023)), with a good overview of approaches for assessing rooftop PV (RTPV) potentials provided in (Mainzer et al. 2014) and (Melius et al. 2013). Concerning the accuracy, approaches which combine statistical measure with building data and even with satellite data, such as done by (Mainzer 2019) are well suited for determining the rooftop PV potential, including an accurate detection of existing PV installation on a municipality scale. The role out on a global scale is however limited due to the computational need. To overcome this limitation, (Joshi et al. 2021) propose a combination of an machine learning approach with a GIS (geo information system) based potential assessment in order to evaluate the rooftop PV potential on a global scale. An alternative approach which also guarantees high accuracy is presented by (Bódis et al. 2019), which the authors classify as high level, complete consensus approach by combining building statistics with multiple high resolved gridded landcover and settlement maps. To some extent this approach corresponds to the approach that has been used in this work. For ground mounted PV, various GIS based approaches may be found in the literature. These approaches range from a regional bottom up analysis based on an hourly performance simulation (Pillot et al. 2020) or (Bao et al. 2022), where the first mentioned authors actually optimize the placement while in the second case the benchmark with existing park layouts is in the focus, to global approaches based on the mean solar radiation on tilted panels (Saxena et al. 2023). In (Yeligeti et al. 2023) a simple statistical fitting is proposed to bridge the gap between those two approaches. For floating PV, which is in a rather early development state, many authors focus on local feasibility studies (Ranjbaran et al. 2019). On a global scale (Jin et al. 2023) presented an approach for assessing the potential on water reservoirs while (Silalahi and Blakers 2023) asses the maritime potential. For solar water heating systems a wide range of technologies and applications might be differentiated as shown in (Jamar et al. 2016; Nanda et al. 2023). From the primary energy resource availability point of view, approaches for determining the potential for rooftop solar water heating (SWH) show a high similarity or are even overlapping with the RTPV case, e.g. (Doorga et al. 2022). The same applies to the literature on ground mounted solar energy potentials, as the suitable areas for CSP, for example computed following (Trieb et al. 2009), are also suitable for ground mounted PV. Besides of the resource availability, many approaches in the literature also consider the integration into local energy management systems as part of the solar energy potential assessment. Especially for SWH this is of great relevance and as shown in (Gaonwe et al. 2022) there are multiple possibilities for combining solar thermal collectors with thermal storages and heat pumps within a local heating system, while (Gaonwe et al. 2022; Kang et al. 2022) providing an overview how SWH might be integrated in district heating systems. The

own approach for modelling solar energy potentials, which is roughly illustrated in the following figure, however, considers only a fraction of the possible applications and focuses on the combination of an hourly generation simulation with a GIS-based bottom-up modelling of the available space with a 100m resolution. For solar rooftop potentials, additionally a top-down assessment based on building statistics or derived metrics is applied and regionalized. Following the classification of (Melius et al. 2013), a combination of a bottom up GIS method and a top-down constant value method is applied in PERSEUS-gECT. An exception in this context is the assessment of the technical floating PV potential, as it actually relies on the wind offshore modelling and the resulting allocation of existing or potential turbines. Assuming that the modules are placed in a ring pattern around the turbines, with an outer/inner radius of a multiple of the rotor diameter (D^o/D^i) such that ships might pass between the turbines and also reach the turbines for maintenance work, the turbine rotor and the park layout determine the potential of the considered floating PV potential. In the default settings simply $D^o = 2, D^i = 1$ and a fill rate of the space of 0.65 is assumed, considering a default 9D/6D spacing between the turbines.

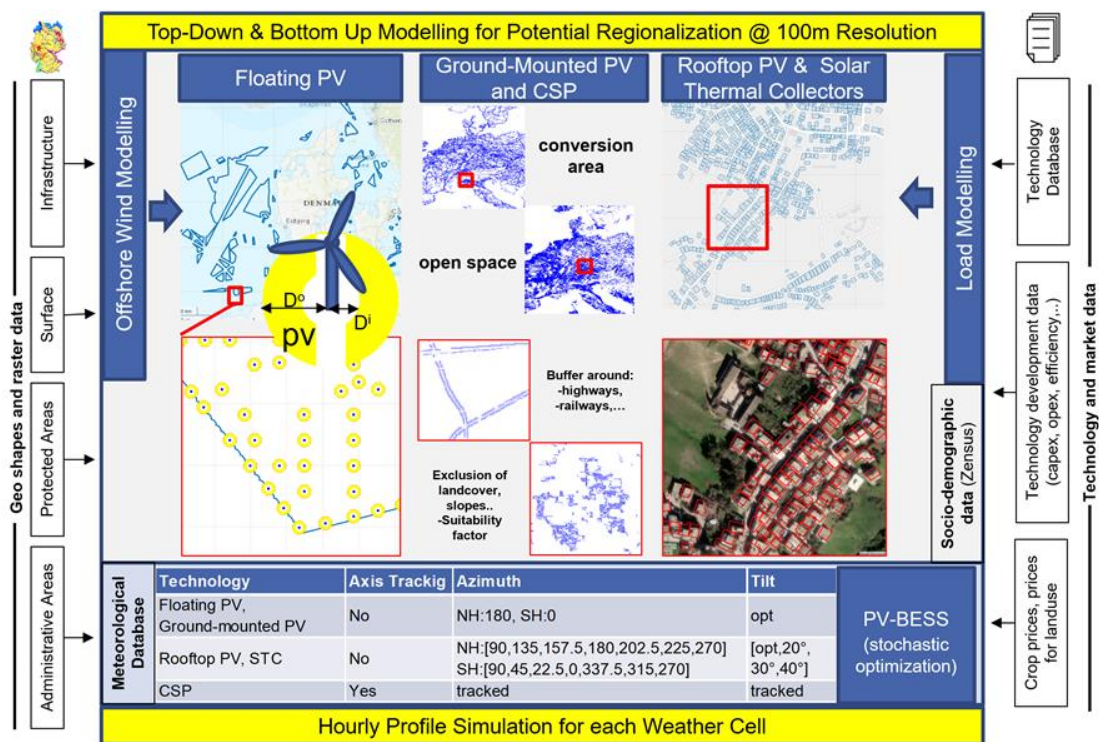


Figure 2.37: General approach for modelling solar energy conversion potentials

For ground mounted PV and CSP potentials basically the same approach as in the first step of the wind onshore potential analysis is used to determine the technical potential. In the default settings, mainly land that is covered by a forest or water as well as urban fabrics and naturally protected areas are excluded. From the topographic point of view altitudes above 2500m and steep slopes in general as well as slighter slopes which are not facing south-west to south-east on the northern hemisphere or in the northern direction in the southern hemisphere, are

excluded. Concerning the infrastructure exclusion, it should be noted that contrary to wind power, actually an explicit inclusion of conversion areas defined by a buffer around highway and railway is considered³⁹. A detailed list of the exclusion settings and the suitability factors can be found in the annex (fig. A.3), although it should be noted that for a practical application the settings are adjusted on a regional basis. Concerning the unit configuration, PERSEUS-gECT currently models an independent investment in solar conversion and storage technologies in the case of utility size PV and assumes a fixed relation between the collector size, the thermal storage and the power generator capacity for CSP units with a differentiation between parabolic through and power tower technologies. The modelling of both CSP technologies is rather simplified and differentiates only in the land-use factors and the economic parameters (Alami et al. 2023; Trieb et al. 2009) while the thermal heat profile is generated based on the same simplified parabolic through modelling approach which is applied in the open source model oemof.thermal (oemof developer group 2020).

The assessment of rooftop PV and STC potentials is based on a combination of a bottom up and top-down assessment of the ground floor area of residential and non-residential buildings and a following statistical calculation of the suitable roof area following (Mainzer et al. 2014). Based on census data available at a subnational level (NUTS3) for the number of dwellings in single, double and multi-family buildings and further statistics such as number of residents and average floor area, the approach for deriving building type specific ground floors in Germany, developed by (Mainzer et al. 2014) is adapted for other European countries in a first step. By multiplying the ground floor area with a utilization factor for each building type and roof type, which might be either flat or slated, the usable roof area is calculated. In previous own work (Slednev et al. 2017b) Corine land cover (CLC) data were taken in a last step for a further regionalization of the calculated building type and roof-type specific usable space for residential PV. While this approach gives an upper bound for the residential rooftop solar energy potential on a national level in Europe, an extension to other regions and sectors as well as the definition of a more precise local lower bound is part of PERSEUS-gECT. As illustrated in the following figure, OSM data allow an exact estimation of the ground floor area of buildings, if available, and therefore might be used for a lower estimation of the available roof area on a 100m resolution, considering that the completeness of the dataset is varying regionally. Additional to the global coverage, which allows a potential assessment outside of Europe, also the potential roof area of non-residential buildings might be estimated based on OSM building data, assuming that the utilization factor and distribution of the roof slopes corresponds to multi-family buildings.

³⁹ Dump sites are also included in the conversion area definition. Also, inactive former military areas could be considered in this context, such as former military used air fields.

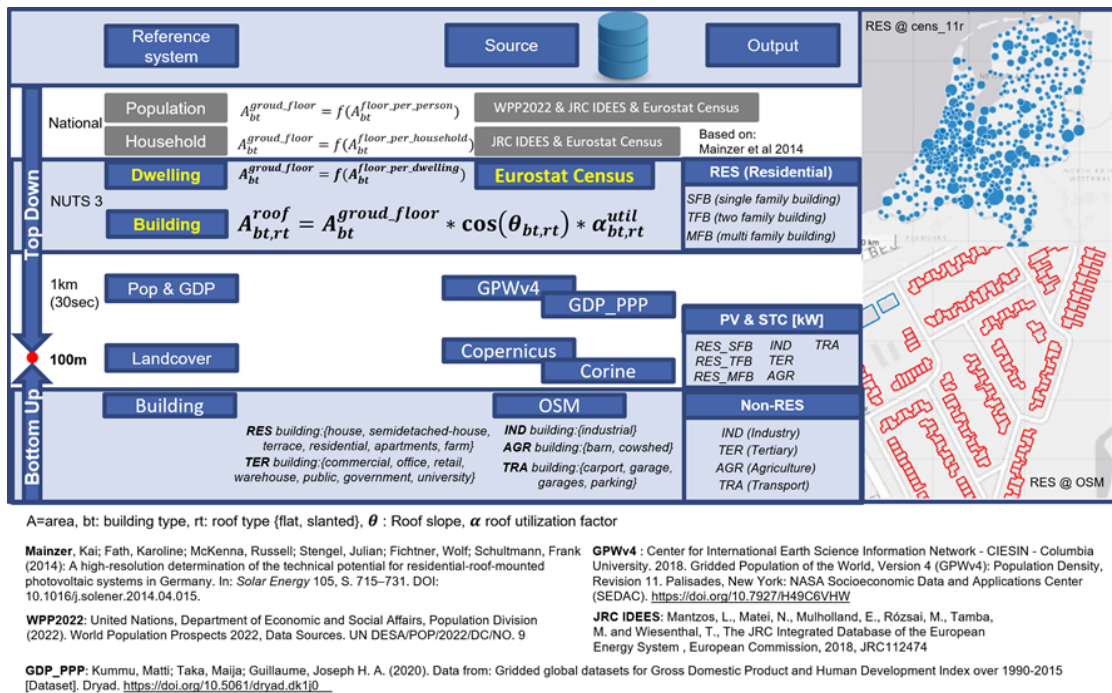


Figure 2.38: Approach for modelling PV and STC potentials

Outside of Europe, the bottom-up based estimation of the suitable residential roof area might be supplemented by a top-down approximation based on globally available population and GDP data in a 1 km grid and the projection of their national development. In the simplest case, the relation between population, household and dwellings on the one hand and the floor area on the other hand is taken from Europe and adjusted to non-European countries. In this context, the approach is quite similar to the one proposed in (Doorga et al. 2022). Subsequently, the data are regionalized based on overlaying the gridded population and GDP data sets with 100m resolved land cover data. By reducing the suitability factor, the higher uncertainty of this simple approximation of the residential rooftop solar energy potential outside of Europe might be taken into account. For non-residential buildings, which are not in the current focus of PERSEUS-gECT, only the OSM-based lower bound of the potential approximation is considered inside and outside of Europe. Overall, the potential for seven building classes and 2 roof types is computed on a 100m scale and combined with the calculated generation profiles for PV and STC for 7 azimuth and 4 tilt configurations in each weather cell. This technical potential is afterwards combined with a database of existing units in order to derive the remaining potential and aggregate within the supply area of grid-connected electricity nodes outside of Europe for each weather cell. Within Europe, an overlay of the electricity and gas supply system and the weather cells is taken to define the aggregation basis for rooftop solar energy. The reason is the consistency with the aggregation basis for final electricity demand processes, considering the endogenously modelled competition between heat pumps and gas boilers for heating applications. Furthermore, to define PV-BESS units, a consistent matching between rooftop PV potentials and the electricity demand is needed. In order to define the optimal dimensioning for such systems, in the default case a linear relation between the yearly electricity demand of a building type and

the PV and battery capacity is assumed following (Ruppert et al. 2019), where the derived data for dimensioning PV-BESS in Northern and Southern Germany in different investment periods is based on a prior optimization conducted with a model described in (Kaschub et al. 2016). In PERSEUS-gECT the north/south differentiation in the dimensioning is simply extended globally and depending on the available rooftop potential and final demand for electricity applications, the greenfield and brownfield potential for PV-BESS is computed. The reason for a fixed dimensioning of the PV-BESS components or for running a prior stochastic optimization is that a maximization of the self consumption is often a primary driver for the investment and dispatch decision for such a system. The described approach is illustrated in the following figure, starting with a regionalization of the PV-BESS systems based on a common 100m regional basis and a subsequential variable aggregation with respect to the grid topology and ending with a stochastic dynamic programming based dispatch optimization for deriving restrictions for the PV-BESS dispatch.

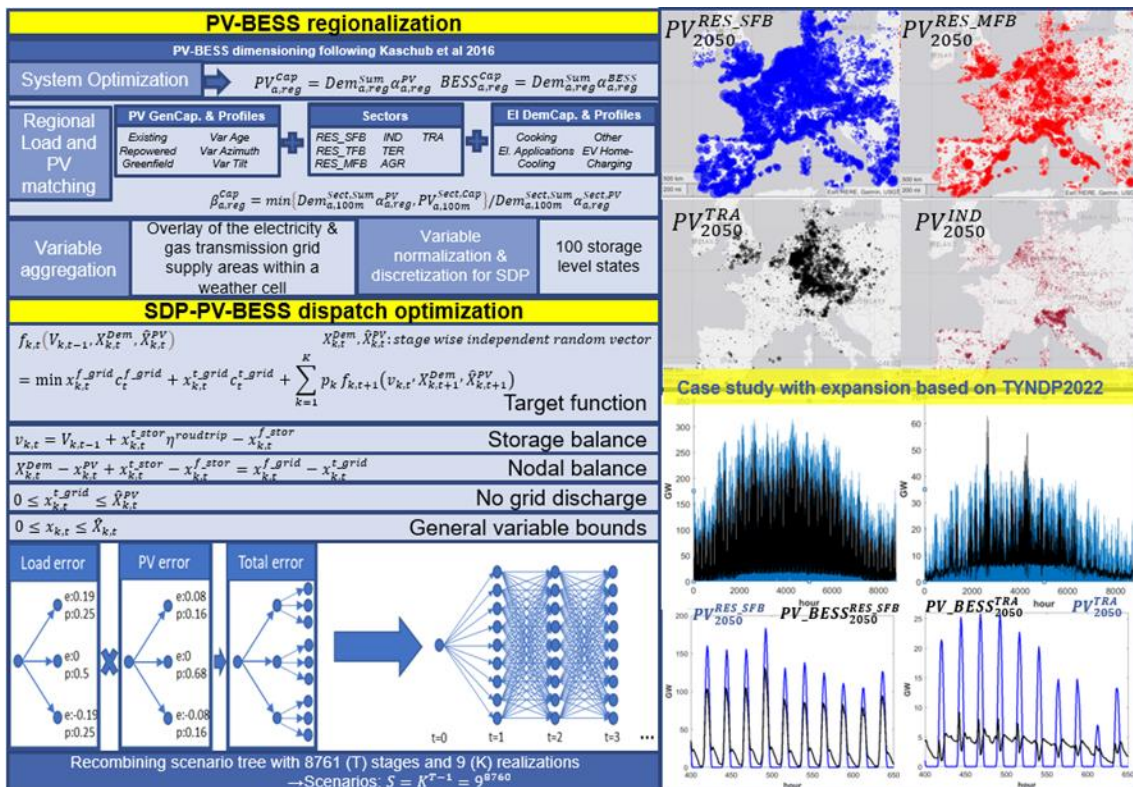


Figure 2.39: Approach for a PV-BESS regionalization and SDP-based dispatch optimization for deriving PV-BESS potentials and dispatch restrictions

In the context of the SDP pre-optimization, meaning prior to the actual PERSEUS-gECT run, it is assumed that the uncertainty about the sectoral demand and the associated available PV generation might be expressed through a stage wise independent random vector, as described in a previous work (Perau et al. 2021). Analogue to the case of wind energy, the regional potential (below the electricity and gas grid level) is afterwards split in three variables (one fixed and two

potentials) and the optimization is run for each investment period, sector and considered weather year. Although the SDP approach requires a discretization of the storage level state space for a quick solution, with 100 steps chosen in the default setting, it has the clear advantage of allowing a fast optimization over 9^{8760} scenarios, assuming an hourly optimization and a division of the probability space for the demand and PV profile in 3 bins. Considering that only for the European region the number of optimized systems is in general over 20000 for each potential type and sector, resulting in over 420000 problems per period and weather year, the fast and easy computation is a key advantage. Depending on the sector, subsequently specific regional bounds for the PV-BESS dispatch might be derived for the further integrated system optimization in PERSEUS-gECT. In the current example the illustrated summed PV-BESS dispatch⁴⁰ in Europe results in a peak shaving pattern for single family households and a partially rather flat dispatch on garages and carports, with the exception in the Easter and summer vacation traveling time, with a high simultaneity in the dispatch. The exemplary results shown in the previous figure are actually based on a prior allocation planning for rooftop PV similar to the described wind-onshore case, assuming that existing units are repowered after the end of their technical lifetime and that the remaining potential for meeting a yearly national capacity target (in this case based on the TYNDP2022) are allocated based on a metric which is not only based on the LCOE but considers sector specific weights which take the available potential, the GDP into account and considers potential sub-national targets or grid restrictions. Although it is also possible to run an optimal allocation planning, as described in (Slednev et al. 2018) considering an approximation of grid restrictions, it might be more favorable in this step to put a stronger focus on an equal sector specific distribution adjusted by the purchasing power. It should be kept in mind that this optional pre-allocation is just used for a definition of the variables and their bounds for a later endogenous expansion in PERSEUS-gECT. Especially for mature PV markets such as Germany, this is of great relevance as illustrated in the following figure based on the sorted LCOE of the potential greenfield units in 37 weather years. If the allocation of the existing units is ignored, a pure LCOE driven approach would lead to a clear regional dominated exploitation of the potentials starting in the sunnier south and ending in the northern part below the coastal regions.

⁴⁰ PV-BESS dispatch is defined shown here as the PV generation plus BESS generation minus BESS demand in an hour.

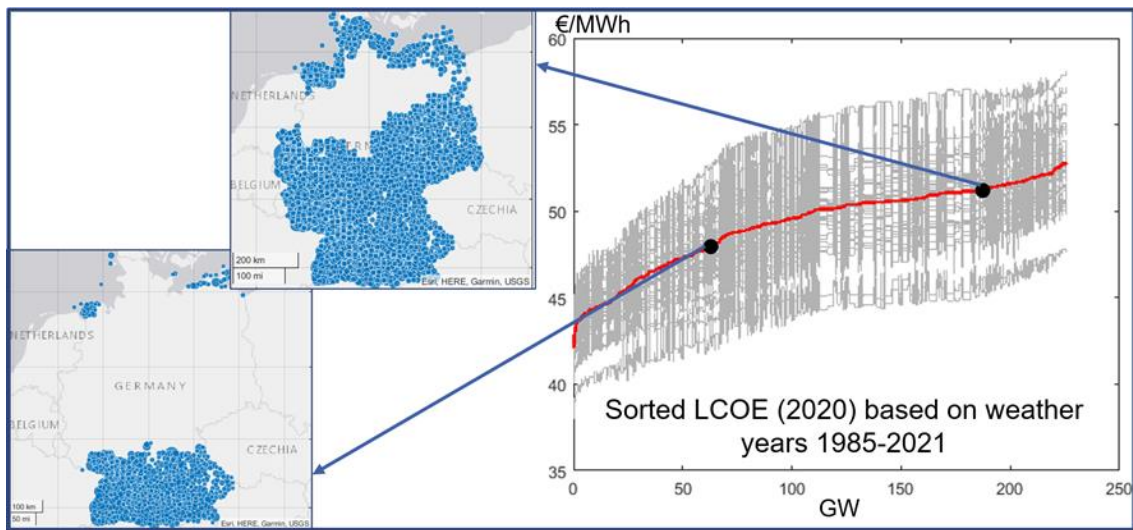


Figure 2.40: Implications of a pure LCOE based allocation of PV, illustrated for the case of Germany

To avoid such unrealistic results in the default settings a stronger weight is put on an equal exploitation of single-family building rooftop potential for example, besides of focusing on including all known units in a database. Currently this database includes over 2 Mio units based on various sources, which were mostly mentioned in the wind onshore chapter. Besides of Germany, where MaStr is a main source, open street map data play an important role in this context on a global scale and are extracted from a dump of the world database based on own scripts and matched with the other databases. Actually, OSM data provide a good starting point for setting up a database for wind and solar wind farms, as shown by (Dunnett et al. 2020) and based on the farm or module polygons they allow an estimation of the capacity, even if the actual capacity information is missing. However, it is clear that these data never reach the quality of national registers or commercial datasets and are therefore used only with conscious. Analogue to the case of parametrizing wind-turbines, missing data such as commissioning years and or capacities to meet reported national values are computed based on a prior allocation planning. In the current state, over 2 Mio. rooftop units and 25000 ground mounted units are included in the database and the computed LCOE of these units in the start year is shown in the following figure, taking into account an annual degradation of 0.75% since the individual commissioning year following (Jordan et al. 2016), the building type for rooftop as well as the individual orientation (tilt, azimuth). Missing data are parametrized analogue to (Slednev et al. 2017b), mainly based on the detailed information on commissioning years, location and orientation from the MaStr.

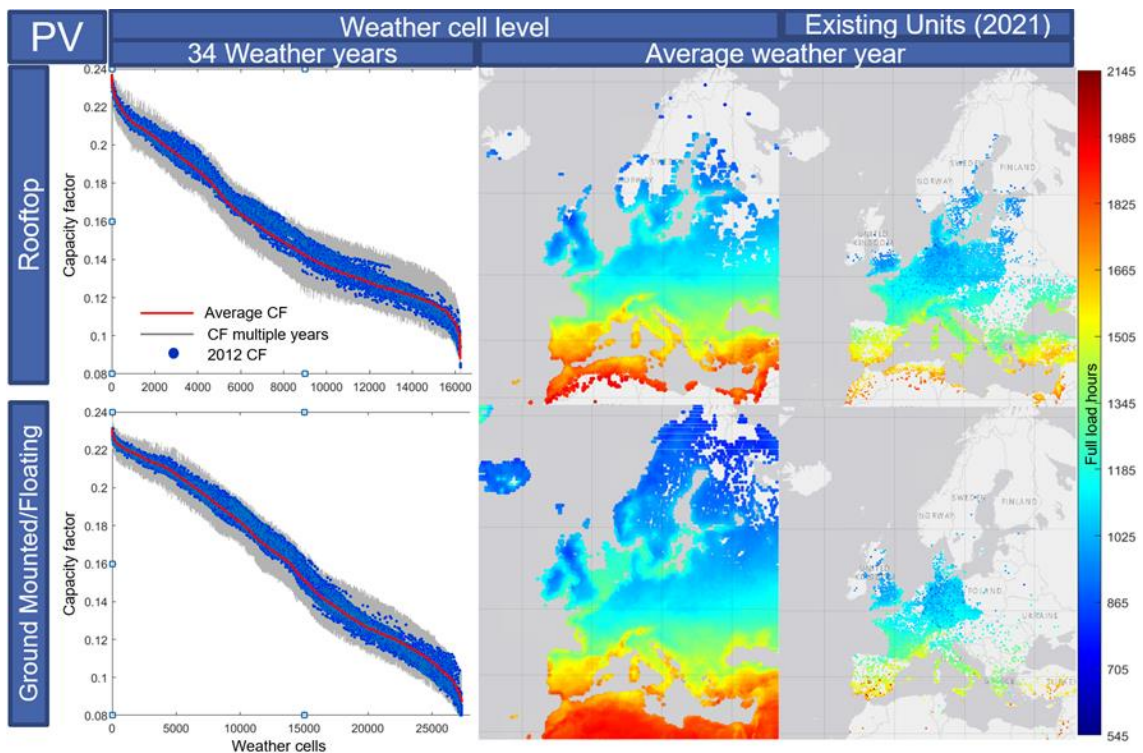


Figure 2.41: Comparison of the distribution of existing and potential ground mounted and rooftop PV units in Europe and North Africa based on the full load hours

Although the distribution of the capacity factors or full load hour shows a clear north/south pattern, which is prominent on the level of the weather cells, the annual variation of these factors, illustrated for Europe in the current figure and previously for Germany, is quite challenging from a system planning point of view. Especially within the same latitudinal zone, the rank of a weather cell, if sorted based on the long year average, might vary to a large degree, as shown by highlighting the weather year 2012. For the selection of a representative weather year for the expansion planning on the one hand and for the calculation of consistent PV and load profile, such as for PV-BESS, on the other hand, a fast profile modelling for solar energy on a (at least) hourly scale is crucial. In this context, the electricity or heat generation availability for each weather cell and process configuration needs to be calculated. Considering that only for the rooftop PV and SWH potential analysis of one investment period in the European region with over 16k weather cells, 28 tilt and azimuth configuration and 30 weather years at least 2.35×10^{10} hourly simulations are needed, in PERSEUS-gECT a rather pragmatic approach is chosen by adapting existing approaches and tools within an own MATLAB code with a focus on a fast computation. A correction of the bottom up modelled data based on measured irradiation data and generation outputs, as described in (Lorenz et al. 2011), is omitted, as well as a statistical calibration based on neural networks. As illustrated in the following figure, in the first step the irradiation on a tilted surface is computed based on an existing toolbox PVLIB developed at Sandia National Laboratories (Stein et al. 2016). While the same tool box is later on taken for computing the PV module performance, the performance calculation of solar thermal collectors relies on a

simple modelling of parabolic through and flat plate collectors following emof.thermal (oemof developer group 2020) and is written in MATLAB. The later toolbox is part of an open source python based energy model (Hilpert et al. 2018), of which only the modelling approach for calculating the thermal losses and the default parameters are considered.

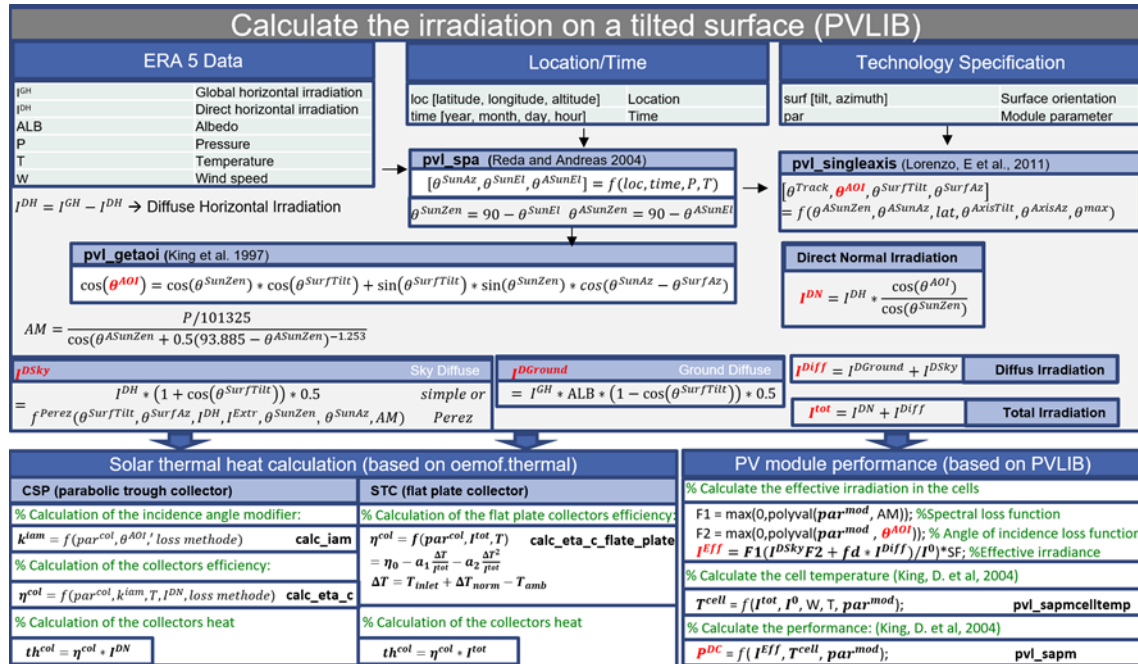


Figure 2.42: Approach for calculating solar thermal (CPS, flat plate collector) and PV profiles

Based on ERA 5 data, which are partially adjusted, such as the wind speed correction to the ground and roof level, in the first step for calculating the irradiation on a tilted surface, the location and time specific irradiation angles such as the sun azimuth (θ^{SunAz}), the sun elevation (θ^{SunEl}) and the apparent sun elevation (θ^{ASunEl}) are calculated. The calculation is based on an approach described in (Reda and Andreas 2004) and performed through the function `pvl_spa`. For units without an axis tracking, in the next step the angle between the surface normal and the sun beam vector (θ^{AOI}) is calculated following (Kratochvil et al. 2004). For collectors and modules with a single axis, tracking the approach of (Lorenzo et al. 2011) implemented in `pvl_singleaxis` is applied. Afterwards the direct normal irradiation might be simply calculated from the direct horizontal irradiation and the cosine of θ^{AOI} and θ^{SunZen} . For the diffuse part, the reflection on the ground and in the sky needs to be considered. In this context multiple models might be selected in PERSEUS-gECT based on PVLIB, which mainly differ in the way how the sky diffuse part is calculated while the ground diffuse is always simply modelled as a function of the albedo and the tilt angle of the surface. A comprehensive description of the models is provided by (Loutzenhiser et al. 2007). In the figure above the simple Isotropic sky model (Duffie and Beckman 2013) and the Perez model (Perez et al. 1990) are illustrated. Once the diffuse irradiation on the tilted surface is calculated and added to the direct irradiation, the total irradiation is known and the models which calculate the thermal efficiency or the PV module

performance are applied. For calculating the PV module performance, first the effective irradiation in the cells is calculated, taken into account soiling losses as well as spectral losses and incidence angle reflection losses based on a 5th order polynomial function which is module dependent. After the correction of the cell temperature, in the last step the 5 points of the PV modules I-V curve are calculated based on the Sandia PV Array Performance Model (Kratovichil et al. 2004), which allows a calculation of the DC performance. Finally, the inverter losses (4.5%) as well as all other losses, except of the degradation, such as additional losses including the deviations of the actual module efficiencies from data sheet information, mismatch between modules, ohmic cable losses, soiling, and deviation of inverter efficiencies from data sheet information, summing up to 9.5% following (Lorenz et al. 2011), are taken into account. The performance calculation of the solar thermal collectors also uses the computed solar radiation on the tilted surface as an input for a rather simple efficiency calculation described in `oemof.thermal`. For concentrated solar power (CSP), in the default settings a loss method based on (Janotte et al. 2014) is used for the calculation of the incidence angle modifier and the collector efficiency while an inlet temperature of 20° and a normal temperature difference of 10° is assumed for flat plate collectors. In both cases the modelling of a thermal storage and in case of CSP, of the power generating turbine, is implemented through separate processes in PERSEUS-gECT which uses the computed thermal heat as an inflow. In the default setting a solar multiple, which defines the ratio between the thermal power which is produced by the collectors field to the power block thermal nameplate capacity (Alami et al. 2023), of 2.4 and a thermal energy storage (TES) of 10 hours is assumed for CSP investment units. The dispatch of the TES, the power cycle or the potential direct use of heat for subsequent processes is modelled endogenously within the optimization. Analogue to RTPV units, the distribution of the tilt and azimuth angles for RTSWH are currently estimated from the known orientation of RTPV installations. Alternatively, country specific values might be specified, as the current database is significantly dominated by German units. Concerning the geographical coverage, Europe and the MENA are currently the main regions where RTPV and RTSWH are modelled while CSP investments are mainly considered as an option for MENA and the Southern part of Central Asia.

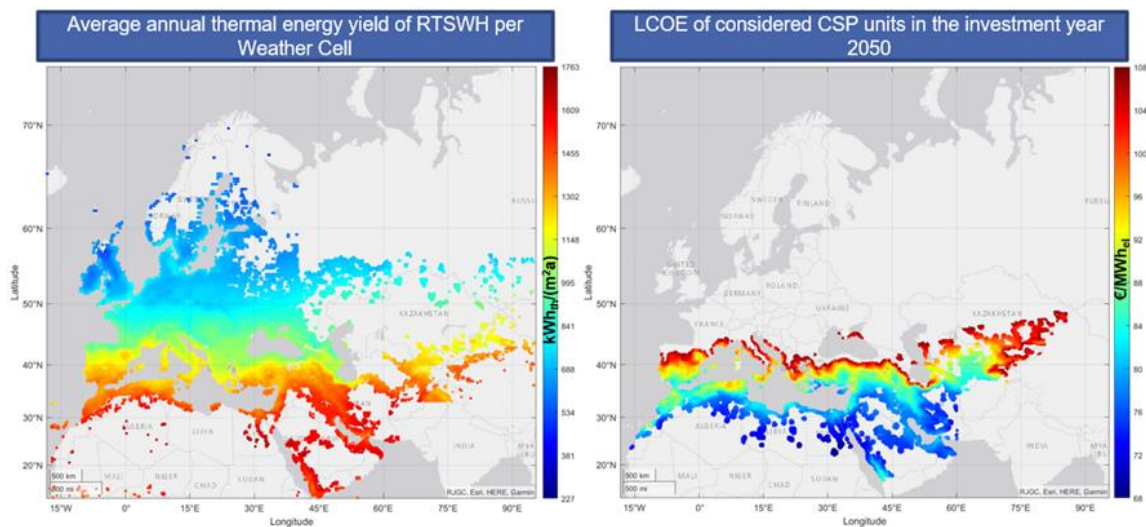


Figure 2.43: Distribution of considered solar thermal potentials in Europa, MENA and Central Asia with respect to the energy yield of RTSWH units (left) and the LCOE of CSP units (right)

Bioenergy and waste

In the current state of PERSEUS-gECT primarily existing conversion processes which produce heat and/or electricity from solid or gaseous biogenic energy carriers are taken into account. In this context the assessment of additional biomass potentials for the regional electricity and heat generation as well as for the further conversion to biogenic based energy carriers, such as biogas, is performed with the focus on deriving the remaining potential for processes which utilize forest, agricultural, industrial or residential biogenic residues with respect of existing bioenergy conversion processes in the transformation or final demand sector. The assessment of the primary energy potential of crops or stem wood for the production of first-generation biofuels is explicitly not part of the potential assessment and existing processes which utilize these biogenic energy carriers are balanced on their emission output but not with respect to the local or global (sustainable) potential for these energy carriers. The same applies for non-biogenic fueled CHP, EOP, or HOP waste processes, which utilize industrial or residential residues. In consequence, PERSEUS-gECT focuses on the regionalization of existing bioenergy and waste-based conversion processes on the one hand and on the other hand on the derivation of potentials for utilizing residues of the forest, agriculture, industry, residential or tertiary sector. A classification of bioenergy-based conversion processes based on their sustainability or in the context of the food or fuel trade-off is therefore not modelled endogenously but defined exogenously based on a scenario. Analogue to the solar energy potential assessment, the general approach is to combine a bottom-up and top-down analysis of the available biomass and waste potential on a 100m resolution in the first step. The considered primary energy sources in this step and their classification, which is largely based on the classification made in the s2biom project (B.S. Elbersen et al. 2017), is shown in the following figure:

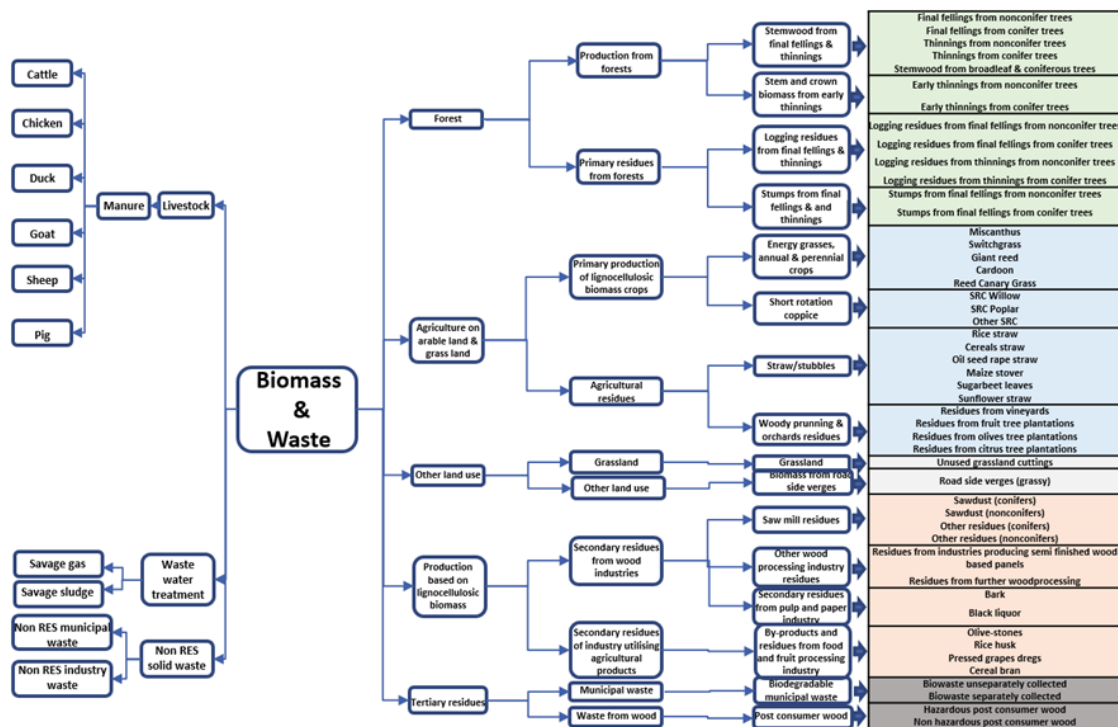


Figure 2.44: Considered resource classes for biomass and waste based conversion processes

For Europe, and including Ukraine and Turkey, the dry mass potentials and their road side cost of the forest and agricultural residues shown on the right side of the figure are taken from the s2biom project⁴¹ and regionalized from the NUTS 3 level to the base resolution of 100m based on Corine Land Cover data (for all biomass types) and population data (for the municipal waste) analog to the PV case. In this context the match between CLC data and the potential classes is provided in the fig. A.6. On a global scale, a rough estimation of the forest and agricultural residues following (Mainzer 2019) is applied based on the Copernicus land cover data and the match between the biomass source and the classes as illustrated in fig. A.7. Either used directly as stem wood or processed to straw bales, pellets, wood chips or cut to firewood, most sources on the right-hand side might be directly utilized in a solid state as an input for the energetic and non-energetic conversion in the transformation and final demand sector. For a subset of the resources, especially for straw and energy grasses, an anaerobic digestion to biogas is taken into account following (B.S. Elbersen et al. 2017). The default delivery form as well as the lower heating value of the solid biomasses considered in PERSEUS-gECT, their biogas yield as well as their CO₂ emission factors, latter one based on (Akagi et al. 2011), are depicted in fig. A.5. While the secondary residues of the forest and food producing industry as well as the biodegradable part of the solid waste collected from the tertiary sector are illustrated on the right-hand side, the

⁴¹ The goal of the project is the “Delivery of sustainable supply of non-food biomass to support a “resource-efficient” Bioeconomy in Europe” <https://research.wur.nl/en/projects/delivery-of-sustainable-supply-of-non-food-biomass-to-support-a-r/datasets/>

remaining residues such as the effluents of the livestock, which might be used for the biogas production as well as the potentials for producing sewage and landfill gas from the waste water treatment and the remaining waste, are shown on the left-hand side. Following the approach of (Scarlat et al. 2018) the potential to produce biogas from manure is calculated in PERSEUS-gECT based on a gridded dataset of the livestock which (Gilbert et al. 2018) generate with respect to the 2010 FAO livestock statistics. Based on land cover data, these potentials are further regionalized to a common 100m resolution prior to an aggregation for investment variables. For the variable definition the topology of district heating, gas and electricity networks is taken into account considering that the produced outputs heat, electricity and gas (biomethane after a subsequent upgrading step), require the corresponds injection nodes. The utilization of the remaining urban waste in solid or gaseous state is currently restricted to Europe and based on the heatmaps project (Scaramuzzino et al. 2019), which provide the unit resolved capacity of 24067 waste water treatment plants as well as the capacity of the municipal waste at NUST 3 resolution, which is subsequently regionalized. An overview of this first step of the potential assessment and the sources is provided in fig. A.4.

Once the biomass potential is defined in PERSEUS-gECT, it is reduced by the energetic and non-energetic demand of existing biomass-based conversion processes in the final demand and transformation sector. Assuming that the final demand of households, tertiary and industrial processes, which are described in a later point, should be covered by the identified regional sustainable biomass potentials, these balancing is modelled first. In this context a simple heuristic approach is applied, by iteratively extending the supply area for each consumer until the demand is covered. In the next step the same approach is applied to cover the average demand of biomass and waste fueled CHP, EOP, or HOP existing units. Analogue to the case of wind and solar energy, the database for existing and planned biomass and waste units is based on various sources which are matched and calibrated with respect to historical national statistics. In the current state, the focus is put on modelling the status quo of EOP and CHP with respect to the electricity generation from primary biomass production or of the utilization of primary, secondary or tertiary residues. As a consequence, heat only plants are missing in the current database and besides of municipal solid waste fuel units, the electricity generation is the dominant output of most existing process classes. As illustrated in the following figure, conversion processes in the transformation sector which utilize bioenergy or waste are differentiated in combustion processes for solids, gas or liquids.

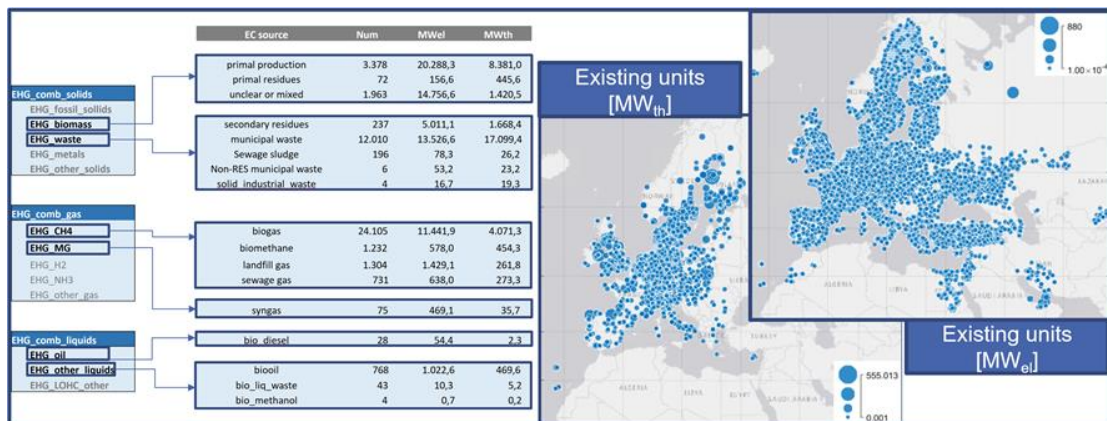


Figure 2.45: Structure, capacity and distribution of biomass and waste driven existing EHG units

In this context, only processes which are mainly operated based on a combustion of solid primary biomass products (mainly wood) or based on primary residues of the forest and agriculture sector by a combustion of wood-chips, pellets or straw bales, are labeled as “EHG_biomass” processes. Currently, this is the largest class in the database regarding the cumulated electrical capacity. Solid secondary residues of the forest and agriculture sector on the other hand are utilized in “EHG_waste” processes. In this class, also units combusting solid municipal waste, sewage sludge and industrial waste are included, with a clear dominance of municipal waste units regarding the number as well as the electrical and thermal output. Regarding the unit number, the database is dominated by gas combusting processes, with a dominance of methane rich gases from an anaerobic digestion, such as biogas, landfill and sewage gas or even biomethane over syngases which are derived from biomass or waste gasification processes. As already mentioned, the balancing of biofuels with respect to the regional sustainable biomass potentials is currently neglected. Nevertheless, the capacity of some of these units is included in the database and for their dispatch it is assumed that the fuel might be imported from an exogenous source.

Regarding the expansion planning, a replacement within the same technology (IC, GT, ST, CC, ORC, as CHP or EOP) and capacity class, but with adjusted techno-economic parameters at the end of lifetime, with and without a carbon capture, is considered as an investment option. For BECC (bioenergy with carbon capture) units, the availability of a gas node within the neighborhood is required. The investments into the CO₂ transport and storage infrastructure and their operation however are modelled endogenously within separate variables and excluded from the BECC CAPEX and OPEX. Assuming that the regional biomass resources are prioritized for replacement decisions, the remaining potential is calculated by excluding these biomass sources in addition to the fixed pre-allocation of biomass to final demand processes. Although these assumptions might seem quite strict, they are made in order to reduce the degree of freedom for modelling the investments into processes which utilize biomass in PERSEUS-gECT, considering that bioenergy conversion chains are highly resource specific and complex. Instead, the focus is laid on assessing the potential of the remaining biomass for producing synthetic natural gas, which might be injected into existing gas grids and on the combined electricity and heat production in regions without a gas infrastructure but with a local heat demand. In this context, it is

assumed that, depending on the biomass source, an anaerobic digestion process or a gasification process with a subsequent upgrading to methane is applied in case of an available gas grid node. For off-grid locations, the upgrading might be omitted and the biogas or syngas directly used as an input for a subsequent biogas CHP engine or a gas-turbine processes. Thus, the utilization of the remaining biomass potential is either modelled through EHG processes with an integrated OCP process for the gas production or through standalone OCP processes which injects methane at a sufficient purity level into a gas grid node. As illustrated in the following figure, a significant potential for biogenic methane is currently included in PERSEUS-gECT and it is assumed that at least in Europe a large part of this methane might be injected into the gas distribution system.

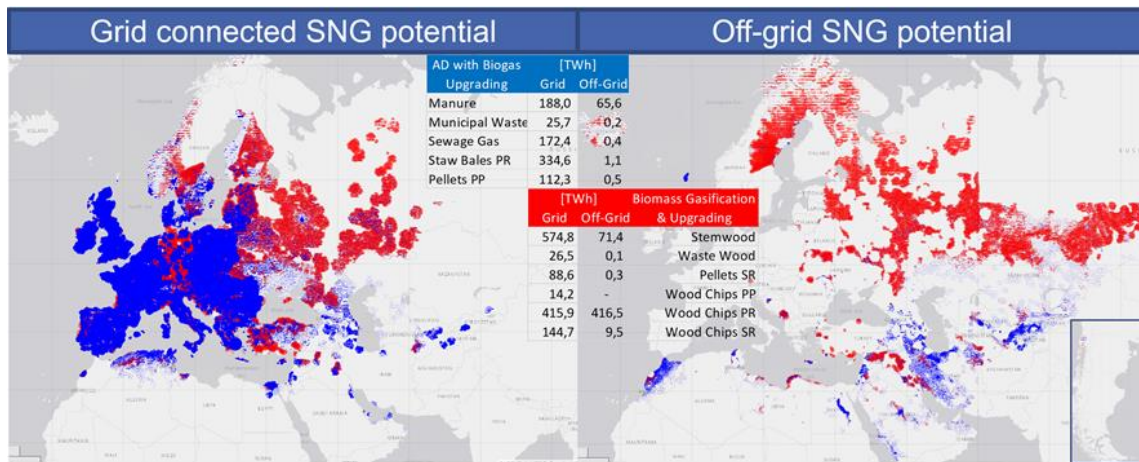


Figure 2.46: Distribution of the considered grid connected (left) and off-grid SNG potential

For the anaerobic digestion with a subsequent upgrading of the biogas, primary agricultural residues based on straw are the main biomass source, followed by manure, sewage and pelletized energy grasses. Besides of manure, which is also available at off grid locations in a significant amount, it is assumed that biomethane produced from most of these sources might be assigned to the next node of the gas transmission grid or an LNG port node based on the injection into an underlying, but not explicitly modelled, gas distribution grid. On the other hand, a significant share of the biomass gasification potentials are assumed to lie in the outskirts of the modelling region without an excess to the gas grid. Especially in Scandinavia and Russia large technical potentials from the utilization of the primary production from forest or from their residues is assumed. In Patagonia some off grid potentials are also considered, but with a negligible share compared to the overall potential. After a first aggregation into grid and off-grid, gasification and AD based conversion paths, 122890 units with weighted parameters of the various biomass sources (road side cost, energy density, emission factor etc.) are defined as investment variables per period. Afterwards this number might be further reduced in order to keep the problem size manageable. With a focus on the future operation of the energy system, a demand driven endogenous dispatch for existing, repowered and potential EHG and OCP based units which convert biomass is assumed. Depending on the scenario, however, upper and lower bounds on the dispatch might be specified based on weekly, monthly or yearly national historical dispatch data

for the bioenergy-based electricity generation. Depending on the region, in this context, monthly data of Eurostat or IEA or hourly data of the transparency platform of the ENTSO-E, aggregated to weekly values, and scaled to the monthly Eurostat values, are used.

Overall, the approach used for modelling biomass conversion chains is rather simple in PERSEUS-gECT, focusing on bioenergy, while relying partly on the regionalization of existing detailed studies and approaches in Europe and on a simple land use based estimation comparable to (Mainzer 2019) or (Bao et al. 2020) outside of Europe. Concerning the general literature in this context, a good overview is provided in (Bentsen and Felby 2012).

Hydro

In the current state of PERSEUS-gECT mainly existing and planned hydroelectric units are considered. Thus, there is a focus on a regional parameterization and grid connection of known capacities and a simple approximation of the inflow, storage and discharge restrictions, neglecting a detailed hydrological modelling. Based on various sources, including specific hydroelectric databases such as the JRC hydro power database⁴² and the Global Dam Tracker (GDAT) by (Zhang and Gu 2023) in addition to the already mentioned public national (MastR, BFE_WASTA⁴³,..) and international (OSM, GEM, OPDS, GPDB, etc.) and commercial (WEEP) power plant database sources, an own database has been created that is illustrated as follows:

⁴² European Commission, Joint Research Centre (JRC) (2019): JRC Hydro-power database. European Commission, Joint Research Centre (JRC) [Dataset] PID: <http://data.europa.eu/89h/52b00441-d3e0-44e0-8281-fda86a63546d>

⁴³ <http://www.bfe.admin.ch/geoinformation>

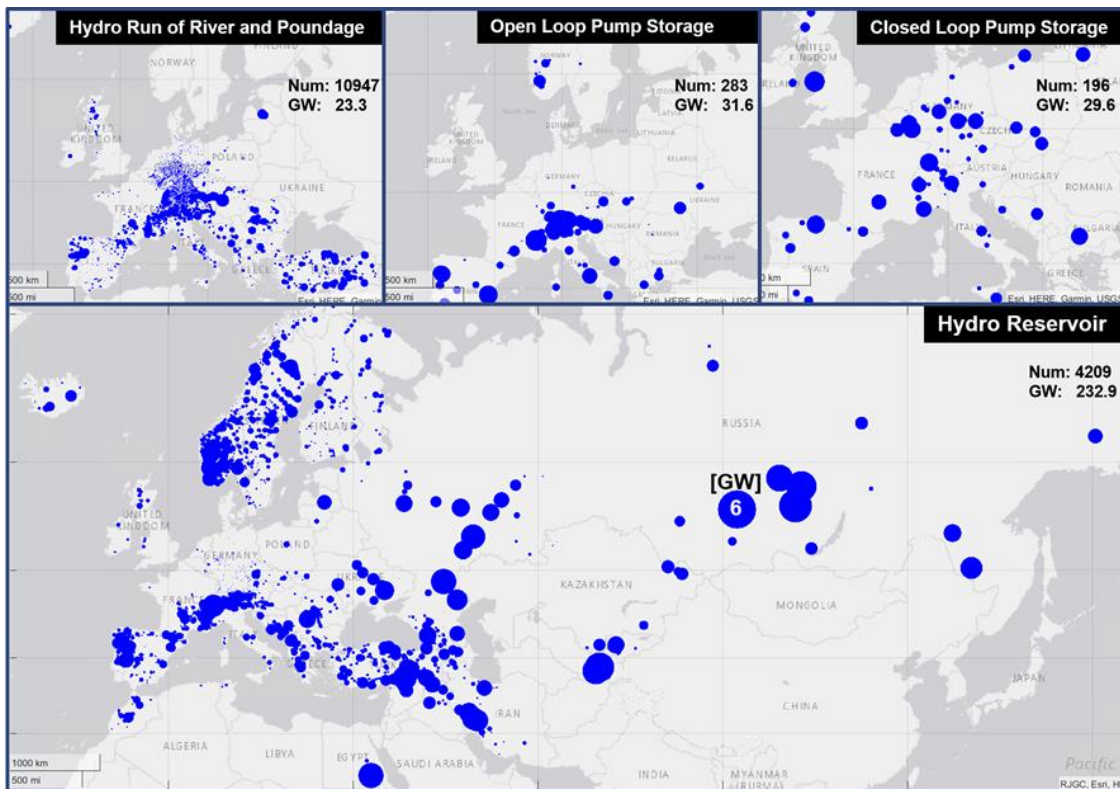


Figure 2.47: Distribution, number and capacity of hydro power units by type

Conventional reservoir power plants with a long-term (seasonal) storage of an upstream hydro inflow currently dominate the database regarding the installed electricity generation capacity. While many large units in this category and the current geographical scope are allocated in the successor states of the former Soviet Union, a large number is modelled in the Scandinavian countries. Existing reservoir storages in the modelled South American region are currently deactivated. Besides of reservoirs, the class of pure hydro power plants comprises run-of-river (ROR) and pondage hydro power plants, which are classified by limited or missing storage capabilities and a natural inflow. Although most of the existing units in the database belong to this category, their average capacity is rather small and most of the units are allocated at the foothills of alpine streams. Considering pump storages, a differentiation between open loop (PS^{ol}) and closed loop (PS^{cl}) units is made, depending on the availability (PS^{ol}) or unavailability (PS^{cl}) of a natural inflow into the storage. While the first ones, often referred to as mixed hydro power plants, are mainly allocated in the Alps and Southern Europe, the pure pump storages are distributed more equally across Europe. The storages, linked to the described pure or pumped hydro power plants, are shown in the following figure.

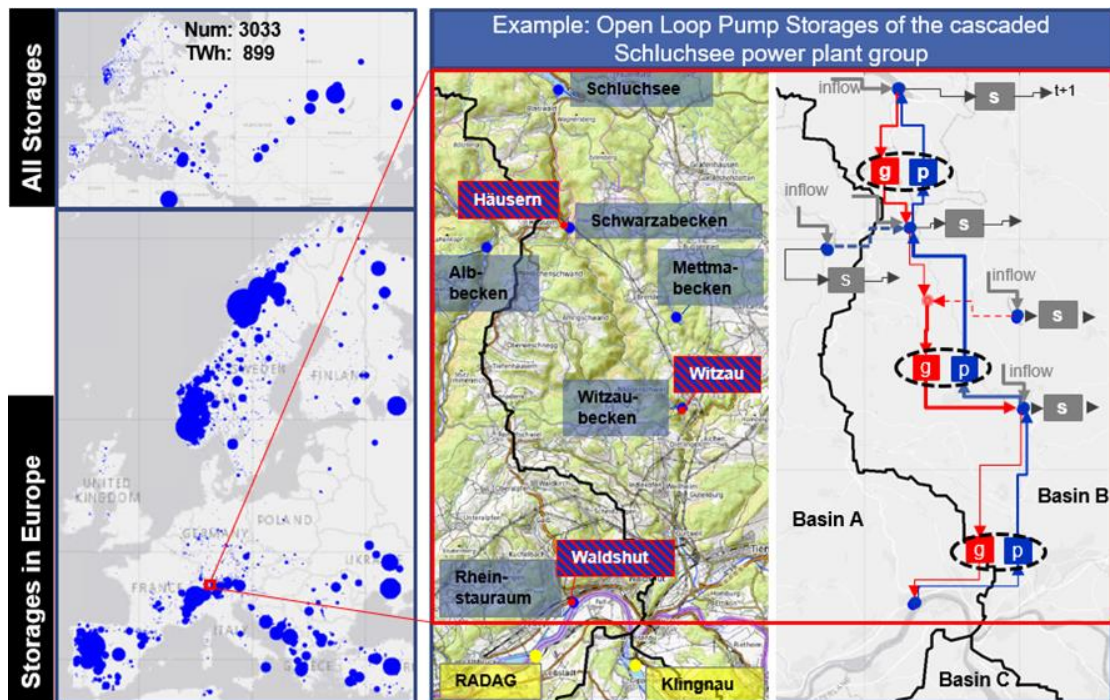


Figure 2.48: Allocation of considered hydro storages and the modelling of cascaded hydro power plants in PERSEUS-gECT

In general, different level of detail for modelling the interaction between uni- or bi-directional pumps and turbines and the associated lower and or upper storage volumes are considered in PERSEUS-gECT, following an approach described in (Ruppert et al. 2016). As illustrated based on the example of the Schluchsee power plant group in Germany, multiple storage processes in different river basins might be connected by a cascade of multiple generators, pump and flow processes over a significant distance. In the current state such a detailed modelling of cascading processes is however limited to specific power plant groups mainly in the alpine region and does not cover a complete hydrological system. In the example, the impact of the outflow to the Rhein river on the operation of the downstream (RADAG) or upstream (Klingnau⁴⁴) ROR and pondage hydro plants is thus neglected. Even the last storage of the cascaded system (“Rheinstauraum”), which is fed by the outflow of the lowest generator and serves as a source for the pumps of the Waldshut power plant, is currently neglected. To decrease the remaining complexity, furthermore different aggregation might be chosen besides of the bundling of parallel generators and pumps into one variable. In the simplest case all generators and pumps of a cascaded group are connected to one summed storage with summed natural inflows. Alternatively, potential equalizing reservoirs are ignored and the cascaded system is separated in

⁴⁴ Lies actually on the inflowing Aare in Switzerland

individual, non-connected subsystems consisting only of a storage and the directly connected downstream generators and pumps⁴⁵.

Concerning the natural inflow into pure hydro or pump storage units and the bounds for the storage volume, generation and pumping, a complex hydrological modelling is omitted. Instead, the hydro power modelling approach and the calculated data of the ENTSOE-E⁴⁶ which provides inflow and storage data based on the PAN European Climate Database (PECD) from 1982 to 2017 on a national level is regionalized to the single unit level in Europe. Outside of Europe, national statistics on the monthly or yearly hydro dispatch are used to approximate the inflow. In both cases unit specific historic dispatch information, based on the WRI Global Power Plant Database, are used for an adjustment on unit level. Additionally, an inflow approximation based on run-off data might be applied to generate unit specific inflow time series as shown in the following example.

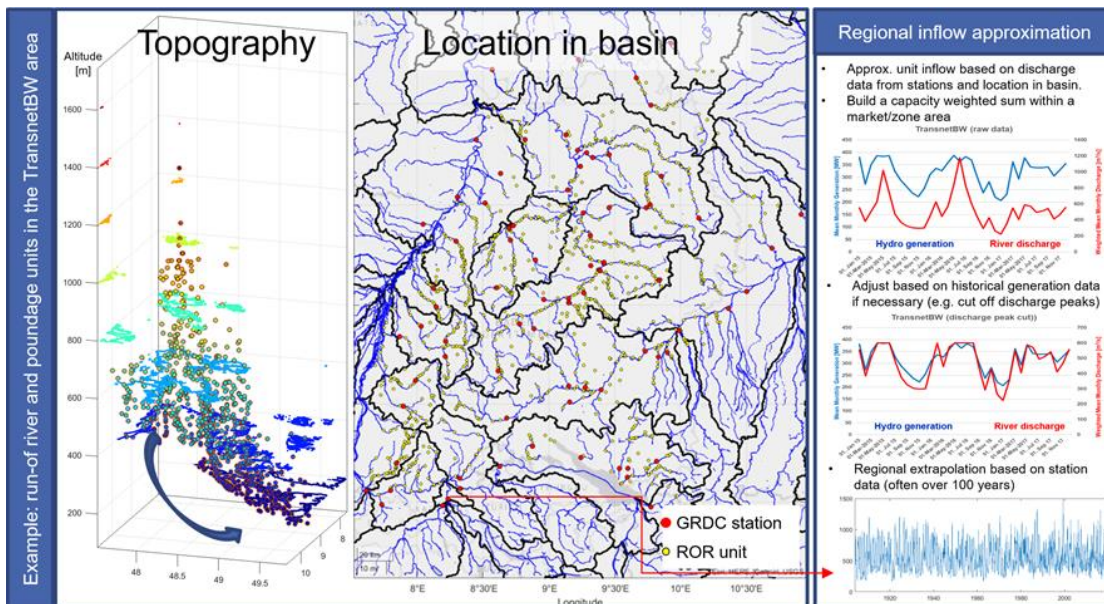


Figure 2.49: Approach for a regional inflow approximating for run-of-river and pondage units

The main motivation for this step lies in the heterogeneity of inflow patterns of different hydrological systems on a subnational level, as shown in the annex (fig. A.8) for the four German control zones. In this context the own run-off approximation on a unit level might be either scaled such that the capacity weighted sum matches the national/zonal target time series (based on

⁴⁵ In the current example the storages of the Albbecken and Mettmabecken might be neglected and three separate pump storages might be defined: Schluchsee+Häusern, Schwarzabecken+Witzau, Witzaubecken+Waldshut.

⁴⁶ https://eepublicdownloads.entsoe.eu/clean-documents/sdc-documents/MAF/2020/Hydro-power_Modelling_New_database_and_methodology_V1_0.pdf

the PECD or historical values) or applied to model the inflow for time periods with missing reference data. Currently, historic daily and monthly run-off data from the Global Runoff Data Centre (BfG - The GRDC 2023) database, which contains measured or calculated data from over 10000 gauging stations⁴⁷, are used to approximate the inflow considering the location of the station and the units within a river basin. As illustrated in the current example of ROR and Pounding plants in the TransnetBW control zone in the southwest of Germany, usually data from multiple stations are available within a sub-basin. By weighting the discharge data accordingly, the zonal data might be calculated and compared with a reference value. In the current example it is obvious that although a general linear correlation of 0.76 between the monthly mean hydro dispatch and the weighted mean station discharge might be observed, the dispatch becomes insensitive for discharges above a certain limit. Once the discharges are cut-off above this limit, the correlation increases to over 0.97. Considering that the GRDC data often cover a long time range, in the current example over 100 years, the inflow might be approximated for a long time horizon with an acceptable accuracy. Furthermore, these data are also available in non-European regions which are not covered by the PECD. In the future, a more advanced approach for fitting the data, like the machine learning based approach of the ENTSO-E, should be applied and combined with simulated run-off data from climate models. In this context the GRDC data might be used for calibrating the hydrological model, as done by (Burek and Smilovic 2022) in another context.

An endogenous expansion planning for hydro power in PERSEUS-gECT is currently only considered for closed loop pump hydro energy storages (PHES) based on the potentials identification and the cost calculation following (Stocks et al. 2021). As an adjustment applied to the potentials identified by the authors, the potential conflicting storage sites are excluded, which are to close the ones included in the own storage database or to the GDAT dam sites. The remaining potentials in the modelled Eurasian region sum up to a storage volume of 123 TWh in case that 6 hour storages with a volume of 2 GWh are considered, as illustrated in fig. A.9. However, it should be noted that in PERSEUS-gECT no focus is put on a detailed PHES expansion planning and that in the default settings this option is neglected.

Geothermal, marine and other

Although the list of existing and potential further non-conventional or fossil electricity and heat generation technologies in the transformation sector is still very large and their contribution might be significant, currently only existing or planned geothermal, marine and coal bed methane-based processes are modelled for the electricity generation. Especially for heating purposes, however, geothermal energy might provide a cheap local alternative for the replacement of fossil fueled heaters in residential building or in the district heating system (Miocic and Krecher 2022). An endogenous expansion planning for the exploitation of one part of this energy source is considered in PERSEUS-gECT, namely by modelling the investment in ground source

⁴⁷ According to Burek and Smilovic 2022 the GRDC database “offers the richest source of global river discharge data” compared to other available public databases.

heat pumps (GSHP) which utilize the shallow geo heating potential. The resource availability restrictions and the actual investment and dispatch restrictions for the GSHP, however, are currently modelled in a very simplified manner. On the one hand the model of the GSHP follows the approach of (Ruhnau et al. 2019)⁴⁸ and rather corresponds to a vertical heat pump as described by (Hou et al. 2022), considering that the ground temperature is taken from ERA 5 at 2 meter and increased by a constant factor. In the current version of PERSEUS-gECT, however, no potential analysis for such heat-pumps, which require a rather large space, is included. Instead, data from the hotmaps project (Pezzutto, S. et al 2018), which provide an upper bound for the bore hole extraction (BHE) based usage of the shallow geothermal potential, are utilized. These potentials are generated based on the G.POT tool as described in (Casasso and Sethi 2016) and are available with a 100 m resolution, assuming a borehole depth of 100m. The potential for extracting this energy source is assessed by overlaying this raster data with the considered residential and tertiary potentials, which are resolved at 100 m and are partially based on hotmaps heating and cooling density raster data. As illustrated in the following figure, this basically reduces the potential in Northern countries (as shown in right figure) and in densely populated cities (as shown by the difference between the left and middle figure). By overlaying the 100 resolved potentials with the electricity and gas supply areas and the weather cell, the final unit potential restrictions might be defined for the model. Therefore, the assumption is made, that the modelled GSHP units, which use the ground temperature from 2 meters, might be only expanded to a certain capacity limit, which is valid for BHE with a depth of 100 meter.

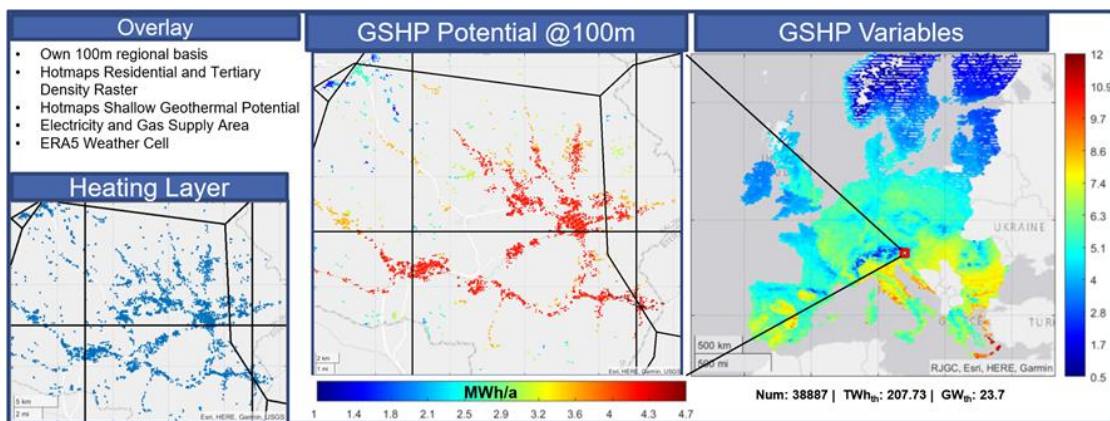


Figure 2.50: Approach for estimating the GSHP potential and defining GSHP variables

While the focus of PERSEUS-gECT does not lie on an exact modelling of GSHP systems, it should be kept in mind that this approximation provides just a simplified estimation of the GSHP potentials. In the literature, more accurate but computationally more expansive approaches might be found, for example by (Miocic and Krecher 2022) who analyze the GSHP potential in the German

⁴⁸ The approach is described in more detail in the section related to final demand processes.

federal state of Baden Württemberg, or of (Walch et al. 2022), were a detailed modelling approach for district heating and cooling based on BHE was developed.

For the considered existing remaining units, the number and the capacity is rather small compared to the other renewable or waste-based technologies. This is illustrated in the following figure. In specific regions, such as geothermal power in Iceland, however, these capacities might play a significant role.

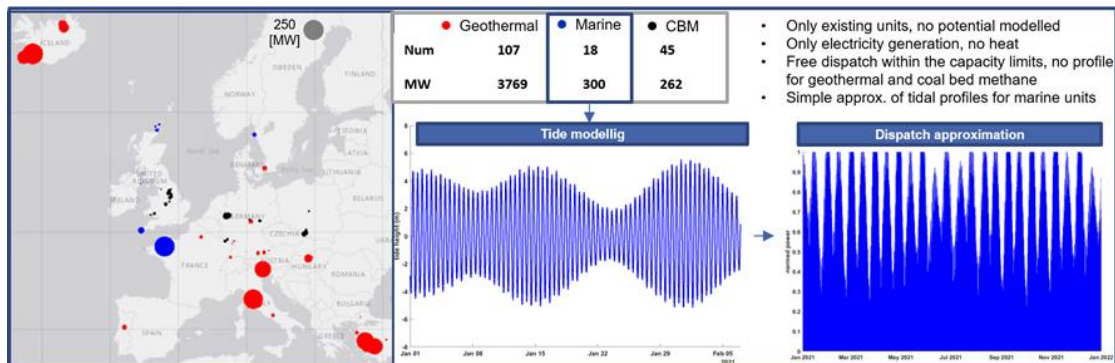


Figure 2.51: Distribution of considered geothermal, marine and CBM units and approach for a tidal profile modelling

Concerning the availability constraint of the dispatch of the units, no further restrictions apart from the unit capacity are assumed for geothermal and coal bedded methane. For the energy generation from marine source, which is differentiated into a tidal, wave and other ocean-based energy conversion, the profile also might be neglected due to the overall neglectable capacity. Considering that currently only the 240 MW Rance Tidal Power Station has any significant market share, a profile approximated from a tide modelling might be chosen. Based on the tidal modelling toolbox TDM3.0⁴⁹ and the global ocean tide model EOT20 from (Hart-Davis et al. 2021), first the tide heights are calculated and afterwards the profile is approximated from the gradient of the tide curve.

⁴⁹ Chad A. Greene, Svetlana Erofeeva, Laurie Padman, Susan Howard, Tyler Sutterley, and Gary Egbert (2023). The Tide Model Driver for MATLAB, version 3.0. <https://github.com/chadagreene/Tide-Model-Driver>.

2.4.3 Approach for defining resource availability constraints for the conversion of non-renewable energy carriers (existing & potential units and profiles)

Natural gas extraction

A detailed modelling of the natural gas extraction is currently not the focus of PERSEUS-gECT. A simplified approximation of the location and extraction cost of the current active and potential gas fields is nevertheless included. The goal is a more realistic modelling of the current and potential pipeline and shipping-based flow directions and quantities of natural gas and LNG. Based on the work of (Aguilera et al. 2009), the extraction cost and volumes per basin, following the USGS⁵⁰ classification, are estimated. A detailed description of the method for estimating the production cost of conventional and unconventional petroleum and a comparison with other approaches is proved by the author in (Aguilera 2014). Field specific extraction rates and location are added to this data based on the GEM database⁵¹ and finally the dataset is parametrized on a national level based on the bp Statistical Review of World Energy 2022⁵² for the gas production and the proven reserves. In the last step this information is matched with the nodes of the modelled gas system. The results of this approach are illustrated below.

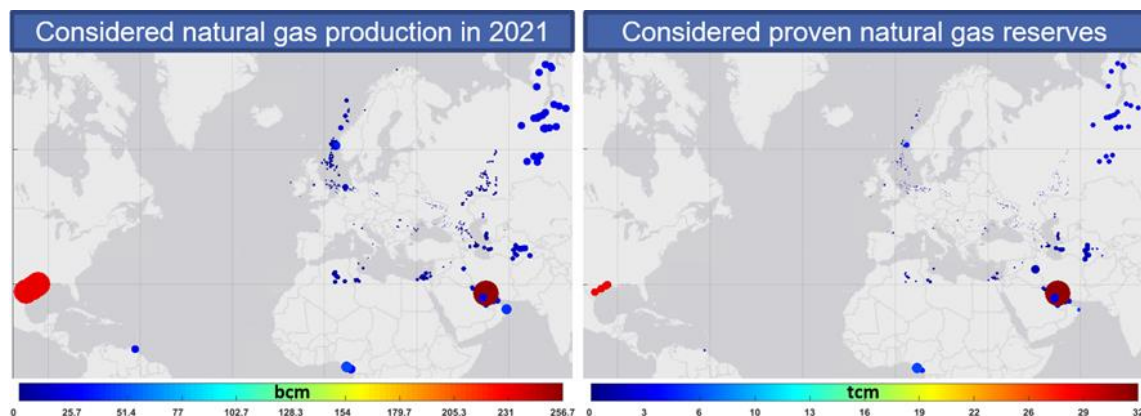


Figure 2.52: Distribution of modelled natural gas production units and their proven reserves

⁵⁰U.S. Geological Survey world petroleum assessment 2000: Description and results. U.S. Geological Survey world petroleum assessment 2000: Description and results (2000).

⁵¹ Additional USGS basins data on undiscovered gas fields and the shapes of existing and potential gas fields are also considered: U.S. Geological Survey World Conventional Resources Assessment Team (2012); Lujala et al. (2007).

⁵² <https://www.bp.com/content/dam/bp/business-sites/en/global/corporate/pdfs/energy-economics/statistical-review/bp-stats-review-2022-full-report.pdf>

Conventional electricity and heat generators

Based on a database, which is maintained at the IIP for several years and contains information from various sources⁵³, the following displayed structure between conversion technologies, displayed on the left, energy carriers in the middle and the overall processes classification on the right is chosen for modelling EHG units:

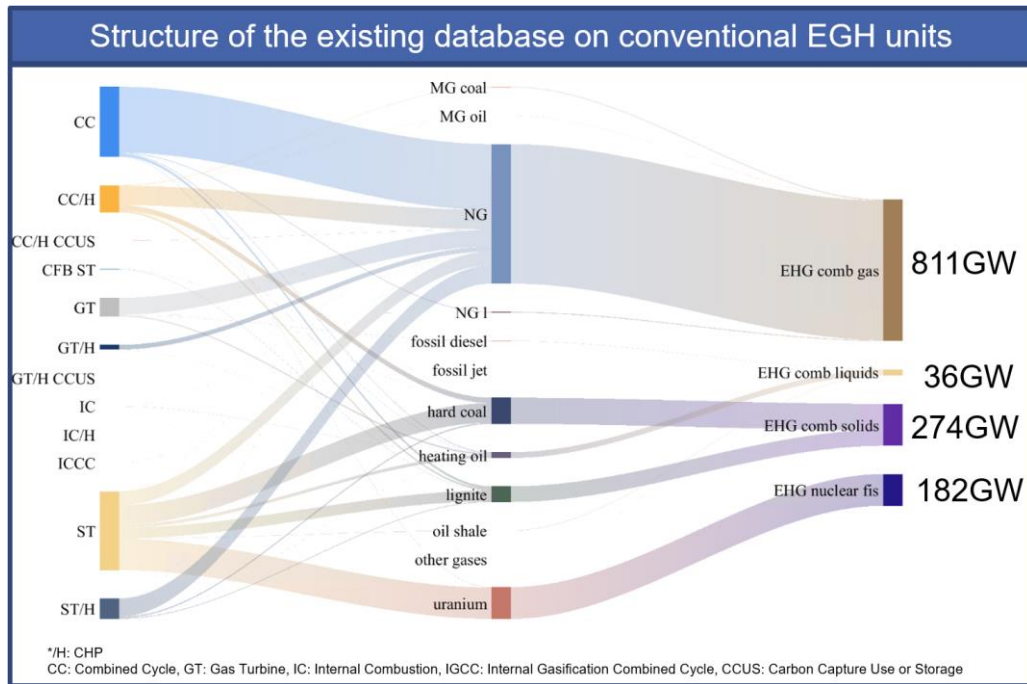


Figure 2.53: Structure and capacity of existing conventional EHG units

The majority of the currently included existing conventional thermal EHG units are thus combined cycle gas turbines which run on natural gas. In general, no further restrictions for the process availability, except of the installed unit capacity is considered in the default settings of PER-SEUS-gECT for the linear dispatch and expansion planning. For smaller problem instances, which focus on a subregion or subsector and in consequence allow the solution of a mixed integer linear problem formulation in an acceptable time, a min-up/min-down unit commitment problem (MUCP) following (Bendotti et al. 2018) is implemented. Besides of the general MUCP restrictions and a consideration of start-up cost, the number of cycles might be additionally restricted⁵⁴. In the default settings this option is however not considered.

⁵³ Mainly based on WEPP and various sources for planned projects or decommissioning such as GEM. Missing parameter such as the efficiency are estimated from a regression taking into account the commissioning date, technology and fuel.

⁵⁴ Alternatively, to a full MILP formulation, the MUCP might be activated with a relaxation on the binary variables.

In the context of a system optimization with the goal of asserting the capacity adequacy to a certain security of supply level, lower bounds for the capacity of dispatchable EHG units might be defined within PERSEUS-gECT on a national level. The utilized approach for this purpose (PERSEUS-ADQ) was initially developed within the DESK project and applied in the context of a security of supply analysis for the European electricity sector with a focus on southern Germany until 2050 (Hartel et al. 2019). The idea is to analyze the national balancing of an exogenously defined hourly electrical load with respect to the non-availability of flexible dispatchable thermal power plants and fluctuating renewables within multiple weather years and the option for a cross border balancing. In this context a Monte-Carlo based drawing of unplanned thermal power plant outages on top of the scheduled maintenance planning is performed for each hour of multiple weather years (usually 15 years) in order to take into account the simultaneous non-availability of thermal power plants, renewables and the weather dependent variation of the electrical load in multiple countries. As illustrated in the following figure, an iterative approach is chosen starting with a first investment period and a two-step allocation planning for minimizing the capacity coverage gap in each Monte-Carlo simulation.

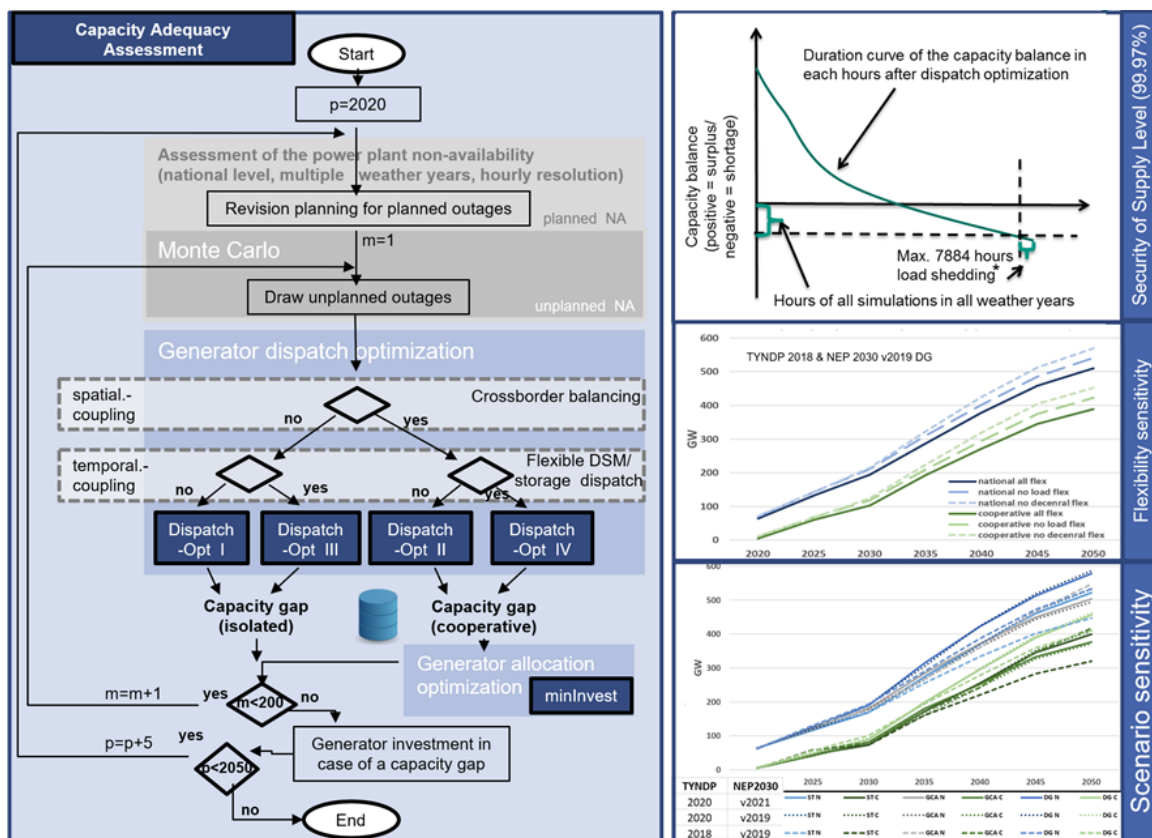


Figure 2.54: Approach for a capacity adequacy assessment in order to derive lower bounds for the expansion of dispatchable EHG units based on (Hartel et al. 2019)

Assuming that the security of supply should be ensured to a certain level (e.g., 99.97%), the national capacity gap is identified by running a dispatch optimization with a subsequent

generator allocation planning. In this context, the dispatch optimization is modelled as a simple linear hourly transport problem with a storage based modelling of central (utility scale batteries and PHES and seasonal hydro storages) and decentral (PV-BESS, DSM for EV and HP) flexibilities following the approach described in (Ruppert et al. 2019). Considering that for 15 weather years with an 8760 hour resolution the resulting problem would include a time coupling of 131400 hourly transport problems in each Monte-Carlo run, the problems are usually decoupled on a weekly or two-weekly basis. This means that the storage level of the first hour of each single or second week depends on the storage level of the last hour of the current or following week. The contribution of decentral and central time-coupled flexibilities to the security of supply during extreme weather events, which last for multiple hours, such as a two weeks' cold spell with low solar irradiation and wind speeds, is thus captured. Besides of the usual nodal balance and storage restriction, which are similar to those used in PERSEUS-gECT, additional constraints are defined in order to assert that each country priorly covers its own demand in case of a shortage. Although this optional condition results in a non-optimal system layout, it is introduced in order to avoid a load shedding in countries which otherwise could cover their demand. In a second step, the relevant hours for the national capacity gap definition of the single countries are identified based on the solution of the current and previous Monte-Carlo dispatch optimization run and a subsequent placement of a generic generator is optimized. Considering that the simultaneous generator unavailability on a European or larger scale is low and that each capacity addition in one country increases the security of supply in all other countries, this second step is introduced as an approximation of the actual allocation problem. The final capacity gap for each country corresponds to the negative part of the sorted national residual capacity balance curve after the spatial and temporal balancing in each Monte-Carlo run taking into account a certain number of hours of unserved load. For example, for 200 Monte-Carlo simulation with 15 weather years and 8760 hours per weather year, a security of supply level of 99.97% corresponds to 7884 hours with load shedding, as illustrated in the previous figure. The results are however highly sensitive regarding the considered flexibilities and the overall scenario framework as exemplary illustrated for the cumulated European capacity gap based on the TYNDP 2018 and TYNDP 2020 in combination with different versions of the German network development plan NEP 2030. In the context of PERSEUS-gECT, where the final electricity demand or the capacity of renewables is not fixed but might be adjusted endogenously, this means that the definition of lower bounds on the capacity expansion of dispatchable EHG units such as hydrogen fired gas-turbines should be considered with caution. One possibility is to apply an iterative approach, starting without or with low capacity requirements for asserting the security of supply in the first run of PERSEUS-gECT, followed by a capacity adequacy assessment based on PERSEUS-ADQ, in order to derive meaningful bounds. Such an iterative approach, with an initial PERSEUS-ADQ optimization followed by a generation expansion planning and a subsequent detailed dispatch optimization was already applied for different analyses of the future European power system (Ruppert et al. 2019; Slednev et al. 2021)

2.4.4 Approach for regionalizing final and useful energy demand and profiles

In the current state there is a specific focus on the regionalization of the final sectoral energy demand for the main energy carriers (electricity, fossil solids, oil, hydrogen, methane, biomass and district heat) based on a reference scenario. With a differentiation in the main classes for the energy use such as heating and cooling (space, process, water, steam), electrical appliances and the different transport modes for passengers and goods, the goal is to model an endogenous fuel switch within the same final energy conversion processes or the replacement of the initially defined heating and cooling process. In consequence, PERSEUS-gECT currently relies on an external energy scenario framework such as the TYNDP or the WEO as a starting base for defining a complete energy balance on a national level. While the non-energetic uses of the considered energy carriers and the yearly demand of electrical appliances, mobility services and specific industrial processes are fixed and might be only shifted intra-annual based on a demand side management process, heating and cooling processes are modelled endogenously but with a fixed useful energy demand. Savings from an improved insulation in the residential sector or a more efficient process which utilizes steam in the industry are therefore still exogenous quantities. In the following figure, the main parameters with their main sources are displayed, which are used for a regional parametrization of processes for the conversion of final energy to useful energy.

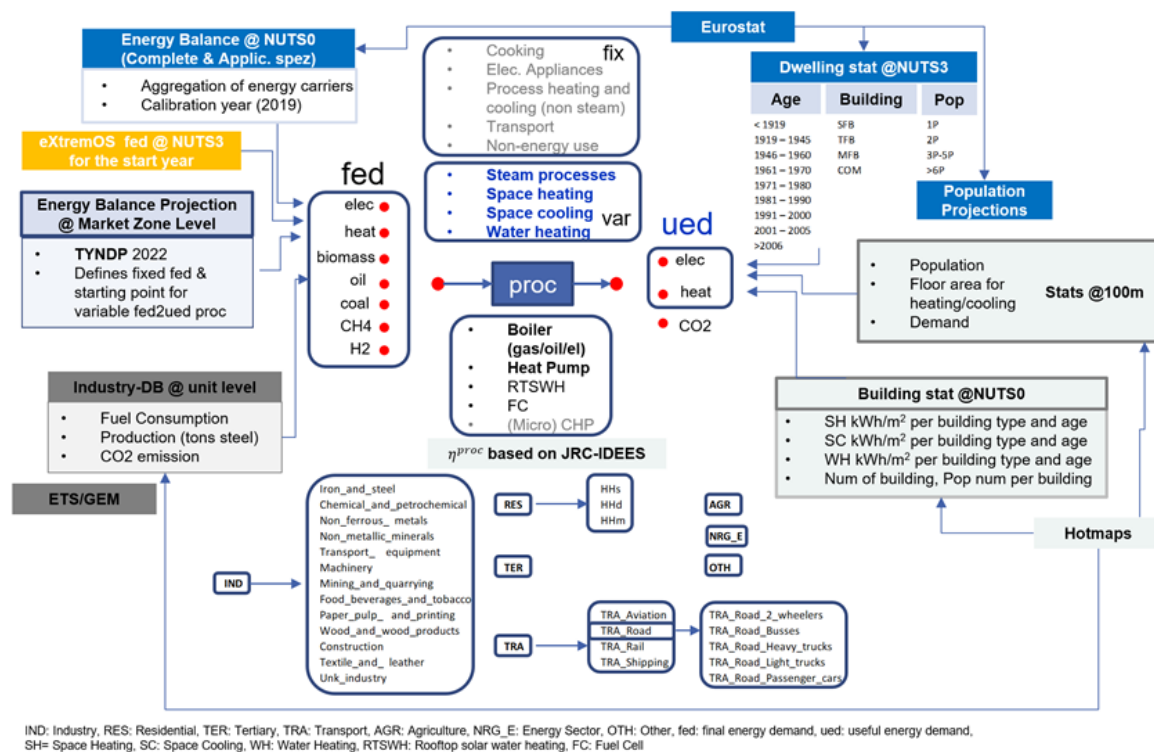


Figure 2.55: Approach for modelling the regional potential of final energy and useful energy demand conversion units

The overall idea for defining regional energy demand potentials and profiles is described next. Instead of a time-series based estimation of the final energy demand of a specific energy carrier (EC), the general idea is to split the sectoral demand into an energy carrier independent useful energy demand (ued) for heating and cooling purposes on the one hand and into the energy carrier dependent final energy demand (fed) for the remaining consumption processes on the other hand. Assuming that processes for generating steam for the industry and space heating (SH), space cooling (SC) and water heating (WH) in buildings are driven by the same ued profile and might be endogenously adjusted within PERSEUS-gECT by changing the conversion technology, the focus is put on modelling regional, highly resolved heating and cooling demands and profiles in the first step. Depending on the conversion efficiencies, which are based on yearly resolved historic national values from the JRC-IDEES database for non-heat pump processes and on hourly resolved simulated temperature dependent local performance coefficients (COP) for space and water heating and cooling processes with heat pumps, the EC dependent demands might be calculated in the second step. Starting from a complete energy balance based on a national level for a historic year and the sector and application specific demands for energy carriers of all fixed (e.g., cooking, electrical appliances) and variable (e.g. SH, SC, WH) processes, the general approach is to calibrate the model in a way such that regional supply potentials, NUTS 3 resolved dwelling statistics and national building statistics might be matched with regards to the local landcover and settlement data. Based on a common regional basis with a 100 resolution, which is also used for modelling primary energy potentials for solar or geothermal energy, in the first step the heating and cooling demand in buildings is calculated. This is done by combining raster data from the hotmaps database concerning the heated and cooled floor area with national building statistics concerning the building and age type specific heating and cooling demands, also taken from the same database and the Census 2011 based dwelling statistics concerning the age, building type and occupancy on a NUTS 3 level. As the population is available on all levels in all sources, in the first step this parameter is fitted such that the numbers match, and afterwards the SH, SC and WH ued is calculated on a 100 resolution for all building, age and population classes and adjusted to the statistically known parameters on a national level. Considering that the different data statistics or values usually don't match, first the population and demand on a NUTS 3 level is fit and afterwards on the actual regional 100m level. This is done by solving multiple quadratic optimization problems which usually minimize the squared deviation of one or more parameters modelled as regionally resolved variable (e.g., population, energy) to the regional reference value (e.g., on NUTS 3 or pixel level) subject to exactly matching with national reference values of the same or a derived parameter, such as the number or buildings, the total population or the energy. Once the ued is known at this lowest spatial level, the local final energy demands for all modelled energy carriers in the reference year, which is currently 2019, are calculated, taken into account the local resource and infrastructure availability and the target values from national statistics. Besides of considering the local potentials of renewable heat sources or of a gas grid connection for methane or hydrogen, in this step the focus is on analyzing the potential or existing supply of heat from district heating grids. This is done by performing a layout optimization for generic district heating grids with a high spatial resolution, considering the location of known heat sources such as CHP units or potential ones,

which will be described at a later point. After the district heating demand of the residential and tertiary sector is defined, the consumption of derived heat in the industry is modelled. This is done either from an auto-production of hot water and steam and injection into an own heat distribution on the plant side or from the public grid. In the first step, this is performed for large consumers, for example from the chemical or paper and pulp producing industry, on a unit basis. The remaining demand is distributed on the regionalized industrial heat demand of smaller units. In this context the industrial heat demand was previously derived by matching the sectoral fed from national statistics to the known or derived demand of the used industrial database of large consumers, which is also taken from hotmaps or GEM and are largely based on the European emission trading system (ETS). The remaining industrial demand was afterwards distributed based on landcover data and downscaled gridded GDP data (from 1 km to 100m) with a 100 resolution on the one hand and employment data in the industry sectors on NUTS 2 level on the other hand. Contrary to residential and tertiary consumers, a differentiation into industrial non-heating related sectoral processes such as electrical appliances and the non-energy use and heating processes was therefore not considered in the first step of the regionalization. This differentiation in the regionalization is also ignored for the remaining sectors such as the transport sector, the agricultural sector and the demand of the energy sector. In these sectors, the final energy demand for a specific fuel in the reference year is considered as the key for the regionalization. Based on values for 2020 taken from the eXtremOS project on the one hand and other further statistics on the other hand, the demands are regionalized. For the transport sector, which is the only relevant remaining sector, the regionalization of the existing final energy demand is dominated by liquids. The Regionalization is additionally either based on the length of the infrastructure (rail, road), the transported freight weight or the passenger number at the nodes (aviation, shipping) or the registered vehicles per type (road) from statistics on NUTS2, NUTS3, city or nodal level or from the transport graph. For agriculture, the biomass potentials from manure and crop residues combined with OSM data on farms are used as a regionalization key. In the energy sector, only refineries taken from the ETS database are used and modelled analogue to the industry and are regionalized. All other consumers of the energy sector, such as liquification/regasification plants and the compressors for natural gas, are not included in this section but modelled as endogenous OCP processes.

Finally, only the remaining non-heating/cooling related demands of the residential and the tertiary sector need to be regionalized, which mainly include the demand of electricity appliances and for cooking. Here the population and the floor area (and GDP for tertiary) on a 100m resolution is used as an approximation for the regionalization of the residual values, which are derived after subtraction the heating/cooling demand from the energy carrier resolved fed data of eXtremOS on NUTS3 level. Such a simplified approach is less detailed, but allows a simple regionalization of these heterogeneous demands including large electrical appliances such as a fridge, oven, washing machine, dry cleaner, etc., or lightning and itc appliances. This approach reflects a more detailed modelling of heating/cooling related processes and a very simplified approximation of the remaining processes. Based on the residual to the eXtremOS, data is also applied for modelling the demand profiles in multiple sectors.

In general, the calculation of the demand profiles combines different sector specific standard load profile (SLP) based approaches which are either taken from the literature (BDEW, SWM) or approximated from time series. Analogue to the differentiation in the energy regionalization, profiles for three categories are modelled: (i) the residential and tertiary space heating/cooling and hot water demand, (ii) the industrial steam and other process heat demand and (iii) the remaining sectoral for non-heating and cooling applications. For the industrial low enthalpy heat, a weighted average of the tertiary space heating/water heating and space cooling profile is assumed. In this context SLP and time series data from different sources such as from the hotmaps and eXtremOS project or from BDEW and SWM are taken and combined with source and sink temperature specific efficiencies of specific conversion processes, such as heat pumps in each weather cell with potential demand in the modelled region. For modelling the heat-pump efficiency, either the more advanced approach following (Ruhnau et al. 2019) or the simple Carnot and quality grade based modelling of heat pumps and chillers following emof.thermal (oemof developer group 2020) is considered while a static country, sector and fuel specific efficiency for boilers (combustion, electric) following the JRC-IDEES database is assumed. In the following figure the approach is illustrated. It is implemented in MATLAB and applied for calculating the hourly profiles in each relevant cell of the ERA 5 weather database for the weather years since 1985. In this context When2Heat references to the approach of (Ruhnau et al. 2019) and includes the BDEW SLP based approach for calculating heating demands.

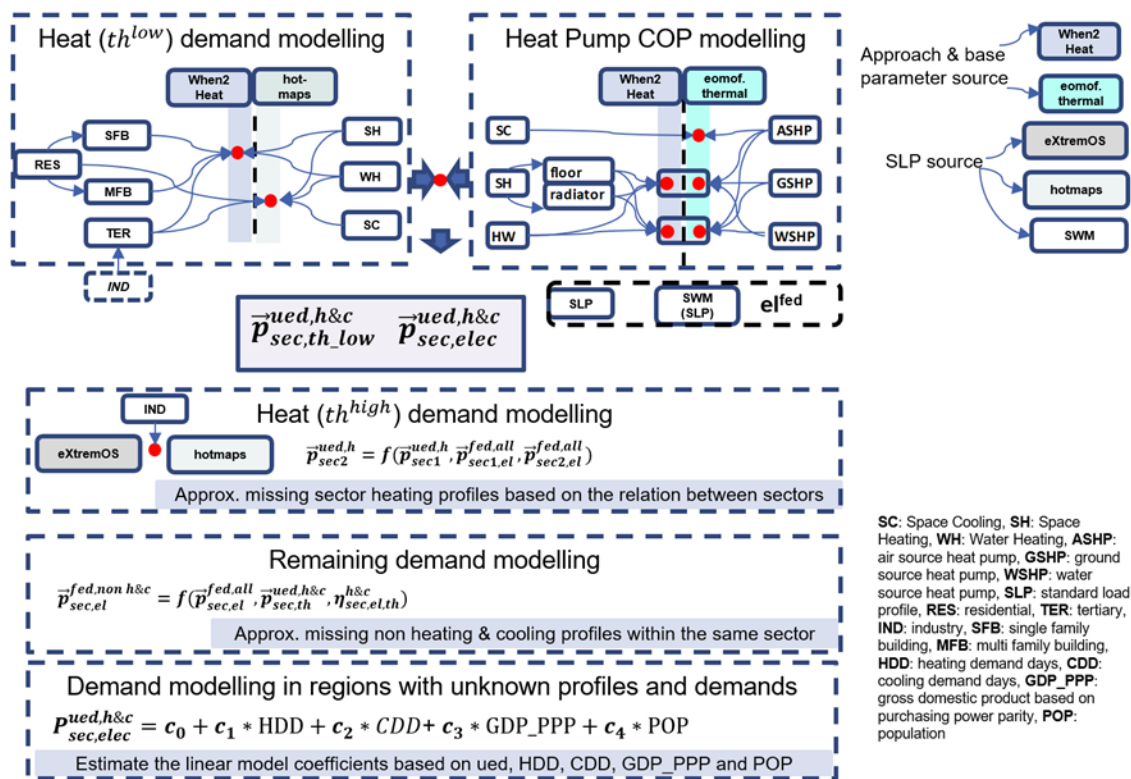


Figure 2.56: Approach for modelling low and high-temperature heating demand profiles

For the low enthalpy heat, currently multiple approaches are implemented and might be combined for calculating a profile for a process. For calculating the fed profile of heat pumps in the residential sector for space heating, multiple options are implemented and tested. Either the SWM based SLP approach might be applied or the ued for SH is first calculated based on the When2Heat or hotmaps approach (for SFB and MFB or for all residential buildings) and is later on divided by the hourly adjusted conversion efficiency of the system. This depends on the floor or radiator based heating system, the heat pump technology (ASHP, GSHP, WSHP) and the chosen heat pump model (When2Heat or eomof.thermal). In the default settings of PERSEUS-gECT the adjusted reference temperature is calculated based on the SWM approach and applied for selecting the daily SLP based on hotmaps. Afterwards, a capacity weighted average of the currently or projected installed heat pumps technologies, which are modelled following (Ruhnau et al. 2019), is chosen depending on the local demand and supply potentials. First it is chosen at the considered common spatial basis, resolved at 100m, and afterwards aggregated to the overlay of the covered areas of the gas, electricity and ERA5 nodes. The consideration of the time-of-use specific demand shift between different countries is applied following the simple approach of hotmaps. The hotmaps database is also the main source for defining high temperature heating profiles for the industry based on the given sectoral SLP on a national level. The sectoral coverage is however less complete than the hourly industry time series provided by eXtremOS, although the later source is only available for Germany and for a specific year without a differentiation of the conversion applications. By combining both sources, sectoral SLP on a national level for the high temperature heating demand are approximated. If for example the ued heating profile of the iron and steel sector is known but not that of non-ferrous metals on the one hand, while the total fed profile for electricity (excluding low enthalpy heat) is known for both parameters, the missing heating profile might be approximated. It is assumed that the structural difference between the electricity demand for the iron and steel production and the non-ferrous metals production also translates to the heating demand, which is a main driver for the energetic use of energy carriers in this sector. Once the high and low temperature heating and cooling profiles in all sectors are parametrized, the remaining sector and fuel specific profiles are approximated based on the definition of new SLPs from the residual of the eXtremOS time series and the own modelled demands. Overall, this approach requires multiple statistics fuel and sector specific parameters which are derived from Eurostat and the JRC IDESS database. Due to the data availability, the previously described detailed modelling of the demand is currently limited to countries which are covered by the Eurostat statistics. Besides of countries of the European Union, this applies with varying degree of detail also to Norway, Switzerland, Iceland, UK, Ukraine, Moldova, Turkey and Georgia as well as all Balkan countries. For the remaining countries the general idea is to estimate the demand based on the regional relation between demand, cooling and heating degree days (CDD, HDD), the population and the gross-domestic product based on purchasing power parity (GDP_PPP). Next to the sectoral demand, all other data are available or calculated on a 100 m resolution for multiple historical years. After aggregation of these parameters to the default variable resolution for heating applications in PERSEUS-gECT, defined by the overlay of the electricity and gas supply area and weather cell grid, in the first step the linear coefficients are estimated in the extended European region based on

the period from 2010 till 2021. Depending on the sector and ignoring district heating (as DH is neglected outside of Europe), this includes 20,000 to 60,000 variables for one year. Afterwards this model is applied to the non-European countries and fitted based on the yearly national final demand for an energy carrier. While currently yearly national data from eia are used, a further adjustment based on monthly net electricity demand (calculated from the cumulated generation with respect to storage demands, grid losses and exchange) and data based on iea could also possibly be used. However, it should be mentioned that a detailed demand modelling outside of the extended European region is currently not the focus of PERSEUS-gECT. It is assumed that such a simple statistical model in combination with the unit-based modelling of some large consumers (e.g., steel plants from the database) provides an acceptable approximation of the electricity grid loads. Although a calculation of the remaining demands, for example for solids and liquids, is also possible, in PERSEUS-gECT they are currently neglected outside of Europe.

Overall, the demand modelling in PERSEUS-gECT is just a means to an end, with the goal of defining fed profiles for fixed demand for non-heating related processes and ued profiles for heating and cooling demand, where the conversion unit might be endogenously adjusted. For this purpose existing approaches and databases are combined and in consequence the level of detail is comparable to other approaches such as open-ego (Büttner et al. 2022) or When2Heat (Ruhnau et al. 2019). Besides of hotmaps, which is used as a starting base for the regional analysis of the heating demand and supply potentials due to the consistency with the utilized profiles, in the literature a lot of other highly resolved approaches for mapping heating and cooling supplies might be found. The Heat Roadmap Europe atlas by (Möller et al. 2018) could be mentioned at this point. For district heating, which will be described in more detail in a later section, the demand assessment itself is also comparable to the mentioned approaches in the literature, although it is less detailed in some points compared to those focusing on this subject such as (Pelda et al. 2021). However, the layout optimization itself in PERSEUS-gECT might be considered as rather advanced due to the actual modelling of flows between 100m resolved variables within a national resolved optimization problem. Concerning the validation of the demand modelling in regions outside the focus area, a comparison with the recently published global heating and cooling by (Staffell et al. 2023) could be interesting due to the challenge of finding valid time series data for benchmarking. The selected approach of modelling the demand based on standard load profiles is a rather simple and widely applied approach with known strengths and drawbacks of the single approaches as reviewed by (Peacock et al. 2021). By combining multiple approaches and a simple estimation of missing parameters, there is a special focus on a balanced and rather complete demand modelling and not on the exact parametrization of the single processes within a single subsector. The results of such an approach, which assumes that the temperature and the date (e.g., summer, winter, workday, weekend, holiday, etc.) are the main driver, is shown in the next figure for the daily German gas demand in 2019. Although the gas demand is entirely modelled from generic heating and non-heating SLPs without any connection to the simulated year and is derived partially or completely from electricity demand patterns in many sectors, a high linear correlation and a small error is achieved by simply stacking the locally modelled raw sectoral demands, without any further dynamization or adjustment.

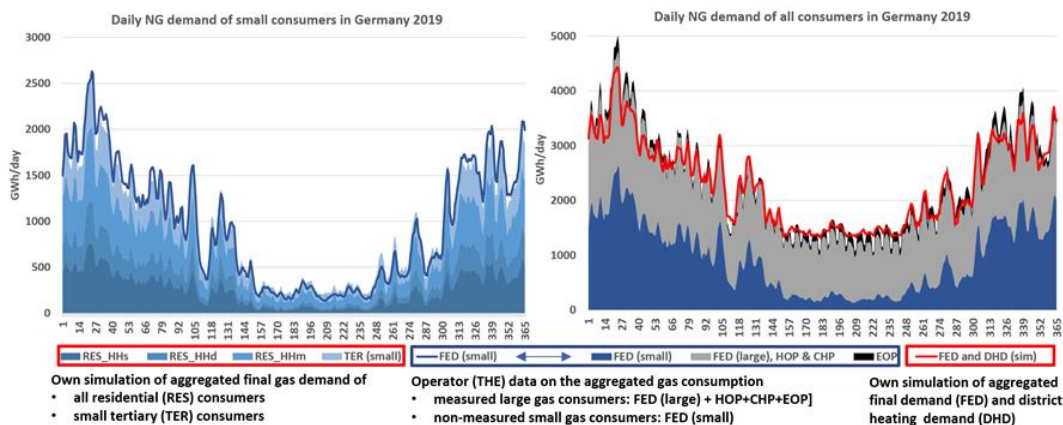


Figure 2.57: Exemplary validation of the bottom-up demand modelling approach based on a comparison of the modelled daily natural gas demand in Germany in 2019 with data from the gas system operators

For small gas consumers, which are not directly measured but estimated from the gas system operators⁵⁵, a linear correlation of 99.5% is observed. This is shown in the left part of the figure and may be observed despite of the circumstance that profiles of tertiary consumers, which are partly non-measured and included here and partially measured and included only in the right part of the figure, are currently not further differentiated. The focus on a detailed regional modelling of heating/cooling demands (over 100000 profiles) thus shows to be valid in the example, on disregard of the actual conversion technology and fuel in the first step and a later technology based adjustment of the conversion efficiency. The matching with the total gas demand shown in the right part of the figure, including the large consumers, is more challenging but still shows a correlation of over 98%. In this group the share of consumers which operate partially or completely independent of the ambient temperature is quite large. Besides of the non-energetic gas demand of the industry, for example for producing fertilizers and specific non steam related gas demands, this group also includes the gas demand of power plants (EOP, HOP, CHP), which complicates the benchmarking as their dispatch is partially or completely determined by the power sector. Based on the published data of the ENTSO-E on the dispatch of gas powerplants and the share of EOP generators in this group, the potential share of the EOP is marked black in the figure. In the results we still observe a quite good match of the simulated and reported gas demand, although in summer a clear weekday/weekend pattern is observed, which might result from a dispatch decision of CHP units running in the electricity markets. As the power plant dispatch is an endogenous variable in PERSEUS-gECT, a deviation at this point is however not necessarily an indication of a badly modelled DH demand for example.

For electricity, the approach is validated on an hourly basis and also provides acceptable results for the given purpose as illustrated in the next figure. In most markets a high correlation is

⁵⁵ In 2019 data of the two German gas network operators NCG and Gaspool, which later merged to THE, are aggregated.

already observed after stacking the regionally computed generation based on the created standard load without any further adjustment.

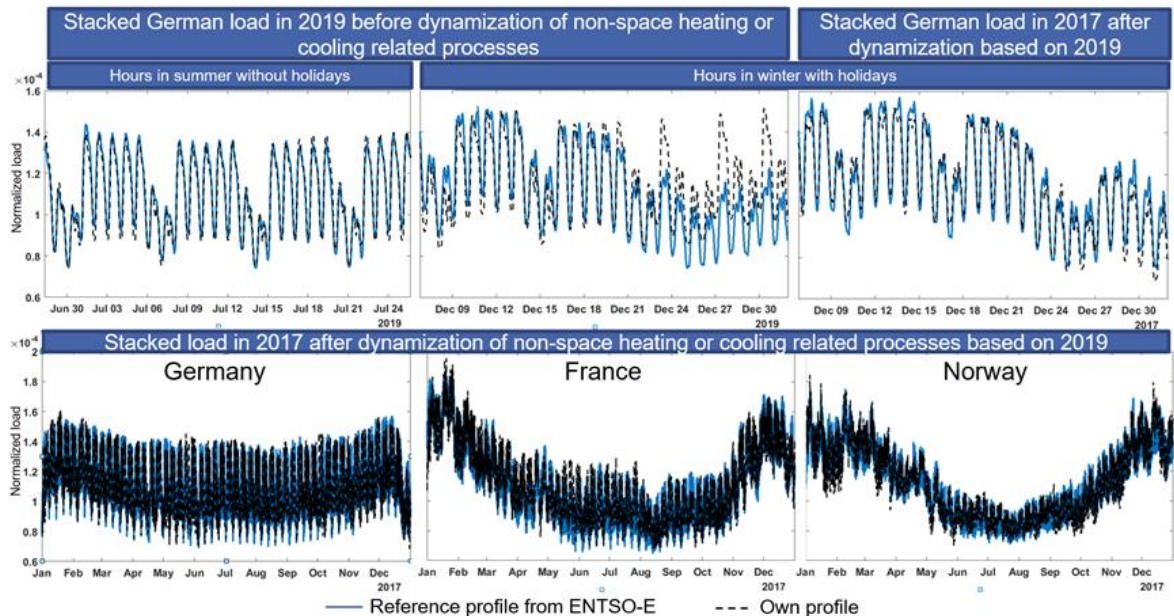


Figure 2.58: Exemplary validation of the bottom-up demand modelling approach based on a comparison of the modelled hourly electricity demand in Germany, France and Norway in 2017 with ENTSO-E data

In Germany for example, already this raw profile without any further dynamization has a linear correlation of over 95% and matches good on normal days. For holidays and bridging days however, the usual SLP pattern of weekday, Saturday and Sunday requires a further adjustment, based on the actual date. Otherwise, the time around Christmas, New Year or Eastern leads to large deviations. Therefore, a simple dynamization is performed based on a calibration year, 2019 in the example, and applied in all further years. Assuming that the deviation results from errors in processes, which are not related to SH, WH or SC, a simple heuristic is applied to shift daily dynamization factors for the remaining SLPs. As illustrated, this approach leads to acceptable results, not only for Germany, where the demand pattern on the days around holidays is consequently met, but also for countries like Norway and France, with a much stronger seasonal pattern.

Until this point, only the modelling and calibration of processes in a historic reference year was described. For the modelling of the further development, an external reference scenario (e.g., TYNDP 2022, WEO) with the general projections on the development of national energy demands needs to be defined. In detail, national projections on the final demands for fixed processes such as for the non-energy related conversion of transport activities on the one hand and the useful demand of heating/cooling related processes on the other hand are needed. The regional development is based on projections of the population development (national, worldwide) and their regional distribution (NUTS3, only Europe), as well as on the projections on

passenger cars registration on a city level (only Europe). For electric vehicles, a matching with the considered carports and garages is taken into account, which are included in the modelling of rooftop PV as described in a previous chapter, and the route fast charging along highways, as described in (Slednev et al. 2021), is modelled. For the charging of electric light trucks, an approximation based on the distribution of warehouses is used to adjust the future distribution of the demand while for electric heavy-duty trucks, the fast charging along the TENT- hubs is considered with a larger weight. For the electrical charging profiles in the transport sector multiple sources from the literature, for example from the TYNDP and from tools developed at the Karlsruhe IIP and partially described in (Slednev et al. 2021) are utilized. For most subsectors and applications however, the parameters used for the regionalization, such as freight weights and passengers in the aviation, are kept constant and only the final demand for a fuel based on the national scenarios is switched.

In general, a further differentiation of the considered processes with the goal of improving the regionalization of future demand potentials is neglected. Only for the steel sector, the process related energy demand for integrated steel plants and for an electric arc furnace is differentiated on a unit level. If the information about planned DRI projects with hydrogen is not known, the previously mentioned differentiation is used to distribute a scenario of defined national increase of hydrogen in the steel sector. However, the level of detail for this processes analysis is rather low and the values are more indicative for a regionalization.

2.4.5 Approach for the definition of the transport network

Overall, multiple systems for the transport of multiple commodities are considered in PERSEUS-gECT and modelled with a varying degree of detail. As illustrated in the following figure, which lists the number of currently considered edges per transport system and commodity and the main data sources, the general approach is based on a combination of multiple sources for the network parametrization⁵⁶.

⁵⁶ The number of nodes per transport system and commodity are listed in the fig. A.10.

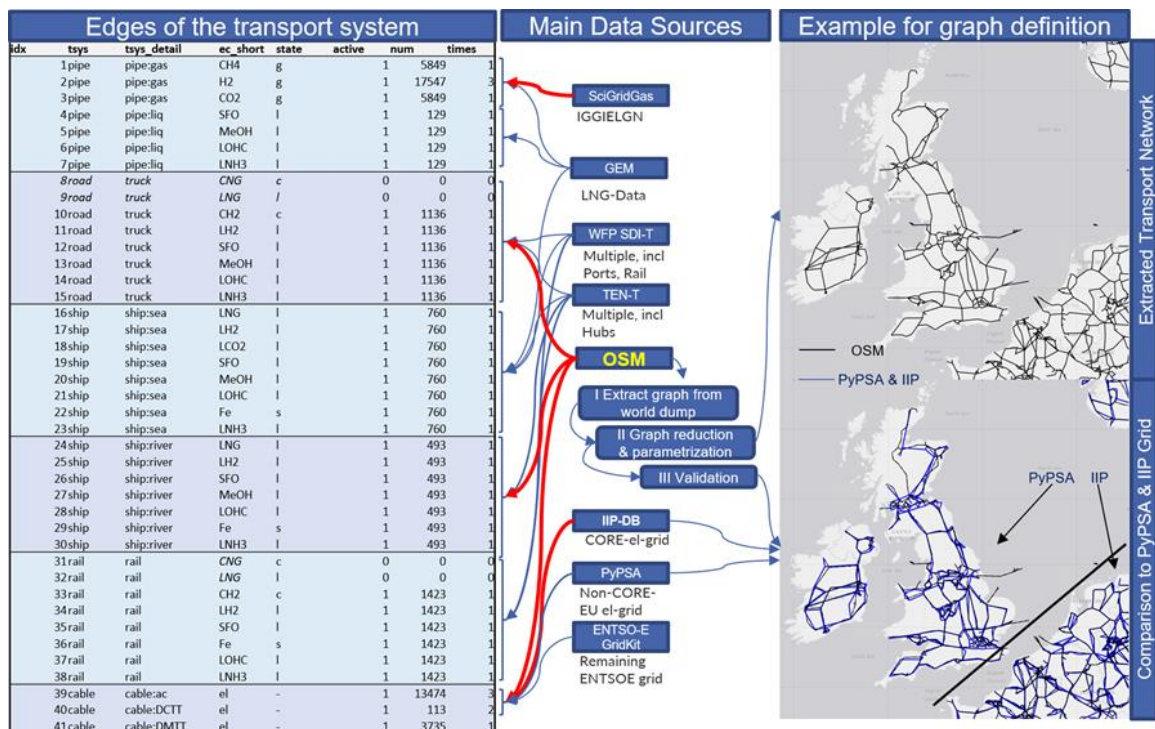


Figure 2.59: Edges of the transport system and main data sources for all networks except district heating and point-to-point connection of offshore units (a) and the exemplary approach for a graph definition (b)

In line with the regionalization of the supply and demand potentials, the entire approach is implemented in MATLAB and open street map data are used as the main data source for the definition of multiple transport systems. Starting from the world dump of this database, a graph of the needed transport system is extracted by reducing the geographically highly resolved node-way annotation of a street or a power line. The goal is to define a connected graph where only the relevant supply, demand and junction nodes remain, while the available information on the connection, such as the number of wires and the voltage level, start and end point for a power line for example, is retained and harmonized. Once the graph is extracted, reduced and cleaned for either unnecessary or missing connections, missing parameters are added, either from the literature or based on a regression from an internal or external database. In the literature, several approaches and tools are available, that basically have the same purpose of a network extraction from OSM data. Especially the methods developed within the SciGRID project (Matke et al. 2016) for defining power networks from OSM data or the subsequent SciGRID_gas project (Pluta et al. 2022), which focuses on the gas network, might be mentioned. Often these data are combined with additional information from system operators or if not directly provided, the information are extracted from a map, such as done by (Wiegmans 2016) for the ENTSO-E map. A rather strong geographical reduction with the focus on using the resulting graph for the power system analysis is included in PyPSA (Hörsch et al. 2023) and is also used for calibrating the own grid for regions which lie outside of the CORE region.

Depending on the system and the model region, data generated by these approaches are utilized within PERSEUS-gECT partially for benchmarking or calibration reasons or even directly for defining the graph. Nevertheless, the own methodology for the network parametrization is applied even if the actual data is utilized, including islands checks and reduction or inconsistency checks, for example on the voltage information of adjacent lines. Finally, for all data, independent of their origin and the methodology used, a time-consuming manual error handling is applied.

In the following, the resulting networks will be shortly described. In general, these networks are modelled in a simplified way as capacitated directed graphs and are therefore characterized by the displayed edges and nodes. Only for the electricity grid, which is modelled based on a DC-OPF approach with quadratic loss approximation, a more detailed line parametrization is considered. For the pipeline-based operation of the oil and gas network, which is displayed in the following, a less detailed parametrization is chosen, as pressure variables and the need for a discrete placement of compressors is ignored. Depending on the known or assumed pipeline diameter, pressure and flow rate, a simplified flow model following (Baufumé et al. 2013) for gas carrying pipelines and (DeSantis et al. 2021) for liquid carrying pipelines is chosen. Thereafter, the capacity of the existing pipelines and potential replacement options or parallel addition options is calculated for each energy carrier. For hydrogen and methane the assumed parameters and calculation steps are displayed based on a definition of the real gas factor z following (Hiller and Walther 2018) and an assumed average operating temperature of 12°C.

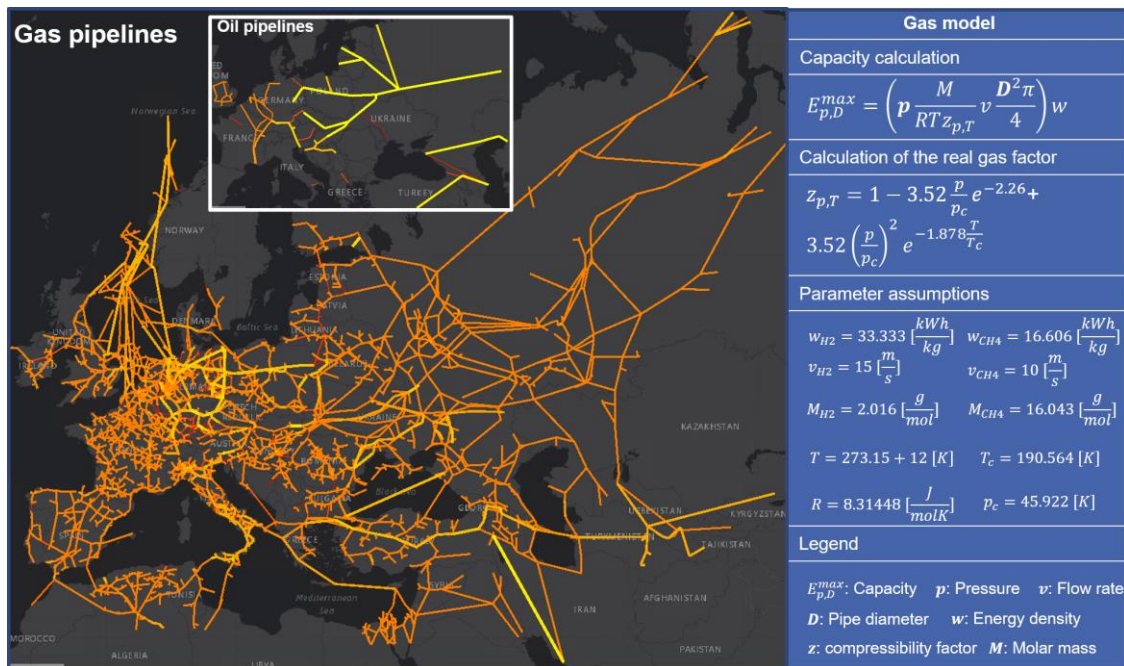


Figure 2.60: Considered gas and oil pipelines in PERSEUS-gECT and approach for defining the capacity in the gas model

In general, each component of the gas and liquids infrastructure, comprising the pipelines, cavern & aquifer storages and the port infrastructure (liquification, regasification, storage tank units) is modeled once for the existing operation with fossil fuels (CH₄, LNG, oil). Alternatively, the option for a replacement or parallel new construction of the components for an operation with hydrogen (H₂/LH₂), ammonia, toluene (LOHC), CO₂ or methanol is included while synthetic fuel oil (SFO) or synthetic natural gas (SNG) might be directly injected in the existing infrastructure. For hydrogen an additional blending into the existing natural gas grid with up to 20% of the pipeline gas volume is assumed. While the geographic information of the pipeline infrastructure is largely based on data from the SciGRID_gas project (Pluta et al. 2022) and the GEM database, the following displayed graph of the road, shipping and railway infrastructure relies on various sources. Starting from the Trans-European Transport Network (TEN-T), which defines the main transport corridors and multi-modal hubs in Europe, mainly open street map data and data from the world food program logistics database (WFP-SDI-t) are used as a starting base for the definition of the illustrated transport graph.

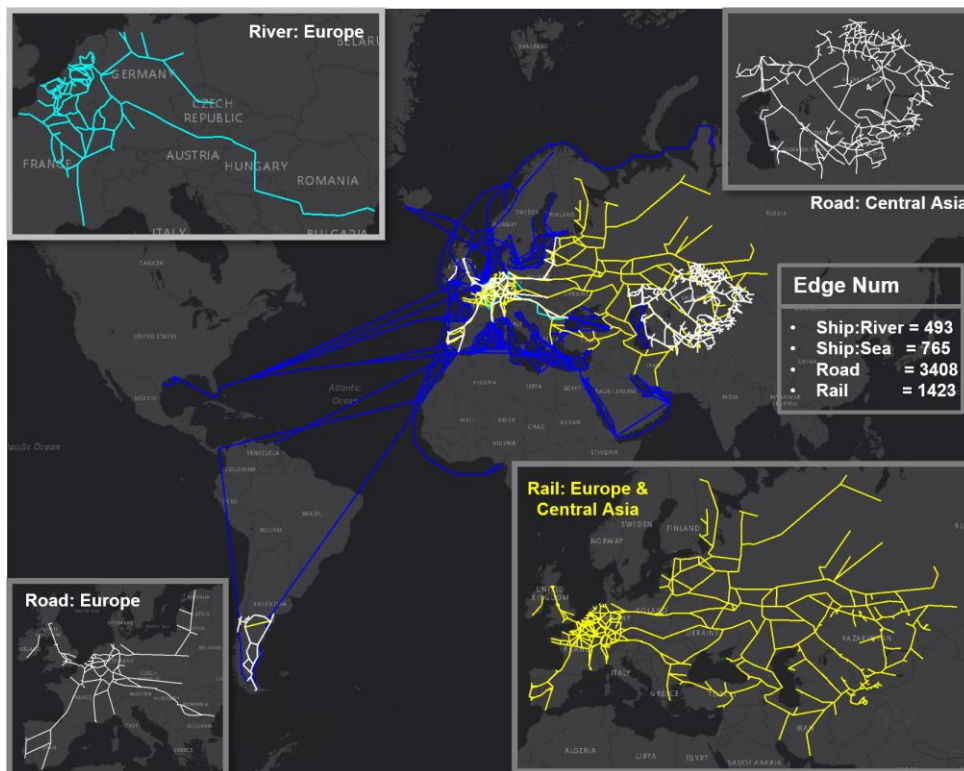


Figure 2.61: Considered ship, road and rail edges

Currently, the expansion of the shipping, truck or rail capacity per edge is assumed to be unrestricted and only depends on edge related investment into ships, trucks and rail wagons on the one hand and node related investments into the port, road or railway turn-over infrastructure on the other hand. In addition to the general inter-modal links at logistic hubs, of which currently 447 are considered (with 538 links within a hub), a direct delivery of commodities to large power

plant locations is modelled at 771 locations with 1083 links. Taking into account that multiple energy carriers are transported, the inter-modal links at logistics hubs increase to 2947.

Considering that the electricity network and the district heating network are modelled rather specifically in PERSEUS-gECT, some aspects of these two networks should be described next.

Electricity grid

The electricity network might be considered as the backbone of the transport infrastructure in PERSEUS-gECT, to which almost all conversion processes are connected either on the input or output side. The majority of these consumers and generators is however not directly linked to the transport grid which is included in PERSEUS-gECT and comprises mainly the extra high voltage grid level (>220 kV)⁵⁷, but indirectly through a connection to the underlying distribution grid, which comprises the high, medium and low voltage level. In previous own work, such as (Slednev et al. 2017b; Slednev et al. 2018), OSM data has also been used for an approximation of the underlying 110 kV distribution grid. As illustrated in the annex (fig. A.11, fig. A.12), this data is available in the entire model region, although the quality might vary significantly depending on the region. In (Slednev et al. 2021), where the combined operation of the transmission and distribution grid in Germany and its neighboring countries was optimized, it has been demonstrated that the extracted distribution grid allows a DC-OPF optimization with a reasonable load flow approximation on the 110 kV level, at least in the central and western European countries⁵⁸. In the scope of this work, however, only the graph information following (Slednev et al. 2017b) is used in order to define supply areas for the electricity transmission grid. By defining Voronoi polygons over the nodes of the high (and partially medium) voltage distribution grid and allocating these nodes to the next available substation with a transformation to the extra high voltage transmission grid level, each existing or potential electricity consuming or generating process might be assigned to a node of the transport system. The resulting supply areas of the transmission grid nodes, which are illustrated in the following figure, are therefore based on the underlying grid topology and allow a reallocation of loads and generators in case of a known substation expansion on the transmission grid level⁵⁹.

⁵⁷ In some regions also parts of the 110 kV high voltage grid are considered as part of the transmission grid.

⁵⁸ A validation, however, has only been performed internally based on the Schleswig-Holstein grid, which is described in Ringler et al. (2016).

⁵⁹ The commissioning of onshore substations at new locations or the decommissioning of old ones is currently only considered in the UCTE grid with a focus on Germany and neighboring countries based on the national grid expansion plans.

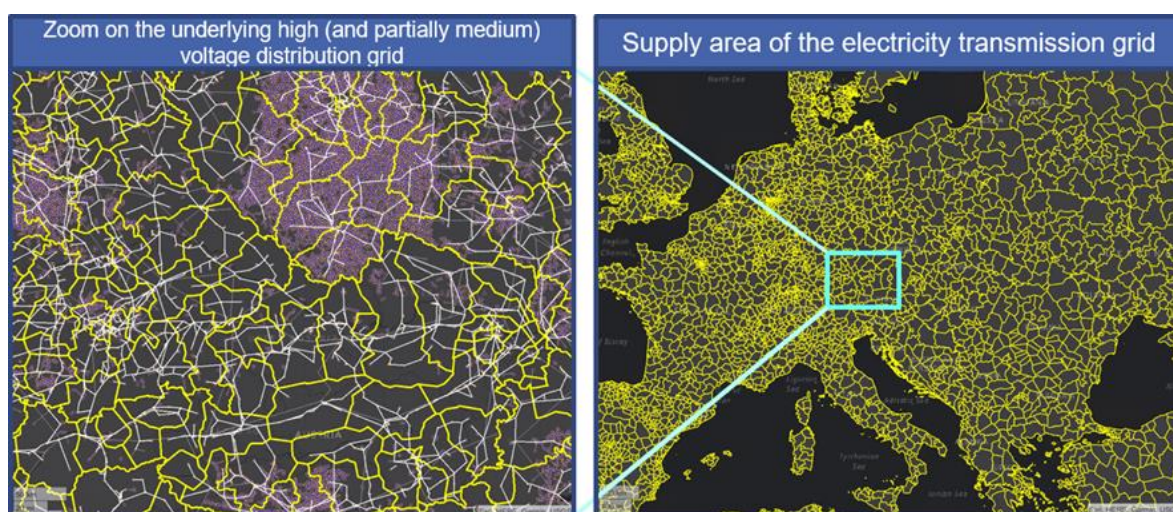


Figure 2.62: Definition of supply areas of the electricity transport grid

For the definition of the actual electricity transmission network, multiple sources are utilized, including publicly non available grid models as well as publicly available data such as static grid models or data from the national expansion project. While Germany and its neighboring countries, including the countries of the CORE CCR region⁶⁰, are modelled with the highest data accuracy concerning the parameters of the transmission lines and transformers, a rather generic parametrization is chosen in the remaining region. The heterogeneity of the of the database is however rather uncritical as the focus of PERSEUS-gECT lies on an endogenous grid expansion planning, which includes the possibility to restructure less accurate parametrized parts of the transmission grid. The AC transmission grid, which is displayed below and contains 13553 substations, 16998 buses, 32348 branches and 5645 transformers excluding endogenous expansion options, thus relies in central parts on a grid which was developed and maintained at IIP by multiple persons and published in multiple studies, such as (Ruppert et al. 2019).

⁶⁰ The Core Capacity Calculation Regions comprise the “geographic areas in which a coordinated capacity calculation is applied” (https://www.entsoe.eu/network_codes/ccr-regions/) and include in addition to Germany and its neighbors further Eastern European countries.

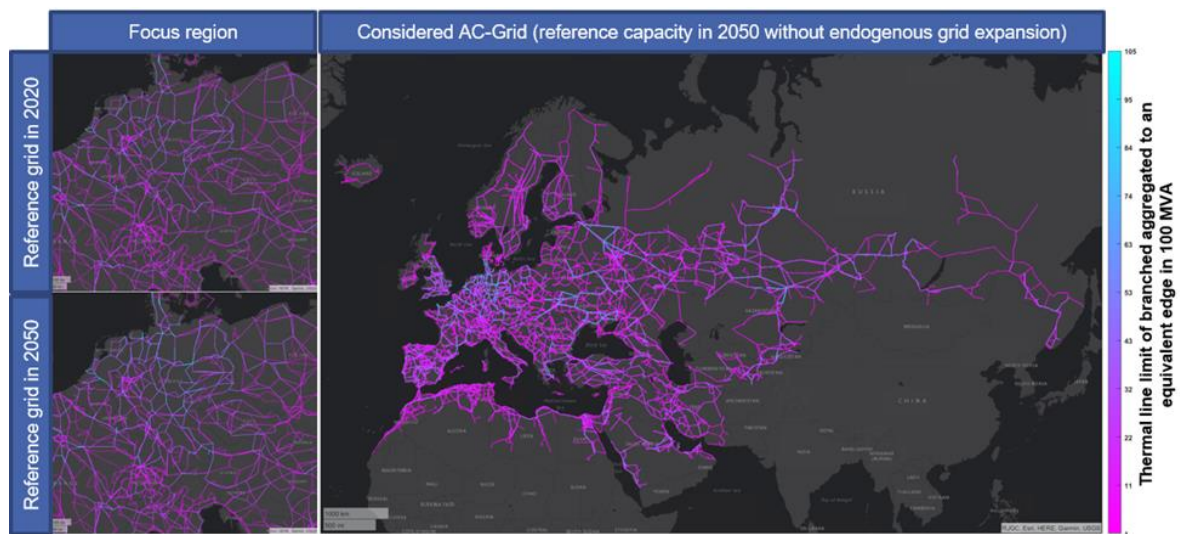


Figure 2.63: Capacity of the considered AC-grid in the reference case in 2050 without endogenous expansion

For the expansion planning two alternative expansion stages per edge in addition to a reference case, which includes only the known and therefore fixed expansion projects, are considered. Depending on the specific parameters of the considered lines per edge, the endogenous expansion with a default new 380 kV overhead line ranges from a rather inexpensive cable replacement within the existing architecture to a parallel construction of a double-circuit line. Alternatively, the dismantling of the existing line and replacement investment of a double-circuit line within the existing corridor is considered. The two expansion stages are thus used for bundling multiple useful discrete upgrading, construction and dismantling decisions into lines, control panels and transformers.

Besides of the AC transmission grid, existing and potential DC converter stations and lines are included in PERSEUS-gECT and shown next. In addition to the existing or planned point to point connection realized through two-terminal DC systems (DCTT), the option to connect specific offshore wind parks either through a DCTT or a multi terminal system (DCMT) with independent investment variables for the converter and transmission lines is considered. In order to model a flexible grid connection or even island operation of offshore generators (wind, PV) or loads (electrolysers, DAC, compressors of NG/H₂/CO₂ storages), these units are actually connected to a virtual electricity node, which might turn out as a node of the DCMT/DCTT system or remain an isolated node. The size of the DC grid depends largely on the modelled wind offshore system, or more precisely, on the selection of the offshore nodes, for which alternative transmission routes should be considered. Overall, 12981 potential offshore converter stations or isolated nodes with the same number of direct point-to-point (DCTT) connections to the next onshore node might be considered. Alternatively, 13855 DCMT edges for linking the offshore based on a meshed grid might be selected. The DCTT connections of the general electricity grid, which is largely based on existing or planned onshore and offshore projects, is much smaller and contains just 113 edges. The following figure illustrates this DCTT and the offshore DCMT grid.

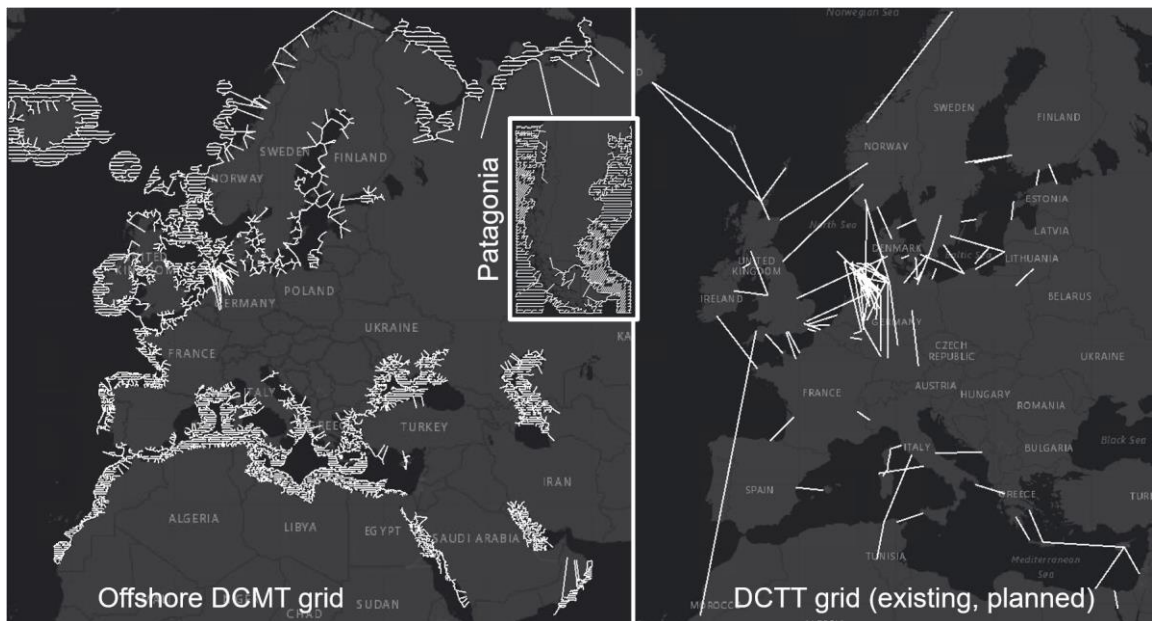


Figure 2.64: Potential and existing edges of the HVDC grid

With a focus on the North-Sea, only a sub-grid of the offshore DCMT is considered in the latter case study. In addition to the offshore connections, this sub-grid however also includes all edges of the onshore DCTT system and of the oil grid and is displayed in figure A.13.

Besides of a bottom-up modelling of weather dependent generation profiles (wind, solar) and demand profiles (space heating and cooling, COP of heat pumps), a consideration of weather dependent and therefore dynamic thermal line ratings for the AC-overhead transmission lines (OHL) is implemented in PERSEUS-gECT. The complex dynamics of weather or climate dependent parameters might be therefore considered in each step of the electricity conversion chain, starting for example from the primary energy conversion in Central Asia or North Africa, followed by the intercontinental transmission and ending at the final energy conversion in Western Europe. Currently a dynamic line rating (DLR) based on the IEEE model (IEC 2021) and the CIGRE model (Cigr WG 22.12 1992) for the calculation of AC OHL thermal limits is implemented. In the default settings the IEEE standard, published in IEC 61597, is applied in combination with ERA5 data for a DLR calculation of multiple weather years, although both models show a similar behavior according to (Arroyo et al. 2015). Instead of splitting each line into the numerous actual segments between the individual towers in order to calculate the actual wind angle for the cooling, currently a simplified direct connection of nodes (substations, junctions) is assumed with a weather cell dependent segmentation in order to reduce the computation time. Within a range of the wind angle of $\pm 15^\circ$, the potential thermal line rating for each segment is calculated for each hour and the lowest values of all segments of a line within the wind angle range is taken as the thermal limit. The rating depends on the line parameters and is therefore calculated for all existing and potential lines. Subsequently, the equivalent edge parameters of the considered expansion stages are calculated based on the hourly single line parameters of the active parallel lines per edge and expansion stage.

Due to the high impact of wind induced cooling on the thermal line rating, the following displayed average impact of DLR is driven by the wind availability. In coastal regions, this cooling effect at locations with good wind conditions might even offset the negative impact of higher irradianations in the southern part of the model region (e.g., Western Sahara, or the Mistral in Southern France).

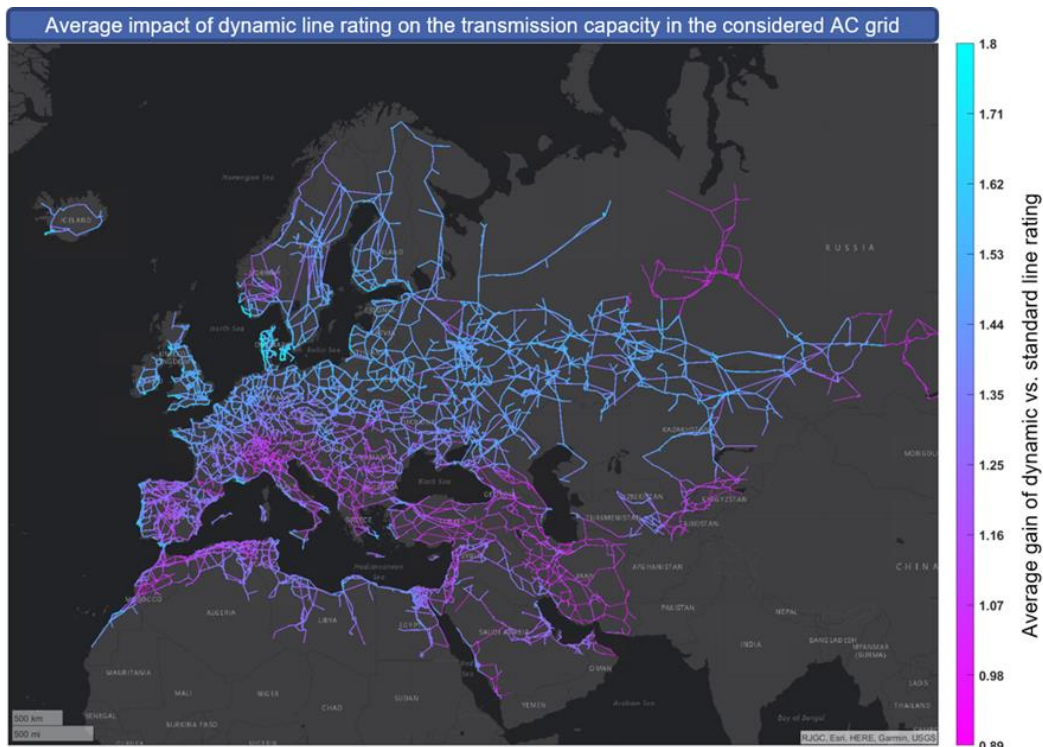


Figure 2.65: Average impact of dynamic line rating on the transmission capacity in the considered AC grid

As illustrated in the annex (fig. A.14), the average gain of dynamic line rating compared to static line rating follows a clear seasonal pattern and is most prominent in winter months. In this context it must be noted that the average capacity weighted value of the DLR impact decreases with a grid expansion in the range of 3 to 4 percentage points due to the spatial effect of adding more capacity in warmer regions and also due to the better temperature performance of new overhead lines. As indicated in these figures, both effects are in the same order of magnitude.

District heating network

In the scientific literature multiple approaches might be found for a detailed analysis of the regional heating and cooling demand assessment which is or might be supplied by district heating and cooling grid (Pelda et al. 2021). In addition, detailed and ready-to-use maps and tools, such as the pan-European Thermal Atlas Peta4 (Möller et al. 2018) give valuable insights on how these demands are distributed. The own selected approach is visualized in the following figure and focuses on the definition of district heating supply areas. The goal is to link the supply and

demand side of the district heating commodity, which is mainly hot water (th_l), within a pre-defined scenario:

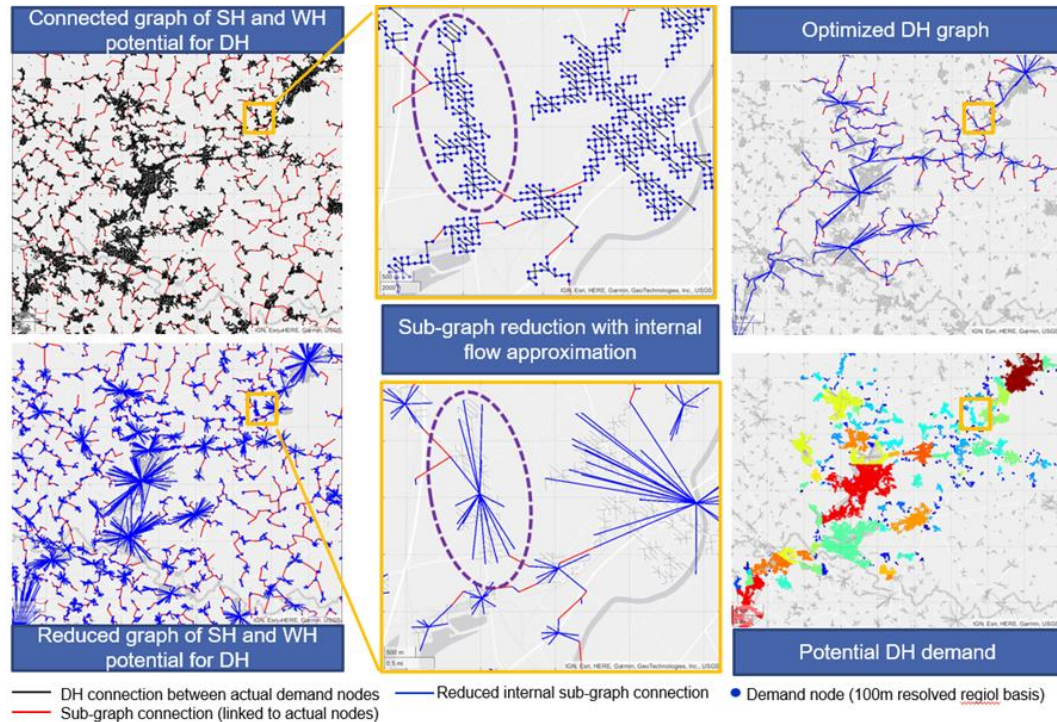


Figure 2.66: Approach of defining the layout of generic district heating networks

In general, the definition of the district heating supply areas follows a simple approach of linking all potential demands and suppliers at a 100m resolution, followed by a graph reduction and a subsequent national optimization for the yearly demand balancing. In detail it starts with the step of connecting all 100 resolved pixel nodes within a certain buffer (default 200 meter). This is done within the overlay of the electricity and gas supply areas and the weather cells. Next, the sub-graphs are defined based on a minimum spanning tree of the interconnected heat pixel nodes. Then, the demand sub-graphs are linked to potential heat sources, which might be existing CHPs, industrial sites with excess heat potentials and potential suppliers located at the nodes of the electricity distribution grid (mainly high voltage and some medium voltage nodes). In the graph reduction step, first the potential links between sub-graphs are reduced by creating a minimum spanning tree. Thereafter, the sub-graphs themselves are internally reduced and the heat demand and the length of the internal connections are distributed on the remaining nodes within a sub graph. Finally, a national optimization with a yearly resolution is run. The goal is to cover an externally defined certain residential and tertiary district heating demand on a national or subnational level such that the distance weighted flows are minimized.

In a calibration step, the generic district heating graph is defined such that the known district heating demands on NUTS3 level in a historic year (currently 2019) might be covered, considering the regionalized potential residential and tertiary space and water heating demand available

for district heating and the available suppliers in that year. Afterwards, the industrial heat demand, which was supplied by hot water and steam grids, is matched with the potential suppliers in the calibration year. Based on an exogenously defined scenario for the development of the district heating demand, a myopic expansion planning for the district heating graphs is run for each investment period. Within this pre-analysis the extent of the district heating supply areas is defined once for a reference case and also for a potential maximum expansion. Finally, the resulting district heating graph is reduced and might be integrated into PERSEUS-gECT. In the current state, distribution losses and transmission limits are ignored in PERSEUS-gECT and only the extent of the district heating supply area is used to link potential demand processes and heat generation processes. The resulting supply areas, that are based on a myopic optimization from 2025 to 2050 in five years resolved periods following the distributed energy scenario of the TYNDP 2022, are illustrated in the following figure for areas with different population densities in Germany. While in the densely populated Rhein-Ruhr metropolitan region large areas are indicated to be suitable for district heating, as shown at the left of the figure, the supply areas in the Rhein-Neckar region are less extensive and focused on the urban areas of cities such as Mannheim/Ludwigshafen/Heidelberg. Nevertheless, the exemplary highlighted district heating graph in the less populated Odenwald region shows that the approach also identifies potentials aside from large agglomerations.

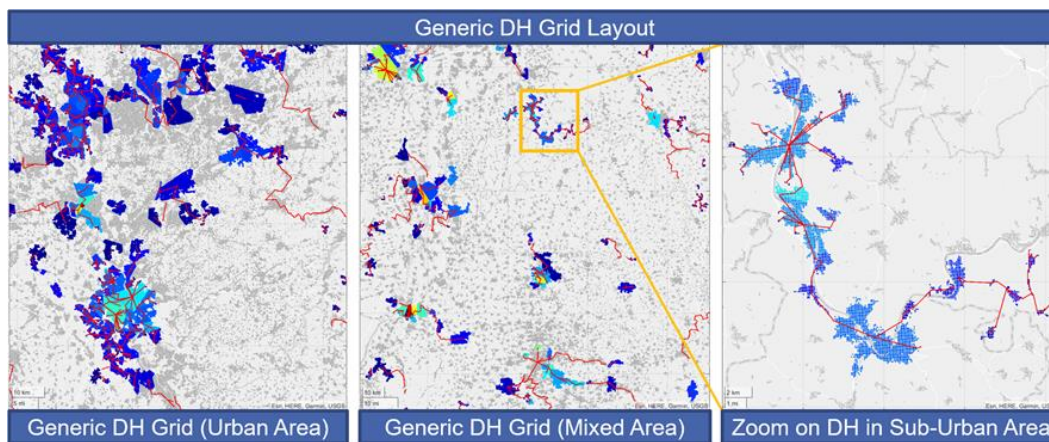


Figure 2.67: Layout of district heating supply areas in selected German regions as a result of a generic district heating planning

Although the linear problem itself is rather simple, the problem size in many countries already lies in the variable range of multiple millions and is therefore non-trivial. The goal of this modeling approach is not the detailed parametrization of the district heating grid but to provide an indication of potentially favorable regions for grid-based balancing of the heat demand.

The final district heating graphs which are considered in PERSEUS-gECT are illustrated in the figure below. Analog to the previous figure, the supply areas are shown as blue points and the links as red lines. In the reference case, an expansion unit 2050 is primarily observed in northern Italy, France and UK compared to the start grid. Although an increasing interconnection between

local grids might be observed, the general structure of the district heating grids remains decentralized. Only in case of a maximum grid expansion, large scale district heating grids spanning over a significant area might be observed in Eastern Europe and Eastern Germany while the general structure in Northern and Western Europe remains rather unchanged compared to the reference case.

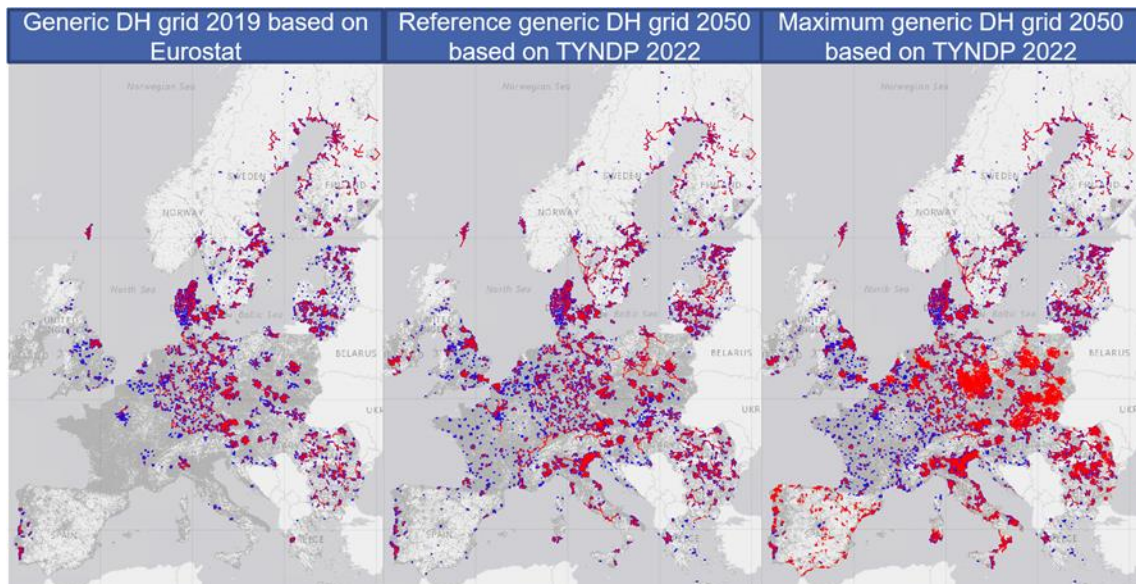


Figure 2.68: Distribution of the considered district heating grids in PERSEUS-gECT

3 Application of the PERSEUS-gECT for modeling the development of the European energy system until 2050 considering energy imports from MENA, Central Asia and Patagonia

3.1 Scenario definition and parametrization

3.1.1 Definition of the general scenario framework

In this chapter, the general functionality of the developed approach will be demonstrated. For the analysis of a possible development path of the European Energy system, a fully parametrized scenario framework, with the goal of achieving carbon neutrality, is chosen as a starting point. From this scenario the projected possible development of the final energy demand is selected for the definition of sector specific and energy carrier specific energetic and non-energetic demand of possible conversion technologies. For electricity and heat generation related applications which are not utilized by final consumers with the primary goal of delivering useful energy for the heating, boiling or cooling of a space or water, the demand is fixed on a yearly basis for a commodity group. While the possibility for producing and utilizing an alternative fuel is maintained, the technology investment decision may not be endogenously adjusted for the demand. The implications of this approach will be discussed in detail in the section of the results. Once these base parametric assumptions are derived from the reference case, the model needs to be parametrized regarding the techno-economics assumptions for investment options and some basic regional exogenous restrictions concerning the development and the suitability of a technology option within a region. This calibration step includes the integration of national or sub-national policy restrictions. As an example, in the current case, known coal phase-out decisions were applied. The underlying case study is to be considered a proof of concept run and must not be mistaken with an actual detailed analysis of the possible development with the goal of deriving policy recommendations. The model run could be directly started based on the already described detailed parametrization of the existing system and the high-level base parameter assumptions provided by the chosen reference case, which is the “distributed generation scenario” of the TYNDP 2022 (ENTSO-E – ENTSOG 2022). For the analysis of the modelling results, the techno economic assumptions from a few data sources, which cover a large spectrum of the needed parameters are considered. These will be described briefly in the next chapter. Due to the large model size and the pure indicative purpose of the scenario, in the next step

multiple parameters are aggregated with the goal of creating a problem instance that can be handled by the commercial mixed integer solver Gurobi without the need for a further decomposition. Obviously, this requires a massive reduction of the temporal dimension in order to allow a model run on a local server¹. In the initial step, some indicative tests with only a few time steps per investment period are performed in order to get at first impression which temporal resolution allows to capture basic system dynamics. For covering the time horizon from 2020 to 2050, seven periods with an equidistant spacing are chosen, such that each period accounts for five years. Prior to the actual optimization, a realistic development for some basic parameters such as the regional expansion of renewables and the potential regional distribution of loads in the grid is computed, in order to derive some useful lower bound on the development of capacities. This is done on a yearly basis with a highest possible spatial resolution and based on the capacity development assumptions derived from the base scenario. In the next step, this information is used for the variable aggregation. For the renewable electricity expansion, next a technology specific national lower bound is defined, which is set between 50% and 80% of the reference TYNDP scenario. Within this case study, the actual highly sectoral resolved parametrization of application specific processes is neglected. Final demand processes are in consequence parametrized with a local weighted average profile and averaged techno-economic parameters. The implication of this approach is that the investment into a technology is potentially locally biased if a specific technology, for example a fuel cell, is unattractive for the majority of consumers while it might be attractive in a specific demand sector. In an area, which is dominated by residential consumers, for example, a potential attractive alternative for the minority is thus underestimated.

Finally, the necessary time steps are computed based on an iterative approach, starting with a resolution of 15 equidistant weighted time steps, which are chosen based on the first model runs. By placing the first investment period into a historic year, this approach is also used as a final calibration step. The first model run, with a computation time of almost 8 days, led to a result, which might be described as an electricity scenario. As illustrated in the annex (fig. A.15), the general properties of the main shipping routes, the placement of hydrogen production units and the expansion of an overlay DCMT grid corresponded to the later shown final results. The availability of large areas with good wind conditions and the possibility to expand the electrical grid shifted the solution to an electricity dominated scenario world. The DCMT expansion in this context ranged over a much larger space and triggered an additional renewable expansion in Germany (compared to the final model run). The initial plan to define the meaningful time slices based on a clustering of the resulting final demand time series of this first model run was however omitted due to the large dominance of a geopolitical area which does not lie within the focus of the current analysis. Nevertheless, the clustering was performed and an additional extreme event for accounting of an hour with expected high residual energy demand was added. Afterwards the new time series for the final clustering were computed without the bias of the

¹ All computations are carried out on an AMD EPYC 7262 8-core processor with a 3.2 GHz and 1024 GB ram.

first time series. The computation of the second model run required 186 hours. In the last step, the time slices were once again adjusted. The selection of the time slices itself is based on a binary optimization problem for the definition of m representative days and n hourly time steps per day from n equidistant segments, considering k fixed extreme events and the goal of minimizing the squared deviation on for the expected wind and solar generation, the final energy demand (fed) and the residual fed². The 16 time steps resulted from the consideration of one extreme event with the hour of the expected highest residual fed and $m = 5$ typical days with $k = 3$ time segments per day. For the scope of this proof-of-concept style case study, this approach showed to provide a sufficient approximation of the temporal characteristics of the problem. As illustrated in the following figure, which already includes the realized renewable generation after the final model run, it was possible to preserve the temporal structure of the main drivers, which is non-trivial considering that the final renewable generation capacities, their allocation as well as the net electricity demand could only be estimated.

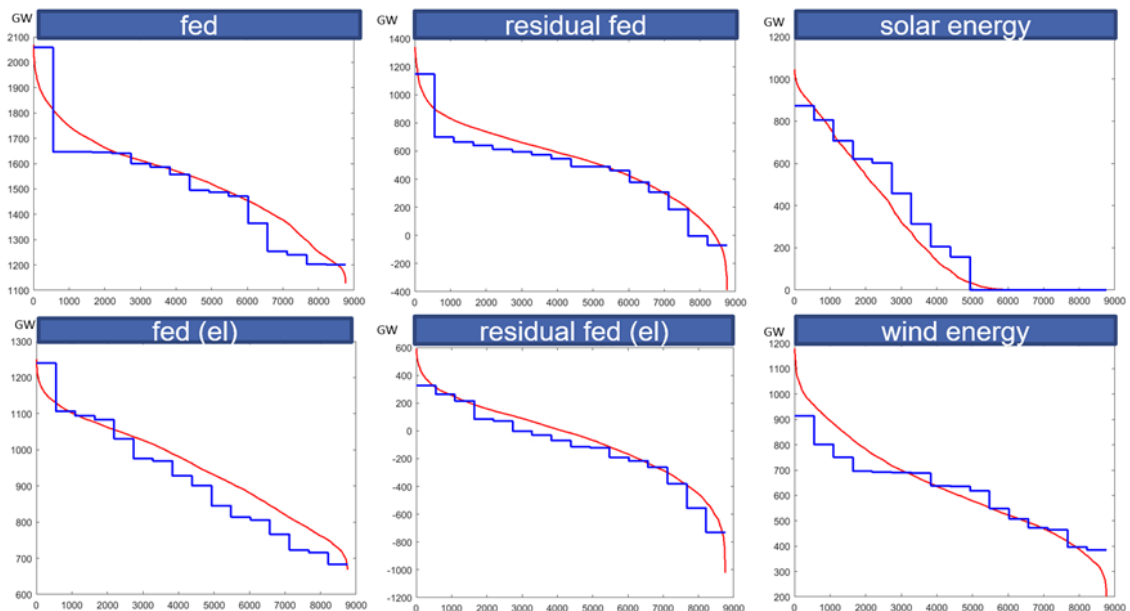


Figure 3.1: Evaluation of the temporal problem reduction based on a comparison of the sorted generation and demand curves for 2050

In (Slednev et al. 2017a) an alternative approach based on the clustering of the expected load flow for the electricity grid expansion planning was presented with the goal of an approximation of the potential critical hours. However, such a procedure might be less suitable for an approach

² The total final energy demand is chosen as a reference, due to the circumstance that the energy carrier specific fed is unknown because of the option to invest into fuel switching processes such as heat pumps, which may replace a gas fired boiler. For the residual fed, the availability of wind and solar power generation and hydro inflows, which are estimated based on the results of a preceding optimization run, are subtracted from the fed.

which might basically shift the entire energy demand from one system to another. A decomposition between the different time steps with the goal of running an optimization with a full 8760 hour resolution, as described in (Ruppert et al. 2018) was tested but not utilized for the final model runs, as this decomposition is not the primary scope of this work. Moreover, the validation of the chosen penalty parameters is also challenging, if the solution is not known. The entire structure of the model definition and coefficient updating is however explicitly formulated to fit in the developed decomposition-based solution approaches and should be validated in the next steps.

In the final model run, which will be analyzed later, the first time period, which was basically included for back testing, is omitted and a linear problem with 103M variables and 118M constraints and 404M nonzeros is solved by Gurobi. Probably due to the selection of more challenging time steps, the solution time also increased in the third run to 487.4 hours. In total thus almost 36 days were spent only by the solver to compute the results of the case study, if taking the two preceding runs for the definition of appropriate time slices into account. The computational needs for the final model solution steps however can be put into perspective when considering the total tool chain of PERSEUS-gECT, which requires multiple preprocessing and pre-optimization steps on a local level (100 m resolution) in order to define and parametrize the variables of the final optimization problem. Considering that already the techno-economic parametrization of candidate wind-offshore turbines for the preceding farm layout problem requires 5.6×10^{11} LCOE calculations per period, the size of the total problem becomes clear. If the LCOE calculating relies only on one profile per weather cell for each unique power-curve-to-hub height configuration, it already requires the simulation of a feed-in time series of 1.65×10^{12} hours for an investment period. Fortunately, most scenario and sensitivity analysis do not require an application of the complete tool box, as performed in this case study.

3.1.2 Techno-economic assumptions for the parametrization of the case study and scenario specification

Within this case study, the Distributed Energy Scenario of the TYNDP 2022 is chosen as a reference for the development of sector and application specific fixed final energy and variable useful energy demand in Europe. Furthermore, a technology specific lower bound for the capacity development of wind and solar conversion technologies is derived from this scenario³. The demand development in non-European countries lies not in the focus of the following study. For a realistic modelling of the power sector, nevertheless, the balancing of the electrical load in these countries is modelled assuming a static demand structure, which is only adjusted based on the population development following the medium scenario of the 2022 World Population prospect of the UN (United Nations 2022). For a consistent modelling of all demand and generation

³ The default lower bound values for the renewable technologies as a share of the zonal TYNDP 2022 capacities are: wind onshore: 0.5, wind offshore: 0.8, PV(-BESS): 0.8 PV (roof): 0.5, PV (ground): 0.5, PV (offshore floating): 0, CSP: 0.5.

profiles and in order to allow a comparison of the results with a historic year which is not affected by extreme event⁴, all profiles are modelled based on the calendric and weather year 2019. The development and distribution of the final energy demand in the reference case is shown in the next figure, while the development of the stacked sectoral hourly final electricity demands for the extended European region is illustrated in figure A.16. In this context, it should be mentioned that only a part of the shown final demand is fixed, while most heating or cooling related demands might be switched. Therefore, this illustration should be interpreted only as a starting point for the optimization, which illustrates on the one hand the region for which a more or less complete energy balancing is considered (Europe including Turkey, Ukraine, Moldova and Georgia) and the location and concentration of electricity demands outside of the extended European region.

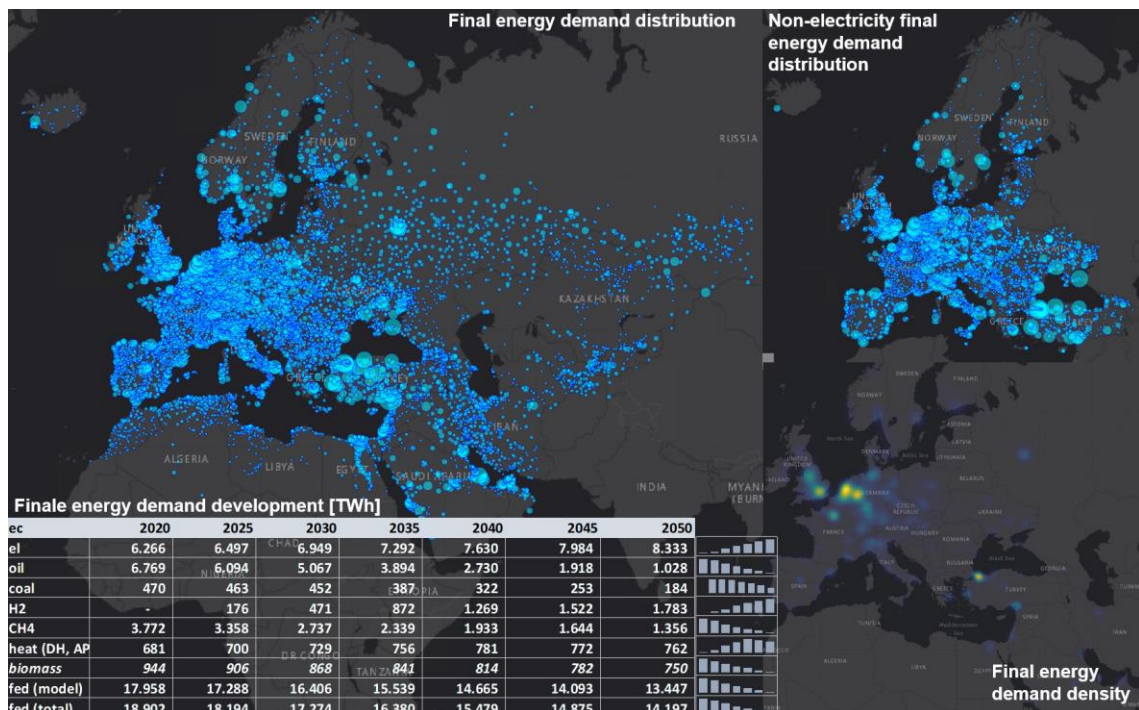


Figure 3.2: Distribution and development of the final energy demand in the reference scenario

If not explicitly stated otherwise, all techno-economic parameters for generation, storage and transmission technologies are derived from the technology data catalog of the Danish Energy Agency⁵ and adjusted to the financial year 2020. For wind and solar energy conversion technologies the economic assumptions are further adjusted in order to align with the TYNDP2022. For conventional electricity and heat related technologies as well as for heat only related conversion

⁴ Due to the demand shock which was caused by the Covid19 pandemic, the year 2020 is not chosen as a reference basis.

⁵ <https://ens.dk/en/our-services/projections-and-models/technology-data>

technologies, assumptions of the EU reference scenario (EUref2020)⁶ are taken and also adjusted to the financial year 2020. In addition, data from the “the future of hydrogen” technology assumption annex (IEA 2019) and from the HYPAT project (Kleinschmitt et al. 2022) are taken for the parametrization of the infrastructure for hydrogen and its derivatives. For the transport of iron the estimations are based on (Jansen et al. 2023). In order to reduce the problem size of this proof-of-concept case study, some technology options which could be modelled, were simplified, neglected or the expansion option was turned off. In this context, solar water heating systems (rooftop for the final demand coverage or ground mounted for district heating systems) were excluded, while the expansion of pumped hydro storages was disabled. By neglecting the flow modelling in the district heating grid and fixing the heat demand, this transport systems are basically reduced to simple nodal heat demands, to which generators might be connected depending on their location. For a conservative estimation of AC transmission capacities and due to a missing consideration of branch outages (N-1) in the expansion planning, the model option of dynamic line rating has been turned off.

In the final optimization, which will be discussed next, the model is run with the objective of minimizing the discounted total system expenses of six investment periods from 2025 to 2050, assuming a global interest rate of 8%. All investment periods apart of the last represent a 5-year range, while the 2050 period represents a 20 years range in order to allow a fair comparison of operation and investment expenses in the last period. In order to account for the effect of varying CAPEX parameters depending on the technology investment region, global CAPEX parameters are adjusted based on national country interest rates taken from the HYPAT project (Kleinschmitt et al. 2022).

3.2 Results of the case study

The goal of this model run lies in the demonstration and evaluation of the general functionality and not in the layout of a desirable or realistic future energy system. On the contrary, a high degree of freedom for a restructuring of the energy system is deliberately chosen. Starting from a consistent energy scenario such as the TYNDP 2022 for Europe, the goal is actually to analyze how such a target and policy orientated energy systems changes if the system boundaries are extended concerning the regional coverage and the granularity of the infrastructure analysis. By fixing only one part of the final energy demand and some lower bounds on the expansion of the renewable energies in a sub-region of the system, it is expected that the results will deviate. If this deviation leads to a system layout which achieves carbon neutrality for lower system expenses, this understanding might be as valuable as the knowledge of fundamental drivers which hamper a desired development. In the following, the results are analyzed from different viewpoints with a focus on the emission balance in 3.2.1, the electricity system related drivers in

⁶https://energy.ec.europa.eu/data-and-analysis/energy-modelling/eu-reference-scenario-2020_en

3.2.2 and the gas system related drivers in 3.2.3. Although the system is optimized in 5-year period steps until 2050, with endogenous capacity additions starting in 2025, the focus will be put on a discussion of the final system configuration in the last period.

3.2.1 Development of the energy system as a result of the emission balance

Considering that the model is driven by the global restriction of defining an energy balance with zero CO₂ emissions until 2050 in the case study, an analysis of the CO₂ balance is clearly a good starting point for the model evaluation. A first indication how this balance is structured is given in the following figure, which displays the net position of the national CO₂ balance in 2050. In this context a global CO₂ balancing through the atmosphere is applied based on a single emission factor for the same commodity. The emissions are attributed to the actual processes which is initially or finally responsible for the change of the atmospheric CO₂ level at the location of the processes. In case that the process is related to a flow of energy or commodities between spatial separated nodes an adequate split is applied. These simple but far-reaching assumptions should be taken into account for the following interpretation of the results. On the one hand they reduce the challenge for a classification of fuels based on their production path, which is rather complicated in a highly meshed system where commodities might cycle between multiple sectors. On the other hand, their implications on the analysis of heterogeneously restricted sub systems within a global optimization should be considered. In the first place they ultimately triggering a direct air capture process or bioenergy-based fuel production, as these are currently the only modelled options for reducing the atmospheric CO₂ level. Without additional, but often arbitrarily defined constraints for the national net balancing in an interconnected system, the actual interesting question is how a heterogeneous system without such constraints would develop towards the global target. The following national net positions⁷, which are displayed with the cumulated electricity generation and the utilization of the electricity and hydrogen grid in the background, are therefore quite interesting for the evaluation of the model.

⁷ A complete shortened National Emission balance is found in the annex in fig. A.1

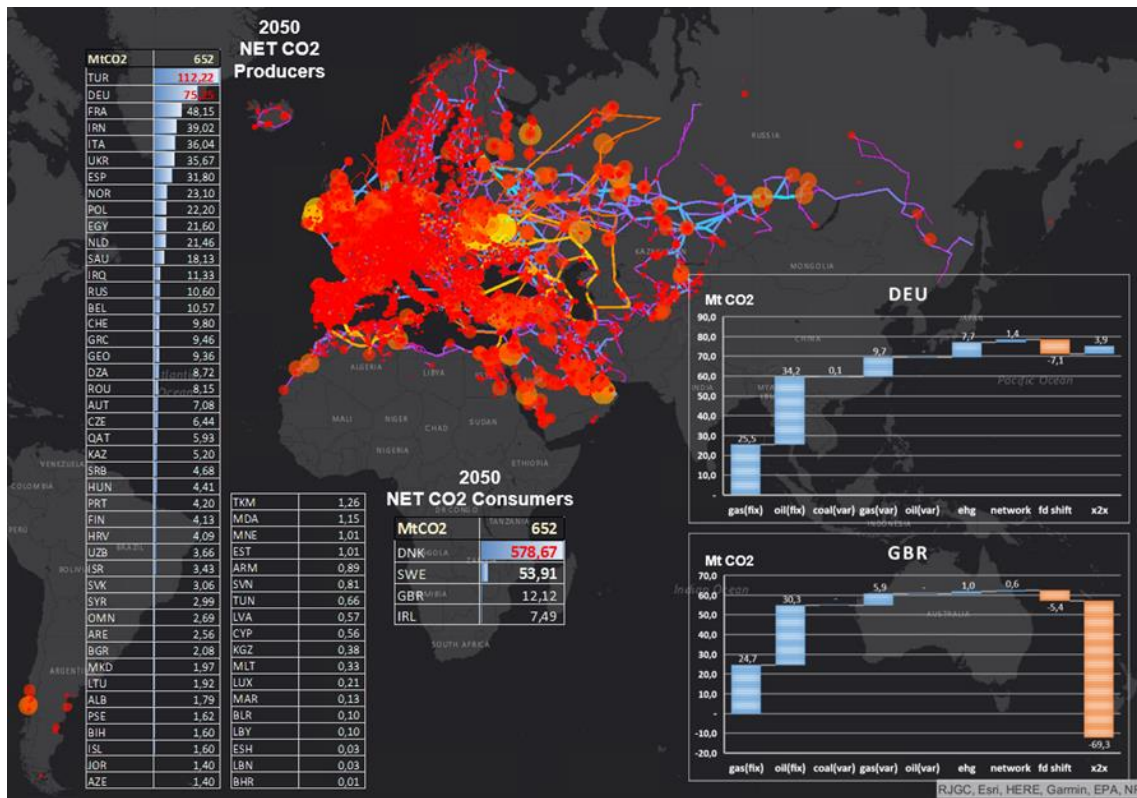


Figure 3.3: Net position of national CO2 emissions in 2050 and comparison of the CO2 balance of Germany and UK against the background of the dispatch of all EHG units and the utilization of the electricity and gas transmission grid.

As expected, the model run did not result in an equal distributed national balance of the emission due to missing corresponding restrictions. The analysis of the drivers is however more complex. On the one hand it is not surprising that countries with a large fixed CO2 emission share, such as Germany, are net CO2 exporters of the fixed CO2 emissions, which largely occur in the transport sector, driven by the aviation demand. Furthermore, it is also foreseeable, that the investment into energy intensive technologies for removing this emission is focused on favorable locations, such as the windy North Sea region, which will be analyzed later. The high positioning of countries for which only the power sector is modelled in the net emission ranking, such as Egypt on the other hand is more interesting. Without a final energy demand for heating applications and a general excess supply due to variable weather conditions, this effect, which also applies to Iran, Iraq and Saudi Arabia, in a later analysis turns out to be a result of a natural gas firing in peak hours. As the only remaining fossil fuel in the power sector with a generation share of 4% as shown later, this results however should not be over interpreted. The overall amount of CO2 from processes for the electricity and heat generation, which might seem unnecessary considering the large dominance of renewables, but is selected nevertheless, account

for 23% of the overall net emissions, which are displayed in the following figure⁸. As expected, these emissions occur mainly in the MENA region, although natural gas is still consumed to a small portion in other regions.

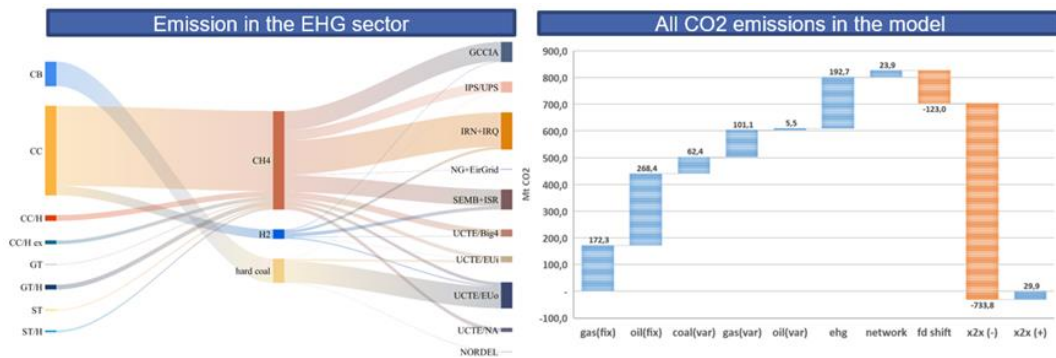


Figure 3.4: Structure of the total CO2 emission balance in 2050

In order to keep the analysis simple and lucid, in the following the countries are loosely grouped referencing to the synchronized electricity system, to which they are connected. GCCIA therefore comprises the six gulf states (ARE, BHR, KWT, OMN, QAT, SAU). In some cases, the regions are merged or split in order to create smaller or larger groups⁹. This is only done for visualizing the results and not on the modelling scale of the networks. One interesting effect is the emission occurring in retrofitted combined cycle plants in order to balance temporal unavailability's in the hydrogen supply. In the Sankey diagram this is indicated by the hydrogen label on the outflows from the technology to the energy carrier. As already mentioned, one part of the emissions is fixed and might not be altered by PERSEUS-gECT. In order to mitigate these emissions, which mainly relate to fossil fuels but also to natural gas, direct air capture units are chosen as the preferred option, although the theoretical option to produce SNG and to store it in tank or cavern storages could be also a theoretically balancing beside of a more logical fuels switch of NG to SNG. While for the fixed gas demand both options are not chosen, a significant amount of synthetic fuel oil is mainly produced in Denmark. While the discussed CO2 balance is neutral towards this production as CO2 is removed already in the preceding process step and no labeling such as green fuel or something else is applied to incentivize this production and the actual emissions occur from a combustion, the reason lies in the utilization of

⁸ In the annex a table with table with the most relevant net CO2 position and their structure for the largest and sink and sources is attached.

⁹ One example of such a merge as the inclusion of Israel into SEMB or the bundling of National Grid (UK) with EirGrid. The UCTE region in this context is split into the group of the big four countries (DEU, FRA, ITA, ESP) and the remaining counties, which themselves are further differentiated into an outer group (UCTE/EUo) including TUR, UKR and MDA, a North Africa (UCTE/NA) group with DZA, ESH, TUN and a remaining inner group UCTE/EUi. It should be noted that Denmark is completely included in UCTE/EUi. A complete list is found in the fig. A.1

process-based gains. As illustrated in the following figure, both technologies, the DAC process and the Fischer-Tropsch based hydrogen to jet production require a transport infrastructure for the input commodities, which will be hydrogen (discussed at a later point) and infrastructure for the output commodity CO₂ or the synthetic fuel. By combing both technologies, at least the need for expanding the CCS infrastructure, of which the cumulated shipping (blue scale) and pipeline (yellow scale) flows are visualized, might be reduced, although for CCS also the investment of the storage and the power demand of the compressors is take into account but not shown here. Besides of a completely model endogenous driven CO₂ pipeline expansion parallel to existing gas pipelines and mainly focused on the industrial spots in Germany, UK, Belgium and the Netherlands, the planned shipping routes of known projects are used within the maritime infrastructure planning. For the oil flows the visualization might be found in fig. A.18.

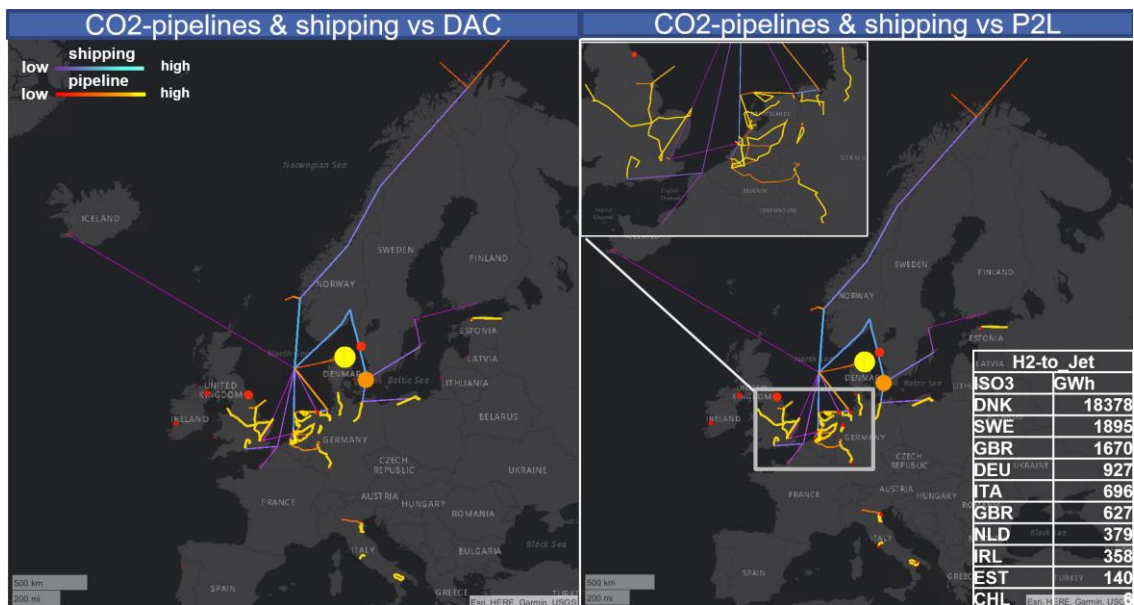


Figure 3.5: Dispatch of direct air capture and hydrogen-to-jet units against the background of pipeline and shipping-based CO₂ flows

Besides of the infrastructure, a lift of heating gains is another reason while both processes (DAC, P2L) are coupled and the P2L unit is not randomly placed somewhere in the oil grid or at the ports. Besides of Chile, where a small DAC unit is realized as an electricity only consumption process, the layout of the DAC as a mainly high temperature heat conversion unit is realized in all other cases and the process heat of the FT process is used for lowering the energy demand. The availability of a district heating grid, where the remaining low temperature heat of both processes might be injected is a further reason for the Danish location, although the main reason is the resource availability of wind and a strong electricity grid due to an AC expansion and a link of multiple wind parks within a meshed DC grid for bundling the generation.

Until this point only the EHG sector and the fixed emissions and possibilities for balancing this emission where discussed. Although the focus of PERSEUS-gECT lies on the modelling of the

transformation sector and the energy transport infrastructure, a simplified modelling of energy related final demand processes is nevertheless included and should be analyzed next. While electricity generating processes are always considered within the modelling of the EHG transformation sector in the developed approach¹⁰, this generally does not apply to the complete heating system. Besides of the district heating system, which is modelled completely endogenously, in the current version only the low enthalpy heating and cooling of space or water in all sectors and the industrial steam generation is modelled in a simplified manner. Besides of a demand side management flexibility, which is also considered for all other fixed demands, this includes the option of endogenous replacing the predefined heating or cooling technology. Considered as an endogenous process class and displayed in the emission balance prior the X2X processes, the investment into the corresponding conversion technology is referred to as final demand switched (fd switch) and should be described next. The following figure gives an impression how an optimization run of PERSEUS-gECT alters the initial scenario defined final demand technologies. Displayed are the model endogenously chosen installed capacities of two technologies heat pumps (HP) and combustion boilers (CB) for replacing a variable final demand. First the development of combustion boiler (CB), which might be fueled by hydrogen or methane and provide an alternative heat supply (ec_new) for residential, tertiary and industrial low and high temperature heating applications¹¹ compared to the default heat source (ec_def) are displayed. Below the realized heat pump installation for the switch of the heating source in low temperature heat application in the residential and tertiary sector are displayed. The options of investing into a fuel cell for low temperature heat or into a classical electric boiler and the unitization of a biomass gasification are not chosen for this specific application¹².

¹⁰ Rooftop PV for example is modelled as part of the power system, independent of the actual allocation on an industrial or residential building

¹¹ The techno-economic parameters are adjusted accordingly for the specific sectors

¹² While the electric boiler is applied in some remote areas, such as Hamerfest in Norway or for a dedicated heat supply, least one biomass gasification unit which injected the excess heat into the district grid was selected

3 Application of the PERSEUS-gECT for modeling the development of the European energy system until 2050 considering energy imports from MENA, Central Asia and Patagonia

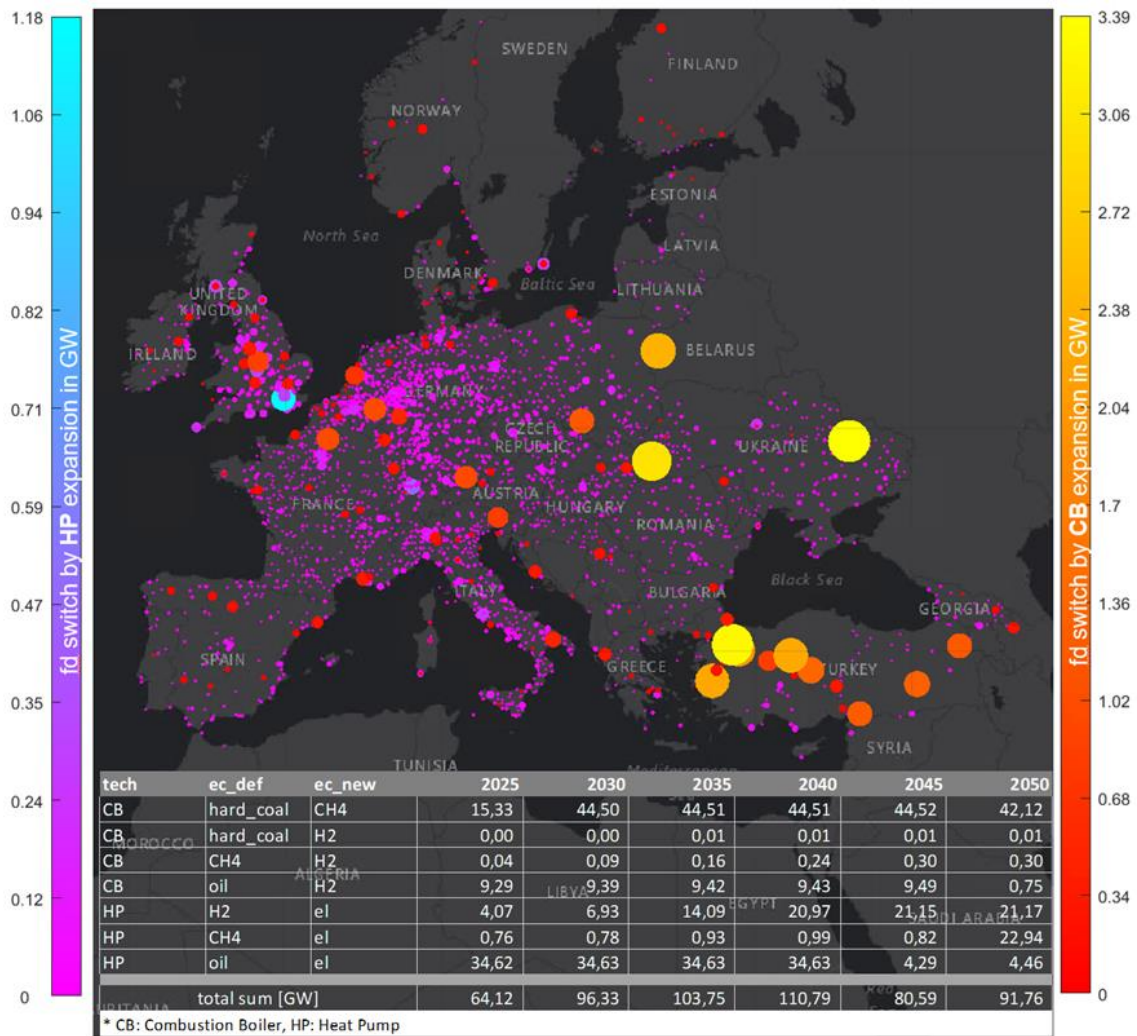


Figure 3.6: Development of final demand switching capacity and comparison of the allocation of heat pumps (blue scale) and combustion boilers (red scale), which are chosen for the final demand-switch

The explanation of this investments, which lead to the previously shown decline in the emission balance, is as follows. In the eastern border of the UCTE region (ECTE/EUo), which basically is dominated by Turkey and Ukraine, the structure of the industrial heating demand was not changed but kept constant in a business-as-usual manner, which was partly due to the missing detailed data in the reference TYNDP scenario. The resulting persisting coal consumption of the industry at the level of the base year is therefore endogenously adjusted by a fuel switch through an investment into an industrial gas boiler. This coal-to-gas fuel switch is actually observed in all regions, but declines in western Europe rapidly over the time as the TYNDP also reduces this heat supply source. This largely explains the energy flows seen in this outer region of Europe¹³.

¹³ It should be mentioned that a direct heat extraction from a CSP is also observed in this graph. Besides of some local impact the overall relevance might be small but it demonstrates the ability of PERSEUS-gECT to endogenously define such links also for the high temperature scale

The option of an oil-to-hydrogen switch for providing industrial high temperature heat on the other hand is observed in a completely different region. In Germany (2.3 GW), UK (1.3 GW) and France (0.7 GW), which dominate this early fuel switch of 9 GW heating capacity, the early availability of a supply and transport infrastructure for hydrogen build in PERSEUS-gECT in order to fulfill the fixed demand¹⁴, also triggers this additional fuel switches in the neighborhood. Thus, an earlier emission reduction at this point is observed than in the reference case. At the end of their technical lifetime these investments are not replaced by the model, as the demand in the reference case already switched. For the low temperature heat, needed by residential and tertiary consumers, partially the same development and partially a complete opposite development is observed. In this case heat pump are the cheapest alternative and as in the case before, existing oil heating in households is directly replaced at the beginning of the optimization and analogously not reinvested at the end of lifetime. For some part of this low enthalpy heat demand for which a methane and hydrogen demand was assumed by the TYNDP, the model instead places heat pumps with an increasing capacity. In line with the increase of hydrogen and at the end also in order to reduce the methane combustion, the heat pumps are primarily expanded in Germany, Italy, Benelux and UK. With a cumulated capacity of around 100 GW the total capacity of final demand switching installations is rather small compared to the total system size, but nevertheless demonstrates the ability of PERSEUS-gECT to model structure changes in the investment of many small consumption units along with capacity development which takes place on much larger scale. This is of great relevance, as bridging the granularity gap between modelling large infrastructure investments on a continental scale, which will be described later, and small-scale investments at a local scale was one of the main goals of this approach. The structural change of this final demand switch in low-temperature heat applications for the relevance in single regions is also shown in fig. A.19. In addition to the utilization of high temperature excess heat (FT. process), the results of the case study indicate that a part of the low temperature heat demand might also be covered by the excess heat of electrolysis, pyrolysis and biomass gasification units. The realized demand coverage is however limited compared to the more model-technical utilization of high temperature heat within low temperature application (fig. A20).

The emission balance is completed by taking the storage- and transport network related emissions and the emissions of the non EHG related transformation sector, which might be either positive or negative, into account. As indicated in the previous figures, the emissions resulting from the transport and storage of energy carriers have only a limited impact on the total emission balance. In the annex (fig. A.21) a differentiation for the transport related emissions is added, which occurred during the pipeline and shipping-based transport of oil, LNG and natural gas. Overall, the highest impact is observed in the Turkish gas pipeline system. On top of these direct transport related emissions, the emissions of the storages (compressors run with carbon-based fuels) and of the gasification and regasification units are included in the previously shown

¹⁴ Within this case study, these first demands are assigned to mainly pilot projects in the steel sector.

balance. The key for balancing of all these previously analyzed emissions from the network, EHG and FD sector finally lies in the transformation sector for non-EHG related processes. Most processes in this sector, such as the hydrogen to jet process, are neutral regarding the CO₂ balance, as they do not directly extract or inject CO₂ into the atmosphere. However, this does not apply to the production of “blue” hydrogen through a methane reformation with CCS or the natural gas pyrolysis. The remaining emissions of these two technologies actually add 30 Mt CO₂ to the atmospheric CO₂ balance. In order to balance all these emissions in the sense of removing the emitted CO₂ from the atmosphere, the model chooses an investment into DAC units. In the final period the processes of the OCP (PERSEUS-gECT) sector, which in this context are often referred to as X2X processes, cause a net-reduction of 700 MtCO₂, which balances the atmospheric CO₂ emissions. However, it should be kept in mind that from the 730 MtCO₂, which are finally extracted by DAC processes from the atmosphere, the part that is used for the production of synthetic carbon-based fuels, appears on both sides of the balance¹⁵.

3.2.2 Development of the energy system as a result of mainly electricity related drivers

While the emission balance gives a first impression of the found solution, the distribution of installed capacities in the EHG sector for the electricity generation and their dispatch explains the fundamental drivers of the solution. As illustrated in the following figure, a primarily wind dominated electricity supply in 2050 is chosen with a share of renewables of 90%. The remaining conventional part of the total generation of almost 10 PWh is dominated by nuclear power plants, while the electricity generation from hydrogen is very small. The generation from carbon capture and storage power plants is also irrelevant while a CHP generation related electricity generation is basically concentrated on biomass technologies. As already mentioned, a limited dispatch of natural gas fired power plants, mainly combined cycle processes, is observed and focused on the MENA region. For this limited amount of natural gas in the power system, the investments into alternatives such as hydrogen firing or CCS are basically neglected and the emissions are balanced by DAC units as described earlier.

¹⁵ The reason is that the combustion of these fuels is modelled with a positive emission in the FD, EHG and network sector.

3 Application of the PERSEUS-gECT for modeling the development of the European energy system until 2050 considering energy imports from MENA, Central Asia and Patagonia

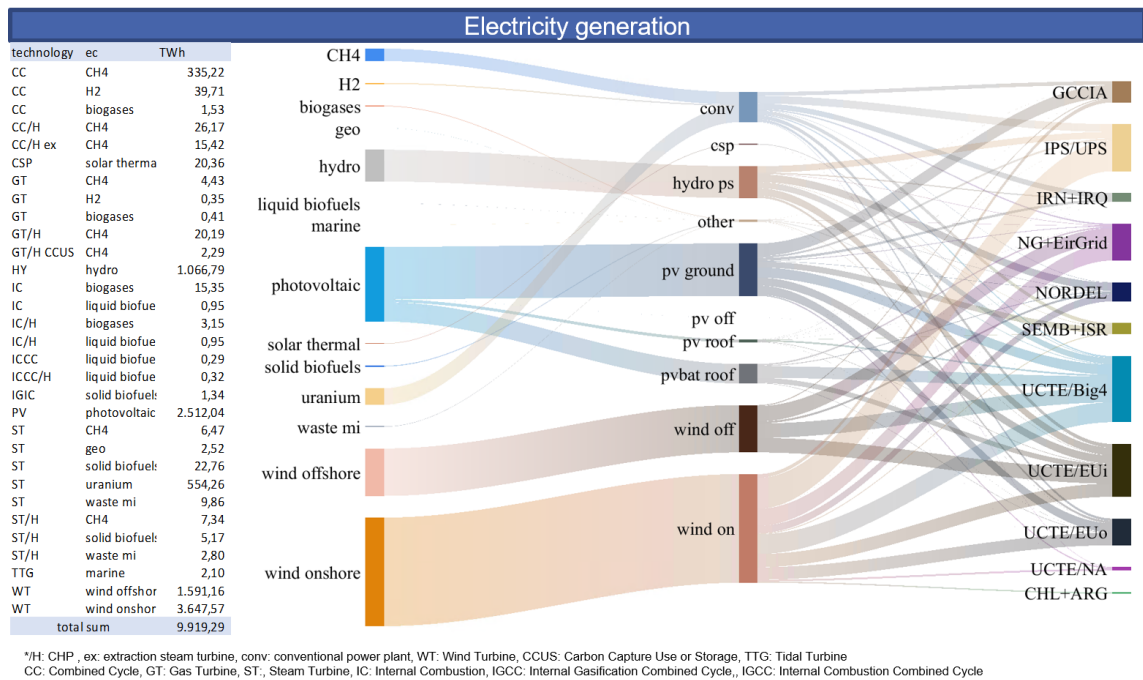


Figure 3.7: Structure of the electricity generation in 2050

Concerning the capacity, the previously observed relation between the electricity generation from solar energy and wind is reversed with a dominance of PV concerning the overall installed capacity. The bulk of this PV capacity, which is dominated by ground mounted installations, is distributed within the UCTE area, although a significant share of the endogenous expansion is allocated at the gulf states (GCCIA). In total rather negligible, but still interesting, is the realization of a 270 MW floating photovoltaic farm in combination with an offshore wind farm south of Sicily. As illustrated in the following figure, the installed electricity generation capacity is doubled within the optimization horizon as a result of the strong increase of WECS and PV installations.

3 Application of the PERSEUS-gECT for modeling the development of the European energy system until 2050 considering energy imports from MENA, Central Asia and Patagonia

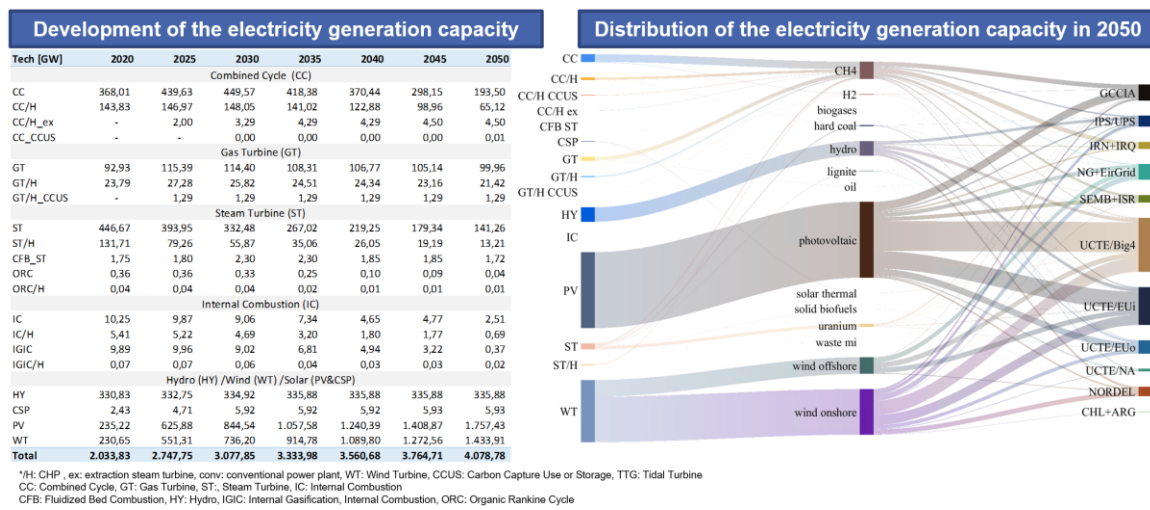


Figure 3.8: Development of the electricity generation capacity of EHG units and their regional distribution

Simultaneously the share of combustion or fission-based electricity generation technologies rapidly decreases, mainly due to the phase out of coal or lignite fired steam turbines. Until 2030 this fuel switch, however, is partially compensated by an increase of gas fired combined cycle and gas turbine power plants. The endogenous capacity investment¹⁶, focuses on the restructuring of the power system in areas which are not covered by the underlying base scenario. As illustrated, these investments are also dominated by wind and PV and are mainly realized in the MENA region and the eastern border of the UCTE region. In Europe, a significant additional wind onshore capacity expansion is observed in UK and Ireland. In this context, overall small investments into hydrogen fueled gas turbines and combined cycle plants might be mentioned in addition to marginal biogas investments, which also trigger the investment into an anaerobic digestion plant in order to produce the biogas¹⁷. Leaving aside batteries, the additional expansion accounts for 20% of the total EHG electricity generation capacity.

¹⁶ This refers to the capacity that is expended beyond the lower bound. Existing units or those under contraction are thus not included.

¹⁷ The endogenous expansion of 60MW CSP is realized by a single unit with the option of extracting steam for a neighboring high temperature heat-based process. While the unit size is rather typical for this technology, the overall relevance for the system is clearly negligible.

3 Application of the PERSEUS-gECT for modeling the development of the European energy system until 2050 considering energy imports from MENA, Central Asia and Patagonia

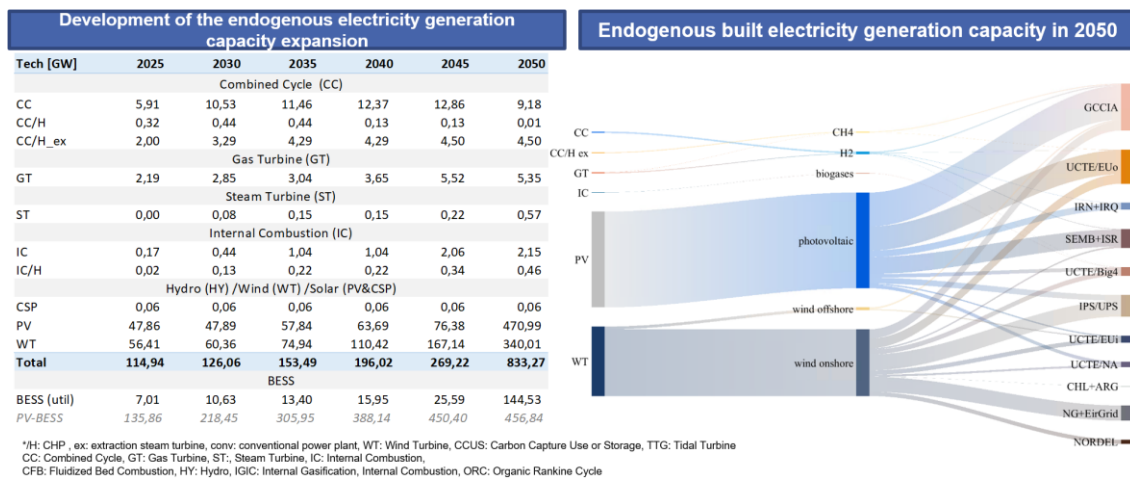


Figure 3.9: Development of the endogenously installed electricity generation capacity of EHG units and their regional distribution

Without any further security of supply restrictions or any national capacity adequacy measures in this case study, the development of the non-volatile and therefore flexibly dispatchable generation capacity is quite interesting. In the first step one might neglect that the contribution of these units to the secured capacity units is non-zero, especially in case of a feed-in into a coupled electricity grid which ranges from -16° to 140° on the longitude scale and 17° to 71° on the latitude scale¹⁸. In this case, the dispatchable capacity is restricted to combustion, fission and hydro based units, as well as CSP units, which are assumed to be secured due to the modelling with a 10-hour storage and a solar multiple of 2.4. Leaving aside batteries, this secured capacity clearly decreases due to the phase out of coal/lignite and later on also gas-based conventional generators. However, a stable development is observed if the battery capacity is taken into account, of which a 144 GW (576 GWh) investment into utility scale units is endogenously driven, while 465 GW (678 GWh) are realized due to the lower bound on PV-BESS systems. Actually, this non-volatile capacity increases by 10% until 2030 and later on drops to the 2020 level in 2045 before it is reduced to 95% of the starting level.

¹⁸ The coupling between non-synchronized grids is either realized by modelling a back-to-back HVDC connection within a station or directly by a HVDC connection, either by a two or a multi-terminal system. While all electrical sub-grids were connected by HVDC expansions in the first optimization run, which was more electricity based, in the final run, which tends to be gas-driven, GCCIA and Iceland are operated as isolated grid.

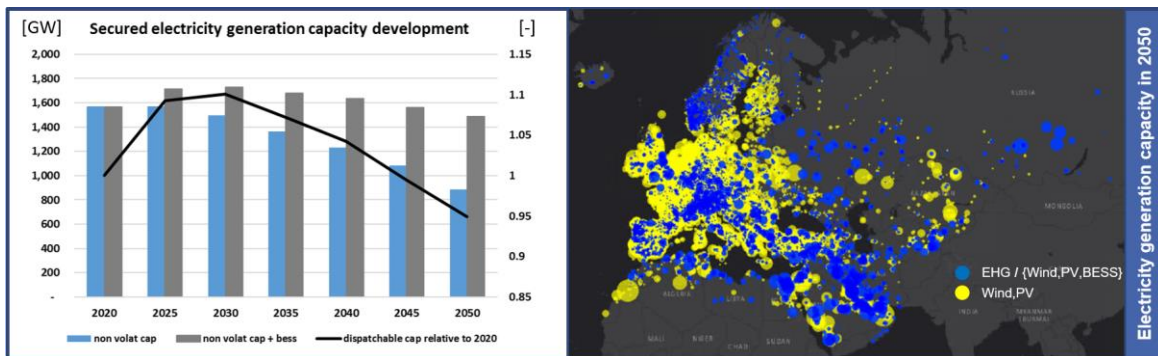


Figure 3.10: Development of the flexibly dispatchable electricity generation capacity of EHG units and their regional distribution

Overall, it should be kept in mind that these results might be only considered as a starting point for a subsequent generation adequacy analysis with the previously described PERSEUS-ADQ approach. With the massive reduction of the temporal resolution and without any additional constraints to ensure the security of supply in case of generator or transmission line outages, the found solution will most certainly require further back-up capacities in addition to the already applied DSM flexibilities, the installation of 1.254 TWh battery storages and a grid expansion, which will be analyzed later. While the drawback of a reduced number of time slices results from the computational limitations of a closed optimization within this case study and could be resolved by applying the developed ADMM based decomposition approach, the challenge of asserting the security of supply within the optimization is a structural problem due to the option of an endogenously final electricity and net electricity demand adjustment¹⁹. Despite all those limitations, the contribution of the fluctuating renewables to the load coverage is nevertheless interesting. In order to isolate this effect from the impact of final demand switching, demand side management and an additional electricity demand of the transformation sector, which all shift the load curve and dynamically react to the renewables availability to a certain extent, in the following figure the initial final electricity of the underlying reference scenario is used to evaluate the impact of fluctuating renewables on the residual load. It should be kept in mind that this electricity demand already includes a very high level of electrification of the overall European energy demand based on the underlying distributed energy TYNDP 2022 scenario or compromises the complete considered energy demand in countries outside of the extended European focus region²⁰. Although the hour of the highest residual load, defined here as the initial

¹⁹ With an increasing deviation between the previously estimated and the finally realized electricity demand a preceding security of supply estimation with PERSEUS-ADQ leads to either an over- or under-estimation of a lower bound for the addition of back-up capacities. With the high degree of freedom within this case study to either substitute all estimated heating or cooling related electricity demand or to define a completely electricity driven energy system, this preceding step is deliberately not chosen.

²⁰ As illustrated in fig. A16 the hourly grid load in Europe already nearly doubles in 2050 compared to 2019 due to the final demand electrification of the underlying scenario.

final electricity demand minus the available (not realized) wind and solar generation, could not be exactly estimated and consequently not validated in the grid model with the time step selection, the following figure already shows that the wind and solar generation has the potential for a broad residual load reduction.

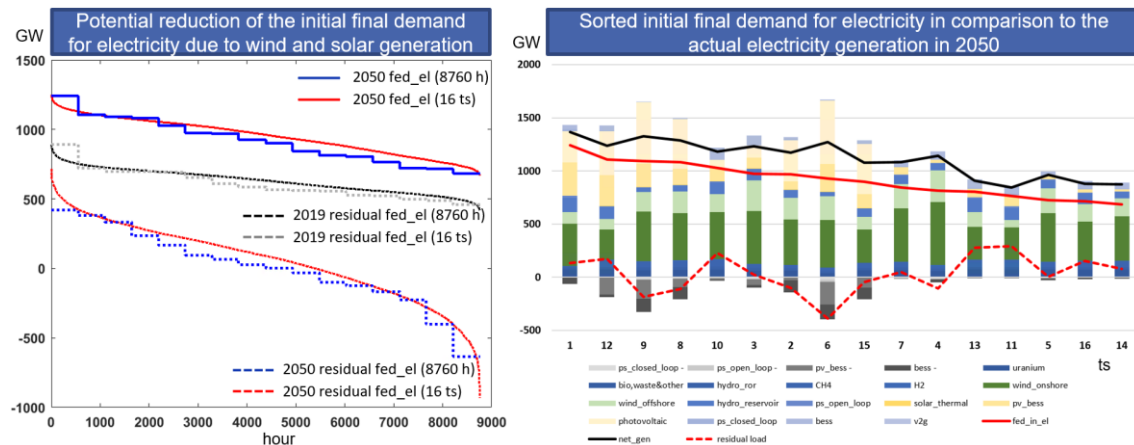


Figure 3.11: Development of the residual load and the contribution of intermittent renewables for the electricity demand balancing

Compared to the 2020 starting year, which is actually calculated based on the 2019 weather year and demand in order to avoid an artificial bias due to a Covid19 related demand reduction pattern, a clear reduction of the residual load might be observed, even in potential critical peak hours. This result is not the trivial cause of a general expansion of wind and solar conversion units but results from a technology and location specific optimization. Combined with an expansion of the electricity transmission, storage and conversion infrastructure, a regional distribution is found, such that the fluctuation of the different intermittent generators might be balanced in order to contribute to the load coverage in all hours of the year. In the underlying TYNDP 2022 scenario with the smaller regional scope and the higher concentration of fluctuating generators in the same region, especially in Germany, this was not the case as illustrated in fig. A.22. In the majority of the analyzed weather years, ranging from 1986 to 2020, the same maximum residual load actually increased in the range of 150 GW, despite of the large expansion of renewables. In contrast to this reference scenario, the found solution allows to reduce the maximum residual load compared to the start year by 176 GW in an 8760 h evaluation prior to any DSM or storage related generation or demand shifting and despite of the increase of this initial final demand by 2 PWh in total or 303 GW in the peak. The identified potential to reduce the need of back-up capacities for fluctuating renewable in the range of 300 GW is quite remarkable, taking into account that the additionally included regions account for 36 % (3 PWh) of the fed for electricity in 2050 and need to be balanced on top of the ENTSO-E demand²¹. The most interesting aspect

²¹ The increase in the initial final electricity demand from the starting year to 2050 is 49% for the ENTSO-E region and 11.11% for the remaining part of the model. In the ENTSO-E region it is

is that the expansion of the geographical scope and demand modelling did not increase the need for a renewables expansion compared to the underlying scenario. Instead, it could be realized by basically redistributing the capacity and technology of intermittent generators in the modelling region. While the overall capacity of WECS and PV remains rather unchanged, with an actual slightly decrease from 3254 GW to 3191 GW and slight shift towards a larger share of wind energy²², the gain is mainly realized on a regional level as shown in fig. A.23, which lists all changes for the technology capacities on a national scale. On the first glance, the comparison of the capacity development with the underlying TYNDP scenario might suggest a concentration of technologies at locations with most favorable resource conditions and a large-scale European import of electricity or power based fuels. Especially the significant capacity decrease in countries with less optimal weather condition (e.g., Germany: -40.1 GW for wind onshore, -3.32 GW wind offshore, -99.37 GW PV), in combination with a capacity increase in countries with good wind conditions (e.g., Kazakhstan: +45.7 GW wind onshore) or good solar conditions (e.g., Saudi Arabia: +97.81 GW or Qatar: +20.7 GW), might lead to this impression. This comparison is however misleading as the non-European countries²³ in the majority use the renewable expansion for a decarbonization of their own power system and in most cases also invest into technologies and locations with less optimal capacity rates but also less correlated (ideally negatively correlated) generation profiles (e.g., Kazakhstan: +14.2 GW PV, Saudi Arabia: +26 GW wind onshore, Qatar: +8/+8.3 GW wind onshore/offshore). As shown later, a non-neglectable share of the renewable generation in regions with existing or potential fossil gas resources is actually not only used for the final demand balancing but for either running the natural gas infrastructure²⁴ or supporting the production of blue hydrogen from natural gas with a subsequent carbon capture and storage²⁵. Apart from that, the example of Germany shows actually that the modelling results tend to decrease and not increase the concentration of generation capacities allocated in the more

mainly driven by a sector coupling related electrification of initially fossil driven technologies, such as the replacement of gas fired boilers through heat pumps in the heating sector or ICEV through BEV I the transport sector. In the remaining regions this is basically neglected and the demand increase results from a classical economic and population related growth.

²² The capacity of wind energy increases from 1,420.26 GW to 1,434.9 GW, with a shift towards wind onshore, which increases from 1,010.5 GW to 1,418.6 GW while offshore was reduced from 409.7 GW to 385.3 GW. Contrary, PV is reduced from 1,833.9 GW to 1,757.4 GW.

²³ In this last model run the Gulf States are actually not even electrically connected to the other grid part, as already outlined.

²⁴ The energy demand of gas compressors, liquification, regasification units etc. is modelled endogenously. In all LNG exporting countries with the option of a renewables expansion, the units are realized as completely or partially power driven processes. Only the LNG terminals in the USA and Nigeria, of which in 2050 only the latter one is supplying LNG to Europe, are operated with natural gas. Venezuela/ Trinidad is not part of the solution in any year.

²⁵ Although the steam reformation is currently modelled as a process which is mainly driven by natural gas, the electricity demand of the subsequent CCS processes, which are mainly compressor units at the CO₂ pipeline and of the gas storage, are realized as electricity driven processes.

or less same weather system. The comparison with the lower bounds on the capacity variables²⁶ shows that for all technology classes actually a small endogenous increase is observed (+500 MW wind onshore, +400 MW wind offshore, +2.26 GW PV) in order to cover a punctual demand. With an installed intermittent capacity of 401 GW, Germany is also still the country with the highest installation in this technology class, concentrating 13 % (previously 17%) of the total capacity in a single country. By redistributing a part of the additional capacity, which could be only realized in less favorable spots²⁷, on the AC or DC interconnected electrical neighboring countries like Denmark (onshore: add 22.13 GW to 10.87 GW) or UK (onshore add 38.75 GW to 64.7 GW), a better balanced system might be realized while utilizing the still available potentials with good resource conditions. The following figure, which shows the summed-up wind onshore grid injection in the AC transmission network (bubbles) with the absolute flow on lines of the reference grid (violet-blue scale) and the expansion grid (red-yellow scale) illustrates a further property of the found solution. In order to balance the North Sea dominated coastal wind onshore cluster (UK, IE, DK, DE), which comes on top of the later shown concentration of wind offshore in this region, a new cluster in Ukraine and Belarus is created and interconnected to the eastern load centers (Moscow, St Petersburg) and the western load centers (Warsaw, Krakow, Budapest) based on a grid expansion. As indicated in this figure, and shown in more detail in fig. A.24, the expansion of the electricity grid is used to support the grid interaction of the wind onshore generation not only in this cluster but also in other local hotspots such as Ireland or the Gulf of Lyon.

²⁶ The choice was not set randomly but based on the analysis of a preceding expansion planning to meet the TYN target.

²⁷ Despite of the expensive need for expending the electricity storage and transmission in order to avoid the already existing problem of congestion management, the previously discussed results, which were basically driven by the German capacity expansion, also showed that adding further 143 GW into the same weather cluster only marginally contributed to secure the supply in critical hours.

3 Application of the PERSEUS-gECT for modeling the development of the European energy system until 2050 considering energy imports from MENA, Central Asia and Patagonia

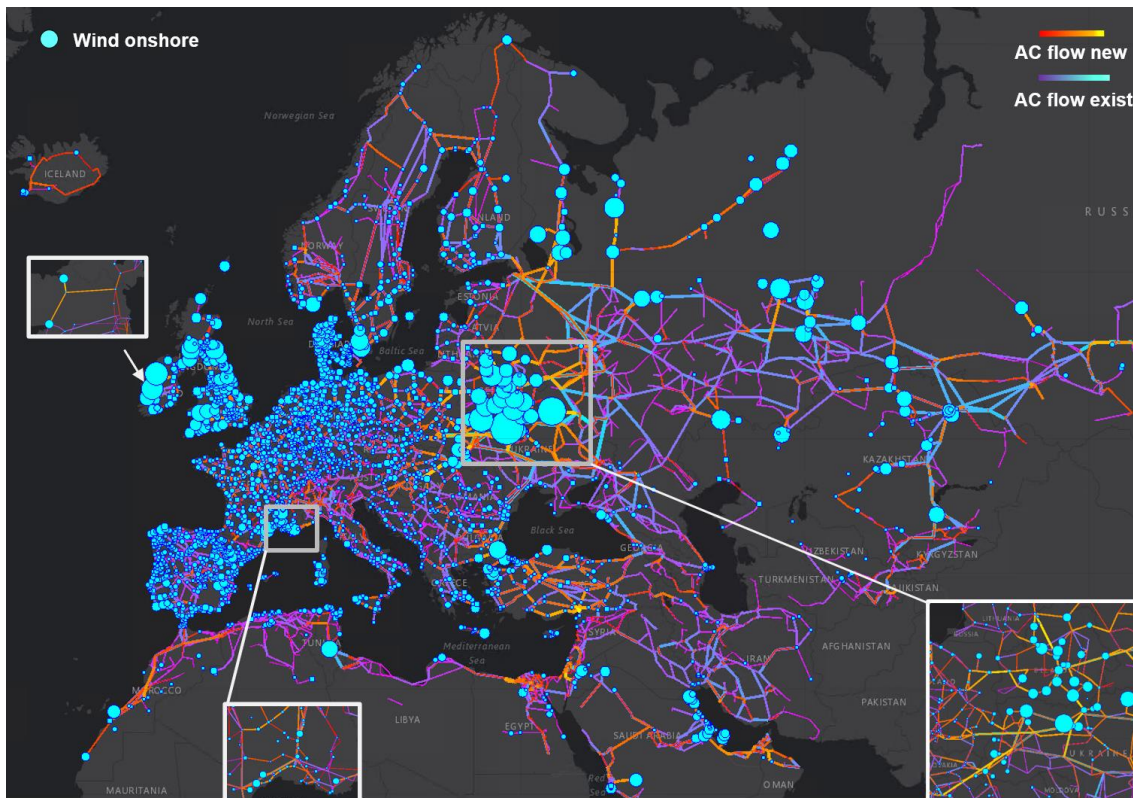


Figure 3.12: Cumulated wind onshore injection into the AC grid and the utilization of the AC grid in 2050

Combined with the expansion of utility scaled battery energy storages, which is shown in fig 3.16 and discussed later, a system is build which allows to utilize almost all available generation. The total curtailment of wind energy, comprising the onshore and offshore generation which is either grid connected or operated in an isolated mode in non-electricity grid balanced onshore systems (Patagonia) or offshore at gas nodes for a hydrogen production (partially in the North Sea) is 3.2 %, as illustrated in fig. A.25. For offshore wind parks, which are discussed next, the grid connection and subsequent grid integration is the most crucial part considering the high concentration of correlated generation in a small focus region in the North Sea. From the capacity density point of view, which is illustrated next, this point is not directly obvious as not only the installed wind onshore, but especially the PV capacity in the triangle of the Benelux States and the western part of Germany (especially the rooftop PV capacity in the German population centers in the Rhein Ruhr metropole region), shifts the focus from the North Sea to the coastal region. From the viewpoint of the total electricity generation from intermittent renewables, illustrated in the left figure (fig. 3.13), the high offshore concentration in the North Sea and the challenge to integrate this generation, becomes however clear. Only the additionally observable counterbalancing wind onshore generation in the Ukraine, Belarus cluster, for which its grid integration was discussed earlier, shows a comparable density.

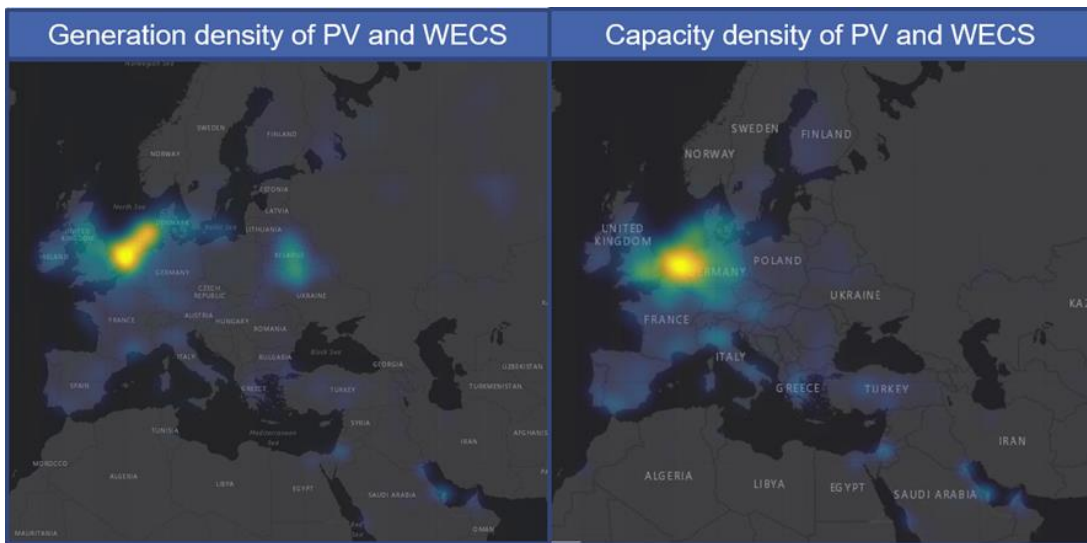


Figure 3.13: WECS and PV electricity generation density (left) and capacity density (right)

For offshore wind parks with the option to decide between a direct point-to-point grid connection (yellow scale) or the connection to a multi terminal HVDC system (blue scale), the realized DC flows are therefore displayed besides of the HVDC flows of the general interconnected electricity grid. While a direct connection to the next onshore substation is chosen in most cases, it is interesting to observe that an overlay DCMT system is built between UK, DK, NL, DE, BE and FR which connects the largest wind parks and increases the cross-border exchange between these countries. In some cases it is actually clear, that the combination of point-to-point based direct wind offshore connection systems and meshed overlay HVDC systems is built to increase the general transmission capacity between these countries. The better grid connection of the offshore generation in these cases is thus rather a positive side effect and not the main reason for the grid expansion²⁸. The allocation of electrolyzers and batteries in this focus region, which will be analyzed later, in combination with the expansion of the hydrogen grid, explains how these very low values for a generation curtailment could be achieved.

²⁸ The meshed overlay HVDC grid, which is built in Germany basically parallel to the existing or planned HVDC north/south corridors and is extended in the North Sea in a way that even load centers in Scotland are connected, in consequence also serves for a distribution of the PV generation from southern Germany. The offshore grid connection is thus not only used for unidirectional flows from the Sea to the Land, or north to south from a German perspective, but may also be operated with a reversed flow direction in hours with low wind feed and high PV penetration. Even offshore electrolyzers are in consequence run with onshore PV generation during these hours.

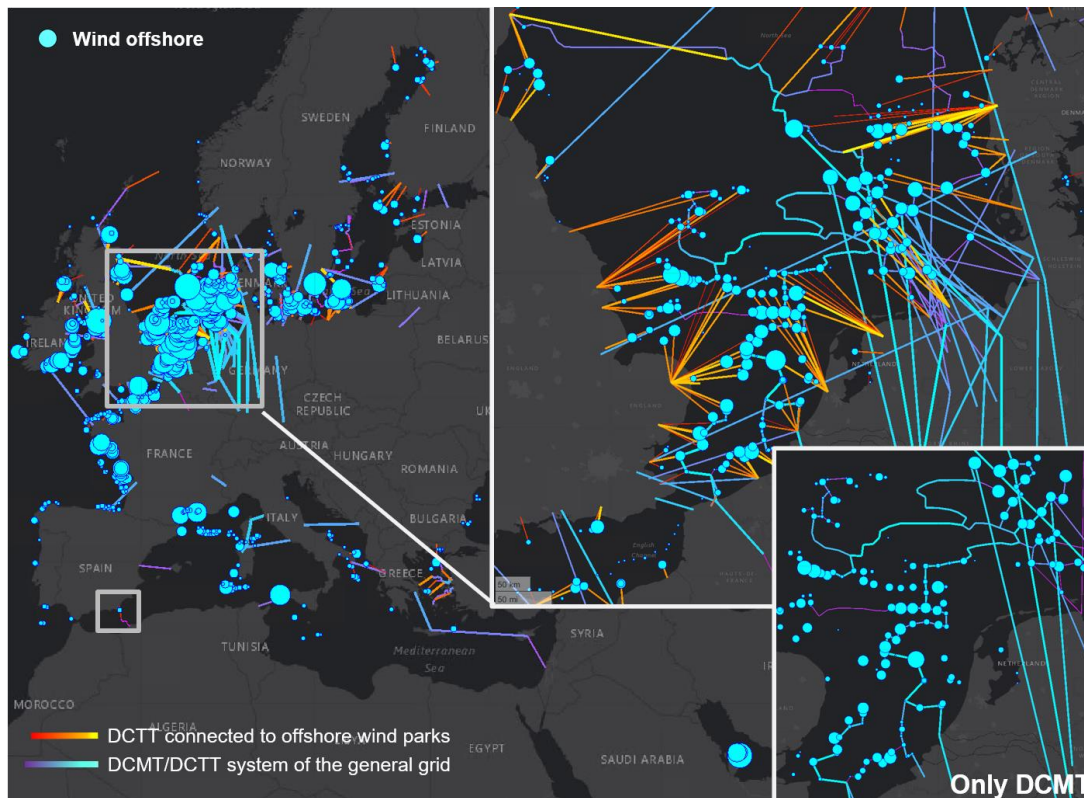


Figure 3.14: Cumulated wind offshore generation and the utilization of the HVDC system in 2050

For the integration of the intermittent PV feed-in with its high daily fluctuation, the expansion of the electricity transmission grid is not the most relevant factor as the expansion of each transmission system seems to follow the rule of being dimensioned with respect to a rather steady operation. In case the PV generation is plotted with the background of the AC grid utilization, in consequence an opposite pattern to the previously observed wind onshore case occurred. Areas with a high flow on expanded transmission lines, for example in the Ukraine, Belarus wind cluster or the Irish wind cluster, show only a few PV injections. Only in selected regions, such as Turkey or Israel, a significant grid expansion next to spots of the main PV injection might be observed. For Israel, which includes the largest single PV park which is connected to one node with a capacity of 12.5 GW, the initial island operation is actually switched. The main connection to the UCTE dominated power grid is realized by realizing a HVDC connection to Cyprus (which is expanded to Greece via Creta)²⁹. In most cases, however, the PV generation is fed in next to load centers, either due to the expansion of rooftop PV, where this is at least partially true at least for the residential part, or by selecting the location on ground mounted PV with respect of minimizing the distance to consumers. This later pattern is often observed in the MENA region, especially in Egypt.

²⁹ Relevant flows to neighboring countries include only one connection to Jordan. The flows are however basically just transit flows to the mentioned endogenously expanded Israel- Greece corridor.

3 Application of the PERSEUS-gECT for modeling the development of the European energy system until 2050 considering energy imports from MENA, Central Asia and Patagonia

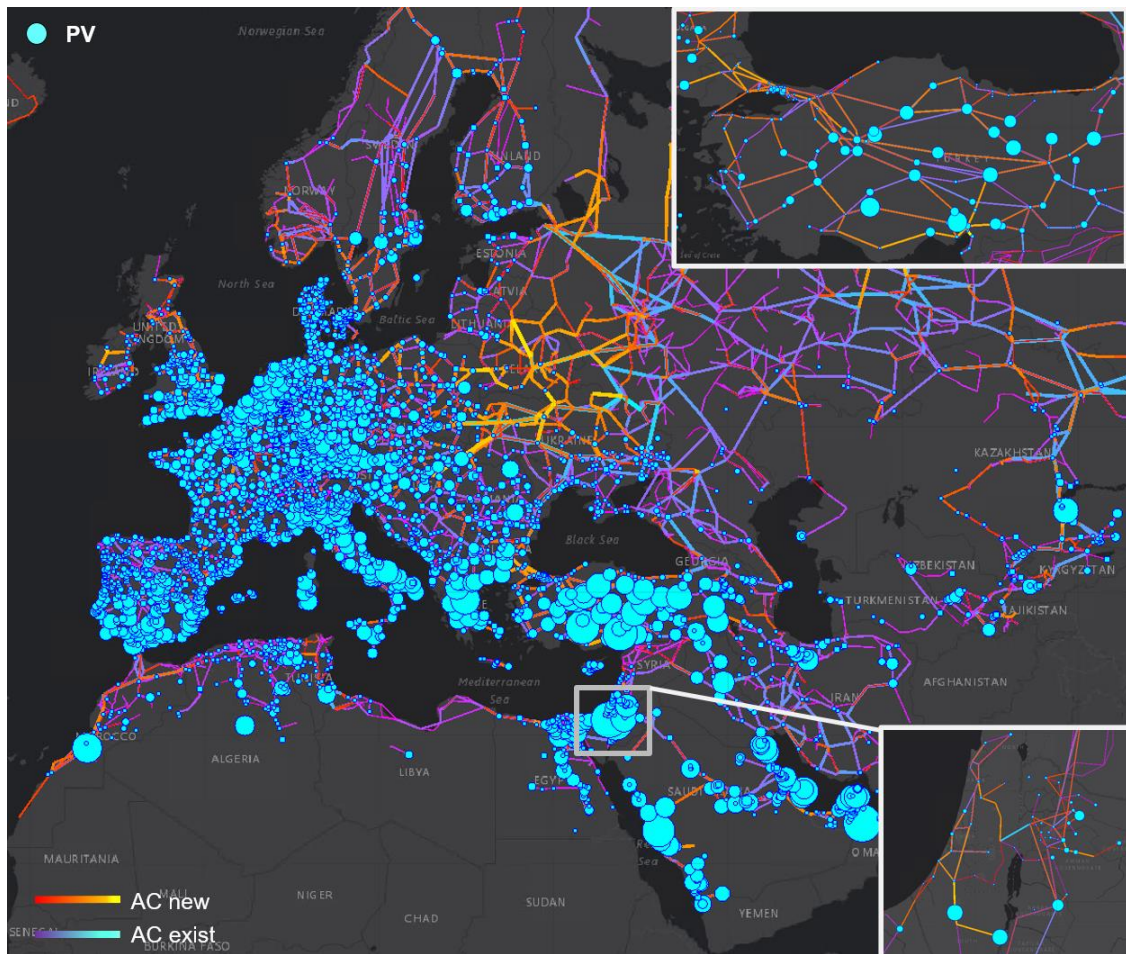


Figure 3.15: Cumulated PV injection into the AC grid and the utilization of the AC grid in 2050

The general observation of a rather local PV utilization is supported by the fact that basically all available projects which focused on a direct HVDC connection from North Africa to Europe with the goal of utilizing the mainly solar dominated generation potential for the demand balancing in Europe are not realized. Although the project sites in Africa showed to be well suited for the energy production and the generation expansion is realized, the connection to Europe through the electricity system and despite of Algeria also through the gas system, is largely omitted. Instead of realizing connections like Xlink (Morocco-UK), TuNur (Tunisia-Italy) or GREGY/EuroAfrica Interconnector (Egypt, Greece), the PV dominated generation expansion is used to decarbonize the local power sector and cover the demand of a growing population.

The most crucial part for the integration of PV, which shows a curtailment of 2.1 % of the total generation (Annex) and is therefore almost completely integrated, has the dimensioning and allocation of battery energy systems in combination with the load of existing or potential conversion processes of the final demand or transformation sector. As illustrated next, the endogenous expansion of utility scaled battery systems at the first glance seems to be concentrated at the same spots as the endogenous PV expansion in the MENA region, Turkey or Central Asia. For Turkey and especially Israel, where the largest BESS unit is connected to the same node as

the largest PV unit in the model, this is true and clearly coincides with the observed electricity grid expansion.

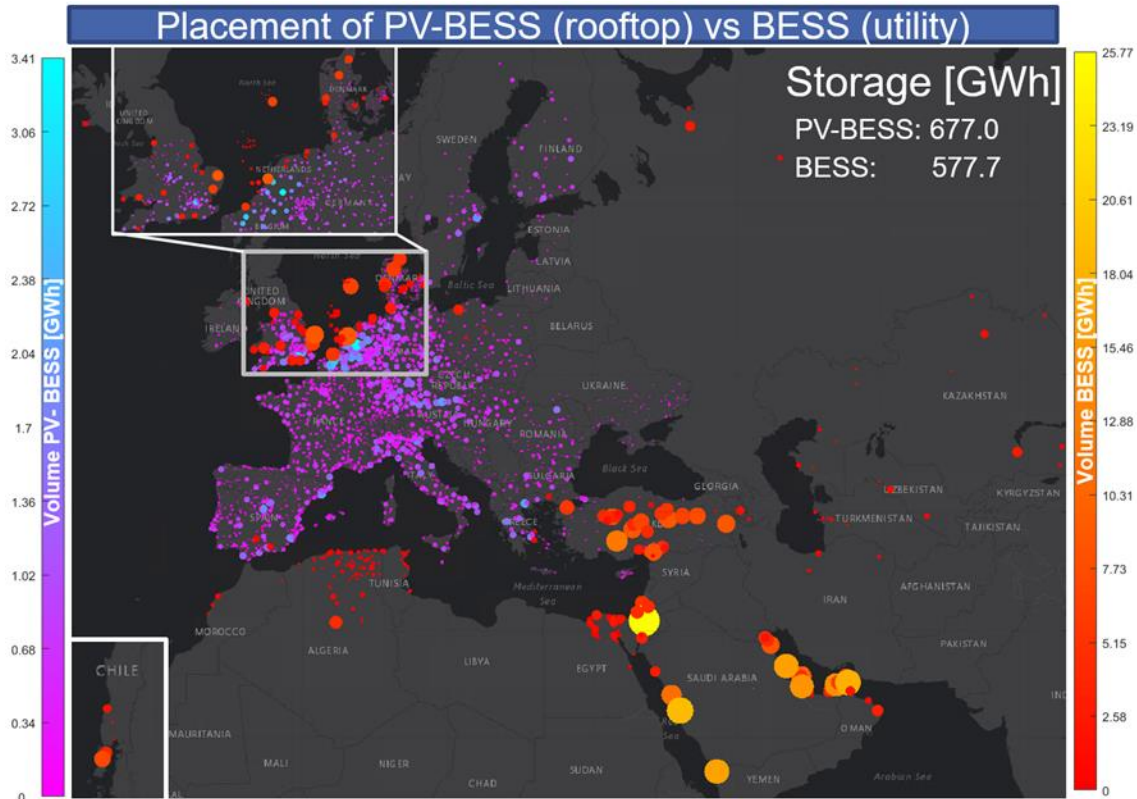


Figure 3.16: Comparison of the allocation of rooftop PV-BESS units and ground-mounted utility scale BESS units

For the Gulf States and Egypt, this observation is however only correct for locations next to central ports. Although these locations are also load centers, they additionally often benefit from a base power supply in order to operate a mainly LNG orientated transport infrastructure. A comparison of the PV location and battery location along the Nile illustrates this effect well. Only in the Nile delta, where in addition to the load centers also the demand of the CCS infrastructure³⁰ needs to be balanced, batteries are installed. As a consequence of this direct PV utilization in North Africa, the capacities are dimensioned in a way that the power might be locally consumed or distributed with only a moderate need for an expansion of the electricity transmission infrastructure. In peak demand hours during the evening the additional moderate wind onshore expansion (EGY: +5.19, DZA: +7.33, MAR: +4.96, ESH: +1.67 GW) thus might be not sufficient to balance the demand if the wind feed-in is additionally moderate. This is especially the case in Egypt but also applies to most Gulf States and explains the investment and dispatch of natural

³⁰ Electricity used to capture and store the CO₂ from the natural gas reformation. Hydrogen is afterwards injected into the new Egypt-Cyprus-Greece interconnector, which will be described later.

gas fired turbines in this region. This explains the initially irritating result, that countries with attractive solar potentials outside of Europe, which only need to decarbonize their power sector, are ranked relatively high in the net emission balance. Considering that the overall net CO₂ emissions, which need to be removed from the atmosphere, are nevertheless quite low, explains the economic attractiveness of this solution. Large scale investments into the storage, transmission and distribution infrastructure are consequently omitted. In Europe, on the other hand, the availability of rooftop PV based battery storages systems (PV-BESS), which are mainly installed in single family or two-family buildings, are the main driver that supported the grid integration of the PV generation, despite of a certain DSM shift, especially from the controlled home charging of battery electric vehicles (BEVs).

Due to the comparably high expanses for such systems, PERSEUS-gECT however does not chose to expand the capacity beyond the scenario defined lower bound. Instead, mainly ground-mounted PV installations are chosen as endogenous decisions without the option of placing a utility scaled battery at the same or neighboring electricity node. In Europe, this technology combination is mainly observed in Turkey and partially in the south of Spain to a significant extent. Besides of these two regions, batteries are mainly placed in the coastal regions or directly offshore in order to support the grid integration of the wind offshore generation in the North-Sea hub. The high expanses for hydrogen liquification, which mainly takes place in Chile and favors a steady operation, additionally triggers a battery expansion in order to support the hydrogen infrastructure in this region from the intermittent wind onshore generation. This economic dimensioning problem between an off-grid wind-onshore generation in a remote area and the investment and operation of electrolyzers, hydrogen tanks, liquefaction, LH₂ tanks, port infrastructure and ship investment on the export site explains the later observed parallel investment into an LH₂ (expansive, lower losses) and LOHC (cheaper, higher losses) infrastructure in Chile³¹.

The sum of these complex interactions between the allocation of intermittent renewables, electricity grid expansion and electricity storage expansion explains how the previously observed potential residual load, which was the initial final demand minus the available WECS and PV generation, could be actually realized in the model. This means, how the WECS and PV units could actually be dispatched without the need of a massive grid or storage expansion or curtailment. The key factor to decrease the maximum residual load and thus the need for dispatchable generators while increasing the regional scope and the final electricity demand of the model, compared to the underlying reference TYNDP scenario, was the technology specific regional allocation planning. This allowed to balance the intermittent generation while actually lowering the installed renewables capacity. The defined final electricity demand in the initial scenario is however non-static. Besides of the possibility of a temporal shift due to DSM processes, the investment into final demand switching processes, which increases the final demand needs to be taken into account for an analysis of the contribution of renewable to the load coverage. In the previous ceteris paribus analysis this effect was deliberately neglected in order to compare the found

³¹ In this context an additional 110 MW ground mounted PV farm was installed next to the chosen export terminal in Chile.

solution with the TYNDP scenario from the capacity adequacy point of view. Taking into account the complete energy system and not just the power system, the question changes regarding the contribution of the intermittent renewables to the total power generation and the contribution of the power sector to the total energy balance. The following figure, which ignores the impact of DSM processes, gives a conservative impression on the suitability of renewables to cover the net demand. In contrast to the previous illustration in fig 3.17 the following figure shows the dispatched of power generating units in chronological temporal order and the impact of additional electricity demands³².

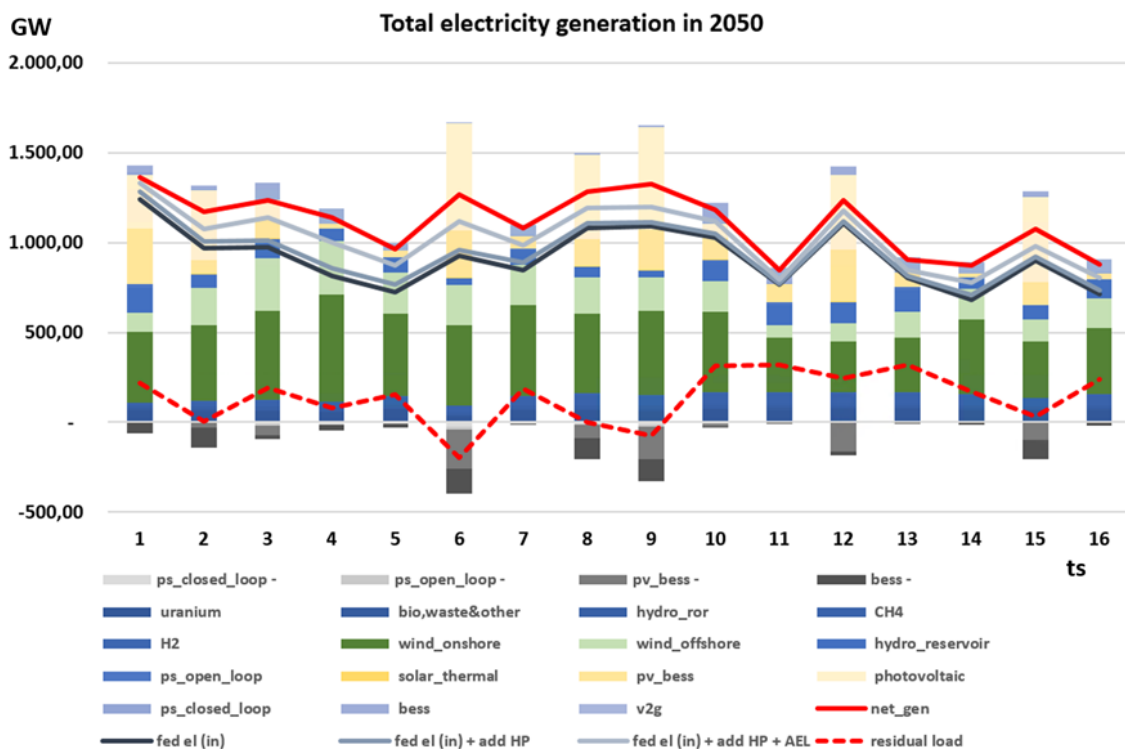


Figure 3.17: Stacked electricity generation of EHG units, differenced by main conversion class in 2050

As expected, the model's choice to invest mainly into heat pumps in addition to the TYNDP scenario defined capacities increases the final electricity demand. For the whole year this resulted in an additional final electricity demand of 233 TWh which is used to mainly lower the natural gas demand in 2050³³. The impact on the total hourly load in single hours however is rather small. In the peak load hour, which is exactly estimated and calculated in the first time slice, the

³² A comparison between the total electricity generation in the System and in Germany is provided in fig. A.26.

³³ As discussed previously, the investment into heat pumps in earlier periods is mainly reducing the oil demand in the residential heating sector. In 2050 this impact is however rather irrelevant as the investments reach the end of their technical lifetime and most oil is phased out in the underlying scenario anyway.

final electricity demand is increased by 45.6 GW. In the peak residual load hour, which lies in a rather wind calm summer evening (ts 11), a small increase of 4.7 GW, mainly for water heating applications, is observed³⁴. Taking the demand of electrolyzes into account, which are mainly realized by an investment into AEL units, an additional load of 783 TWh and 156 GW peak demand is included, which adds 43.5 GW in the peak load hour and 20,4 GW in the peak residual load hour. The previous figure consequently illustrates the significant contribution for a demand coverage in peak load and peak residual load hours which might be provided by intermittent renewable if their allocation and technology shares are locally optimized. Even without DSM the maximum residual load remains quite low and a comfortable margin between the realized net generation and this hypothetical load remains for covering the electricity demand of other processes of the transformation sector and the losses of the electricity transmission and storage. With the right mix of generation profiles and a more balanced distribution in the transmission grid it is possible to balance the already in the TYNDP scenario included demand increase of processes from coupled sectors such as the transport sector (BEV) or heat sector (HP) without an increase of the maximum residual load. The model decision to cover the additional demand of the non-European region while slightly decreasing the capacity or renewables, however, has the drawback that electricity for a large-scale hydrogen production from power is missing. Overall PERSEUS-gECT choses to produce only 519 TWh of hydrogen from electrolyzers in the case study. Partially this might be explained by an overall lower hydrogen consumption compared to the TYNDP scenario, as this fuel is basically irrelevant in the power sector in the case study. Furthermore, the expansion of heat pumps for the production of low temperature heat was not only targeting at lowering the natural gas demand in the heating sector, but also at lowering the hydrogen demand, when possible³⁵. In order to cover the remaining hydrogen demand, which results either from fixed processes or the replacement of fossil fueled boiler through a hydrogen combustion in the industry³⁶, an additional production of 1.1 PWh H₂ from natural gas is realized. To a certain degree, the process chain for the production of this “blue” hydrogen is a driver of the electricity demand and covered by the installed intermittent renewables. In this case the renewables are either used directly in the conversion phase for the natural gas pyrolysis, which accounts for 10% of the blue hydrogen production while the majority is based on a steam reformation with CCS, or in the subsequent or preceding processes chain. As already outlined, this includes the electricity demand of compression, cooling and heating processes of the NG, LNG and CO₂ production, transmission (mainly pipeline or shipping) and storage (tank, cavern) in addition to the same process chains for the H₂ handling. Besides of losses and the demand of

³⁴ Such a max residual load case is quite easy to handle in a wind dominated system, with this large geographical scope, as it occurs during the low wind periods in summer nights, where the batteries, either from PV-BESS system or the standalone utility size BESS, might be charged.

³⁵ With an average COP above 3.5 for heat pumps and efficiency below 1 for gas boilers the additional 233 TWh electricity demand replaces a multiple of the natural gas and hydrogen demand if the processes are switched.

³⁶ As high temperature heat pumps are not considered it is possible that some part of this hydrogen demand might be also mitigated by an alternative electrification route.

DAC processes this natural gas related electricity demand partially explains the observed margin between the electricity net generation and the sum of final and electrolysis related demand processes. While the gas flows will be analyzed at a later point, the allocation and dispatch of electrolyzers in the electricity grid is displayed next.

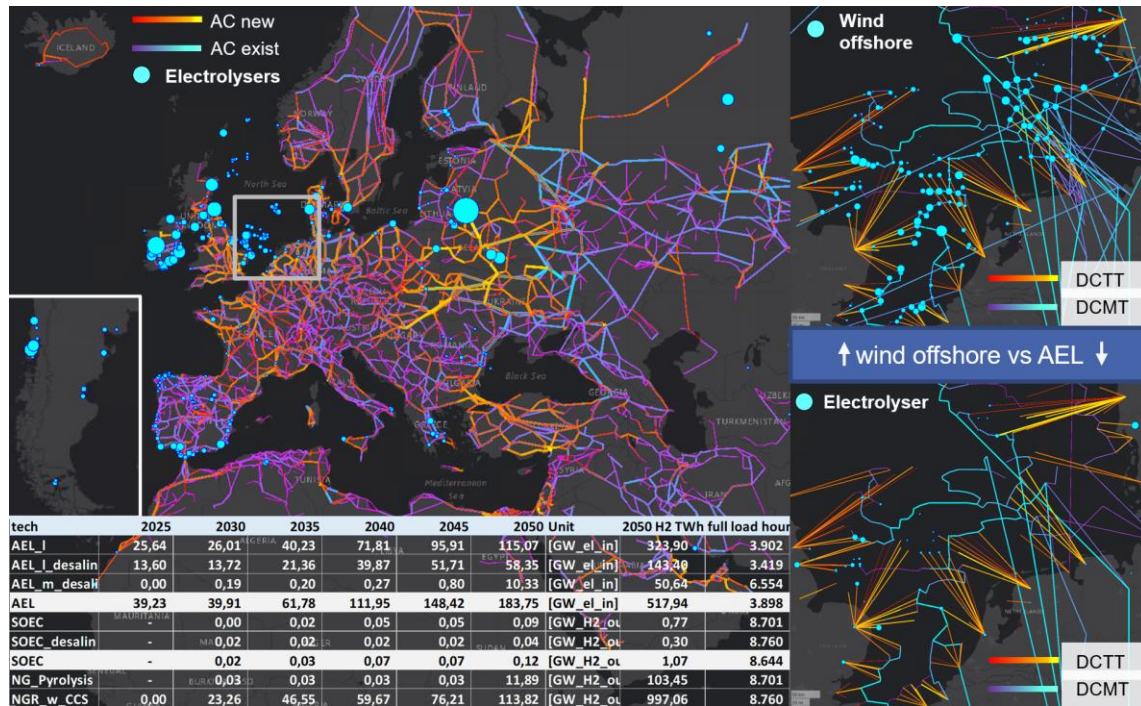


Figure 3.18: Cumulated electricity demand of electrolyzers in the AC grid and comparison with the wind offshore generation in 2050

In comparison with the previously shown allocation and dispatch of wind onshore, offshore and PV, the technology choice, dimensioning and dispatch of electrolyzers might be explained. The general observation is that the expansion of electrolyzers is focused on large scale alkaline units which are allocated in the neighborhood of renewable generation clusters which are located apart from load centers. As shown later, this development is accompanied by investments into the hydrogen transport and storage infrastructure (pipeline, shipping), which is expanded for this task. For the system integration of fluctuating renewables which are located apart from load centers, an indirect conversion route is chosen which reduces the expansion of the electricity grid. With respect to electricity storages the impact of electrolyzers is less clear. On the one hand, an investment into BESS is observed at insolated regions (Patagonia, Siberia) with the goal of increasing the capacity factor of electrolyzers or facilitating the grid integration of wind-offshore in the North-Sea. In the second case BESS units are either allocated offshore at the same node as the wind park and the AEL unit or onshore at the landing points along with AEL units. For wind onshore such an effect is however not observed while for PV the effect tends to be reverted. In Spain and Greece the demand of electrolyzers, which are dimensioned rather and small and distributed, actually seems to reduce the need for a large scale BESS expansion,

especially when comparing with the centralized PV and BESS expansion in Turkey and Israel, where this demand is missing. Overall, multiple clusters might be identified. From a technological point of view, the allocation of large scale AEL units, which do not require a desalination process is favored and dominates the installations in northern European countries. For offshore applications or in dry regions, the units are realized with an additional desalination process. As these units are also more often allocated at remote areas (Chile/Patagonia) or supplied by PV, which shows a higher fluctuation than wind, the full load hour of this second class of AEL units is a little bit lower than of the first class, as visualized in the table in the previous figure. Finally, also medium scaled AEL units with a desalination are realized on a smaller scale than in Algeria or Siberia and dimensioned in a way that they might be operated with higher full load hours (6954 vs. 3902 (AEL_I) or 3419 (AEL_I_desalin)) in order to compensate the higher investment expenses. This is also the main criteria for the dimensioning of SOEC units, which produce just 1 TWh of hydrogen. The few realized units are all allocated at the landing point of offshore HVDC connections and are basically operated in base load mode due to the overall small H₂ production capacity compared to the capacity of the HVDC converter unit. While in most cases the attribution of the renewable power source to the electrolysis based hydrogen production is clear, such as wind onshore in Patagonia or Ireland or for PV in Spain, the situation in countries with nuclear energy production is ambiguous. For Hinkley Point, Sizewell C (UK) and Flammenville (France) the relation between the dispatch and allocation of nuclear power plant, wind offshore and onshore generators and electrolyzers is illustrated in the Annex for 2050. The last two mentioned units are dispatched in a direct neighborhood to the onshore grid connection of offshore wind farms, where also rather smaller scaled electrolysis units are operated. Considering the relatively small hydrogen production it might be assumed that the utilization of nuclear power at this point was not the main motivation for electrolysis allocation. At the Belarus-Lithuanian border region, the situation is however not that clear and the question whether the nuclear power plant fleet plays a significant role for the hydrogen production or not might play a much more significant role. Next to already described onshore wind cluster in this region the largest hydrogen production from power is observed as shown in the next figure. In a relatively small area an installed electrical electrolysis capacity of 21.9 GW is concentrated, which is quite large, considering that this is comparable to the 21.19 GW offshore units (21.1 GW onshore) units in UK. Additionally, a nuclear power plant is dispatched in the neighborhood. Although the highest power flows are observed from the wind cluster to the electrolysis units, the additionally observed significant flows from the nuclear power plant, reinforce the assumption that the electrolyzers are partially operated with generation from the nearby nuclear power plant (2.4 GW) in addition to the available renewables (e.g., from the 30.4 GW Belarus wind onshore cluster)³⁷.

³⁷ It is observed that the electricity from the Belarus cluster tends to flow in the east direction (Russia) while electricity from the Ukrainian cluster shows a clear flow direction towards west.

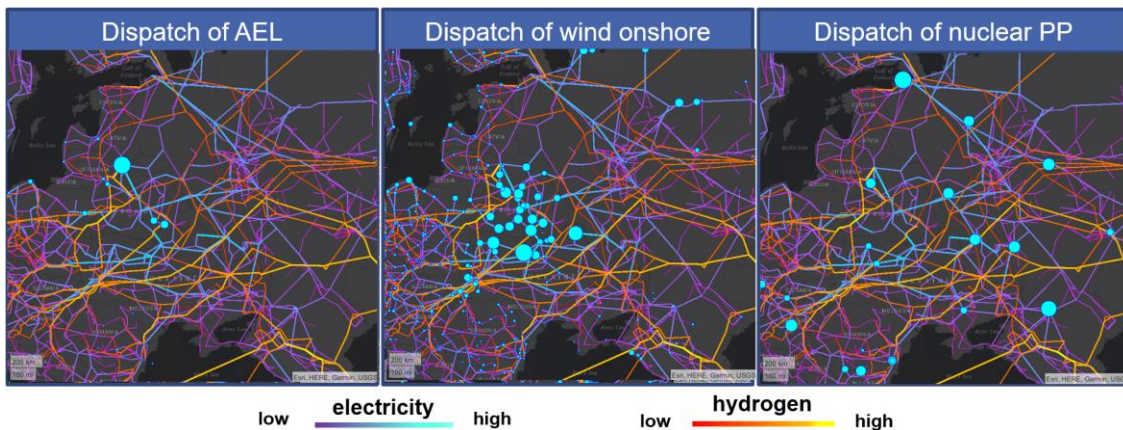


Figure 3.19: Comparison of the dispatch of electrolyzers (left), wind onshore units (middle) and nuclear power plants (right) with respect to the utilization of the hydrogen and AC grid in Eastern Europe in 2050

Overall, this example illustrates how the expansion of intermittent renewables and electrolyzers is affected by the structure of the existing gas and electricity infrastructure. The existing natural gas pipeline infrastructure, which is retrofitted to a hydrogen transport at this region as shown later and the availability of a CO₂ free dispatchable nuclear generation capacity, which guarantees a certain minimum utilization of the electrolyzers during calm wind hours, might have been drivers why this wind onshore cluster was realized, besides of the good wind conditions. Basically, the same conditions (high wind potentials, existing gas grid, existing nuclear power plant fleet) are also available in the Ukraine cluster, but in this case the retrofit of the natural gas grid is used for a transit of “blue” hydrogen produced in the Caspian region. Before analyzing the results with a focus on the gas grid, in the following the electricity grid expansion is briefly summarized.

Although the need for an electricity grid expansion is reduced due to the placement decision of electrolyzers, some expansion is still needed and illustrated below. In the AC grid a net expansion of 2.2 TW (absolute 3.31 TW) or 11.8% compared to the reference case is observed. However, it should be mentioned that this reference grid already includes some fixed expansion projects, in specific regions such as Germany. Although the capacity addition is rather moderate, it should be considered that the average utilization of expanded lines is 53% compared to 18% in the remaining grid. This effect underpins the general observation that the energy system is dimensioned in a way such that each component might be operated with high full load hours.

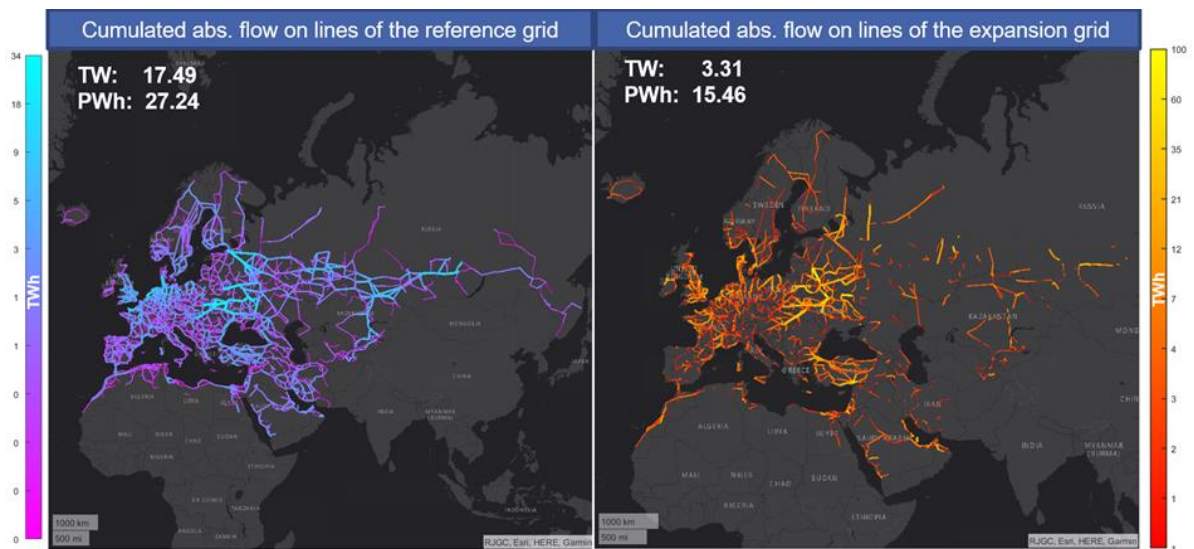


Figure 3.20: Comparison of AC line flows on edges of the reference grid and the expansion grid in 2050

As expected, the AC grid expansion is focused on regions with a high wind onshore expansion and on strengthening the grid in the coastal regions where the offshore generation has to be integrated. Besides of stronger grid expansion along the Baltic coastline, it is interesting to observe that there is basically no significant grid expansion which increases the East-West transit capacity in Eastern European countries like Poland, the Czech Republic or Austria and that Spain, Italy and the Balkan also face just minor expansions. Therefore, on the AC side no backbone grid is built which substantially increases the transport capacity between Africa and Europe or Central Asia and Europe or even between the North Sea based wind cluster and the Eastern European wind cluster. As shown in the next figure, such an electricity grid expansion is also not realized in the HVDC grid. From the point of view of a large-scale coupling of remote parts of the power system, only the Israel-Cyprus-Creta-Greece-Italy corridor might be mentioned³⁸. Overall, the expansion of the HVDC grid is driven by the expansion of the wind offshore generation or related to this task. From a structural point of view, it increases the interconnection of littoral states of the Baltic Sea and the Nordic Sea as well as the north-south transmission capacity in Germany. On top of the direct connection of offshore wind farms, nevertheless, the expansion of a meshed DCMT overlay grid for the interconnection of offshore wind farm is chosen and the decision is driven by the structure of the underlying gas grid and linked by the investment into offshore electrolysis.

³⁸ However, only the Israel-Cyprus section was an actual endogenous decision

3 Application of the PERSEUS-gECT for modeling the development of the European energy system until 2050 considering energy imports from MENA, Central Asia and Patagonia

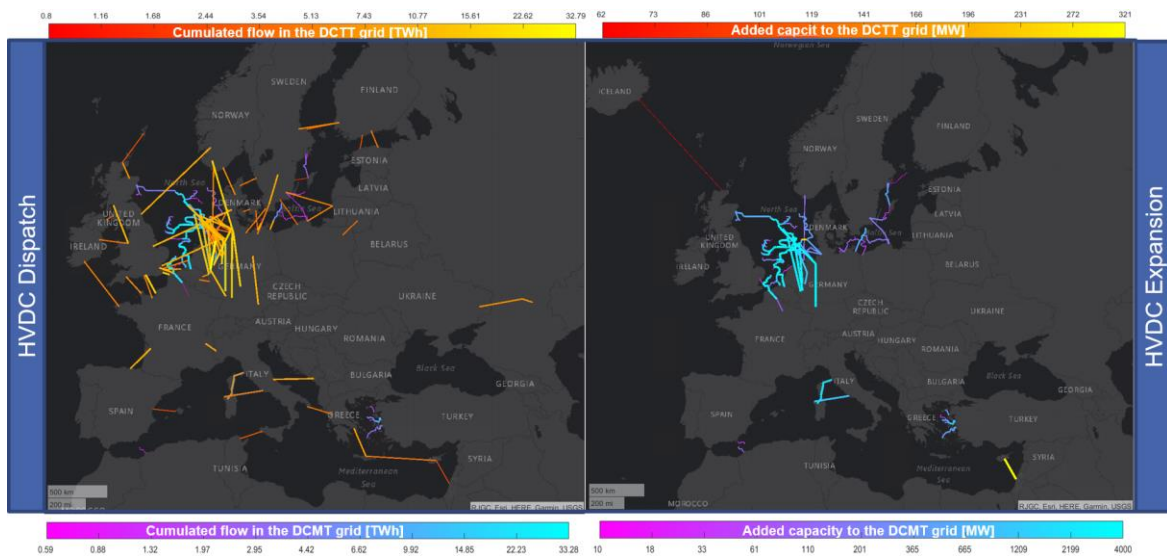


Figure 3.21: Comparison of the dispatch of the HVDC transmission system (left) and the HVDC expansion (right) in 2050

In line with this mainly renewable driven grid expansion for interconnecting wind farms, the interconnection between coastal regions and the grid connection of islands is improved. For example, a maximum expansion of 2x2GW transmission capacity is chosen in order to tighten the ring from Italy, Sardinia and Corsica. This is done in order to integrate the observed wind offshore expansion around these islands. Also, the connection between Aegean islands is improved in the attempt to optimize the grid connection of offshore wind farms in this region. In the Baltic region an additional overlay grid starting from linking the windfarms around Bornholm is realized with the goal of strengthening the transmission capacity between Germany, Norway and Sweden. Overall, the focus of the expansion however lies in the North Sea with the goal of increasing the interconnection between Germany, UK, Denmark Belgium and the Netherlands. The basis for these expansions are the existing offshore converter stations in the German North sea and their point-to-point connections. On top of this capacity, an additional 4 GW layout is added which is basically parallel to the existing lines and branches out offshore. Finally, this leads to the following displayed line flows, which illustrates the utilization of the AC grid on the yellow scale and the HVDC grid on the blue scale. Besides of the already described pattern, which led to mainly wind onshore and nuclear driven large line flows in states of the former Soviet Union³⁹, it is interesting to observe which corridors are highly utilized in Northwestern Europe and the Baltic states⁴⁰. As expected, high flows are observed on the corridor from Norway to southern Germany and on a smaller scale also from Sweden to southern Germany, where the linking of offshore wind farm around Bornholm is used in order to create a new cross border exchange.

³⁹ In this context two hotspots are identified, one in the European part of this former Soviet Union grid, which is driven by wind onshore in Belarus, Ukraine and nuclear in Russia and one in the central Asian part, which is dominated by hydro in Russia and wind onshore in Kazakhstan.

⁴⁰ An illustration of the main electricity transport corridors in Germany is provided in fig. A.28.

3 Application of the PERSEUS-gECT for modeling the development of the European energy system until 2050 considering energy imports from MENA, Central Asia and Patagonia

The longest direct path, which was realized based on the topology of potential offshore wind-farms is the link between Scotland and northern Germany, which is actually extended further south. The utilization of the meshed offshore grid between UK, NL, DE and DK is also quite high.

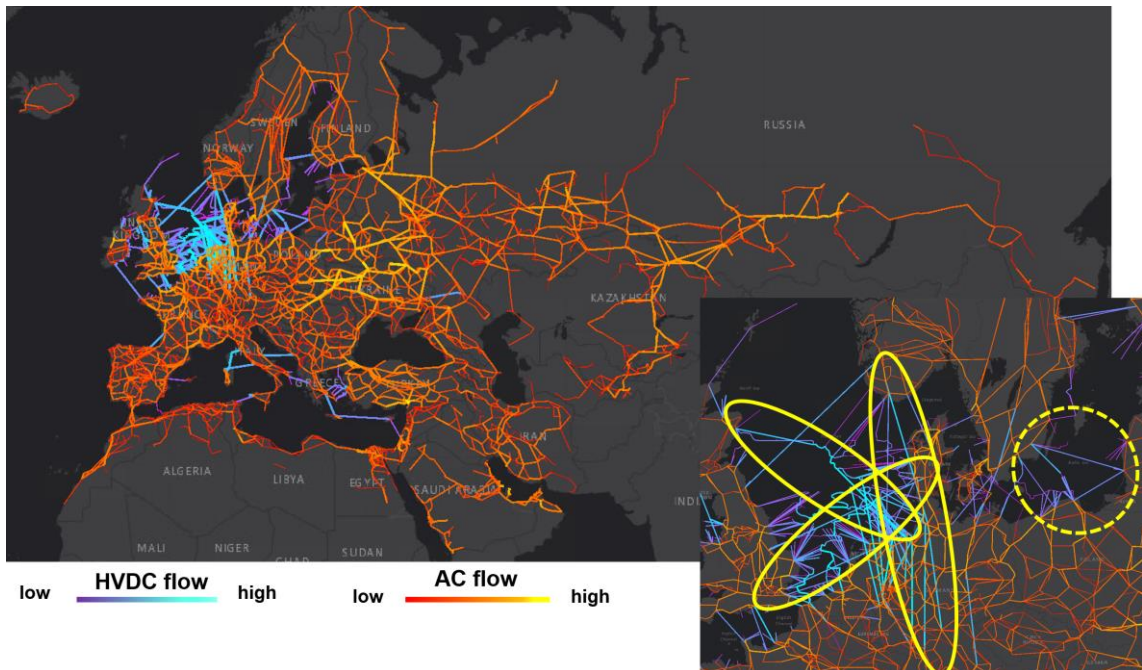


Figure 3.22: Cumulated flows on lines of the electricity transmission system and identification of main transport corridors in the North Sea and Baltic Sea in 2050

For a direct comparison of the main drivers, the generation of wind onshore and PV is displayed once again below.

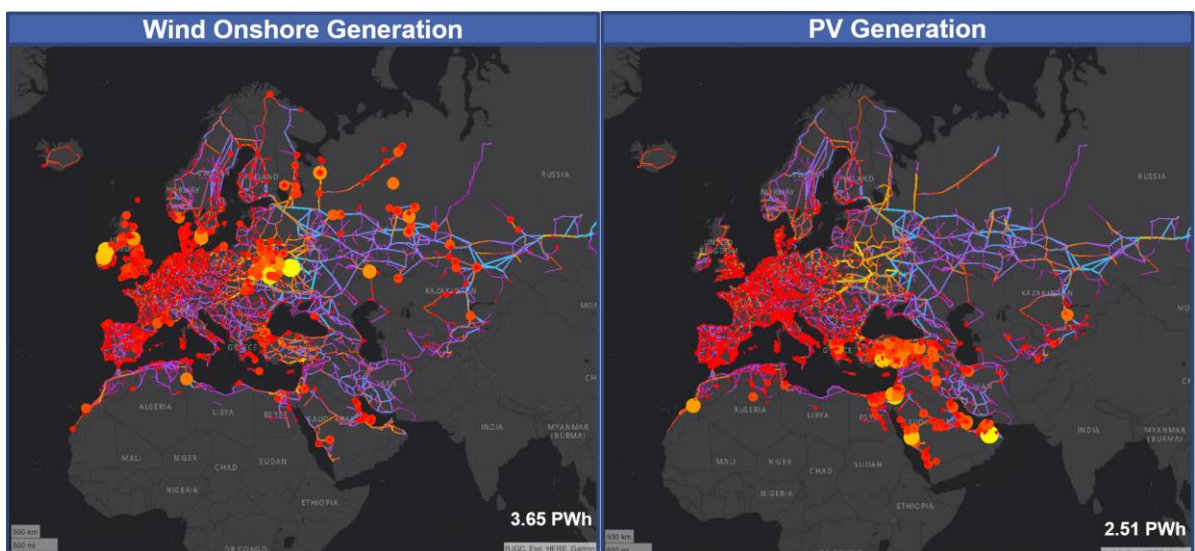


Figure 3.23: Comparison of the wind onshore and PV generation in the AC grid in 2050

3.2.3 Development of the energy system as a result of mainly gas related drivers

Complementary to the power system, which was previously shown to be designed with a focus on a regional balancing of supply and demand, the gas system is used for a long-distance transport of energy from renewable or fossil sources. From the set of available transport options and energy carriers, the pipeline based transport of hydrogen and methane and the maritime shipping of LNG, LH2 and LOHC are chosen as the main options for the intercontinental transport of energy carriers and should be analyzed next. The previously shown pipeline or river shipping-based transport of oil from the European border to hubs in the hinterland, should not be part of the analysis as it is more or less predetermined through the remaining demand of the final demand sector (mainly transport) and plays only a minor role for the system integration of renewables. Also, the CO₂ transport is already described and is not part of the following analysis. Without any constraints for the use of carbon-based energy carriers besides of a quantity limit on the conversion process based net emission of CO₂ into the atmosphere within this case study, the question remains if the gas system supports the expansion and integration of renewables or maintains the existing carbon-based structure in combinations with CCS. Overall, the results of this case study are ambiguous in this context as already outlined in the previous chapter with a focus on the electricity based production of hydrogen. From the viewpoint of the gas transport infrastructure, the following figure provides a compact overview of the conversion process chain of hydrogen and its relevance for the final energy demand balancing compared to other energy carriers with a transport modelling. Compared to the underlying TYNDP scenario, the already discussed expansion of heat pumps led to a slight shift in the final demand from gaseous energy carriers like methane and hydrogen to electricity. Although this shift in Western Europe was partially compensated by the coal-to-natural gas fuel switch of industrial final energy conversion processes in Turkey and Ukraine, which were additionally modelled with a complete energy balancing compared to the TYNDP scenario, the following figure supports the impression that hydrogen- or methane-based energy carriers play only a minor but complementary role for the overall electricity dominated system.

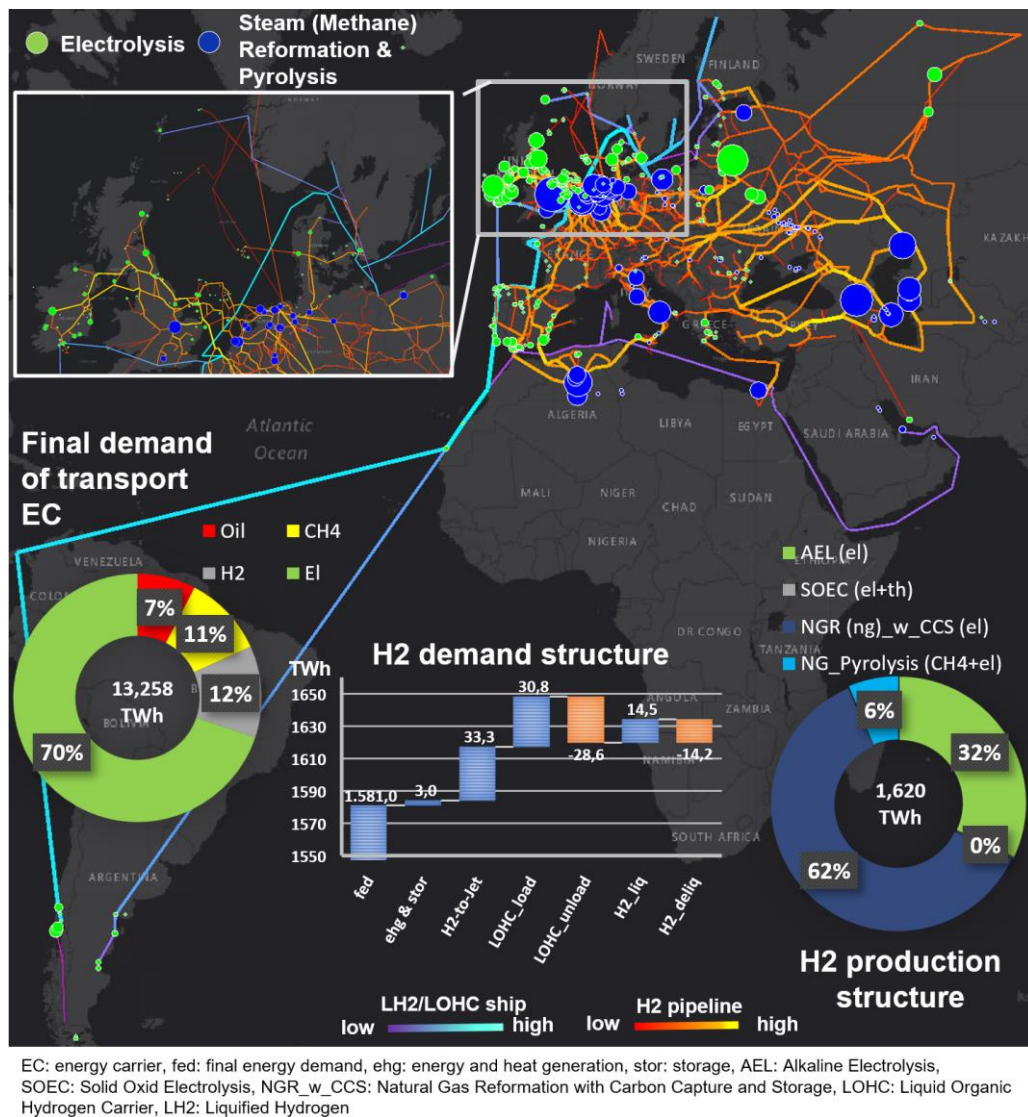


Figure 3.24: Structure of the hydrogen production and transport

In order to balance the chosen final energy demand level of 1,581 TWh for hydrogen in Europe, which lies above the lower bound of 1,394 TWh⁴¹, as well as some minor demands of the transformation sector⁴², a tight processes conversion chain is chosen, which mainly relies on natural gas. As long as good renewable power resource conditions (wind, solar) and/or the availability of alternative dispatchable low carbon generators (hydro, nuclear) allows a dispatch of

⁴¹ The structure of the final hydrogen demand is shifted towards high temperature heat processes in the industry while most low temperature heat demands in the residential sector are covered by heat pumps. The final demand lies 204 TWh below the reference level but 187 TWh above the lower bound.

⁴² The production of 25 TWh Fischer Trofsch fuels from 33.3 TWh H2 corresponds to only 2.5% of the oil demand and is only realized due to processes optimization with preceding (heat source) and succeeding conversion and transmission processes, as described earlier.

electrolysers with high full load hour and reduces the need for an electricity transmission grid expansion, the model selects the electrolysis process for the hydrogen production. As shown in the next figure based on the Zoom on the North Sea region, the allocation and dispatch of renewable generators (wind-onshore and offshore units), the electricity transmission system (HVDC and AC), the gas transmission system (pipeline, shipping) and the hydrogen production units (electrolysis, NG-to-H₂) interacts and support each other.

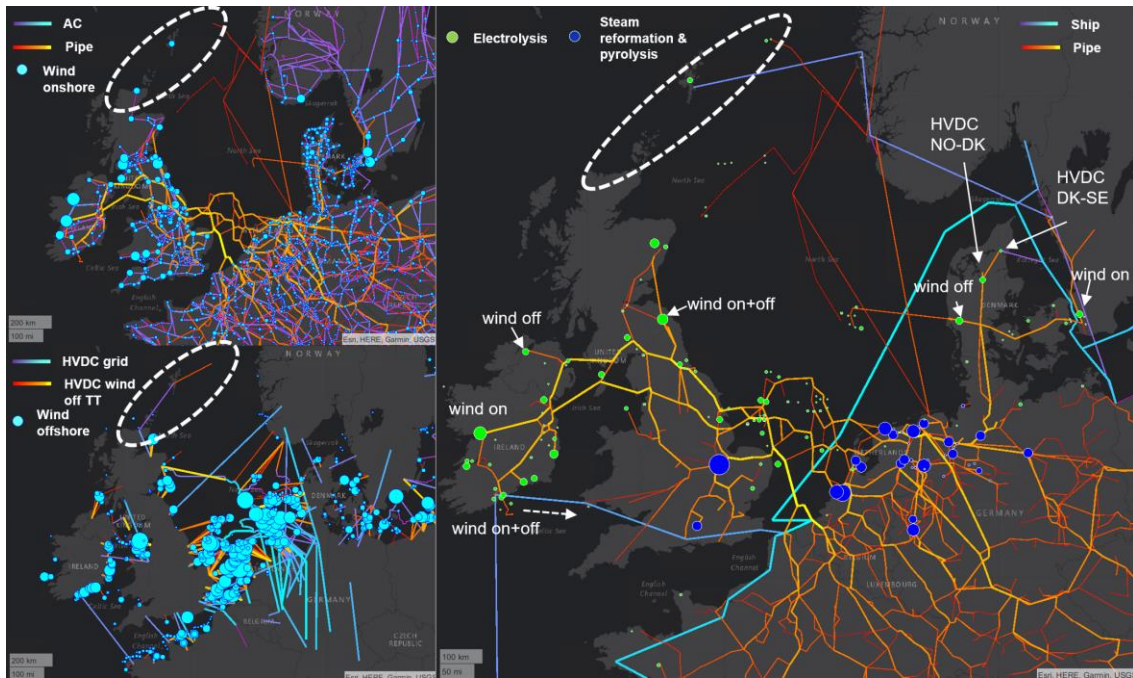


Figure 3.25: Interdependency between components of the hydrogen and electricity system in the North Sea. Right part: hydrogen production and hydrogen pipeline and shipping flows, upper left corner: wind onshore and flows in the AC grid and hydrogen pipelines, lower left: Wind offshore and flows in HVDC lines

With a focus on the hydrogen production and transport on the right side and a comparison of the wind onshore generation (upper left corner) and the wind offshore generation (lower left corner), several dimensioning decisions might be observed. On the one hand, it can be observed that processes for the power-to-hydrogen and methane-to-hydrogen process are allocated in different but neighboring parts of the gas pipeline system, which is later shown to be largely retrofitted for the hydrogen transport in this region. As the methane-to-hydrogen process is basically operated in base load mode (as show in fig 4.18), this combination allows a high utilization of the new hydrogen pipeline system without the risk of a temporal pipeline congestion and the need for a further expansive parallel expansion. Instead, this combination improves the economic perspective of converting a larger part of the natural gas system to hydrogen. The previously discussed power-to-hydrogen based grid integration of large wind onshore and offshore clusters is furthermore clearly visible in the hydrogen pipeline flows, which indicates that the electricity grid expansion is actually reduced in this context. The allocation of large

electrolysers in the northern electricity grid of Denmark-West at the converter stations of the interconnectors to Norway and Sweden is a further indication that the ability of the Nordic hydro power for a flexible dispatch is not only used in the electricity grid but also to increase the full load hours of electrolyzers. The most interesting interaction between transmission systems in this region is however observed around Shetland. Instead of increasing the electricity transmission capacity from the most northern part of Scotland towards the south or choosing an expansion of the pipeline system, the wind onshore and offshore injection around and north of Inverness is bundled and directed north to Shetland. In combination with an onshore wind expansion in Shetland, this island is chosen for creating a hub for the hydrogen production and liquification. As already mentioned, this conversion route is quite expansive and requires high full load hours in order to be economically attractive. If electricity is however not scarce but can be provided at low cost with a flat profile, the electricity demand of the liquification becomes irrelevant and the option economically attractive. This effect explains why the hydrogen demand of liquification units and the hydrogen production of regasification units shows just a small gap in fig 4.24, as most energy demands in the conversion and reconversion phase are balanced with electricity. Contrary to Chile, where the largest liquification unit with a production of 7.1 TWh in a real island mode is realized and requires an expansion of expensive batteries, the Shetland Island with a production of 4.4 TWh is actually grid connected such that the investment into batteries is omitted. Analogous to the described dimensioning task in Chile, a parallel LOHC production is allocated at the same site with the goal of dispatching a cheaper unit with higher losses and a more volatile profile. Due to the grid connection, the dimensioning proportions are however reverted, as the more volatile site in Chile produces 16.9 TWh LOHC and the Shetland site 1.12 TWh. Additionally, the Shetland energy island provides power for small scale offshore electrolyzers in Norway which blend their hydrogen production into the existing natural gas system. At this point it should be mentioned that this is actually the only real energy island which the model chooses, as comparable sites in the Faroe Islands or Bornholm are not developed in the same way. The meshed DCMT grid which is built in and around the Doggerbank basically fulfils the same function like an energy island, but shows a more decentralized structure and is therefore less comparable. While the hydrogen liquification and shipping is concentrated on the previously mentioned countries, it is interesting to observe where the remaining LOHC is injected and which countries are the importers. Besides of Argentina, which was already mentioned and which produces 5.4 TWh LOHC, the remaining production focuses on Ireland (1.9 TWh), Western Sahara (1.4 TWh), Lithuania (2.4 TWh) and Estonia (1.5 TWh). In Ireland, it is interesting to observe in the previous figure, that the LOHC production is located at the southern corner of the wind onshore cluster and next to an HVDC connection to France and provides an alternative transport option for the energy conversion in this region to the pipeline grid transport and AC or DC grid. Western Sahara on the other hand lies on the route from Southern America to Europe, as illustrated next, and the transport option starts next to the point where the model could alternatively invest into an HVDC cable for linking this region with UK (Xlinks). On a smaller scale, this Morocco-UK project is thus actually realized in the sense that energy is transported from Africa to Europe, although only a smaller fraction of the realized power generation is sent north and is consumed in the Nordic countries Norway (7.1 TWh), Sweden (7.5 TWh) and Finland (8.5

TWh) and to a minor extend in Denmark (2.6 TWh) and Sardinia (1.8 TWh). The focus on the import Nordic import countries, where no hydrogen pipeline grid is built, also explains the production in Lithuania and Estonia. Compared to the 1.62 PWh hydrogen production which is almost entirely transported through pipelines, and which should be analyzed next, the shipping however plays only a minor role.

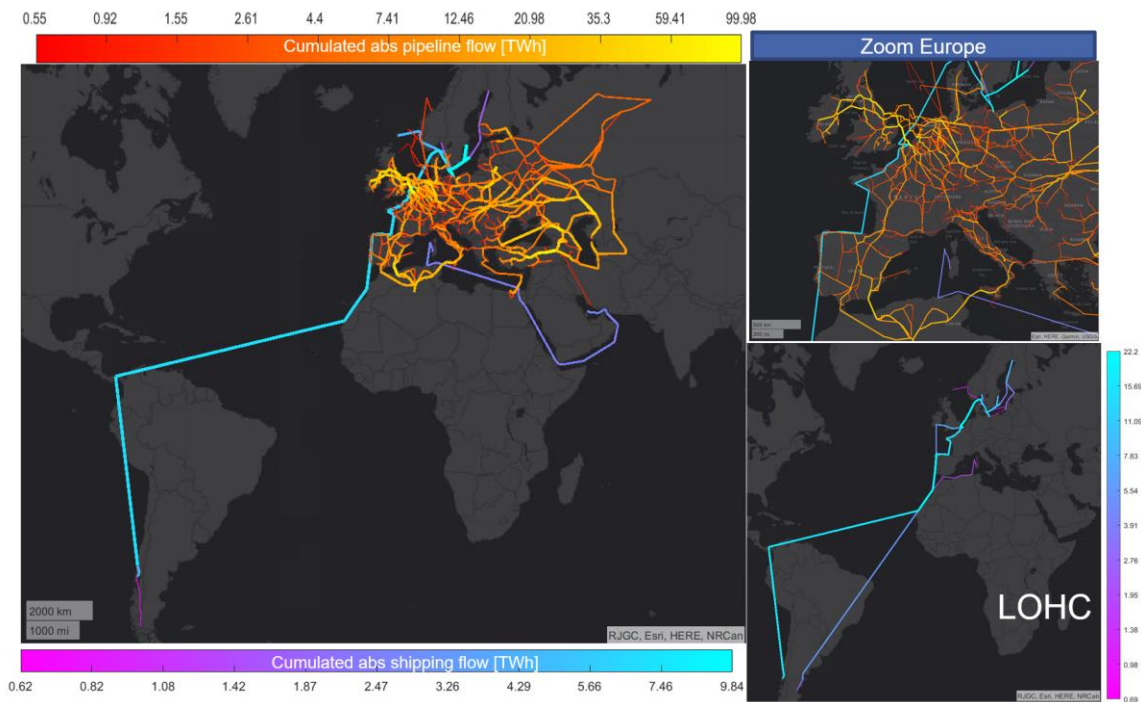


Figure 3.26: Comparison of the cumulate hydrogen pipeline flows with the shipping of LH2 and LOHC

With the model choice to rely on natural gas as the main energy source for the hydrogen production and to electrify only the auxiliary direct processes in the case of the methane pyrolysis or the subsequent CCS processes, the overall need for a low carbon or renewable electricity production is significantly reduced. As the majority of the CO₂ emissions is directly stored (NGR_w_CCS) or used (combination with Fischer Tropsch) or does not even occur (NG_pyrolysis), only the electricity demand of auxiliary processes and for the preceding natural gas conversion chain or the final direct air capture units remain. Despite of the open question if such a conversion route is useful or publicly accepted, the question remains where the conversion takes place (at the natural gas producing countries or the importing countries), and how the methane transport systems will change in this context. Although the conversion chain for the hydrogen transport is expensive and requires additional investments, the already observed finding that some part of the hydrogen production is nevertheless allocated in the production countries is interesting. Although this could be partially explained with the availability of suitable CO₂ storages in depleted gas fields for the subsequent CCS processes after the natural gas reformation, which is by far the most dominant conversion technology in this case study, the actual allocation of the units and the already observed investment into CO₂ grids in northwestern

Europe indicate that this is just a minor point. Overall, several drivers, which depend on the location and technology of the potential methane-to-hydrogen processes might be identified. A comparison in the following figure, which shows the cumulated dispatch of steam reformation and pyrolysis units and the hydrogen flows on the left and the natural gas flows on the right, reveals that natural gas-based hydrogen conversion processes are either focused in existing pipeline-connected natural gas production countries in North Africa or in the coastal riparian regions of the North Sea. Furthermore, it is observed that the choice of the preferred energy carrier for the transport varies between LNG or pipeline connected producer countries. Despite of Qatar, which complements its LNG exports with a small LH2 production of 4.6 TWh, all LNG producer regions basically stick to the LNG export or quit the production (Russian LNG) by 2050.

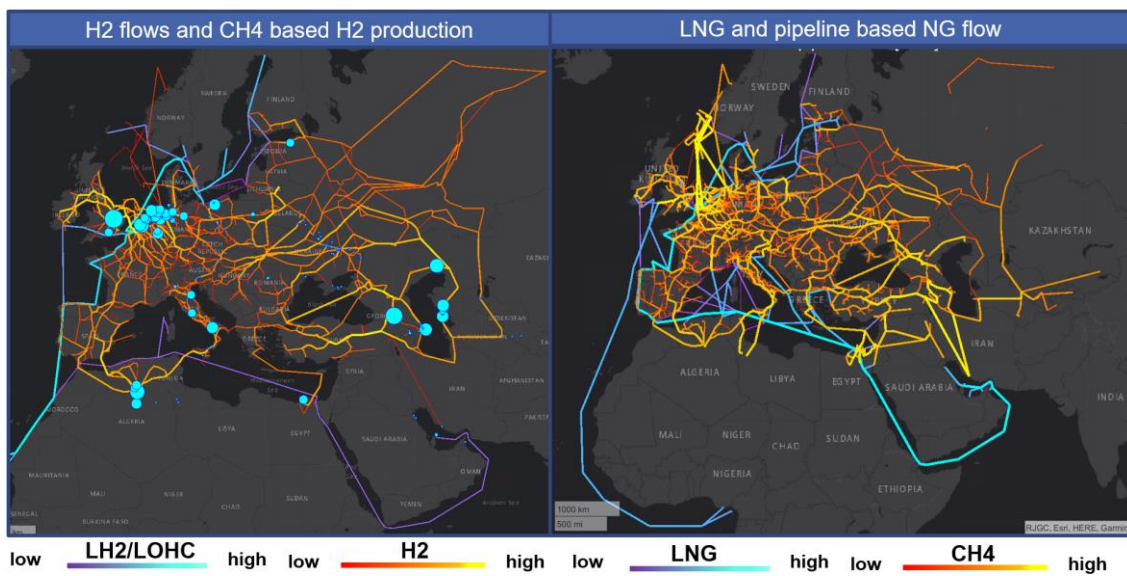


Figure 3.27: Comparison between the cumulated hydrogen pipeline and shipping flows (left) and the natural gas pipeline and shipping flows (right)

The renewable power generation at LNG exporting locations is consequently only used for auxiliary processes of the natural gas conversion chain despite of the coverage of the local load. Considering the high energy demand for the hydrogen liquification or the production of derivatives, this outcome is less surprising than the partially observed switch to hydrogen production and pipeline-based export in North Africa (Algeria, Egypt) and the Caspian Sea. One possible explanation might lie in the trade-off between the emission reduction at an early state of the supply chain, which reduces transport and storage related CO₂ emissions in cases where the transport fuel is used for the compressor operation⁴³ and the investment expenditure for

⁴³ In the current case study, the simplification of modelling all compressors for the pipeline operation based on a loss factor, corresponds to the assumption that only gas driven compressors are utilized. For existing storages on the other hand electricity driven compressors were

converting long distance pipelines to hydrogen transport in cases where the transport demand exceeds the assumed blending potential of 20%vol. Another explanation might lie in the already discussed interdependency between availability of attractive renewable power resources (wind and solar irradiation) and the auxiliary power demand of the methane conversion and possible subsequent CCS processes. In the following figure this question is analyzed by comparing the allocation of pyrolysis and steam reformation units on the one hand in the large left figure and the CCS conversion chain of pipeline transport/ shipping and storage on the other hand in the smaller figures on the right. At least for the MENA region and Central Asia the illustration shows a clear preference of an investment into natural gas steam reformation units at natural gas production sites with a direct injection at deleted fields in the same region. Taking the previously shown distribution of renewables into account and the correlation with battery storages in PV dominated MENA region, the illustration gives a good indication that the allocation and dimensioning of CH₄-to-H₂ processes follows at least to some extent the same logic as discussed for electrolysers. As most energy is however taken from the natural gas itself, the needed renewable energy for the observed base load operation of the conversion is significantly lower, compared to the power-to-gas process.

assumed if the grid connection was possible. For investments both options are available. The results show that the electricity connection is chosen whenever possible.

3 Application of the PERSEUS-gECT for modeling the development of the European energy system until 2050 considering energy imports from MENA, Central Asia and Patagonia

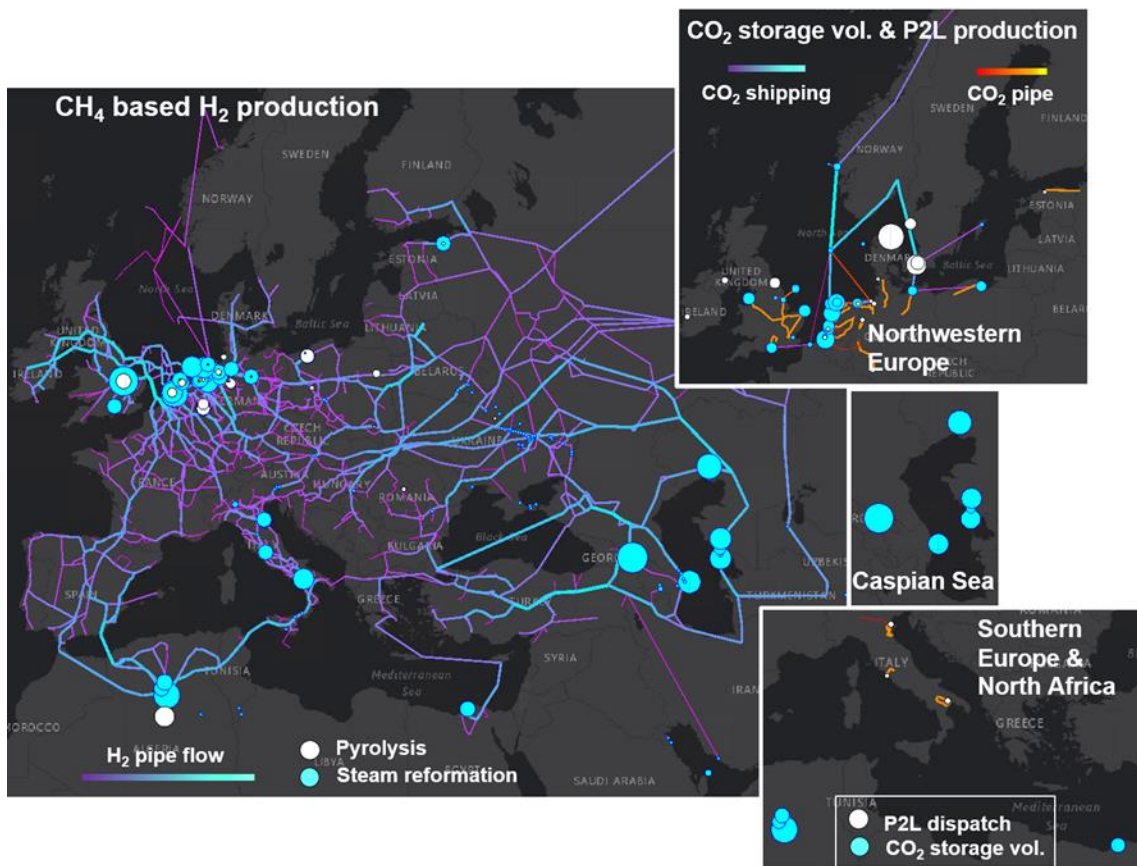


Figure 3.28: Cumulated dispatch of methane based hydrogen production processes and comparison of the unit placement with the placement of possible CO2 sinks

At the end of the optimization horizon the production of blue hydrogen is increasingly directly coupled to the renewables availability with an increasing investment into plasma assisted methane pyrolysis. Backed-up by a BESS, the largest unit is realized in Algeria at the source of a main hydrogen supply corridor with a production of 27.37 TWh and a direct electricity demand of 6.99 TWh in 2050. For the transport of the produced hydrogen from the MENA and Central Asian region a focus on four main corridors is observed. Compared to the existing and still utilized natural gas-based pipeline system, the transport from these regions seems rather focused on the main south-north (1: Algeria-(Morocco)-Spain-France, 2: Algeria-Tunisia-Italy), and east-west pipelines (3: Turkey via TurkStream and TANAP, 4: Kazakhstan-Slovakia via the Soyuz pipeline and Ukraine). To a smaller extent, also the East-Med-pipeline, which is linked to Egypt via the Aphrodite gas field south of Cyprus delivers hydrogen to Europe. Although the binary condition on the variables for modelling the replacement or parallel addition of pipelines was relaxed in this case study and the results should be taken with caution, the following illustrated analysis of the respective pipeline flows supports the impression of a concentrated hydrogen flow along the main transport routes. As the blending capacity in the main corridors is not sufficient, a

partial replacement is often chosen in this linear approximation. An even more expansive parallel addition is however mainly restricted in the previously described Ireland, UK, ARA corridors⁴⁴.

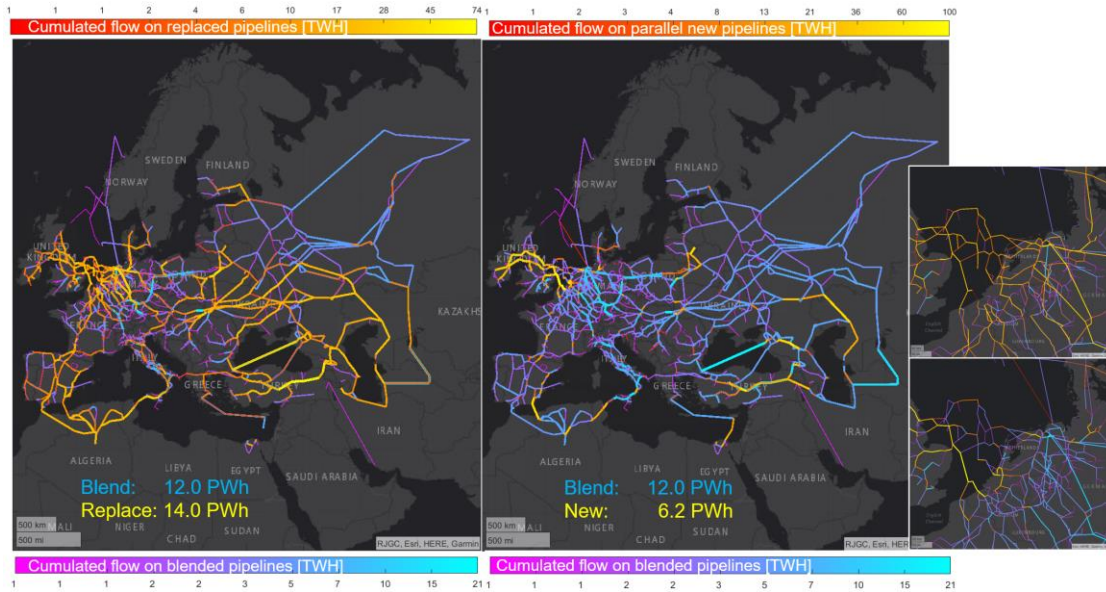


Figure 3.29: Comparison between the cumulate hydrogen pipeline flows in 2050 in blended or replacement NG pipelines (left) and blended (NG) or parallel new H2 pipelines (right)

Unlike to the previously described methane-based hydrogen production outside of Europe, the analysis of the reason for producing this so called “blue” hydrogen in Europe is more complex. Analog to the discussion in the context of the CO₂-balance analysis and the relation between DAC and P2L processes, the potential to couple processes and realize efficiency gains showed to be a main driver for the observed allocation. Additionally, it could be observed that the temporal dimension of the ramp of the hydrogen infrastructure, which goes along with the question which sector (transformation e.g., power and/or heat generation or final demand e.g., industry or transport), is supplied first and where the transformation of the hydrogen to natural gas infrastructure is realized first, had a significant impact on the solution. Nevertheless, some global trends might be observed. In line with the observed trend in natural gas producing countries, the bulk of the hydrogen production in importing countries is focused on the production in the

⁴⁴ Due to the large capacities on major pipelines, the logarithmic scale, the different scales between new/replaced and blended flows and the possibility to realize a replacement only partially, the false impression may occur that a replacement decision has no impact on the existing flows. Technically this is partially true as the blending comes for free and a small-scale partial replacement offers the option of adding high capacities without significantly reducing the old flows, due to the larger capacity of the replaced pipeline. Contrary to the AC-modelling, where an equivalent edge is modelled, parallel pipelines in the gas grid are modeled individually. If only one pipeline is replaced and the pipeline capacity is large thus high flows on both pipelines on the same edge (replaced and old) are shown.

neighborhood of potential CO₂ storages in depleted gas fields or at least in the coastal region, where the pipeline or shipping distance to the next potential storage is minimized. In consequence, large capacities are realized next to the existing LNG import terminals in the ARA region, the German North Sea coast and UK. In combination with the large-scale electrolysis-based hydrogen production in UK, Ireland and the North-Sea offshore hotspot, which reaches the continental European North Sea shore and some smaller scale cavern storage, investments with a focus on UK and Ireland for balancing the intermittent renewables on the hydrogen site (fig. A.29) are implemented. The base load hydrogen production allows a high and steady energy dispatch of the hydrogen transmission infrastructure in Western Europe. As the North-South and East-West divide in the hydrogen transmission system basically mirrors the structure of the power system and is established in an early phase of the optimization, following the distribution of renewables and the flow directions of the existing natural gas system, the main transmission corridors are already established when the methane pyrolysis becomes economically attractive in 2050⁴⁵. With the much higher energy transmission capacity of the hydrogen system per edge compared to the power system and the already realized investment which established a clear flow direction, this new hydrogen production units are similarly placed at the source nodes of the hydrogen transmission system in Europe where a steady supply with methane and electricity is guaranteed.

Besides of this global trend, the analysis on a local scale reveals how the model tries to optimize synergies by coupling processes and how the path dependency and interaction with the power system impacts the single allocation decision. Based on some examples, illustrated in the following figure, for the coupling of Fischer Tropsch based hydrogen-to-liquid (H₂tL) processes and the natural gas steam reformation with other processes in Germany, Benelux and Italy, the interdependency between single technology allocation and dimensioning decision should be explained next. Analog to the already described H₂tL -DAC coupling at the same location, where the process heat of the Fischer Tropsch process is used to reduce the energy demand of the DAC process and might utilize the CO₂, the coupling between LOHC unloading (also utilizes high temperature heat) and the H₂tL processes observed in Demark (upper right corner) follows the same goal of coupling process inputs and outputs on the same site. In this case heat and hydrogen are exchanged. The carbo capture after the steam reformation offers an alternative CO₂ source for the H₂tL process and reduces the need for a CO₂ storage or a DAC unit or their size. While the first case might be basically observed in all CO₂ grids, the second case is also not uncommon, as indicated here in Groningen (NL). While in most cases the layout of the CO₂ grid follows the goal of minimizing the distance between the source (NGR_w_CCS, DAC) and the sink (H₂tL unit, CO₂ storage, port for CO₂ liquification and shipping), in some cases a ring flow is observed which results in the misuse of the pipeline as a temporal storage (IT). In cases where the NGR units are

⁴⁵ Besides of the improved techno-economic parameters, the effort to remove the remaining CO₂ emission sources from system increases with reduced emission limits. In the last period, in which no net emission into the atmosphere is allowed, the missing alternative to produce hydrogen cheaply promotes the investment into this technology.

not directly placed next to a CO₂-storage or H₂tL unit, the structure of the power grid and the demand of the chemical industry for hydrogen and/or high temperature heat showed to be a main driver. SOEC units, for example, were only realized at locations, where the grid connection allowed a base operation. Besides of the location at the former nuclear power plant site Emsland (currently a CCGT site), which showed to have a favorable position in the electricity grid, all units were realized directly at large wind offshore landing nodes. Of the two processes options, either with an electricity only input or with external high temperature heat supply of round about 20%, only the second option was selected. In order to avoid an additional energy conversion, all units were dimensioned in a way that the process heat after the Fischer Tropsch conversion, which was built at the same site, was sufficient to provide the additional energy to the major electricity driven process. While the CO₂ for the H₂tL processes was taken from the NGR units, these processes were only allocated in Emsland at the same spot. For other units the trade-off between the optimal allocation in the hydrogen, natural gas, CO₂ and electricity grid was balanced.

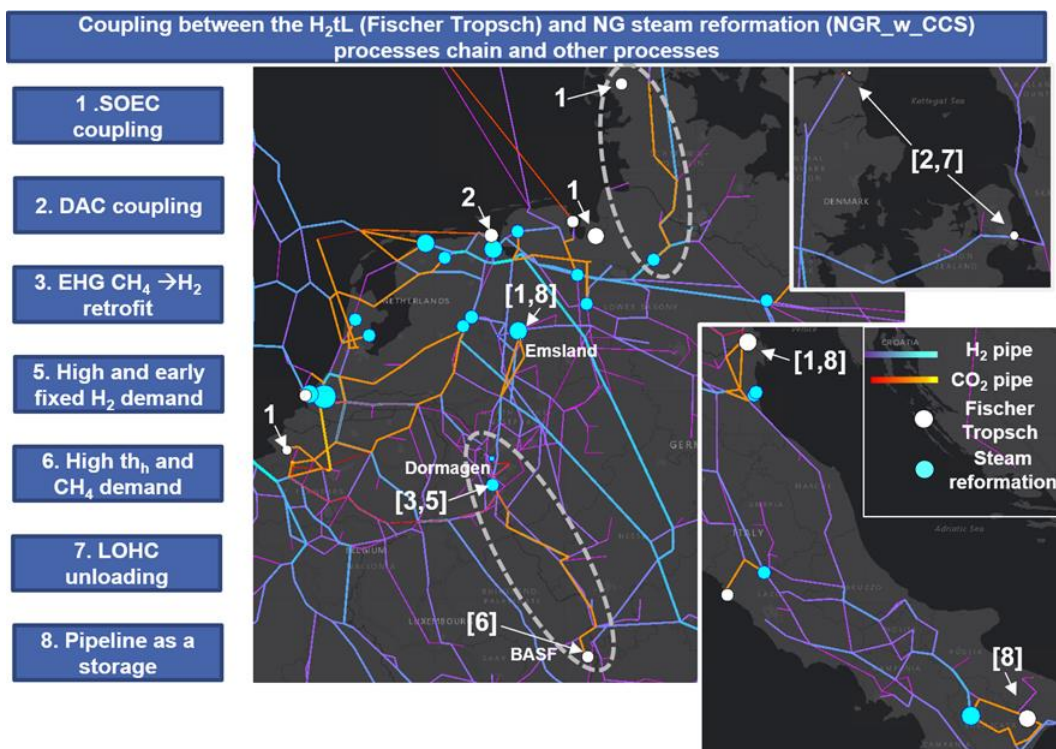


Figure 3.30: Process coupling examples involving Fischer Tropsch and steam reformation processes

The trade-off between an external or onsite generation of hydrogen and heat and the placement of NGR and H₂tL units might be further shown based on the example of the chemical sites in Dormagen (Bayer) and Ludwigshafen (BASF). With the currently high natural gas demand at the BASF location, which is partially used to produce steam for processes and the future high hydrogen demand, the model decides already in an early phase to link this site to the main north-south (and also partially east-west) hydrogen corridors. By integrating an additional Fischer

Tropsch (FT) process at the site, the utilization of the remaining process heat allows the model to reduce the natural gas demand. The needed hydrogen for the FT process, in this context, is just a fraction of the fixed hydrogen demand at this site which is needed to cover other non-energetic conversion processes. For the chemical plant site in Dormagen, which does not lie on the main hydrogen corridor, mainly a local hydrogen production from NGR units with additional supply from the Emsland site is chosen. Instead of directing the complete CO₂ from the CCS process at this site to the storages and the ports in the ARA region, the CO₂ flows to the BASF location and is used for producing synthetic fuels there. At the end of the optimization horizon and with a doubling of the hydrogen production capacity by installing pyrolysis units, the Dormagen node turns from a hydrogen sink to a source. A further interesting finding is the retrofit of natural gas fired power plants to a hydrogen firing next to chemical site location (e.g., Infraserb Höchst, Knapsack, Haiming). In the medium term, these units benefit from the early available hydrogen at the location sites. As the operation of retrofitted gas turbines with methane was however not forbidden and hydrogen is the scarce resource in the last period (high demand of the industry for decarbonizing the remaining processes) while electricity from renewables dominates the system, it is observed that these units switch back to a methane firing in the few hours when they are dispatched. This degree of freedom is consequently used for reducing the spatial and temporal coupling of the energy system. The option to balance these avoidable CO₂ emissions in any time slice of the period by any DAC process has the same effect like a flexible global load for the integration of fluctuating renewables, which otherwise would require additional investments (actual DSM, storage and grid expansion).

4 Conclusion and limitations

4.1 General approach

Within the scope of this work an approach was developed in order to provide a profound decision support for energy system planners, based on a spatial and temporal highly resolved analysis of the fundamental drivers of the energy system. The main goal of this approach was to develop a method, which bridges the granularity gap in energy system models between investment decisions on a local level and overall infrastructure changes on a continental level. Driven by the need to cover a useful energy demand of heating, cooling and electricity appliances as well as the final energy demand of other conversion processes for the main energy carriers (oil, methane, coal, biomass besides of heat and electricity) on the one hand and the varying spatial and temporal availability of primary energy sources on the other hand, an optimal conversion path for the balancing of energy supply and demand has been found. In this context a particular focus is laid on a detailed and consistent modelling of the impact of varying weather conditions on all processes for the conversion, storage and transmission of energy carriers and a balancing of the resulting CO₂ emissions.

The developed approach starts from a common regional basis for the analysis of energy demand and primary energy supply potentials with a resolution of 100 meter. In many cases this requires the computation of hourly weather dependent generation and demand profiles¹, which are modelled based on ERA5 reanalysis data for multiple weather years (often 1985-2022) for each cell of the weather database. For the balancing of this regional highly resolved supply and demand potentials based on conversion, storage and transmission of energy carriers, an aggregation approach is developed which allows a flexible definition of variables depending on the topology of existing or potential transmission networks. In this context the multimodal transport of liquid², gaseous³ and solid⁴ commodities by pipelines, ships (river, maritime), trucks and

¹ Weather dependent conversion processes include the electricity or heat generation from wind (onshore, offshore) and solar (PV, CSP, RTSWH). On the demand site, the electricity-to-heat conversion of heat pumps and in general the low enthalpy space heating and cooling demand in the residential, tertiary and industry sector might be mentioned. Hydro inflows are a spatial case and if not taken from an external source currently only the inflow into run-of-river plants might be modelled bottom up.

² Considered liquid or liquified commodities: Oil/SFO, MeOH, LOHC, LH₂, LNG, NH₃, LCO₂. As Ammonia is liquid already at relatively low pressure and ambient temperature it is modelled as a liquid fuel in this model

³ Considered gaseous commodities: CH₄ (NG, SNG, biomethane), H₂, CO₂. Compresses gaseous commodities: CNG, CH₂

⁴ Reactive metals (Fe).

railways, in combination with the AC or HVDC⁵ based electricity transmission, is considered. The aggregation of decentral conversion processes in a system with a high degree of sector coupling and non-overlapping transmission system topologies, however, might rapidly increase the problem size as generation or demand processes might be balanced by multiple competing systems. The developed aggregation approach resolves this problem by defining variables in a way such that each potential supply or demand might flexibly switch the transmission system.

With the target of minimizing all system expenses, the developed model PERSEUS-gECT allows a multi-commodity, multi-period co-optimization of the dispatch and expansion planning of the energy conversion, transmission and storage. Taking into account the path dependency and the impact of existing or planned assets of the energy systems, especially of the power system, the focus is primarily laid on a detailed parametrization of the existing electricity generation and transmission system. For a modelling of flows in the AC grid, therefore, a DC-OPF approach with a quadratic line loss approximation is chosen, while a simplified capacitated directed flow modelling approach with transmission losses approximates the transport problem of all other commodities.

In order to test the developed approach, the transformation of the energy system, which covered significant parts of the Eurasian continent, North Africa and Patagonia, was optimized with the goal of a decarbonization until 2050. Disregarding of the different scales of final demand investments in an kW range and energy balancing in transmission systems on a PWh range, a validation of reasonable dispatch and investment decisions could be provided. The overall target of covering the energy demand while reducing the overall emissions to net zero was validated based on an analysis of the emission balance and the development of the power and gas system.

4.2 Mathematic problem formulation

Starting from the general approach of a directed energy graph, which models all energy flows from the source to the sink and is driven by nodal demand outflows to the sink and supply inflows from the source, an own approach is developed that introduced the concept of a generic conversion process, which might be limited by a generic unit. This generic process combines the properties of a process, which converts energy carriers at one producer node with the properties of an edge, which links between nodes and the properties of a storage, which establishes a flow of energy along the temporal dimension. Doing so, decentral generation and demand potentials might be attached to virtual producer nodes and flexibility redistributed between nodes of different transmission systems without the need of defining additional balancing nodes and flows. Thus, the general advantage of energy flow graphs, which allow a complex coupling of conversion processes in one node, was preserved. In real transmission systems with non-overlapping topologies, where most consumers and producers are not directly linked to a transmission node

⁵ Includes the DC point-to-point connections (DCTT) and meshed grids (DCMT).

but indirectly through a distribution grid, therefore supply switching decision might be easily modelled. Based on the concept of an abstract process, where the same process variable might have multiple functions, an energy system model is defined, which starts from 100 m resolved sectoral demand and supply conversion processes, aggregates these processes with a minimum loss of information and optimizes their balancing. In a multi period optimization, which minimizes the system cost for a load coverage, the unit capacities, which limit the activity level of processes, are adjusted.

Within the case study, the general function of the combined conversion, storage and transmission network, dispatch and expansion planning model PERSEUS-gECT was demonstrated based on a closed linear optimization with 6 and 7 time periods (each representing five full years) and a time resolution of 16 time slices per period. As PERSEUS-gECT is actually formulated as a mixed integer linear problem (MILP), this was done by relaxing the integrality constraints on the unit variables. Also, the included option to run PERSEUS-gECT with minimal-uptime/downtime unit commitment constraints was turned off. In order to optimize the problem with a full temporal resolution of 8760 hours, which is the clearly next goal, or for switching from an LP to a MILP problem class, a decomposition of the problem is needed. Although first decomposition tests with an ADMM based approach, with a separation between the single time steps, showed some promising results, the size of the sub-problems was still too large for a fast convergence. As already seen in the closed optimization, the large dimensional differences between the different energy systems remain numerically challenging - even if the problem size is reduced. Therefore, further research is needed, especially with a focus on defining adequate subsystems for the decomposition. A decoupling between the gas, electricity and heating system might be a good starting point.

4.3 Data model

A spatial and temporal highly resolved analysis of final and primary energy conversion potentials and profiles in combination with a detailed parametrization of the existing and planned generation, transmission and storage capacities is the basis for a data driven definition of a reference energy system. With a focus on the power system, where most generators are parametrized on a single unit base (e.g., existing or potential single wind turbines) or at least with a spatial and sectoral resolution of 100 m (e.g., RTPV on SFB, TFB, MFB⁶), a variable aggregation scheme with respect to the modelling of alternative conversion and supply paths is developed. Driven largely by the need to balance a heating or cooling demand or the potential to exploit renewable energy potentials at remote sites with a high resource availability, the data structure is defined in a way that a switching of energy carriers and transport systems is taken into account. Through an overlay of electricity and gas supply areas with the weather cells of a meteorological database, for example, an aggregation basis is defined which allows to model multiple conversion paths for

⁶ E.g., rooftop PV (RTPV) an single-, two-, and multifamily builds (SFB,TFB,MFB)

covering a decentral space heating demand, ranging from an electricity grid balancing⁷ or gas grid balancing⁸ to a local balancing⁹. Contrary to the previous example, which is determined by the parametrization of the existing energy infrastructure¹⁰, modelled with a high level of detail in PERSEUS-gECT, the developed approach also offers the possibility to define the layout of an energy conversion and transmission infrastructure from the scratch in remote areas. Starting for example from a placement of single offshore wind turbines and clustering into wind farms during a preprocessing step, the model afterwards may endogenously find a path to suitable nodes of the existing logistic onshore or offshore infrastructure (e.g., port, gas node, railway station) based on interconnection to neighboring wind farms and the built of a potential meshed multi terminal DC (DCMT) network or through a point-to-point connection (DCTT). Alternatively, to a complete balancing within the electricity system, PERSEUS-gECT thus allows to evaluate alternative conversion paths, with the option to endogenously define complex conversion chains at any point of the system, which are often referred to as energy islands.

For the definition of the input data of PERSEUS-gECT, many preprocessing and also preoptimization steps are needed. The reason lies in limitation of large-scale energy system models to adequate approximate decentral decisions, such as an optimal techno-economic configuration of single wind turbines within a windfarm or the district heating layout-optimization at single building level. In both examples an elaborate preprocessing is performed. For defining the wind offshore farm layout, for example, a discrete turbine placement in multiple investment years with respect to wind-ellipse based distance restrictions is performed, taking into account the techno-economic parameters of 16 investment options at 5 hub-heights (120, 140, 160, 180, 200) and the site topography¹¹. Also, for the layout of the districting heating networks a spatial resolution of 100 m is chosen and the balancing of potential demand and supply is pre-optimized on a national level with respect to potential flows between the various demand nodes.

Besides of the computation of the generation profiles of renewable energies, which is performed on a global scale with a high spatial resolution for a large set of existing and potential technology configurations (e.g., individual hub-height, over 800 power curves for existing wind turbines) and validated against data of the transmission system operators, the modelling of highly resolved sectoral demand profiles for the considered energy carrier is included in PERSEUS-gECT. By focusing on a detailed bottom-up modeling of heating and cooling related profiles and

⁷ E.g., by heat pumps (HP) or electro boilers (EB)

⁸ E.g., by fuels cells (FC) or combustion boilers (CB) which are fueled by hydrogen or methane

⁹ E.g., by combining PV-BESS, HP, demand side management (DSM) and thermal energy storages (TES)

¹⁰ E.g., by the layout of the electricity distribution grid (110 kV) or the parameters of existing PV units (capacity, age, azimuth, slope)

¹¹ This includes for example the water-depth, distance to next port, distance to next potential substation, gas node, etc. An evaluation of the investment options requires 5.6 e11 LCOE calculations per period. For only one profile per weather cell, 78667 weather cells, 16 turbines, 5 hub height and 30 weather years and 8760h this already included a time series of 1.65e12 hours.

combining this approach with a top-down modelling of the remaining loads, it could be shown that even without a further calibration the staking of modelled profiles showed a high accuracy compared to gas or electricity grid operator data on a national level.

4.4 Case study

Based on the TYNDP2022 “decentral energy” scenario, which serves as a starting point for the projection of a demand development¹², and for the definition of lower bounds on the expansion of renewable energies, the general functionality of PERSEUS-gECT was demonstrated. With the target of achieving net-zero emission for all processes which convert, store or transport energy carriers, the development of the energy system was modelled for a case where the additional electricity demand in neighboring regions in Eurasia (continental Europe and rest of Russia, Central Asia) and North Africa, as well as their primary energy potentials and the RES-E potentials in Patagonia are considered. With the goal to test the general performance of the model, a high degree of freedom for the restructuring of the energy system was chosen.

Despite of the rather high degree of freedom, which offers the model the possibility to reduce the number of conversion technologies and to concentrate the primary energy conversion on favorable sites, the results show a trend for a balanced solution. By combining multiple conversion and transmission paths aligned with an optimized allocation of renewables, the resulting system layout shows a trend towards maximizing the utilization of components. The most astonishing results, which draws a light on the impact of a harmonized renewables allocation planning, is the finding that an overall slight reallocation of intermittent renewables (WECS, PV)¹³ capacities and technologies, compared to the TYNDP 2022 scenario, allowed an unexpected good balancing of the final electricity demand. Although the results should be taken with caution, as only a limited number of load situation was calculated in the grid model, the hourly (8760h) analysis of the residual load, nevertheless, indicates a significant decrease in peak hours, compared to the reference case. This finding comes despite of the circumstance that additional demand regions are included while the intermittent renewables capacity in the complete system is overall slightly lower compared to Europe alone. Even prior to any demand side management flexibilities, the maximum electricity residual load in 2050 decreases compared to the start year (2019). With the same load curve in Europe alone but with a more concentrated renewables allocation in Germany, the opposite is the case. A better balancing of profiles becomes possible by reducing the massive WECS and PV capacity concentration in Germany¹⁴ and a reallocation in neighboring countries (UK, DK) and partially in Eastern Europe (UA, BY). Nevertheless,

¹² For heating and cooling related conversion processes only the useful energy demand was fixed. A significant part of the final energy demand for energy carriers is therefore variable. The demand and production of energy carriers in the transformation sector is modeled completely endogenously without any restrictions.

¹³ WECS: Wind Energy Conversion System, PV: Photovoltaics

¹⁴ From 544 GW to 401 GW

Germany still remains the country with the most renewables capacity (what indicates that the massive expansion is useful). Despite of the capacity reallocation, the general trend of high north-south power flows in Northwestern Europe and an expansion of the HVDC corridors in this direction, did not deviate from the underlying TYNDP scenario¹⁵.

From a sector coupling point of view, the interaction between the gas and electricity system reveals some interesting dynamics. Besides of the global dimensioning trend (i0) that each added conversion or transmission capacity is operated with high full load hours, three general trends, from the point of view of the RES-E system integration, might be identified:

- (i) In case of an RES-E expansion, the electricity is typically first used to cover a local final electricity demand (in case of the possibility to increase this demand by heat pumps, they are expanded).
- (ii) In case of a medium scale RES-E supply imbalance and (ii1) the possibility of a regional or temporal balancing, an AC grid expansion for wind onshore and BESS expansion for PV (partially in combination with an electrolysis) is chosen. If not possible (ii2), auxiliary energy for conversion processes of the transformation sector (e.g., CCS after steam reformation) and for the transport of energy carriers (e.g., compressors, liquefaction) is provided.
- (iii) In case of a large-scale RES-E supply imbalance, if possible (iii1) an electricity grid expansion (AC: wind onshore, DCMT and DCTT for wind offshore) is chosen for a regional but not intercontinental transport of a part of the generation. For the remaining part, or if an expansion is not possible, an alternative conversion route is chosen. This might be (iii2) the production (AEL) and transport (pipeline, ship) of hydrogen or derived energy carriers (2/3 LOHC, 1/3 LH₂), or (iii3) a direct are capture with a subsequent CO₂ transport and storage (iii3a) or production of synthetic fuel oil (iii3b). In all cases (iii2, iii3), the conversion units are either placed in the direct neighborhood of the renewables hotspot or partly offshore and at the first landing node at the shore.

While the first point (i) is quite obvious in densely populated areas with limited high quality resource potential (like Germany), this also might be the main reason why no large scale direct (electricity) or indirect (“green” hydrogen and derivatives) renewable energy imports from the MENA region or Central Asia are observed. In the first place, the renewable generation in these countries is used for a decarbonization of the own power system and the balance of an increasing power demand due to a population growth. The circumstance that these often PV dominated countries (with less developed electricity transmission systems as a start base) do not end the firing of natural gas in the power system, is a further indication for the observed development.

¹⁵ By doubling the electricity transmission capacity on most German North-South HVDC corridors and increasing the cross-border transmission capacities to Nordic countries, the results actually strengthen the findings of the transmission system operators.

As the precondition (i0) is not given, these countries switch to providing auxiliary energy for reducing the emissions of the natural gas-based energy conversion chain (ii2). Although PV also plays a significant role in the Spanish or Greece system, the placement of electrolyser capacities next to large PV capacities in these countries (ii1) and their relatively high utilization rate¹⁶, indicates that the electricity grid might improve the integration of renewables even if they are not producing. Potentially due to their placement within the highly interconnected UCTE grid, the electrolyser in Spain in Greece continued their operation during night hours. With higher full load hours, the economical properties of an PV-AEL system increased, while a large-scale expansion of the electricity transmission or storage system for an integration of the peak generation could be avoided. In the North-Sea and the bordering coastal regions (iii), finally the largest concentration of wind onshore and offshore units is observed. In order to integrate this generation into the system, the model uses a combination of multiple conversion and transmission paths. One important element is the AC expansion in the coastal grid for integrating the feed-in from onshore units and strengthening the grid around offshore landings, which are realized through an expansion of the HVDC connections and may reach to the load centers in the inland (Germany, partially France). In this context a combination of direct point-to-point HVDC connections, to connect the offshore wind farms to the onshore grid, with a meshed DCMT overlay grid, for linking the offshore wind farms and increasing the cross-border exchange capacity, is observed. In order to avoid an over dimensioning of the electricity system, the RES-E expansion is accompanied by a nearby expansion of the hydrogen conversion chain. Being directly located next to generation hotspots (onshore and offshore) or directly at the first landing point for wind offshore at the shore, the power-to-gas units reduce the need for an electricity grid expansion by injecting the generation into a hydrogen transmission grid, which is built. The example of Shetland, which is a hub (energy island) for the hydrogen production, liquification and shipping and bundles the generation off the most northern part of Scotland, further demonstrates that the choice of a transmission system and transport energy carrier is not only optimized within the technology class (e.g., LH2 vs. LOHC shipping in Chile) but across. In this case the AC and HVDC expansion is weighted against the pipeline (H2 replaces CH4) and shipping (LH2 vs LOHC) expansion. The possibility to identify and expand complex conversion chains from the scratch leads also to the interesting finding that the meshed DCMT offshore grid basically fulfills the function of a virtual energy island by bundling the generation from multiple offshore windfarms. This bundling facilitates the steady dispatch of offshore electrolyser, such that the expansion of offshore BESS units, which are also observed in this constellation, might be reduced.

While the current conclusion focused on the analysis of the electricity system, which clearly dominates the whole energy system, it should be mentioned that the majority of the hydrogen production is chosen from a natural gas steam reformation. In this context the renewable generation is just as an auxiliary energy for decarbonizing the preceding natural gas conversion chain (production, storage, compression liquification, etc.), the process itself (electricity demand

¹⁶ These units are dispatched in PV dominated systems with only little lower full load hours, compared to wind dominated systems in the north.

of pyrolysis units) and for the subsequent emission reduction (CCS after NGR, DAC and storage, DAC and H₂toL). In this context it could be mentioned that the general structure and the flow directions of the natural gas or “blue hydrogen” transmission systems remains quite stable. While LNG exporting countries like the Gulf States continue the LNG supply to Europe, where the blue hydrogen production is concentrated next to import terminals in the North Sea region (e.g., ARA, Wilhelmshaven, Hamburg), a part of the natural gas production around the Caspian Sea, and in Algeria (and on a smaller scale Egypt) switches to the hydrogen production. The produced hydrogen in the latter case is exported via pipelines to Europe.

Although the results of the case study should not be overinterpreted, they demonstrate the ability of the approach for a cross-sectoral balance of conversion and storage processes on a local scale in combination with a cross-energy carrier balancing of transmission systems on an intercontinental scale. Based on the example of the allocation decision for Fischer-Tropsch processes and its local and transmission network spanning coupling with preceding and succeeding conversion processes of the transformation sector (EHG, X2X) and the final demand sector (chemical industry) it was demonstrated how the optimization of local energy and material flows (e.g., BASF in Ludwigshafen) interacts with the global layout of the energy system.

4.5 Limitations and Outlook

The developed tool chain for an integrated analysis of the energy system relies on multiple techno-economic parameter assumption for the modelling of existing and future energy conversion, storage and transmission processes. While the parameters of the existing energy system are partially unknown due to their proprietary nature and may only be approximated, the uncertainty about the future technological development is an additional challenge. For technologies in the early development state a broad range of parameter estimations may be found in the literature. In the course of the case study, the sensitivity against this parameter uncertainty was not tested. As a consequence, multiple technologies which are currently at an early state of their development, such as the fusion, were not included. From a methodological point of view it should be mentioned, that the choice of an optimization with perfect foresight, is also less suitable for addressing this kind of uncertainty, compared to other approaches such as stochastic or robust optimization. Besides of neglecting the parametrization uncertainty, the current approach also does not take the impact of the stochastic nature of weather-related generating and demand profiles (and of transmission capacities in case of an DLR of power lines) into account. Only in a preprocessing step this impact is considered for deriving valid bounds for the dispatch of PV-BESS units¹⁷.

¹⁷ In an SDP based dispatch optimization, the sectoral demand and PV generation stochastic is considered based on a recombining tree with 8760 stages and 9 realizations. For Europe this results in solving 420000 optimization problems for one investment period and weather year

The general choice for a mono-criterial minimization of the total system expenses under the assumption of complete information and perfect competition has also some far-reaching implications and limitations. With respect to the public acceptance of certain technology options in certain regions and the trade-off between certain model outcomes, a combination with approaches of the multi-criteria decision analysis (MCDA) or even a multi-criteria optimization might be more suited. Within the case study, this aspect was rudimentary addressed in the pre-computation phase for an estimation of the regional demand and renewables development. For the regionalization of lower bound for the technology specific renewables expansion or the sectoral market penetration of PV-BESS systems or EVs, a multi criteria approach was chose. In an earlier work (Slednev et al. 2014), the combination of a preceding version of PERSEUS-gECT (PERSEUS-NET) with the multi attribute value theory (MAVT) based toolbox Simada (Bertsch and Fichtner 2016) was demonstrated and could be also applied to the described energy system model. Considering the large problem size, the switch to a multi-objective optimization however seems less promising in the short-to-medium term. Concerning the suitability of the assumption of a perfect competition, the answer is unclear and will probably depend on the question if a deep sector coupling is actually realized or not. In general, it should be stressed that the results of energy system models like PERSEUS-gECT should not be interpreted as market results but from a normative point of view perspective. Depending of the type of competition in a market, this normative perspective is however, more or less related to the observed developments. From the power sector point of view in the integrated European market, the inherent assumption of perfect competition in PERSEUS-gECT, seems to be less critical, considering that a use of market power on a large scale could not be observed despite of the high concentration of the generation capacity. For the gas sector on the other hand, and especially for the LNG sector, the modelling of a Cournot or Stackelberg oligopoly could be more appropriate, but would require to switch from a LP/MILP problem formulation to a MCP (mixed complementary problem), which is non-linear. In case the energy system is largely dominated by electricity for covering the demand of the final energy and transformation sector (high sector coupling), it might be assumed that the perfect competition assumption might be less critical in future. However, also the opposite might be the case.

A further critical point is the consideration of security of supply in PERSEUS-gECT with respect to the generation and transmission capacity adequacy. This aspect was neglected within the case study, as only one part of the developed tool chain (PERSEUS-gECT) was demonstrated. In an iterative approach the developed sub-module PERSEUS-ADQ could be applied to evaluate the capacity adequacy in the power sector considering generator outages and the hourly residual load for a long range of weather years. An integrated consideration of the outage or failure of transmission lines (electricity), pipes (gas) or transport routes (waterway, rail, road) or of conversion capacities in the transformation sector (EHG, OCP), however, remains a challenge, and might be part of future research. Also, the consideration of outages of the transmission and transport infrastructure, which were previously (Hartel et al. 2019) considered only for the N-1 case of the electricity grid based on an ADMM decomposition and a rolling horizon approach in a smaller region, remains challenging and should be addressed in future work.

Finally, the increase of the spatial coverage (remaining world) and of the sectoral coverage (global complete energy balance everywhere, not only in Europe) should be part of future work. In this context, especially the modelling of sector specific demand profiles (industry!), apart of low enthalpy heating and cooling related applications, remains a challenge. The tool-chain for the other component models (transport\transmission, renewable potentials and heating profiles, generator database) however already allows a global coverage.

References

Aguilera, Roberto F. 2014. Production costs of global conventional and unconventional petroleum. *Energy Policy* 64:134–140. doi: 10.1016/j.enpol.2013.07.118.

Aguilera, Roberto F., Roderick G. Eggert, Gustavo Lagos C.C., and John E. Tilton. 2009. Depletion and the Future Availability of Petroleum Resources. *The Energy Journal* 30 (1): 141–174.

Akagi, S. K., R. J. Yokelson, C. Wiedinmyer, M. J. Alvarado, J. S. Reid, T. Karl, J. D. Crouse, and P. O. Wennberg. 2011. Emission factors for open and domestic biomass burning for use in atmospheric models. *Atmospheric Chemistry and Physics* 11 (9): 4039–4072. doi: 10.5194/acp-11-4039-2011.

Alami, Abdul Hai, A. G. Olabi, Ayman Mdallal, Ahmed Rezk, Ali Radwan, Shek Mohammod Atiqure Rahman, Sheikh Khaleduzzaman Shah, and Mohammad Ali Abdelkareem. 2023. Concentrating solar power (CSP) technologies: Status and analysis. *International Journal of Thermofluids* 18:100340. doi: 10.1016/j.ijft.2023.100340.

Arroyo, Alberto, Pablo Castro, Raquel Martinez, Mario Manana, Alfredo Madrazo, Ramón Lecuna, and Antonio Gonzalez. 2015. Comparison between IEEE and CIGRE Thermal Behaviour Standards and Measured Temperature on a 132-kV Overhead Power Line. *Energies* 8 (12): 13660–13671. doi: 10.3390/en81212391.

B.S. Elbersen, H.L.E. de Groot, I.G. Staritsky, Matthias Dees, Pawan Datta, and Sylvain Leduc. 2017. *Final version of: 1) D4.3: Fully populated database including all data accumulated in the project and used by the tools 2) D4.4: Data viewer, download and analysis tool for biomass cost-supply/ 3) D4.5: Tool for viewing characteristics of technologies and matching biomass to pre-treatment and conversion technologies 4) D4.6: Tool for viewing market demand and policies for biomass for bioenergy and biobased products 5) D4.7/D4.8: Validated tools for optimal design and evaluation of biomass delivery chains and networks at Pan-European, national, regional and local scale (BeWhere & LocaGISStics) 6) D4.9: Comprehensive general user interface (GUI) that integrates the tools and S2BIOM database: Version: 0.2.* S2Biom.

Bao, Keyu, Rushikesh Padsala, Volker Coors, Daniela Thrän, and Bastian Schröter. 2020. A Method for Assessing Regional Bioenergy Potentials Based on GIS Data and a Dynamic Yield Simulation Model. *Energies* 13 (24): 6488. doi: 10.3390/en13246488.

Bao, Keyu, Louis Kalisch, Thunyathep Santhanavanich, Daniela Thrän, and Bastian Schröter. 2022. A bottom-up GIS-based method for simulation of ground-mounted PV potentials at regional scale. *Energy Reports* 8:5053–5066. doi: 10.1016/j.egy.2022.03.187.

Baufumé, Sylvestre, Fabian Grüger, Thomas Grube, Dennis Krieg, Jochen Linsen, Michael Weber, Jürgen-Friedrich Hake, and Detlef Stolten. 2013. GIS-based scenario calculations for a nationwide German hydrogen pipeline infrastructure. *International Journal of Hydrogen Energy* 38 (10): 3813–3829. doi: 10.1016/j.ijhydene.2012.12.147.

- Bendotti, Pascale, Pierre Fouilhoux, and Cécile Rottner. 2018. The min-up/min-down unit commitment polytope. *Journal of Combinatorial Optimization* 36 (3): 1024–1058. doi: 10.1007/s10878-018-0273-y.
- Bentsen, Niclas Scott, and Claus Felby. 2012. Biomass for energy in the European Union - a review of bioenergy resource assessments. *Biotechnology for biofuels* 5 (1): 25. doi: 10.1186/1754-6834-5-25.
- Bertsch, Valentin, and Wolf Fichtner. 2016. A participatory multi-criteria approach for power generation and transmission planning. *Annals of Operations Research* 245 (1-2): 177–207. doi: 10.1007/s10479-015-1791-y.
- BfG - The GRDC. 2023. https://www.bafg.de/GRDC/EN/01_GRDC/grdc_node.html. Accessed 2 November 2023.
- Bódis, Katalin, Ioannis Kougias, Arnulf Jäger-Waldau, Nigel Taylor, and Sándor Szabó. 2019. A high-resolution geospatial assessment of the rooftop solar photovoltaic potential in the European Union. *Renewable and Sustainable Energy Reviews* 114:109309. doi: 10.1016/j.rser.2019.109309.
- Brown, Thomas, Jonas Hörsch, and David Schlachtberger. 2018. PyPSA: Python for Power System Analysis. *Journal of Open Research Software* 6 (1): 4. doi: 10.5334/jors.188.
- Burek, Peter, and Mikhail Smilovic. 2022. *The use of GRDC gauging stations for calibrating large-scale hydrological models*.
- Büttner, Clara, Jonathan Amme, Julian Endres, Aadit Malla, Birgit Schachler, and Ilka Cußmann. 2022. Open modeling of electricity and heat demand curves for all residential buildings in Germany. *Energy Informatics* 5 (S1): 1–21. doi: 10.1186/s42162-022-00201-y.
- Carrillo, C., A. F. Obando Montaña, J. Cidrás, and E. Díaz-Dorado. 2013. Review of power curve modelling for wind turbines. *Renewable and Sustainable Energy Reviews* 21:572–581. doi: 10.1016/j.rser.2013.01.012.
- Casasso, Alessandro, and Rajandrea Sethi. 2016. G.POT: A quantitative method for the assessment and mapping of the shallow geothermal potential. *Energy* 106:765–773. doi: 10.1016/j.energy.2016.03.091.
- Cigr WG 22.12. 1992. The thermal behaviour of overhead conductors, section 1 and 2: mathematical model for evaluation of conductor temperature in the steady state and the application thereof. Electra. *Electra*.
- DeAngelo, Julianne, Inês Azevedo, John Bistline, Leon Clarke, Gunnar Luderer, Edward Byers, and Steven J. Davis. 2021. Energy systems in scenarios at net-zero CO2 emissions. *Nature communications* 12 (1): 6096. doi: 10.1038/s41467-021-26356-y.

DeSantis, Daniel, Brian D. James, Cassidy Houchins, Genevieve Saur, and Maxim Lyubovsky. 2021. Cost of long-distance energy transmission by different carriers. *iScience* 24 (12): 103495. doi: 10.1016/j.isci.2021.103495.

Doorga, Jay, Soonil Rughooputh, and Ravindra Boojhawon. 2022. Optimizing on Rooftop Solar Technologies—Photovoltaic and Solar Water Heating. In *Geospatial Optimization of Solar Energy*, 53–64. Springer, Cham.

Dranka, Géremi Gilson, Paula Ferreira, and A. Ismael F. Vaz. 2021. A review of co-optimization approaches for operational and planning problems in the energy sector. *Applied Energy* 304:117703. doi: 10.1016/j.apenergy.2021.117703.

Duffie, John A., and William A. Beckman. 2013. *Solar Engineering of Thermal Processes*. John Wiley & Sons.

Dunnett, Sebastian, Alessandro Sorichetta, Gail Taylor, and Felix Eigenbrod. 2020. Harmonised global datasets of wind and solar farm locations and power. *Scientific data* 7 (1): 130. doi: 10.1038/s41597-020-0469-8.

Dupré, Aurore, Philippe Drobinski, Jordi Badosa, Christian Briard, and Riwal Plougonven. 2019. Air Density Induced Error on Wind Energy Estimation. *Annales Geophysicae Discussions* 1–10. doi: 10.5194/angeo-2019-88.

Earth Resources Observation, and Science Center, U.S. Geological Survey, U.S. Department of the Interior. 1997. USGS 30 ARC-second Global Elevation Data, GTOPO30. Boulder CO: Research Data Archive at the National Center for Atmospheric Research, Computational and Information Systems Laboratory. doi: 10.5065/A1Z4-EE71.

ENTSO-E – ENTSOG. 2020. TYNDP 2020, SCENARIO BUILDING GUIDELINES. https://2020.entsos-tyndp-scenarios.eu/wp-content/uploads/2020/06/TYNDP_2020_Scenario_Building_Guidelines_Final_Report.pdf.

ENTSO-E – ENTSOG. 2022. TYNDP 2022, Scenario Report. https://2022.entsos-tyndp-scenarios.eu/wp-content/uploads/2022/04/TYNDP2022_Joint_Scenario_Full-Report-April-2022.pdf. Accessed 18 December 2023.

EU. 2023. 2050 long-term strategy. https://climate.ec.europa.eu/eu-action/climate-strategies-targets/2050-long-term-strategy_en. Accessed 18 December 2023.

Eurek, Kelly, Patrick Sullivan, Michael Gleason, Dylan Hettinger, Donna Heimiller, and Anthony Lopez. 2017. An improved global wind resource estimate for integrated assessment models. *Energy Economics* 64:552–567. doi: 10.1016/j.eneco.2016.11.015.

Gaonwe, Tsholofelo Priscilla, Kanzumba Kusakana, and Percy Andrew Hohne. 2022. A review of solar and air-source renewable water heating systems, under the energy management scheme. *Energy Reports* 8:1–10. doi: 10.1016/j.egy.2022.10.065.

Gilbert, Marius, Gaëlle Nicolas, Giusepina Cinardi, Thomas P. van Boeckel, Sophie O. Vanwambeke, G. R. William Wint, and Timothy P. Robinson. 2018. Global distribution data for cattle, buffaloes, horses, sheep, goats, pigs, chickens and ducks in 2010. *Scientific data* 5 (1): 180227. doi: 10.1038/sdata.2018.227.

Gils, Hans Christian, Thomas Pregger, Franziska Flachsbarth, Mareike Jentsch, and Constantin Dierstein. 2019. Comparison of spatially and temporally resolved energy system models with a focus on Germany's future power supply. *Applied Energy* 255:113889. doi: 10.1016/j.apenergy.2019.113889.

Global administrative boundaries - Data Europa EU. 2023. <https://data.europa.eu/data/datasets/jrc-10112-10004?locale=en>. Accessed 11 October 2023.

González-Longatt, F., P. Wall, and V. Terzija. 2012. Wake effect in wind farm performance: Steady-state and dynamic behavior. *Renewable Energy* 39 (1): 329–338. doi: 10.1016/j.renene.2011.08.053.

Hart-Davis, Michael G., Gaia Piccioni, Denise Dettmering, Christian Schwatke, Marcello Passaro, and Florian Seitz. 2021. EOT20: a global ocean tide model from multi-mission satellite altimetry. *Earth System Science Data* 13 (8): 3869–3884. doi: 10.5194/essd-13-3869-2021.

Hartel, Rupert, Viktor Slednev, Hasan Ümitcan Yilmaz, Armin Ardone, Dogan Keles, Wolf Fichtner, Anke Eßer, Marian Klobasa, Matthias Kühnbach, Pia Manz, Joachim Globisch, Rainer Elsland, and Martin Wietschel. 2019. Dekarbonisierung des Energiesystems durch verstärkten Einsatz erneuerbaren Stroms im Wärme-, Verkehrs- und Industriesektor bei gleichzeitigen Stilllegungen von Kraftwerken – Auswirkungen auf die Versorgungssicherheit in Süddeutschland. *2194-2404* 31. doi: 10.5445/KSP/1000087897.

Hemmati, R., R.-A. Hooshmand, and A. Khodabakhshian. 2013a. Comprehensive review of generation and transmission expansion planning. *Generation, Transmission & Distribution, IET* 7 (9): 955–964. doi: 10.1049/iet-gtd.2013.0031.

Hemmati, Reza, Rahmat-Allah Hooshmand, and Amin Khodabakhshian. 2013b. State-of-the-art of transmission expansion planning: Comprehensive review. *Renewable and Sustainable Energy Reviews* 23:312–319. doi: 10.1016/j.rser.2013.03.015.

Hersbach, Hans, Bill Bell, Paul Berrisford, Shoji Hirahara, András Horányi, Joaquín Muñoz-Sabater, Julien Nicolas, Carole Peubey, Raluca Radu, Dinand Schepers, Adrian Simmons, Cornel Soci, Saleh Abdalla, Xavier Abellan, Gianpaolo Balsamo, Peter Bechtold, Gionata Biavati, Jean Bidlot, Massimo Bonavita, Giovanna de Chiara, Per Dahlgren, Dick Dee, Michail Diamantakis, Rossana Dragani, Johannes Flemming, Richard Forbes, Manuel Fuentes, Alan Geer, Leo

Haimberger, Sean Healy, Robin J. Hogan, Elías Hólm, Marta Janisková, Sarah Keeley, Patrick Laloyaux, Philippe Lopez, Cristina Lupu, Gabor Radnoti, Patricia de Rosnay, Iryna Rozum, Freja Vamborg, Sebastien Villaume, and Jean-Noël Thépaut. 2020. The ERA5 global reanalysis. *Quarterly Journal of the Royal Meteorological Society* 146 (730): 1999–2049. doi: 10.1002/qj.3803.

Hiller, Benjamin, and Tom Walther. 2018. Modelling compressor stations in gas networks. *1438-0064*.

Hilpert, S., C. Kaldemeyer, U. Krien, S. Günther, C. Wingenbach, and G. Plessmann. 2018. The Open Energy Modelling Framework (oemof) - A new approach to facilitate open science in energy system modelling. *Energy Strategy Reviews* 22:16–25. doi: 10.1016/j.esr.2018.07.001.

Hörsch, Jonas, Henrik Ronellenfitsch, Dirk Witthaut, and Tom Brown. 2018. Linear optimal power flow using cycle flows. *Electric Power Systems Research* 158:126–135. doi: 10.1016/j.epsr.2017.12.034.

Hou, Gaoyang, Hessem Taherian, Ying Song, Wei Jiang, and Diyi Chen. 2022. A systematic review on optimal analysis of horizontal heat exchangers in ground source heat pump systems. *Renewable and Sustainable Energy Reviews* 154:111830. doi: 10.1016/j.rser.2021.111830.

IEA. 2019. The Future of Hydrogen,. <https://www.iea.org/reports/the-future-of-hydrogen>, License: CC BY 4.0.

IEC. 2021. *Overhead electrical conductors. Calculation methods for stranded bare conductors: IEC 61089*. London: International Electrotechnical Commission.

Jager, Tobias, Russell McKenna, and Wolf Fichtner. 2015. A bottom-up method for feasible wind energy potential assessments, turbine and park placement. In *2015 12th International Conference on the European Energy Market (EEM)*, 1–5. 2015 12th International Conference on the European Energy Market (EEM). doi: 10.1109/EEM.2015.7216738.

Jamar, A., Z.A.A. Majid, W. H. Azmi, M. Norhafana, and A. A. Razak. 2016. A review of water heating system for solar energy applications. *International Communications in Heat and Mass Transfer* 76:178–187. doi: 10.1016/j.icheatmasstransfer.2016.05.028.

Janotte, N., G. Feckler, J. Kötter, S. Decker, U. Herrmann, M. Schmitz, and E. Lüpfer. 2014. Dynamic Performance Evaluation of the HelioTrough® Collector Demonstration Loop—Towards a New Benchmark in Parabolic Trough Qualification. *Energy Procedia* 49:109–117. doi: 10.1016/j.egypro.2014.03.012.

Jansen, Erik, Julia Schuler, Armin Ardone, Viktor Slednev, Wolf Fichtner, and Marc E. Pfetsch. 2023. Global Logistics of an Iron-based Energy Network: A Case Study of Retrofitting German Coal Power Plants. In *Working Paper Series in Production and Energy ; 70*. doi: 10.5445/IR/1000158253.

- Jin, Yubin, Shijie Hu, Alan D. Ziegler, Luke Gibson, J. Elliott Campbell, Rongrong Xu, Deliang Chen, Kai Zhu, Yan Zheng, Bin Ye, Fan Ye, and Zhenzhong Zeng. 2023. Energy production and water savings from floating solar photovoltaics on global reservoirs. *Nature Sustainability* 6 (7): 865–874. doi: 10.1038/s41893-023-01089-6.
- Jordan, Dirk C., Sarah R. Kurtz, Kaitlyn VanSant, and Jeff Newmiller. 2016. Compendium of photovoltaic degradation rates. *Progress in Photovoltaics: Research and Applications* 24 (7): 978–989. doi: 10.1002/pip.2744.
- Joshi, Siddharth, Shivika Mittal, Paul Holloway, Priyadarshi Ramprasad Shukla, Brian Ó Galachóir, and James Glynn. 2021. High resolution global spatiotemporal assessment of rooftop solar photovoltaics potential for renewable electricity generation. *Nature Communications* 12 (1): 1–15. doi: 10.1038/s41467-021-25720-2.
- Kang, A., I. Korolija, and D. Rovas. 2022. Photovoltaic Thermal District Heating: A review of the current status, opportunities and prospects. *Applied Thermal Engineering* 217:119051. doi: 10.1016/j.applthermaleng.2022.119051.
- Kaschub, Thomas, Patrick Jochem, and Wolf Fichtner. 2016. Solar energy storage in German households: profitability, load changes and flexibility. *Energy Policy* 98:520–532. doi: 10.1016/j.enpol.2016.09.017.
- Khan, Jibrán, and Mudassar H. Arsalan. 2016. Solar power technologies for sustainable electricity generation – A review. *Renewable and Sustainable Energy Reviews* 55:414–425. doi: 10.1016/j.rser.2015.10.135.
- Kleinschmitt, C., J. Fragoso Garcia, K. Franke, D. Teza, L. Seidel, A. Ebner, and M. Baier. 2022. Weltweite Potenziale erneuerbarer Energien: HYPAT Working Paper 03/2022. https://hypat.de/hypat-wAssets/docs/new/publikationen/HYPAT_Working_Paper_P03-22_EE-Potentiale_FINAL.pdf. Accessed 2023.
- Kratochvil, Jay, William Boyson, and David King. 2004. *Photovoltaic array performance model*. Office of Scientific and Technical Information (OSTI).
- Krishnan, Venkat, Jonathan Ho, Benjamin F. Hobbs, Andrew L. Liu, James D. McCalley, Mohammad Shahidehpour, and Qipeng P. Zheng. 2016. Co-optimization of electricity transmission and generation resources for planning and policy analysis: review of concepts and modeling approaches. *Energy Systems* 7 (2): 297–332. doi: 10.1007/s12667-015-0158-4.
- Kueppers, Martin, Stephany Nicole Paredes Pineda, Michael Metzger, Matthias Huber, Simon Paulus, Hans Joerg Heger, and Stefan Niessen. 2021. Decarbonization pathways of worldwide energy systems – Definition and modeling of archetypes. *Applied Energy* 285:116438. doi: 10.1016/j.apenergy.2021.116438.

- Latorre, G., R. D. Cruz, J. M. Areiza, and A. Villegas. 2003. Classification of publications and models on transmission expansion planning. *Power Systems, IEEE Transactions on* 18 (2): 938–946. doi: 10.1109/TPWRS.2003.811168.
- Li, Can, Antonio J. Conejo, Peng Liu, Benjamin P. Omell, John D. Siirola, and Ignacio E. Grossmann. 2021. Mixed-integer linear programming models and algorithms for generation and transmission expansion planning of power systems. *European Journal of Operational Research*. doi: 10.1016/j.ejor.2021.06.024.
- Liu, Andrew, Qipeng Zheng, Jonathan Ho, Venkat Krishnan, Benjamin Hobbs, Mohammad Shahidehpour, and James McCalley. 2013. Co-optimization of Transmission and Other Supply Resources. NARUC Project No. 3316T5. http://www.naruc.org/grants/Documents/Co-optimization-White-paper_Final_rv1.pdf.
- Lopion, Peter, Peter Markewitz, Martin Robinius, and Detlef Stolten. 2018. A review of current challenges and trends in energy systems modeling. *Renewable and Sustainable Energy Reviews* 96:156–166. doi: 10.1016/j.rser.2018.07.045.
- Lorenz, Elke, Thomas Scheidsteger, Johannes Hurka, Detlev Heinemann, and Christian Kurz. 2011. Regional PV power prediction for improved grid integration. *Progress in Photovoltaics: Research and Applications* 19 (7): 757–771. doi: 10.1002/pip.1033.
- Lorenzo, E., L. Narvarte, and J. Muñoz. 2011. Tracking and back-tracking. *Progress in Photovoltaics: Research and Applications* 19 (6): 747–753. doi: 10.1002/pip.1085.
- Loutzenhiser, P. G., H. Manz, C. Felsmann, P. A. Strachan, T. Frank, and G. M. Maxwell. 2007. Empirical validation of models to compute solar irradiance on inclined surfaces for building energy simulation. *Solar Energy* 81 (2): 254–267. doi: 10.1016/j.solener.2006.03.009.
- Lujala, Päivi, Jan Ketil Rod, and Nadja Thieme. 2007. Fighting over Oil: Introducing a New Dataset. *Conflict Management and Peace Science* 24 (3): 239–256. doi: 10.1080/07388940701468526.
- Mainzer, Kai. 2019. Analyse und Optimierung urbaner Energiesysteme - Entwicklung und Anwendung eines übertragbaren Modellierungswerkzeugs zur nachhaltigen Systemgestaltung. Dissertation, Karlsruher Institut für Technologie (KIT). <https://publikationen.bibliothek.kit.edu/1000092481/24544203>.
- Mainzer, Kai, Karoline Fath, Russell McKenna, Julian Stengel, Wolf Fichtner, and Frank Schultmann. 2014. A high-resolution determination of the technical potential for residential-roof-mounted photovoltaic systems in Germany. *Solar Energy* 105:715–731. doi: 10.1016/j.solener.2014.04.015.

Mathew, Manuel S., Surya Teja Kandukuri, and Christian W. Omlin. 2022. Estimation of Wind Turbine Performance Degradation with Deep Neural Networks. *PHM Society European Conference* 7 (1): 351–359. doi: 10.36001/phme.2022.v7i1.3328.

Matke, Carsten, Wided Medjroubi, and David Kleinhans. 2016. SciGRID - An Open Source Reference Model for the European Transmission Network (v0.2). <http://www.scigrid.de>.

McKenna, R., S. Hollnaicher, and W. Fichtner. 2014. Cost-potential curves for onshore wind energy: A high-resolution analysis for Germany. *Applied Energy* 115:103–115. doi: 10.1016/j.apenergy.2013.10.030.

McKenna, Russell, Stefan Pfenninger, Heidi Heinrichs, Johannes Schmidt, Iain Staffell, Christian Bauer, Katharina Gruber, Andrea N. Hahmann, Malte Jansen, Michael Klingler, Natascha Landwehr, Xiaoli Guo Larsén, Johan Lilliestam, Bryn Pickering, Martin Robinius, Tim Tröndle, Olga Turkovska, Sebastian Wehrle, Jann Michael Weinand, and Jan Wohland. 2022. High-resolution large-scale onshore wind energy assessments: A review of potential definitions, methodologies and future research needs. *Renewable Energy* 182:659–684. doi: 10.1016/j.renene.2021.10.027.

Melius, J., R. Margolis, and S. Ong. 2013. Estimating Rooftop Suitability for PV: A Review of Methods, Patents, and Validation Techniques. <https://www.osti.gov/biblio/1117057>.

Miocic, Johannes M., and Marc Krecher. 2022. Estimation of shallow geothermal potential to meet building heating demand on a regional scale. *Renewable Energy* 185:629–640. doi: 10.1016/j.renene.2021.12.095.

Möller, Bernd, Eva Wiechers, Urban Persson, Lars Grundahl, and David Connolly. 2018. Heat Roadmap Europe: Identifying local heat demand and supply areas with a European thermal atlas. *Energy* 158:281–292. doi: 10.1016/j.energy.2018.06.025.

Nanda, Iksan Riva, Nugroho Agung Pambudi, and Muhammad Aziz. 2023. Review on the Progress of Solar Water Heaters and Their Future Perspectives. *Energy Technology* 11 (10): 2300191. doi: 10.1002/ente.202300191.

Neumann, Fabian, and Tom Brown. 2020. Transmission Expansion Planning Using Cycle Flows. In *Proceedings of the Eleventh ACM International Conference on Future Energy Systems*, 253–263. e-Energy '20. doi: 10.1145/3396851.3397688.

oemof developer group. 2020. *oemof-thermal: Thermal energy components in oemof*. Zenodo.

Open Data Science Europe Metadata Catalog. 2022. Nomenclature of Territorial Units for Statistics (NUTS) - Statistical Units - Data sets (2003 - 2021). <https://data.opendatascience.eu/geonetwork/srv/api/records/4b6369cc-3db4-4aa5-9cbe-4058fc63d0df>. Accessed 11 October 2023.

- OpenStreetMap contributors. 2017. Planet dump retrieved from <https://planet.osm.org>.
- Parzen, Maximilian, Hazem Abdel-Khalek, Ekaterina Fedotova, Matin Mahmood, Martha Maria Frysztacki, Johannes Hampp, Lukas Franken, Leon Schumm, Fabian Neumann, Davide Poli, Aristides Kiprakis, and Davide Fioriti. 2023. PyPSA-Earth. A new global open energy system optimization model demonstrated in Africa. *Applied Energy* 341:121096. doi: 10.1016/j.apenergy.2023.121096.
- Peacock, Malcolm, Aikaterini Fragaki, and Bogdan J. Matuszewski. 2021. Review of Heat Demand Time Series Generation for Energy System Modelling. *Energy and Sustainable Futures* 53–60. doi: 10.1007/978-3-030-63916-7_7.
- Pelda, Johannes, Stefan Holler, and Urban Persson. 2021. District heating atlas - Analysis of the German district heating sector. *Energy* 233:121018. doi: 10.1016/j.energy.2021.121018.
- Perau, Christian, Viktor Slednev, Manuel Ruppert, and Wolf Fichtner. 2021. Regionalization of four storylines for the decarbonization of the European power system including flexibilities. In *12. Internationale Energiewirtschaftstagung, IEWT: Das Energiesystem nach Corona: Irreversible Strukturänderungen - Wie? 8. - 10. September 2021, Karlsplatz & Online, TU Wien*.
- Perez, Richard, Pierre Ineichen, Robert Seals, Joseph Michalsky, and Ronald Stewart. 1990. Modeling daylight availability and irradiance components from direct and global irradiance. *Solar Energy* 44 (5): 271–289. doi: 10.1016/0038-092X(90)90055-H.
- Pillot, Benjamin, Nadeem Al-Kurdi, Carmen Gervet, and Laurent Linguet. 2020. An integrated GIS and robust optimization framework for solar PV plant planning scenarios at utility scale. *Applied Energy* 260:114257. doi: 10.1016/j.apenergy.2019.114257.
- Ranjbaran, Parisa, Hossein Yousefi, G. B. Gharehpetian, and Fatemeh Razi Astarai. 2019. A review on floating photovoltaic (FPV) power generation units. *Renewable and Sustainable Energy Reviews* 110:332–347. doi: 10.1016/j.rser.2019.05.015.
- Reda, Ibrahim, and Afshin Andreas. 2004. Solar position algorithm for solar radiation applications. *Solar Energy* 76 (5): 577–589. doi: 10.1016/j.solener.2003.12.003.
- Ringler, Philipp, Hans Schermeyer, Manuel Ruppert, Marian Hayn, Valentin Bertsch, Dogan Keles, and Wolf Fichtner. 2016. Decentralized Energy Systems, Market Integration, Optimization. *2194-2404*. doi: 10.5445/KSP/1000053596.
- Rosen, J. 2008. The future role of renewable energy sources in European electricity supply. A model-based analysis for the EU-15. Dissertation, Karlsruher Institut für Technologie (KIT). <https://www.osti.gov/etdeweb/biblio/21085511>.

- Ruhnau, Oliver, Lion Hirth, and Aaron Praktiknjo. 2019. Time series of heat demand and heat pump efficiency for energy system modeling. *Scientific data* 6 (1): 189. doi: 10.1038/s41597-019-0199-y.
- Ruppert, Manuel, Viktor Slednev, Valentin Bertsch, and Wolf Fichtner. 2016. The impact of microeconomic decisions in electricity market modelling on load flows in transmission grids. In *13th International Conference on the European Energy Market*, 1–5. EEM, Porto, Portugal. doi: 10.1109/EEM.2016.7521238.
- Ruppert, Manuel, Viktor Slednev, Armin Ardone, and Wolf Fichtner. 2018. Dynamic Optimal Power Flow with Storage Restrictions Using Augmented Lagrangian Algorithm. In *2018 Power Systems Computation Conference (PSCC)*, 1–7. doi: 10.23919/PSCC.2018.8442993.
- Ruppert, Manuel, Viktor Slednev, Rafael Finck, Armin Ardone, and Wolf Fichtner. 2019. Utilising Distributed Flexibilities in the European Transmission Grid. In *Advances in Energy System Optimization – Proceedings of the 2nd International Symposium on Energy System Optimization*, 81–101. Birkhäuser Verlag. doi: 10.1007/978-3-030-32157-4_6.
- Sadeghi, Hadi, Masoud Rashidinejad, and Amir Abdollahi. 2017. A comprehensive sequential review study through the generation expansion planning. *Renewable and Sustainable Energy Reviews* 67:1369–1394. doi: 10.1016/j.rser.2016.09.046.
- Saint-Drenan, Yves-Marie, Romain Besseau, Malte Jansen, Iain Staffell, Alberto Troccoli, Laurent Dubus, Johannes Schmidt, Katharina Gruber, Sofia G. Simões, and Siegfried Heier. 2020. A parametric model for wind turbine power curves incorporating environmental conditions. *Renewable Energy* 157:754–768. doi: 10.1016/j.renene.2020.04.123.
- Saxena, Ankita, Calum Brown, Almut Arneht, and Mark Rounsevell. 2023. Modelling the global photovoltaic potential on land and its sensitivity to climate change. *Environmental Research Letters* 18 (10): 104017. doi: 10.1088/1748-9326/acf86f.
- Scaramuzzino, Chiara, Giulia Garegnani, and Pietro Zambelli. 2019. Integrated approach for the identification of spatial patterns related to renewable energy potential in European territories. *Renewable and Sustainable Energy Reviews* 101:1–13. doi: 10.1016/j.rser.2018.10.024.
- Scarlat, Nicolae, Fernando Fahl, Jean-François Dallemand, Fabio Monforti, and Vincenzo Motola. 2018. A spatial analysis of biogas potential from manure in Europe. *Renewable and Sustainable Energy Reviews* 94:915–930. doi: 10.1016/j.rser.2018.06.035.
- Schweppe, Fred C. 2000. *Spot pricing of electricity*, 4th edn. Boston: Kluwer Acad. Publ.
- Silalahi, David Firnando, and Andrew Blakers. 2023. Global Atlas of Marine Floating Solar PV Potential. *Solar* 3 (3): 416–433. doi: 10.3390/solar3030023.

- Slednev, Viktor, Valentin Bertsch, Christoph Nolden, and Wolf Fichtner. 2014. Multi-Criteria Decision Support for Power Grid Expansion Planning. *Decision analysis and multiple criteria decision making : proceedings of the Joint GOR- and DASIG-Conference, Hamburg, Germany, September 23rd - 24th, 2013*. Ed.: S. Langton 133.
- Slednev, Viktor, Valentin Bertsch, and Wolf Fichtner. 2017a. A Multi-objective Time Segmentation Approach for Power Generation and Transmission Models. In *Operations Research Proceedings 2015*, 707–714. Cham: Springer International Publishing. doi: 10.1007/978-3-319-42902-1_95.
- Slednev, Viktor, Manuel Ruppert, Valentin Bertsch, Wolf Fichtner, Nico Meyer-Hübner, Michael Suriyah, Thomas Leibfried, Philipp Gerstner, Michael Schick, and Vincent Heuveline. 2017b. Regionalizing Input Data for Generation and Transmission Expansion Planning Models. In *Advances in Energy System Optimization*, ed. Valentin Bertsch, Wolf Fichtner, Vincent Heuveline and Thomas Leibfried, 205–217. Cham: Springer International Publishing.
- Slednev, Viktor, Valentin Bertsch, Manuel Ruppert, and Wolf Fichtner. 2018. Highly resolved optimal renewable allocation planning in power systems under consideration of dynamic grid topology. *Computers & Operations Research* 96:281–293. doi: 10.1016/j.cor.2017.12.008.
- Slednev, Viktor, Patrick Jochem, and Wolf Fichtner. 2021. Impacts of electric vehicles on the European high and extra high voltage power grid. *Journal of Industrial Ecology*. doi: 10.1111/jiec.13216.
- Staffell, Iain, Stefan Pfenninger, and Nathan Johnson. 2023. A global model of hourly space heating and cooling demand at multiple spatial scales. *Nature Energy* 1–17. doi: 10.1038/s41560-023-01341-5.
- Stein, Joshua S., William F. Holmgren, Jessica Forbess, and Clifford W. Hansen. 2016. PVLIB: Open source photovoltaic performance modeling functions for Matlab and Python. In *IEEE 43rd Photovoltaic Specialists Conference (PVSC)*, 3425–3430, Portland, OR, USA. doi: 10.1109/PVSC.2016.7750303.
- Stocks, Matthew, Ryan Stocks, Bin Lu, Cheng Cheng, and Andrew Blakers. 2021. Global Atlas of Closed-Loop Pumped Hydro Energy Storage. *Joule* 5 (1): 270–284. doi: 10.1016/j.joule.2020.11.015.
- Trieb, F., C. Schillings, M. O. Sullivan, T. Pregger, and C Hoyer-Klick. 2009. Global Potential of Concentrating Solar Power. In *Proceedings of Solar Power and Chemical Energy Systems Conference*. Berlin.
- U.S. Geological Survey world petroleum assessment 2000: Description and results. 2000. US Geological Survey. doi: 10.3133/ds60.

- Walch, Alina, Xiang Li, Jonathan Chambers, Nahid Mohajeri, Selin Yilmaz, Martin Patel, and Jean-Louis Scartezzini. 2022. Shallow geothermal energy potential for heating and cooling of buildings with regeneration under climate change scenarios. *Energy* 244:123086. doi: 10.1016/j.energy.2021.123086.
- Weinand, Jann M., Russell McKenna, and Kai Mainzer. 2019. Spatial high-resolution socio-energetic data for municipal energy system analyses. *Scientific data* 6 (1): 243. doi: 10.1038/s41597-019-0233-0.
- Weinand, Jann Michael, Maximilian Hoffmann, Jan Göpfert, Tom Terlouw, Julian Schönau, Patrick Kuckertz, Russell McKenna, Leander Kotzur, Jochen Linßen, and Detlef Stolten. 2023. Global LCOEs of decentralized off-grid renewable energy systems. *Renewable and Sustainable Energy Reviews* 183:113478. doi: 10.1016/j.rser.2023.113478.
- Wiegmans, Bart. 2016. *Gridkit Extract Of Entso-E Interactive Map*. Zenodo.
- Yeliget, Madhura, Wenxuan Hu, Yvonne Scholz, Ronald Stegen, and Kai von Krbeke. 2023. Cropland and rooftops: the global undertapped potential for solar photovoltaics. *Environmental Research Letters* 18 (5): 54027. doi: 10.1088/1748-9326/accc47.
- Zhang, Alice Tianbo, and Vincent Xinyi Gu. 2023. Global Dam Tracker: A database of more than 35,000 dams with location, catchment, and attribute information. *Scientific data* 10 (1): 111. doi: 10.1038/s41597-023-02008-2.

Annex

ISO2	CO2 Emission in 2050 in kT		INPUT:: fix_CO2_Emission			INPUT:: var_CO2_Emission			Output					
	ISO3	CNTR_Name Cluster	Coal	Gas	Oil	Coal	Gas	Oil	fix	OCP	EHG	STOR	TST	
AL	ALB	Albania	UCTE/EUi	0,00	89,74	1.172,09	877,23	1,75	161,90	1.261,83	-	516,04	6,05	9,31
AE	ARE	United Arab	GCCIA	-	-	-	-	-	-	-	0,22	2.422,34	-	135,88
AR	ARG	Argentina	CHL+ARG	-	-	-	-	-	-	-	-	-	-	-
AM	ARM	Armenia	IRN+IRQ	-	-	-	-	-	-	-	-	719,23	-	166,20
AT	AUT	Austria	UCTE/EUi	-	4.268,92	2.311,20	-	810,37	-	6.580,12	0,07	144,31	187,81	166,87
AZ	AZE	Azerbaijan	IPS/UPS	-	-	-	-	-	-	-	1.240,33	0,50	-	155,85
BE	BEL	Belgium	UCTE/EUi	0,05	2.855,88	4.749,50	2,31	1.428,70	-	7.605,43	-	1.426,26	518,21	1.016,92
BG	BGR	Bulgaria	UCTE/EUi	-	879,85	937,64	296,97	52,19	-	1.817,48	-	179,27	2,92	79,05
BH	BHR	Bahrain	GCCIA	-	-	-	-	-	-	-	-	0,70	-	12,31
BA	BIH	Bosnia and H	UCTE/EUi	-	103,16	1.457,92	-	118,66	81,45	1.561,08	-	-	33,12	6,68
BY	BLR	Belarus	IPS/UPS	-	-	-	-	-	-	-	0,23	56,08	2,35	44,69
CH	CHE	Switzerland	UCTE/EUi	-	1.857,93	6.731,90	-	2.251,57	1.103,90	8.589,83	-	1,03	1.173,32	33,08
CL	CHL	Chile	CHL+ARG	-	-	-	-	-	-	-	-	-	-	-
CY	CYP	Cyprus	UCTE/EUi	-	50,80	421,54	-	10,70	-	472,34	-	-	4,50	86,34
CZ	CZE	Czech Repub	UCTE/EUi	-	3.094,80	2.356,89	-	1.528,45	-	5.451,69	-	428,79	518,15	38,35
DE	DEU	Germany	UCTE/Big4	0,21	25.454,82	34.178,24	86,70	9.698,39	-	59.633,27	4.125,95	7.687,62	2.911,16	1.123,40
DK	DNK	Denmark	UCTE/EUi	0,42	1.745,71	3.399,02	15,83	342,26	-	5.145,16	-	10,01	77,97	111,70
DZ	DZA	Algeria	UCTE/NA	-	-	-	-	-	-	-	3.016,81	5.150,25	-	555,31
EG	EGY	Egypt	SEMB+ISR	-	-	-	-	-	-	-	562,08	19.892,00	-	1.151,16
EH	ESH	Western Sah	UCTE/NA	-	-	-	-	-	-	-	-	-	-	29,19
ES	ESP	Spain	UCTE/Big4	0,22	13.729,72	15.930,96	11,31	3.006,72	-	29.660,90	-	77,24	1.024,90	1.034,81
EE	EST	Estonia	UCTE/EUi	0,03	190,35	259,23	5,00	72,70	-	449,61	503,78	3,12	8,29	41,40
FI	FIN	Finland	NORDEL	0,20	696,94	3.387,95	7,78	3,87	-	4.085,09	-	17,56	0,80	24,99
FR	FRA	France	UCTE/Big4	0,12	15.020,61	27.560,17	276,18	10.561,13	21,30	42.580,90	-	170,38	3.389,75	2.015,26
GB	GBR	United Kingd	NG+EirGrid	-	24.696,69	30.286,53	-	5.908,47	-	54.983,23	2.520,74	1.033,91	547,07	644,86
GE	GEO	Georgia	IPS/UPS	-	1.793,83	1.366,33	947,68	1.444,33	28,91	3.160,16	3.455,42	2.051,37	482,41	209,71
GI	GIB	United Kingd	NG+EirGrid	-	-	-	-	-	-	-	-	-	-	-
GQ	GNQ	Equatorial G-	-	-	-	-	-	-	-	-	-	-	-	-
GR	GRC	Greece	UCTE/EUi	0,11	1.280,40	4.463,49	108,81	253,61	-	5.744,01	-	2.254,68	74,51	1.391,31
HR	HRV	Croatia	UCTE/EUi	0,00	1.327,00	2.146,22	498,10	334,49	-	3.473,22	-	445,11	62,66	109,91
HU	HUN	Hungary	UCTE/EUi	-	2.344,57	1.549,75	-	1.480,00	-	3.894,32	0,12	273,97	177,35	63,21
IE	IRL	Ireland	NG+EirGrid	-	1.103,95	2.231,19	3,55	589,00	-	3.335,14	-	247,66	67,89	71,62
IR	IRN	Iran	IRN+IRQ	-	-	-	-	-	-	-	-	38.788,80	-	228,02
IQ	IRQ	Iraq	IRN+IRQ	-	-	-	-	-	-	-	-	11.177,78	-	154,33
IS	ISL	Iceland	NORDEL	-	-	1.169,35	425,38	-	10,13	1.169,35	-	-	431,43	-
IL	ISR	Israel	SEMB+ISR	-	-	-	-	-	-	-	-	3.305,60	-	129,09
IT	ITA	Italy	UCTE/Big4	0,22	10.610,70	16.271,71	337,87	9.769,72	-	26.882,62	2.591,09	3.765,47	1.628,81	1.174,19
JO	JOR	Jordan	SEMB+ISR	-	-	-	-	-	-	-	-	1.325,62	-	76,60
KZ	KAZ	Kazakhstan	IPS/UPS	-	-	-	-	-	-	-	4.011,95	1.131,30	-	94,07
KG	KGZ	Kyrgyzstan	IPS/UPS	-	-	-	-	-	-	-	-	379,14	-	-
KW	KWT	Kuwait	GCCIA	-	-	-	-	-	-	-	0,09	0,16	-	1,21
LB	LBN	Lebanon	SEMB+ISR	-	-	-	-	-	-	-	-	0,23	-	25,16
LY	LYB	Libya	SEMB+ISR	-	-	-	-	-	-	-	-	18,19	-	80,70
LT	LTU	Lithuania	UCTE/EUi	-	1.377,82	479,32	-	93,20	-	1.857,14	-	29,40	0,93	30,17
LU	LUX	Grand Duchy	UCTE/EUi	-	125,53	-	-	193,96	-	125,53	-	0,14	78,01	6,16
LV	LVA	Latvia	UCTE/EUi	-	200,64	347,84	-	94,18	-	548,49	-	0,06	2,05	21,55
MA	MAR	Morocco	UCTE/EUi	-	-	-	-	-	-	-	-	127,64	-	0,09
MD	MDA	Moldova	UCTE/EUo	0,00	-	956,94	268,05	-	31,74	956,94	-	153,81	12,05	24,19
MK	MKD	Macedonia	UCTE/EUi	-	46,94	1.912,28	-	20,65	113,47	1.959,22	-	0,28	10,84	4,26
MT	MLT	Malta	UCTE/EUi	-	8,88	211,69	-	6,22	-	220,57	-	-	6,58	99,11
ME	MNE	Croatia	UCTE/EUi	-	-	674,99	534,70	-	26,07	674,99	-	314,03	24,41	-
NG	NGA	Nigeria	-	-	-	-	-	-	-	-	-	-	-	-
NL	NLD	Netherlands	UCTE/EUi	0,06	6.352,69	12.274,42	1.967,33	3.792,68	-	18.627,16	7.300,59	1.311,78	777,69	444,65
NO	NOR	Norway	NORDEL	0,17	8.703,94	11.425,40	2.133,68	215,55	817,59	20.129,51	-	657,85	1.264,54	1.046,64
OM	OMN	Oman	GCCIA	-	-	-	-	-	-	-	-	2.347,22	-	343,54
PL	POL	Poland	UCTE/EUi	0,15	10.056,69	8.633,69	768,76	3.374,23	-	18.690,53	504,59	2.223,89	466,14	318,34
PT	PRT	Portugal	UCTE/EUi	-	1.080,58	2.889,40	0,30	104,27	-	3.969,98	-	23,73	8,54	197,92
PS	PSE	Palestine	SEMB+ISR	-	-	-	-	-	-	-	-	1.598,32	-	25,74
QA	QAT	Qatar	GCCIA	-	-	-	-	-	-	-	76,75	5.854,71	-	-
RO	ROU	Romania	UCTE/EUi	0,00	2.783,44	4.354,34	533,85	1.188,53	-	7.137,78	0,22	806,18	135,31	69,37
RU	RUS	Russia	IPS/UPS	-	-	-	-	-	-	-	0,39	9.750,02	0,17	849,75
SA	SAU	Saudi Arabia	GCCIA	-	-	-	-	-	-	-	-	18.125,79	-	-
RS	SRB	Serbia	UCTE/EUi	-	1.068,96	3.283,69	-	824,43	233,58	4.352,64	-	37,49	256,50	30,16
SK	SVK	Slovakia	UCTE/EUi	-	1.649,91	1.263,00	-	720,90	-	2.912,91	-	0,46	115,90	30,14
SI	SVN	Slovenia	UCTE/EUi	-	233,74	308,78	-	104,60	-	542,52	-	176,25	25,34	69,17
SE	SWE	Sweden	NORDEL	-	1.842,72	3.332,72	-	571,49	-	5.175,44	-	0,69	126,33	57,78
SY	SYR	Syria	SEMB+ISR	-	-	-	-	-	-	-	-	2.836,60	-	150,01
TJ	TJK	Tajikistan	IPS/UPS	-	-	-	-	-	-	-	-	-	-	0,91
TM	TKM	Turkmenista	IRN+IRQ	-	-	-	-	-	-	-	0,12	1.038,69	-	218,02
TT	TTO	Trinidad and	-	-	-	-	-	-	-	-	-	-	-	-
TN	TUN	Tunisia	UCTE/NA	-	-	-	-	-	-	-	0,70	279,53	-	379,25
TR	TUR	Turkey	UCTE/EUo	0,01	13.482,56	40.835,74	35.338,44	30.017,88	2.693,08	54.318,31	-	26.099,18	26.430,61	5.377,44
UA	UKR	Ukraine	UCTE/EUo	0,00	10.137,59	10.845,24	16.946,21	10.090,11	202,78	20.982,83	2,42	10.235,29	3.541,96	906,21
US	USA	United States	-	-	-	-	-	-	-	-	-	-	-	-
UZ	UZB	Uzbekistan	IPS/UPS	-	-	-	-	-	-	-	0,20	3.573,42	-	84,58

Figure A.1: Country info and complete CO2 emission balance in 2050

Aggregation Rank	Level Type	Code_To	Name_To	Code_From	Name_From	default	renewable	fossil	other
5 sum	1 sum	1.0.0.0.0	EHG_all	EHG_all	EHG_all	1	1	1	1
3 val	0 val	1.0.0.0.0	EHG_comb_lval	EHG_comb_lval	EHG_comb_lval	1	1	1	1
2 val	0 val	2.0.0.0.0	EHG_other_nongas	EHG_other_nongas	EHG_other_nongas	0	0	0	0
2 val	0 val	3.0.0.0.0	EHG_nuclear	EHG_nuclear	EHG_nuclear	0	0	0	0
3 val	0 val	4.0.0.0.0	EHG_wind	EHG_wind	EHG_wind	0	0	0	0
5 val	0 val	5.0.0.0.0	EHG_solar	EHG_solar	EHG_solar	1	0	0	0
3 val	0 val	6.0.0.0.0	EHG_hydro	EHG_hydro	EHG_hydro	1	0	0	0
2 val	0 val	7.0.0.0.0	EHG_geo	EHG_geo	EHG_geo	1	0	0	0
2 val	0 val	8.0.0.0.0	EHG_marine	EHG_marine	EHG_marine	0	1	0	0
4 val	0 val	9.0.0.0.0	EHG_other_res	EHG_other_res	EHG_other_res	0	1	0	0
4 val	0 val	10.0.0.0.0	EHG_battery	EHG_battery	EHG_battery	0	0	0	0
2 val	0 val	11.0.0.0.0	EHG_P2H	EHG_P2H	EHG_P2H	0	0	0	0
2 val	0 val	12.0.0.0.0	EHG_TES	EHG_TES	EHG_TES	0	0	0	0
2 sum	2 sum	0.1.0.0.0	EHG_comb_fuel	EHG_comb_fuel	EHG_comb_fuel	1	1	1	1
2 val	1 val	1.1.0.0.0	EHG_comb_solids	EHG_comb_solids	EHG_comb_solids	1	1	1	1
2 val	1 val	1.2.0.0.0	EHG_comb_gas	EHG_comb_gas	EHG_comb_gas	1	1	1	1
2 val	1 val	1.3.0.0.0	EHG_comb_liquids	EHG_comb_liquids	EHG_comb_liquids	1	1	1	1
1 sum	0 sum	0.3.0.0.0	EHG_nuclear	EHG_nuclear	EHG_nuclear	0	0	0	0
0 val	0 val	3.0.0.0.0	EHG_nuclear_fis	EHG_nuclear_fis	EHG_nuclear_fis	0	0	0	0
0 val	0 val	3.0.0.0.0	EHG_nuclear_fus	EHG_nuclear_fus	EHG_nuclear_fus	0	0	0	0
2 sum	2 sum	0.4.0.0.0	EHG_wind	EHG_wind	EHG_wind	0	0	0	0
2 val	1 val	4.1.0.0.0	EHG_wind_off	EHG_wind_off	EHG_wind_off	0	1	0	0
2 val	1 val	4.2.0.0.0	EHG_wind_on	EHG_wind_on	EHG_wind_on	0	1	0	0
4 sum	4 sum	0.5.0.0.0	EHG_solar	EHG_solar	EHG_solar	1	0	0	0
4 val	1 val	5.1.0.0.0	EHG_pv	EHG_pv	EHG_pv	1	0	0	0
4 val	1 val	5.2.0.0.0	EHG_hydro	EHG_hydro	EHG_hydro	1	0	0	0
5 sum	5 sum	0.6.0.0.0	EHG_hydro	EHG_hydro	EHG_hydro	1	0	0	0
2 val	1 val	6.1.0.0.0	EHG_hydro_pure	EHG_hydro_pure	EHG_hydro_pure	1	0	0	0
2 val	1 val	6.2.0.0.0	EHG_hydro_reserve	EHG_hydro_reserve	EHG_hydro_reserve	1	0	0	0
0 sum	0 sum	0.7.0.0.0	EHG_geo	EHG_geo	EHG_geo	0	0	0	0
0 val	0 val	7.0.0.0.0	EHG_geo_shallow	EHG_geo_shallow	EHG_geo_shallow	0	1	0	0
0 val	0 val	7.0.0.0.0	EHG_geo_deep	EHG_geo_deep	EHG_geo_deep	0	1	0	0
1 sum	0 sum	0.8.0.0.0	EHG_marine	EHG_marine	EHG_marine	0	0	0	0
0 val	0 val	8.1.0.0.0	EHG_tide	EHG_tide	EHG_tide	0	1	0	0
0 val	0 val	8.2.0.0.0	EHG_wave	EHG_wave	EHG_wave	0	1	0	0
0 val	0 val	8.3.0.0.0	EHG_ocean	EHG_ocean	EHG_ocean	0	0	0	0
3 sum	0 sum	0.10.0.0.0	EHG_battery	EHG_battery	EHG_battery	0	0	0	0
0 val	0 val	10.1.0.0.0	EHG_battery_utility	EHG_battery_utility	EHG_battery_utility	0	0	0	0
3 val	1 val	10.2.0.0.0	EHG_battery_small	EHG_battery_small	EHG_battery_small	0	0	0	0
3 val	1 val	10.3.0.0.0	EHG_battery_v2g	EHG_battery_v2g	EHG_battery_v2g	0	0	0	0
0 sum	0 sum	1.1.0.0.0	EHG_P2H	EHG_P2H	EHG_P2H	0	0	0	0
0 val	0 val	11.0.0.0	EHG_P2H_direct	EHG_P2H_direct	EHG_P2H_direct	0	0	0	0
0 val	0 val	11.2.0.0.0	EHG_P2H_ambient	EHG_P2H_ambient	EHG_P2H_ambient	0	0	0	0
1 sum	0 sum	0.12.0.0.0	EHG_TES	EHG_TES	EHG_TES	0	0	0	0
0 val	0 val	12.1.0.0.0	EHG_TES_OH	EHG_TES_OH	EHG_TES_OH	0	0	0	0
0 val	0 val	12.2.0.0.0	EHG_TES_RES	EHG_TES_RES	EHG_TES_RES	0	0	0	0
0 val	0 val	12.3.0.0.0	EHG_TES_TER	EHG_TES_TER	EHG_TES_TER	0	0	0	0
0 val	0 val	12.4.0.0.0	EHG_TES_MND	EHG_TES_MND	EHG_TES_MND	0	0	0	0
1 sum	1 sum	1.1.0.0.0	EHG_comb_solid	EHG_comb_solid	EHG_comb_solid	1	1	1	1
0 val	0 val	1.1.1.0.0	EHG_fossil_solids	EHG_fossil_solids	EHG_fossil_solids	0	1	0	0
0 val	0 val	1.1.2.0.0	EHG_biomass	EHG_biomass	EHG_biomass	0	1	0	0
0 val	0 val	1.1.3.0.0	EHG_waste	EHG_waste	EHG_waste	0	1	0	0
0 val	0 val	1.1.4.0.0	EHG_metals	EHG_metals	EHG_metals	0	0	0	0
0 val	0 val	1.1.5.0.0	EHG_other_solids	EHG_other_solids	EHG_other_solids	0	0	0	0
0 sum	2 sum	1.2.0.0.0	EHG_gas	EHG_gas	EHG_gas	1	0	0	0
0 val	0 val	1.2.1.0.0	EHG_CH4	EHG_CH4	EHG_CH4	1	0	0	0
0 val	0 val	1.2.2.0.0	EHG_MG	EHG_MG	EHG_MG	1	0	0	0
0 val	0 val	1.2.3.0.0	EHG_H2	EHG_H2	EHG_H2	1	0	0	0
0 val	0 val	1.2.4.0.0	EHG_MH3	EHG_MH3	EHG_MH3	1	0	0	0
0 val	0 val	1.2.5.0.0	EHG_other_gas	EHG_other_gas	EHG_other_gas	1	0	0	0
1 sum	1 sum	1.3.0.0.0	EHG_comb_liquid	EHG_comb_liquid	EHG_comb_liquid	1	1	1	1
0 val	0 val	1.3.1.0.0	EHG_OH	EHG_OH	EHG_OH	1	1	1	1
0 val	0 val	1.3.2.0.0	EHG_LOHC	EHG_LOHC	EHG_LOHC	1	0	0	0
0 val	0 val	1.3.3.0.0	EHG_other_liquids	EHG_other_liquids	EHG_other_liquids	1	0	0	0
1 sum	1 sum	1.4.1.0.0	EHG_wind_off	EHG_wind_off	EHG_wind_off	0	1	0	0
0 val	0 val	4.1.1.0.0	EHG_wind_off_fixed	EHG_wind_off_fixed	EHG_wind_off_fixed	0	1	0	0
0 val	0 val	4.1.2.0.0	EHG_wind_off_floating	EHG_wind_off_floating	EHG_wind_off_floating	0	1	0	0
1 sum	1 sum	1.4.2.0.0	EHG_wind_on	EHG_wind_on	EHG_wind_on	0	1	0	0
0 val	0 val	4.2.1.0.0	EHG_wind_on_DS	EHG_wind_on_DS	EHG_wind_on_DS	0	1	0	0
0 val	0 val	4.2.2.0.0	EHG_wind_on_F	EHG_wind_on_F	EHG_wind_on_F	0	1	0	0
3 sum	3 sum	1.5.1.0.0	EHG_pv	EHG_pv	EHG_pv	0	1	0	0
3 val	3 val	5.1.1.0.0	EHG_pv_roof	EHG_pv_roof	EHG_pv_roof	0	1	0	0
3 val	3 val	5.1.2.0.0	EHG_pv_ground	EHG_pv_ground	EHG_pv_ground	0	1	0	0
2 sum	2 sum	5.1.3.0.0	EHG_pv_floating	EHG_pv_floating	EHG_pv_floating	0	1	0	0
3 val	3 val	5.2.1.0.0	EHG_solar_th_ground	EHG_solar_th_ground	EHG_solar_th_ground	1	1	0	1
3 val	3 val	5.2.2.0.0	EHG_solar_th_roof	EHG_solar_th_roof	EHG_solar_th_roof	1	1	0	0
1 sum	1 sum	1.6.1.0.0	EHG_hydro_pure	EHG_hydro_pure	EHG_hydro_pure	0	1	0	0
0 val	0 val	6.1.1.0.0	EHG_ror	EHG_ror	EHG_ror	0	1	0	0
0 val	0 val	6.1.2.0.0	EHG_hydro_reserve	EHG_hydro_reserve	EHG_hydro_reserve	0	1	0	0
1 sum	1 sum	1.6.2.0.0	EHG_ps	EHG_ps	EHG_ps	1	1	0	1
0 val	0 val	6.2.1.0.0	EHG_ps_open_loop	EHG_ps_open_loop	EHG_ps_open_loop	1	1	0	1
0 val	0 val	6.2.2.0.0	EHG_ps_closed_loop	EHG_ps_closed_loop	EHG_ps_closed_loop	0	0	0	1
2 sum	2 sum	1.10.2.0.0	EHG_battery_small	EHG_battery_small	EHG_battery_small	0	0	0	0
2 val	2 val	10.2.1.0.0	EHG_battery_small_RES	EHG_battery_small_RES	EHG_battery_small_RES	0	0	0	1
0 val	0 val	10.2.2.0.0	EHG_battery_small_TER	EHG_battery_small_TER	EHG_battery_small_TER	0	0	0	1
0 val	0 val	10.2.3.0.0	EHG_battery_small_MND	EHG_battery_small_MND	EHG_battery_small_MND	0	0	0	1
0 val	0 val	10.2.4.0.0	EHG_battery_small_AGR	EHG_battery_small_AGR	EHG_battery_small_AGR	0	0	0	1
0 val	0 val	10.2.5.0.0	EHG_battery_small_TRA	EHG_battery_small_TRA	EHG_battery_small_TRA	0	0	0	1
0 sum	0 sum	1.10.3.0.0	EHG_battery_v2g	EHG_battery_v2g	EHG_battery_v2g	0	0	0	0
2 val	2 val	10.3.1.0.0	EHG_battery_v2g_RES	EHG_battery_v2g_RES	EHG_battery_v2g_RES	0	0	0	1
0 val	0 val	10.3.2.0.0	EHG_battery_v2g_TER	EHG_battery_v2g_TER	EHG_battery_v2g_TER	0	0	0	1
0 sum	0 sum	1.1.1.0.0	EHG_coal	EHG_coal	EHG_coal	0	0	0	0
0 val	0 val	1.1.1.2.0	EHG_ignite	EHG_ignite	EHG_ignite	0	0	1	0
2 sum	2 sum	2.5.1.1.0	EHG_pv_roof	EHG_pv_roof	EHG_pv_roof	0	1	0	0
2 val	2 val	5.1.1.1.0	EHG_pv_roof_RES	EHG_pv_roof_RES	EHG_pv_roof_RES	0	1	0	0
0 val	0 val	5.1.1.2.0	EHG_pv_roof_MND	EHG_pv_roof_MND	EHG_pv_roof_MND	0	1	0	0
0 val	0 val	5.1.1.3.0	EHG_pv_roof_AGR	EHG_pv_roof_AGR	EHG_pv_roof_AGR	0	1	0	0
0 val	0 val	5.1.1.4.0	EHG_pv_roof_TRA	EHG_pv_roof_TRA	EHG_pv_roof_TRA	0	1	0	0
0 val	0 val	5.1.1.5.0	EHG_pv_roof_OTH	EHG_pv_roof_OTH	EHG_pv_roof_OTH	0	1	0	0
1 sum	1 sum	2.5.1.2.0	EHG_pv_ground	EHG_pv_ground	EHG_pv_ground	0	1	0	0
0 val	0 val	5.1.2.1.0	EHG_pv_ground_DS	EHG_pv_ground_DS	EHG_pv_ground_DS	0	1	0	0
0 val	0 val	5.1.2.2.0	EHG_pv_ground_CS	EHG_pv_ground_CS	EHG_pv_ground_CS	0	1	0	0
1 sum	1 sum	2.5.2.1.0	EHG_solar_th_ground	EHG_solar_th_ground	EHG_solar_th_ground	1	1	0	0
0 val	0 val	5.2.1.1.0	EHG_solar_th_ground_DS	EHG_solar_th_ground_DS	EHG_solar_th_ground_DS	1	1	0	1
0 val	0 val	5.2.1.2.0	EHG_solar_th_ground_CS	EHG_solar_th_ground_CS	EHG_solar_th_ground_CS	1	1	0	0
2 sum	2 sum	2.5.2.2.0	EHG_solar_th_roof	EHG_solar_th_roof	EHG_solar_th_roof	0	1	0	0
3 val	3 val	5.2.2.1.0	EHG_solar_th_roof_RES	EHG_solar_th_roof_RES	EHG_solar_th_roof_RES	0	1	0	0
0 val	0 val	5.2.2.2.0	EHG_solar_th_roof_MND	EHG_solar_th_roof_MND	EHG_solar_th_roof_MND	0	1	0	0
0 val	0 val	5.2.2.3.0	EHG_solar_th_roof_AGR	EHG_solar_th_roof_AGR	EHG_solar_th_roof_AGR	0	1	0	0
0 val	0 val	5.2.2.4.0	EHG_solar_th_roof_TRA	EHG_solar_th_roof_TRA	EHG_solar_th_roof_TRA	0	1	0	0
0 val	0 val	5.2.2.5.0	EHG_solar_th_roof_OTH	EHG_solar_th_roof_OTH	EHG_solar_th_roof_OTH	0	1	0	0
1 sum	1 sum	2.10.2.1.0	EHG_battery_small_R	EHG_battery_small_R	EHG_battery_small_R	0	0	0	0
0 val	0 val	10.2.1.1.0	EHG_battery_small_RES_SF1	EHG_battery_small_RES_SF1	EHG_battery_small_RES_SF1	0	0	0	1
0 val	0 val	10.2.1.2.0	EHG_battery_small_RES_TF1	EHG_battery_small_RES_TF1	EHG_battery_small_RES_TF1	0	0	0	1
0 val	0 val	10.2.1.3.0	EHG_battery_small_RES_MF	EHG_battery_small_RES_MF	EHG_battery_small_RES_MF	0	0	0	1
1 sum	1 sum	3.5.1.1.0	EHG_pv_roof_RES	EHG_pv_roof_RES	EHG_pv_roof_RES	0	1	0	0
0 val	0 val	5.1.1.1.1	EHG_pv_roof_RES_SF1	EHG_pv_roof_RES_SF1	EHG_pv_roof_RES_SF1	0	1	0	0
0 val	0 val	5.1.1.1.2	EHG_pv_roof_RES_TF1	EHG_pv_roof_RES_TF1	EHG_pv_roof_RES_TF1	0	1	0	0
0 val	0 val	5.1.1.1.3	EHG_pv_roof_RES_MF1	EHG_pv_roof_RES_MF1	EHG_pv_roof_RES_MF1	0	1	0	0
1 sum	1 sum	3.5.2.2.1.0	EHG_solar_th_roof_R	EHG_solar_th_roof_R	EHG_solar_th_roof_R	0	1	0	0
0 val	0 val	5.2.2.1.1	EHG_solar_th_roof_RES_SF1	EHG_solar_th_roof_RES_SF1	EHG_solar_th_roof_RES_SF1	0	1	0	0
0 val	0 val	5.2.2.1.2	EHG_solar_th_roof_RES_TF1	EHG_solar_th_roof_RES_TF1	EHG_solar_th_roof_RES_TF1	0	1	0	0
0 val	0 val	5.2.2.1.3	EHG_solar_th_roof_RES_MF1	EHG_solar_th_roof_RES_MF1	EHG_solar_th_roof_RES_MF1	0	1	0	0

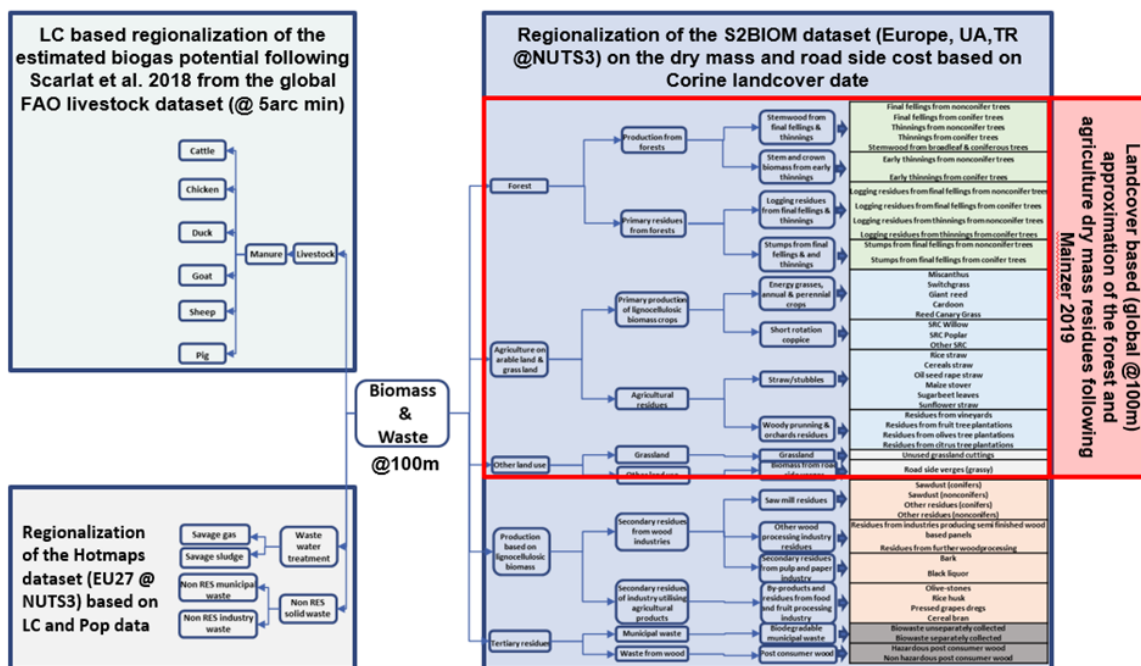
Figure A.2: Classification of EHG processes

ARC GIS IFCLC-Class	CLC Name	ground-mounted suitability	ground-mounted Buffer [m]	roof top surface suitability
1	111 Continuous urban fabric	0	0	1
2	112 Discontinuous urban fabric	0	0	1
3	121 Industrial or commercial units	0	0	1
4	122 Road and rail networks and associated	0.4	0	0
5	123 Port areas	0	0	0
6	124 Airports	0	0	0
7	131 Mineral extraction sites	1	0	0
8	132 Dump sites	1	0	0
9	133 Construction sites	0	0	0
10	141 Green urban areas	0	0	0
11	142 Sport and leisure facilities	0	0	0
12	211 Non-irrigated arable land	0.525	0	0
13	212 Permanently irrigated land	0.525	0	0
14	213 Rice fields	0.525	0	0
15	221 Vineyards	0.1	0	0
16	222 Fruit trees and berry plantations	0.1	0	0
17	223 Olive groves	0.1	0	0
18	231 Pastures	0.1	0	0
19	241 Annual crops associated with permanent	0.4	0	0
20	242 Complex cultivation patterns	0.4	0	0
21	243 Land principally occupied by agriculture	0.4	0	0
22	244 Agro-forestry areas	0.4	0	0
23	311 Broad-leaved forest	0	300	0
24	312 Coniferous forest	0	300	0
25	313 Mixed forest	0	300	0
26	321 Natural grasslands	0.65	0	0
27	322 Moors and heathland	0	0	0
28	323 Sclerophyllous vegetation	0.65	0	0
29	324 Transitional woodland-shrub	0.65	0	0
30	331 Beaches, dunes, sands	0	0	0
31	332 Bare rocks	1	0	0
32	333 Sparsely vegetated areas	1	0	0
33	334 Burnt areas	1	0	0
34	335 Glaciers and perpetual snow	0	0	0
35	411 Inland marshes	0	1000	0
36	412 Peat bogs	0	0	0
37	421 Salt marshes	0	0	0
38	422 Salines	0	0	0
39	423 Intertidal flats	0	1000	0
40	511 Water courses	0	1000	0
41	512 Water bodies	0	1000	0
42	521 Coastal lagoons	0	1000	0
43	522 Estuaries	0	1000	0
44	523 Sea and ocean	0	1000	0
45	999 else	0	0	0

Map code	UN LCCS	Land Cover Class	ground-mounted suitability	Buffer [m]	roof top surface suitability
0		No input data available	0	0	0
111	A12A3A10B2	Closed forest, evergreen needle leaf	0	300	0
113	A12A3A10B2	Closed forest, deciduous needle leaf	0	300	0
112	A12A3A10B2	Closed forest, evergreen, broad leaf	0	300	0
114	A12A3A10B2	Closed forest, deciduous, broad leaf	0	300	0
115	A12A3A10	Closed forest, mixed	0	300	0
116	A12A3A10	Closed forest, unknown	0	300	0
121	A12A3A11B2	Open forest, evergreen needle leaf	0	300	0
123	A12A3A11B2	Open forest, deciduous needle leaf	0	300	0
122	A12A3A11B2	Open forest, evergreen broad leaf	0	300	0
124	A12A3A11B2	Open forest, deciduous broad leaf	0	300	0
125	A12A3A12	Open forest, mixed	0	300	0
126	A12A3A12	Open forest, unknown	0	300	0
20	A12A4A20B3	Shrubs	0.1	0	0
30	A12A2(A6)A2	Herbaceous vegetation	0.1	0	0
90	A24A2A20	Herbaceous wetland	0	1000	0
100	A12A7	Moss and lichen	0.325	0	0
60	B16A1(A2)	Bare / sparse vegetation	0.4	0	0
40	A11A3	Cultivated and managed vegetation/agricu	0.2625	0	0
50	B15A1	Urban / built up	1	0	1
70	B28A2(A3)	Snow and ice	0	0	0
80	B28A1B1	Permanent water bodies	0	0	0
200	B28A1B11	Open sea	0	1000	0

Exclusion List	
Topography	altitude > 2500 [m]
	slope >15° everywhere & >3° if not SW-SE Azimut in NH or NW-NE Azimut in SH
Protected Areas	yes WPDA/NATURA2000 +150 [m] Buffer
Infrastructure	pipeline +150 [m] Buffer
	highway yes
	overhead lin/yes
	rail yes
	waterway +100 [m] Buffer
Weather	Irradiation <4 KWh/(day m*2)
Inclusion List	
Infrastructure	highway +200 [m] Buffer around the excluded cell
	rail +200 [m] Buffer around the excluded cell

Figure A.3: Default parameters for the definition of the land cover based suitability



Scarlat N, Fahl F, Dallemand J-F, Monforti F, Motola V, 2018. A spatial analysis of biogas potential from manure in Europe. *Renewable and Sustainable Energy Reviews*, 94, 915–930, <https://www.sciencedirect.com/science/article/pii/S1364032118304714>

FAO 2010: Gilbert. M. et al. Global distribution data for cattle, buffaloes, horses, sheep, goats, pigs, chickens and ducks in 2010. *Sci. Data*. 5:180227 doi: 10.1038/sdata.2018.227 (2018).

S2BIOM : Elbersen, B. (Creator), de Groot, H. (Creator), Staritsky, I. (Creator), Dees, M. (Creator), Datta, P. (Creator), Leduc, S. (Creator) (2016). S2BIOM DATA. Wageningen University & Research.

Hotmaps: Scaramuzzino C, Garegnani G, Zambelli P, 2019. Integrated approach for the identification of spatial patterns related to renewable energy potential in European territories. *Renewable and Sustainable Energy Reviews*, 101, 1–13, <https://www.sciencedirect.com/science/article/pii/S1364032118307275>

Figure A.4: Considered main resource classes for the assessment of the biomass potential and their data sources

CATO	categorie	subcategorie	short_name	LHV [kWh/kg]	CO2_fact [kgCO2/kWh]	Biogas yield from AD [m ³ _{biogas} /tonne _{DM}]	Default EC Class	CAT_long
Forest	Production from forests	Stemwood from final fellings & thinnings	Final fellings from nonconifer trees	5.278	0.310	0	Stemwood	primal production
			Final fellings from conifer trees	5.361	0.305	0		
			Thinnings from nonconifer trees	5.278	0.310	0		
			Thinnings from conifer trees	5.333	0.307	0		
			Stemwood from broadleaf & coniferous trees	5.333	0.307	0		
			Stem and crown biomass from early thinnings	5.278	0.310	0		
	Primary residues from forests	Logging residues from final fellings & thinnings	Early thinnings from nonconifer trees	5.278	0.310	0	Wood_Chips	primal residue
			Early thinnings from conifer trees	5.333	0.307	0		
			Logging residues from final fellings from nonconifer trees	5.194	0.315	0		
			Logging residues from final fellings from conifer trees	5.333	0.307	0		
		Stumps from final fellings & and thinnings	Logging residues from thinnings from nonconifer trees	5.194	0.315	0		
			Logging residues from thinnings from conifer trees	5.333	0.307	0		
			Stumps from final fellings from nonconifer trees	5.167	0.317	0		
			Stumps from final fellings from conifer trees	5.167	0.317	0		
Agriculture on arable land & grass land	Primary production of lignocellulosic biomass crops	Energy grasses, annual & perennial crops	Miscanthus	4.994	0.310	244.5	Pellets	primal production
			Switchgrass	4.622	0.335	244.5		
			Giant reed	4.828	0.321	244.5		
			Cardoon	4.325	0.366	244.5		
			Reed Canary Grass	4.583	0.346	244.5		
		Short rotation coppice	SRW Willow	5.111	0.303	0	Wood_Chips	
			SRW Poplar	5.111	0.303	0		
			Other SRC	5.028	0.315	0		
	Agricultural residues	Straw/stubbles	Rice straw	4.019	0.385	244.5	Straw_Bales	primal residue
			Cereals straw	4.431	0.349	244.5		
			Oil seed rape straw	4.908	0.315	244.5		
			Maize stover	4.733	0.327	244.5		
			Sugarbeet leaves	4.611	0.336	237.6		
			Sunflower straw	5.611	0.276	244.5		
			Residues from vineyards	4.861	0.326	0		
			Residues from fruit tree plantations	4.778	0.332	0		
			Residues from olives tree plantations	4.778	0.332	0		
			Residues from citrus tree plantations	4.639	0.342	0		
Other land use	Grassland	Grassland	Unused grassland cuttings	5.194	0.298	495	Straw_Bales	
	Other land use	Biomass from road side	Road side verges (grassy)	5.194	0.298	495		
Production based on lignocellulosic biomass	Secondary residues from wood industries	Saw mill residues	Sawdust (conifers)	5.214	0.297	0	Other	secondary residue
			Sawdust (nonconifers)	5.214	0.314	0		
			Other residues (conifers)	4.992	0.328	0		
			Other residues (nonconifers)	4.992	0.328	0		
		Other wood processing industry residues	Residues from industries producing semi finished wood based	5.106	0.321	0	Wood_Chips	
			Residues from further woodprocessing	5.106	0.321	0		
	Secondary residues of industry utilising agricultural products	Secondary residues from pulp and paper industry	Bark	5.333	0.307	0	Other	
			Black liquor	3.194	0.512	0		
			Olive-stones	5.650	0.281	0		
		By-products and residues from food and fruit processing industry	Rice husk	5.094	0.311	0	Pellets	
			Pressed grapes dregs	5.411	0.293	0		
			Cereal bran	5.792	0.274	0		
Tertiary residues	Municipal waste	Biodegradable municipal waste	Biowaste unseparately collected	3.000	0.484	144	Other	municipal waste
			Biowaste separately collected	1.194	0.484	144		
	Waste from wood	Post consumer wood	Hazardous post consumer wood	3.944	0.415	0		waste wood
			Non hazardous post consumer wood	4.444	0.415	0		

Figure A.5: Properties of the main considered biomass resource classes

CATO	category	subcategory	short_name	Cropland		Forest															
				40		111	112	113	114	115	116	117	118	119	120	121	122	123	124	125	126
Forest	Production from forests	Stemwood from final fellings & thinnings	Final fellings from nonconifer trees			1	1	1	1	1	1	1	1	1	1	1	1	1	1	1	
		Thinnings from nonconifer trees	Thinnings from nonconifer trees			1	1	1	1	1	1	1	1	1	1	1	1	1	1	1	1
		Stemwood from broadleaf & coniferous trees	Stemwood from broadleaf & coniferous trees			1	1	1	1	1	1	1	1	1	1	1	1	1	1	1	1
		Early thinnings from nonconifer trees	Early thinnings from nonconifer trees			1	1	1	1	1	1	1	1	1	1	1	1	1	1	1	1
		Stemwood from oak	Stemwood from oak			1	1	1	1	1	1	1	1	1	1	1	1	1	1	1	1
	Primary residues from forests	Logging residues from final fellings & thinnings	Logging residues from final fellings from nonconifer trees	Logging residues from final fellings from conifer trees			1	1	1	1	1	1	1	1	1	1	1	1	1	1	1
		Logging residues from thinnings	Logging residues from thinnings from nonconifer trees	Logging residues from thinnings from conifer trees			1	1	1	1	1	1	1	1	1	1	1	1	1	1	1
		Stumps from final fellings & thinnings	Stumps from final fellings from nonconifer trees	Stumps from final fellings from conifer trees			1	1	1	1	1	1	1	1	1	1	1	1	1	1	1
		Stumps from final fellings & thinnings	Stumps from final fellings from nonconifer trees	Stumps from final fellings from conifer trees			1	1	1	1	1	1	1	1	1	1	1	1	1	1	1
		Stumps from final fellings & thinnings	Stumps from final fellings from nonconifer trees	Stumps from final fellings from conifer trees			1	1	1	1	1	1	1	1	1	1	1	1	1	1	1
Agriculture on arable land & grass land	Primary production of lignocellulosic biomass crops	Energy grasses, annual & perennial crops	Miscanthus	1																	
		Switchgrass	Switchgrass	1																	
		Giant reed	Giant reed	1																	
		Cardoon	Cardoon	1																	
		Need Canary Grass	Need Canary Grass	1																	
		SRK Willow	SRK Willow	1																	
		SRK Poplar	SRK Poplar	1																	
		Other SRC	Other SRC	1																	
		Rice straw	Rice straw	1																	
		Cereals straw	Cereals straw	1																	
Agricultural residues	Straw/stubbles	Oil seed rape straw	Oil seed rape straw	1																	
		Maize stover	Maize stover	1																	
		Sugarbeet leaves	Sugarbeet leaves	1																	
		Sunflower straw	Sunflower straw	1																	
		Residues from vineyards	Residues from vineyards	1																	
		Residues from fruit tree plantations	Residues from fruit tree plantations	1																	
		Residues from olive tree plantations	Residues from olive tree plantations	1																	
		Residues from citrus tree plantations	Residues from citrus tree plantations	1																	
		Unused grassland cuttings	Unused grassland cuttings	1																	
		Road side verges (grassy)	Road side verges (grassy)	1																	
Other land use	Secondary residues from wood industries	Sawdust (conifers)	Sawdust (conifers)			1	1	1	1	1	1	1	1	1	1	1	1	1	1	1	
		Saw mill residues	Saw mill residues			1	1	1	1	1	1	1	1	1	1	1	1	1	1	1	
		Other residues (nonconifers)	Other residues (nonconifers)			1	1	1	1	1	1	1	1	1	1	1	1	1	1	1	
		Other residues (conifers)	Other residues (conifers)			1	1	1	1	1	1	1	1	1	1	1	1	1	1	1	
		Residues from industries producing semi finished wood based panels	Residues from industries producing semi finished wood based panels			1	1	1	1	1	1	1	1	1	1	1	1	1	1	1	1
		Residues from further woodprocessing	Residues from further woodprocessing			1	1	1	1	1	1	1	1	1	1	1	1	1	1	1	1
		Bark	Bark			1	1	1	1	1	1	1	1	1	1	1	1	1	1	1	1
		Black liquor	Black liquor			1	1	1	1	1	1	1	1	1	1	1	1	1	1	1	1
		By products and residues from food and agricultural processing	By products and residues from food and agricultural processing			1	1	1	1	1	1	1	1	1	1	1	1	1	1	1	1
		Olive-stones	Olive-stones			1	1	1	1	1	1	1	1	1	1	1	1	1	1	1	1
Rice husk	Rice husk			1	1	1	1	1	1	1	1	1	1	1	1	1	1	1	1		
Pressed grapes drags	Pressed grapes drags			1	1	1	1	1	1	1	1	1	1	1	1	1	1	1	1		
Cereal bran	Cereal bran			1	1	1	1	1	1	1	1	1	1	1	1	1	1	1	1		

Figure A.7: Match between Copernicus land cover classes and biomass resource classes

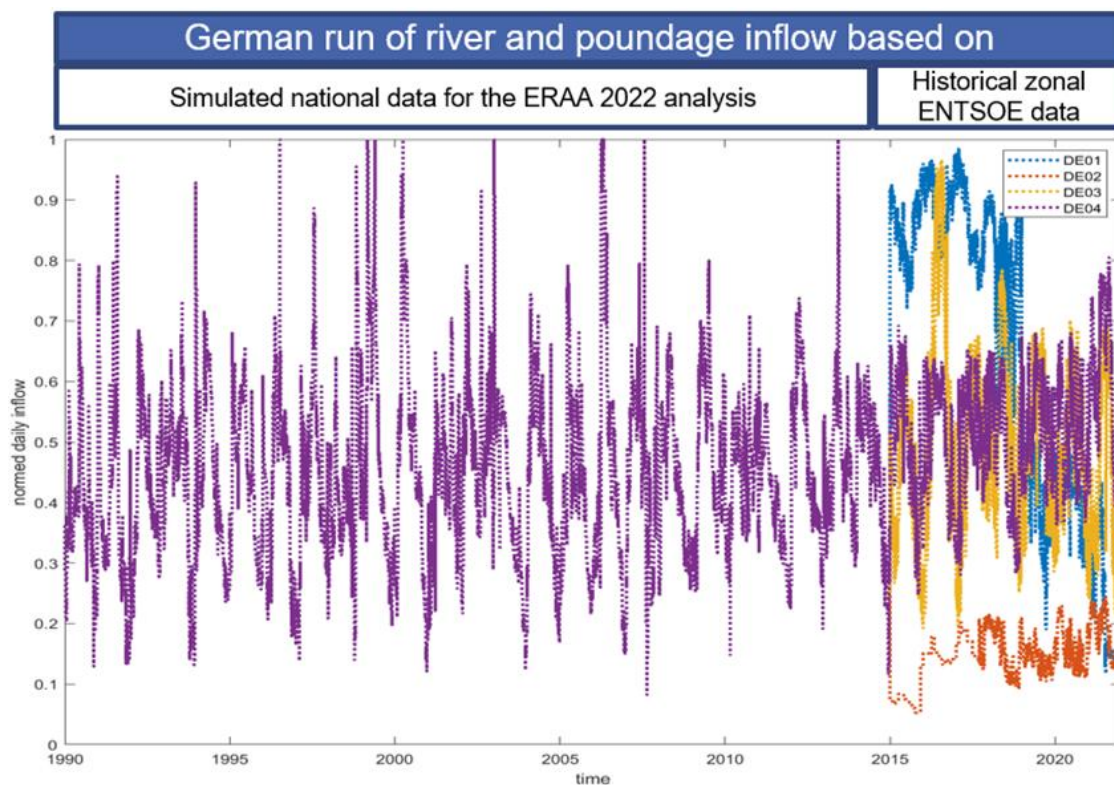


Figure A.8: Comparison of the ERAA and ENTSOE run-of-river time series for Germany

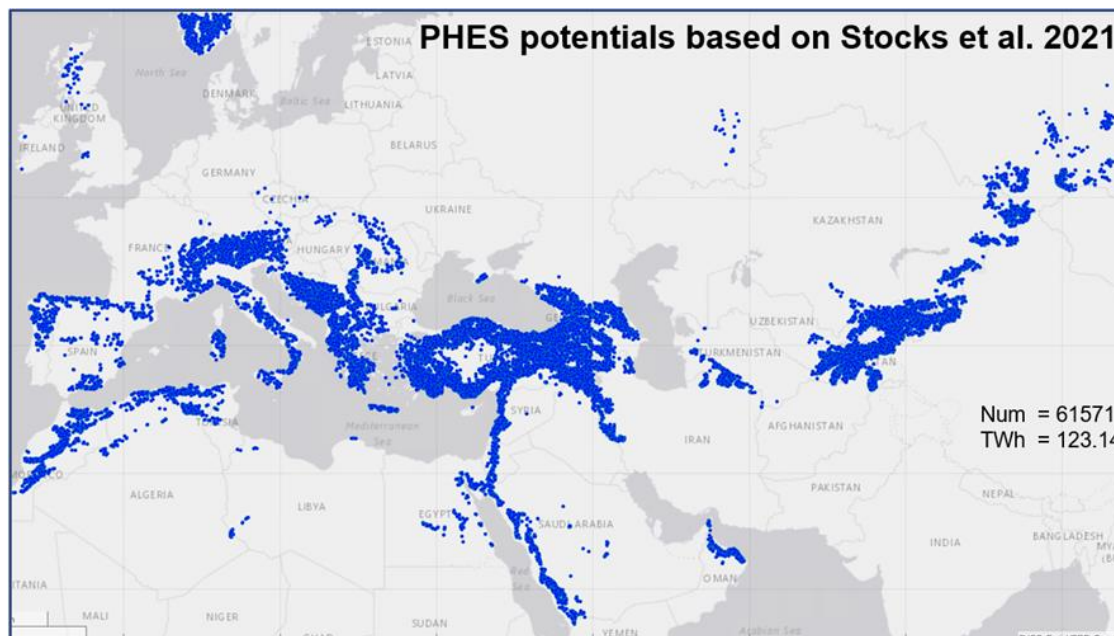


Figure A.9: Considered PHES Potential

Node included in PERSEUS-gECT											
system	sub-system	ec	no	system	sub-system	ec	no	system	sub-system	ec	no
bulk	ship:sea	oil	660	el	el_grid	el	14656	storage	bat	el	2558
bulk	ship:sea	CO2	118	el	el_grid	th_h	1527	storage	cavern_exist	CH4	270
bulk	ship:sea	Fe	660	el	el_grid	th_l	1903	storage	cavern_exist	H2	270
bulk	ship:sea	H2	252	el	el_DCMT_grid	el	3740	storage	lng_exist	LH2	116
bulk	ship:sea	LH2	660	el	el_iso_off	el	136	storage	lng_exist	LNG	116
bulk	ship:sea	LNG	660	el	el_iso_gas	el	99	storage	field_exist	CO2	453
bulk	ship:sea	LNH3	660	el	el_iso_gas	th_h	97	storage	field_exist	CH4	533
bulk	ship:sea	LOHC	660	el	el_iso_road	el	245	storage	g2l	LH2	594
bulk	ship:sea	MeOH	660	el	el_iso_road	th_h	242	storage	l2g	LH2	194
bulk	ship:sea	th_h	112	el	el_iso_rail	el	43	storage	ccus_stor	CO2	26
bulk	ship:sea	hard_coal	197	el	el_iso_rail	th_h	43	storage	dsm	el	2535
bulk	ship:river	oil	410	el	el_iso_ship	el	22	storage	dsm	th_h	11012
bulk	ship:river	Fe	410	el	el_iso_ship	th_h	22	storage	dsm	th_l	12531
bulk	ship:river	LH2	410	el	-	-	22775	storage	pv-bess	el	5795
bulk	ship:river	LNG	410	gas	gas	el	1123	storage	csp	th_h	3015
bulk	ship:river	LNH3	410	gas	gas	CO2	4780	storage	hydro	el	2485
bulk	ship:river	LOHC	410	gas	gas	CH4	4784	storage	tank	H2	1941
bulk	ship:river	MeOH	410	gas	gas	H2	4784	storage	-	-	44444
bulk	rail	oil	1135	gas	-	-	15471				
bulk	rail	CO2	180	oil	oil	oil	134				
bulk	rail	CH2	1135	oil	oil	LNH3	134				
bulk	rail	Fe	1135	oil	oil	LOHC	134				
bulk	rail	H2	190	oil	oil	MeOH	134				
bulk	rail	LH2	1135	oil			536				
bulk	rail	LNH3	1135	CO2	air	CO2	82				
bulk	rail	LOHC	1135	district_heat	district_heat	th_h	2164				
bulk	rail	MeOH	1135	district_heat	district_heat	th_l	2164				
bulk	rail	th_h	9	district_heat			4328				
bulk	road	oil	954	plant	conv_plant	CO2	415				
bulk	road	CO2	329	plant	conv_plant	CH4	709				
bulk	road	CH2	954	plant	conv_plant	Fe	289				
bulk	road	H2	336	plant	conv_plant	H2	722				
bulk	road	LH2	954	plant	conv_plant	LNH3	519				
bulk	road	LNH3	954	plant	conv_plant	LOHC	519				
bulk	road	LOHC	954	plant	-	-	3173				
bulk	road	MeOH	954								
bulk	road	th_h	7								
bulk	-	-	22889								

Figure A.10: Considered nodes per system in PERSEUS-gECT

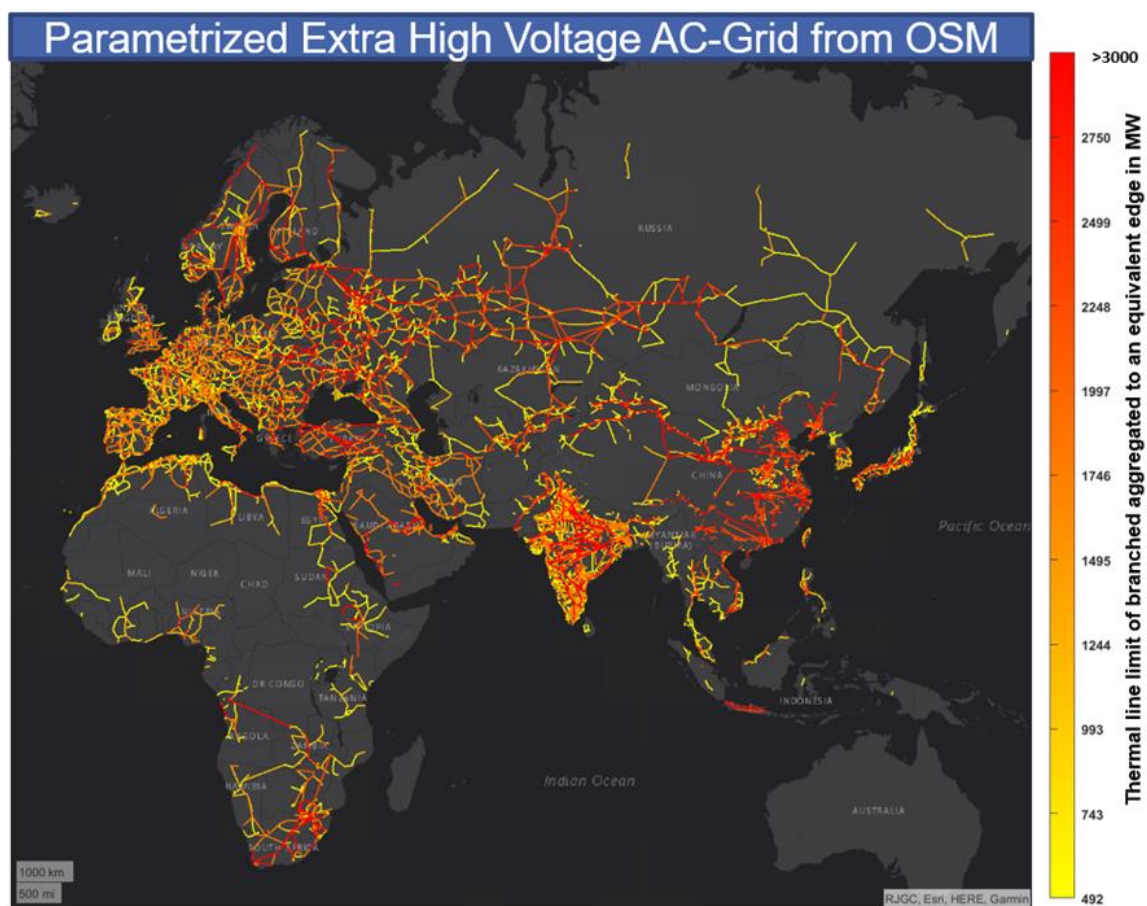


Figure A.11: Extract of the OSM based extra high voltage transmission grid in PERSEUS-gECT for Eurasia and Africa

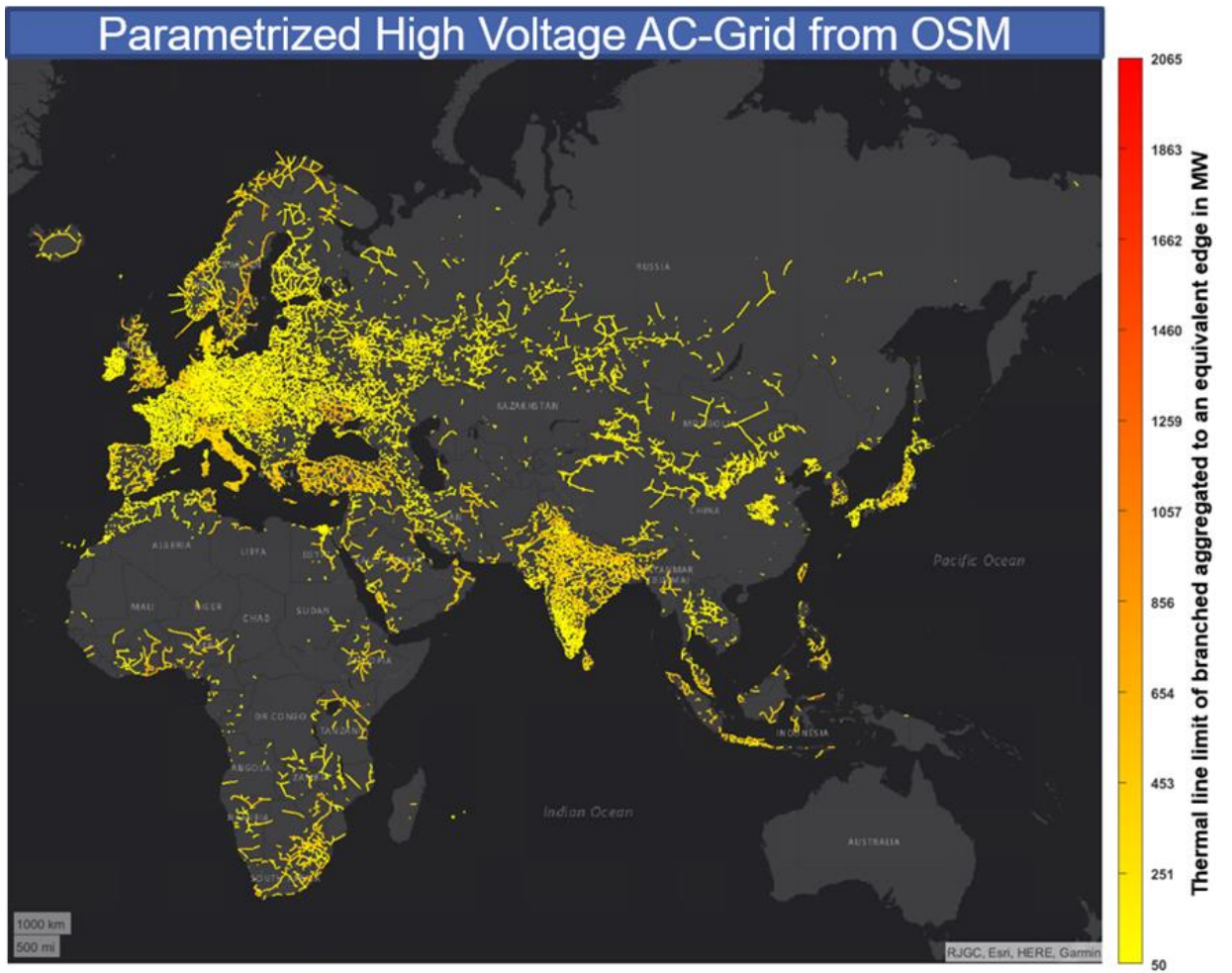


Figure A.12: Extract of the OSM based high voltage grid in PERSEUS-gECT for Eurasia and Africa

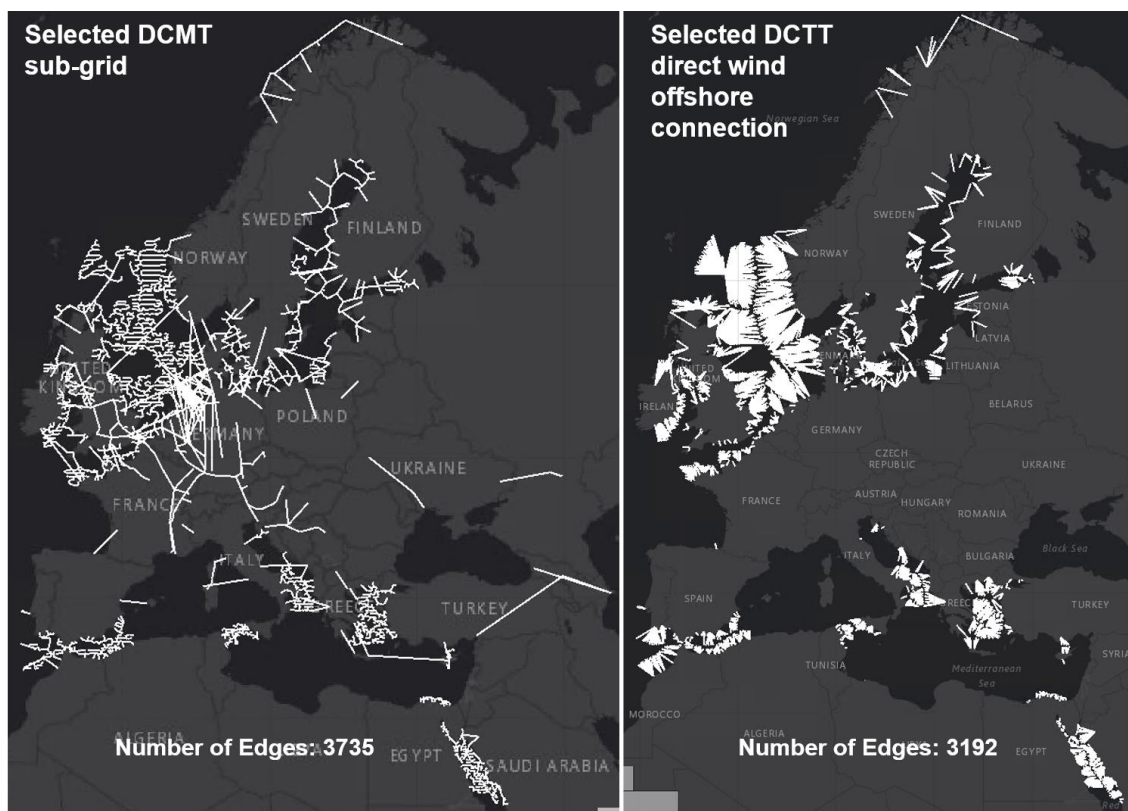


Figure A.13: Selected potential DCMT and DCTT (direct offshore grid connection) HVDC sub-grid in the case study

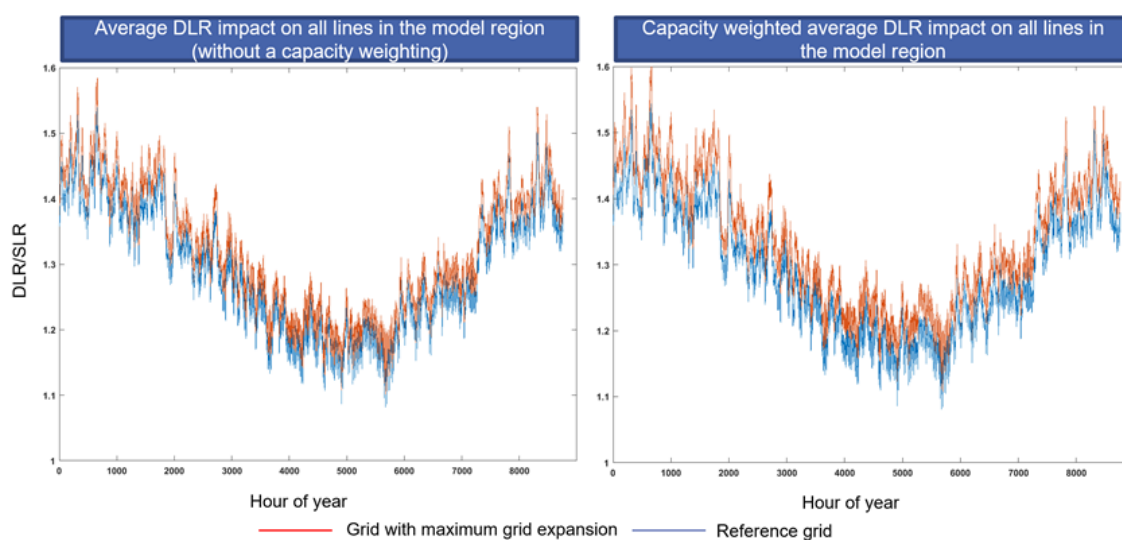


Figure A.14: Hourly timeseries of the DLR impact in the transmission grid in weather year 2019

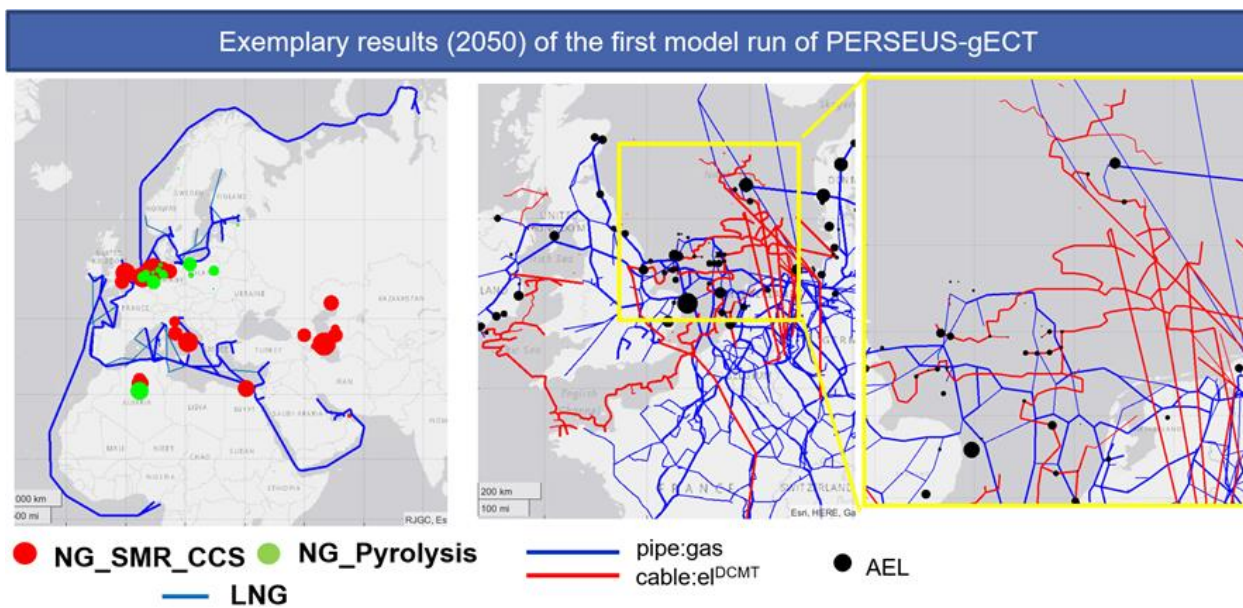


Figure A.15: Exemplary results of the transport system in 2050 of the first model run in the case study

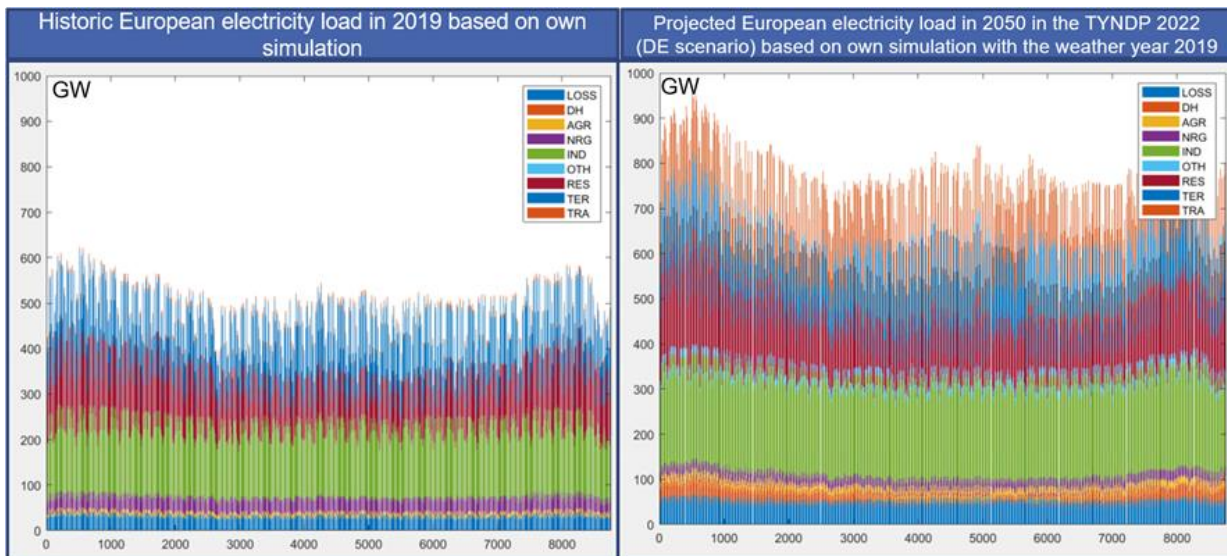


Figure A.16: Comparison of the simulated hourly time series of the reference electricity final demand in Europe of 2019 and 2050

MT CO2 Country	FD (fix)		FD (var)			EHG	TraStor	VarRem	X2X	Netto Position		
	Gas	Oil	Coal	Gas	Oil							
TUR	13,5	40,8	35,3	30,0	2,7	26,1	5,5	26,3	-	0,0	112,2	
DEU	25,5	34,2	0,1	9,7	-	7,7	1,4	2,7	3,9		75,3	
FRA	15,0	27,6	0,3	10,6	0,0	0,2	2,0	3,4	-	0,0	48,2	
IRN	-	-	-	-	-	38,8	0,2	-	-	0,0	39,0	
ITA	10,6	16,3	0,3	9,8	-	3,8	1,2	1,6	2,6		36,0	
UKR	10,1	10,8	16,9	10,1	0,2	10,2	0,9	3,5	0,0		35,7	
ESP	13,7	15,9	0,0	3,0	-	0,1	1,0	1,0	-	0,0	31,8	
NOR	8,7	11,4	2,1	0,2	0,8	0,7	1,0	1,3	-	0,0	23,1	
POL	10,1	8,6	0,8	3,4	-	2,2	0,3	0,5	0,5		22,2	
EGY	-	-	-	-	-	19,9	1,2	-	0,6		21,6	
NLD	6,4	12,3	2,0	3,8	-	1,3	0,4	0,8	0,3		21,5	
SAU	-	-	-	-	-	18,1	-	-	-	0,0	18,1	
IRQ	-	-	-	-	-	11,2	0,2	-	-		11,3	
RUS	-	-	-	-	-	9,8	0,8	-	-	0,0	10,6	
BEL	2,9	4,7	0,0	1,4	-	1,4	1,0	0,5	-	0,0	10,6	
CHL	-	-	-	-	-	-	-	-	-	0,2	-	0,2
IRL	1,1	2,2	0,0	0,6	-	0,2	0,1	0,1	-	11,2	-	7,5
GBR	24,7	30,3	-	5,9	-	1,0	0,6	0,5	-	69,3	-	12,1
SWE	1,8	3,3	-	0,6	-	0,0	0,1	0,1	-	59,3	-	53,9
DNK	1,7	3,4	0,0	0,3	-	0,0	0,2	0,0	-	584,0	-	578,7

Figure A.17: Zoom on the CO2-emission balance of the largest positive and negative net-emission countries in 2050

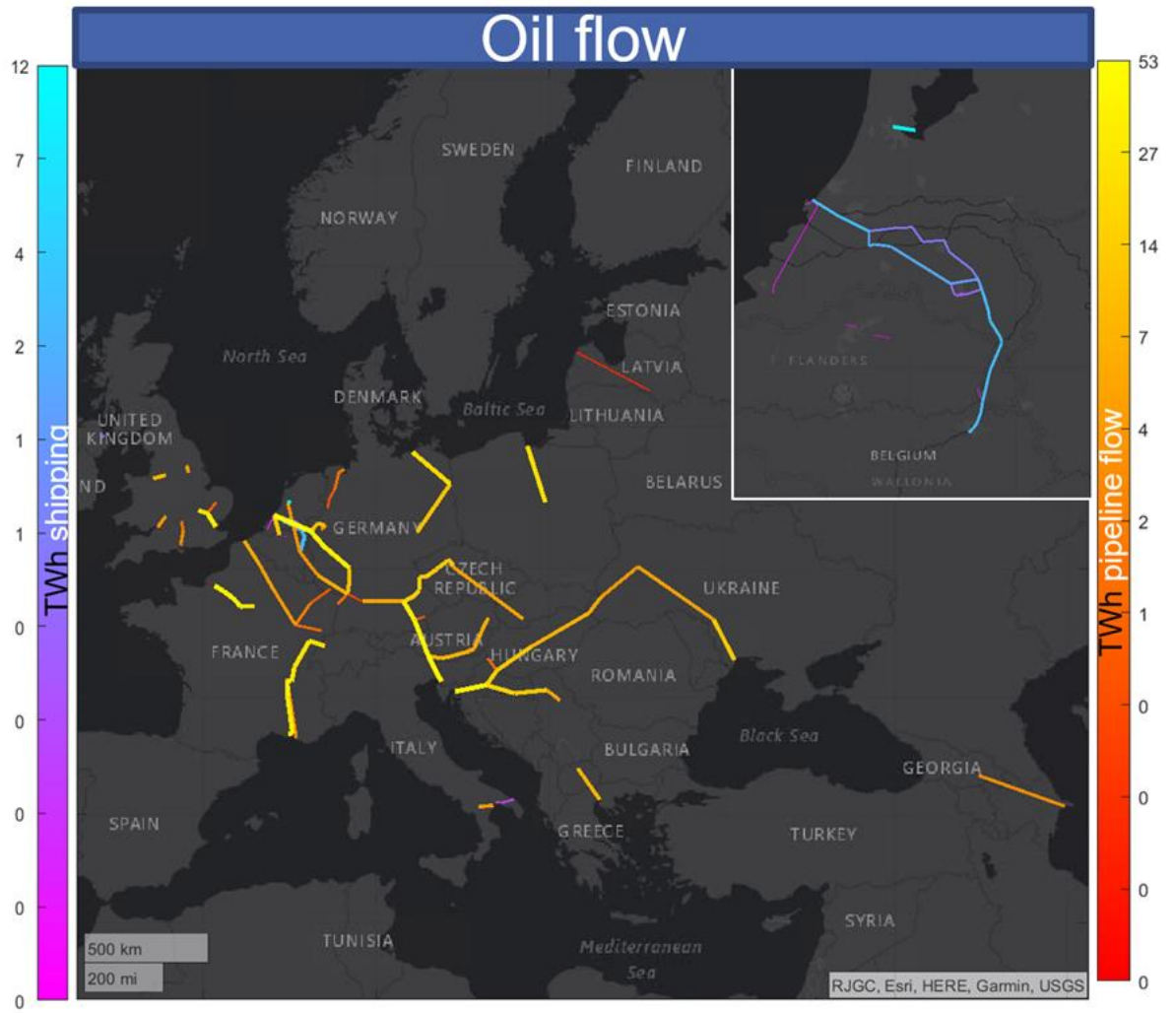


Figure A.18: Oil flows in 2050

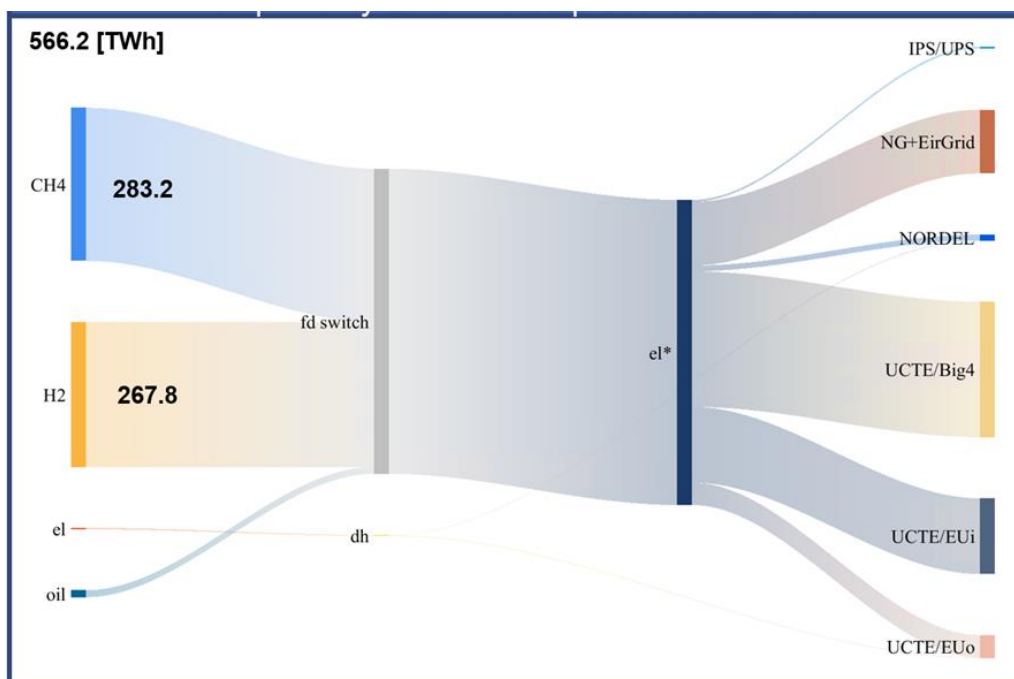


Figure A.19: Structure of the final demand switching for low temperature heat in 2050

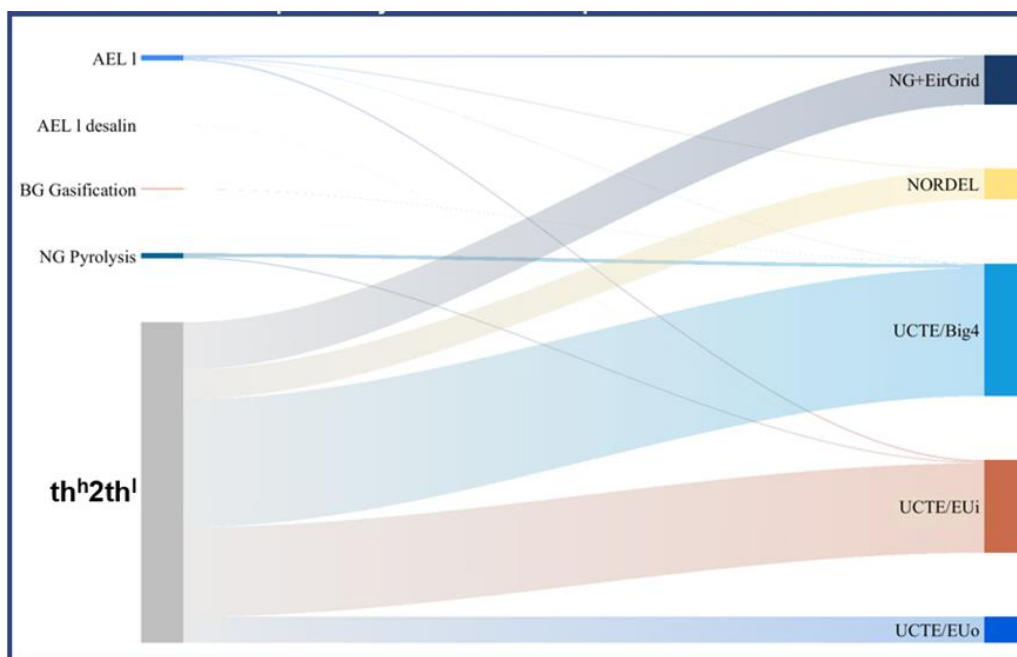


Figure A.20: Structure of the low temperature supply from non-primarily EHG related processes in 2050

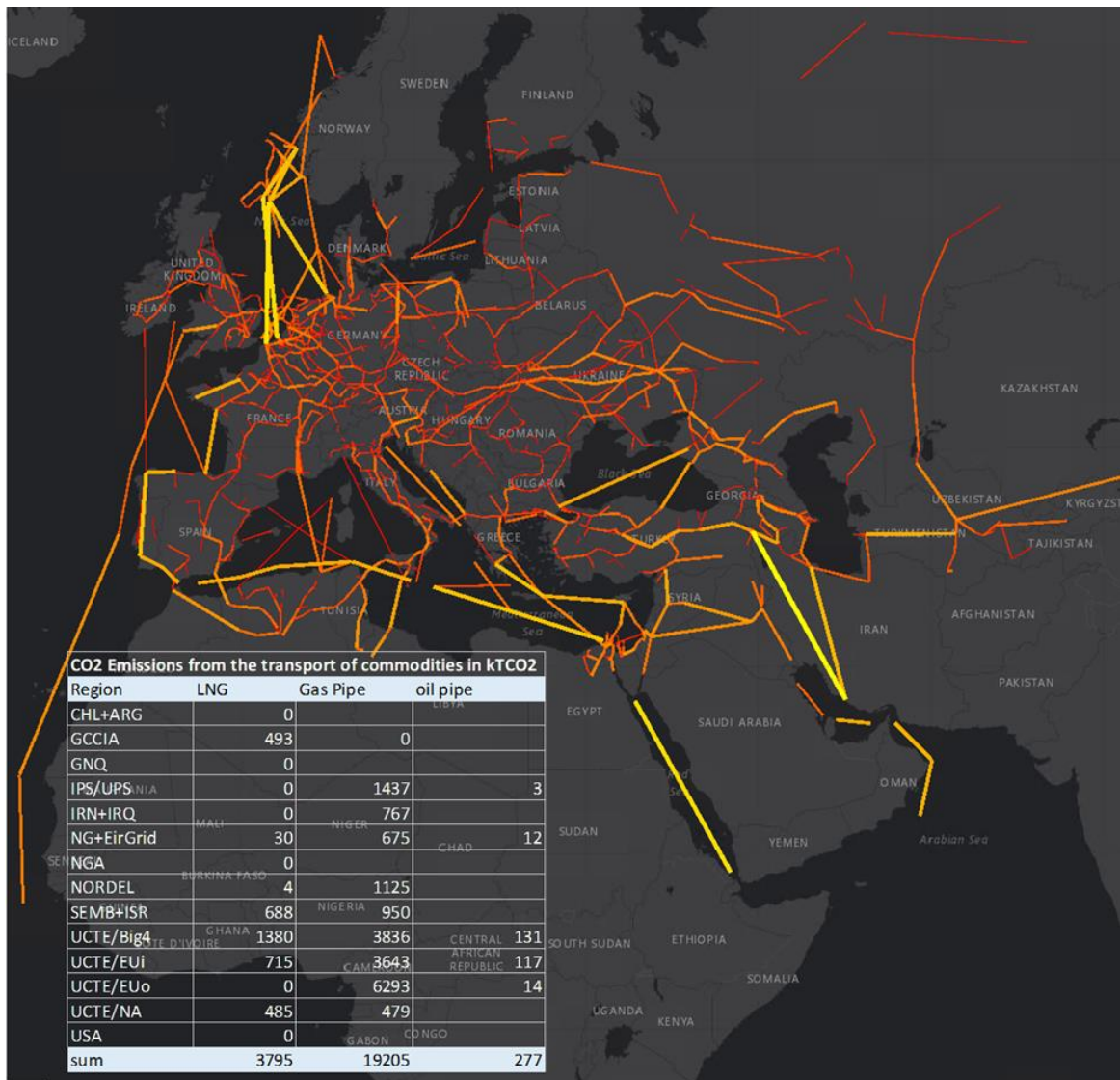


Figure A.21: Distribution of transport related CO2 emissions excluding ports and storages

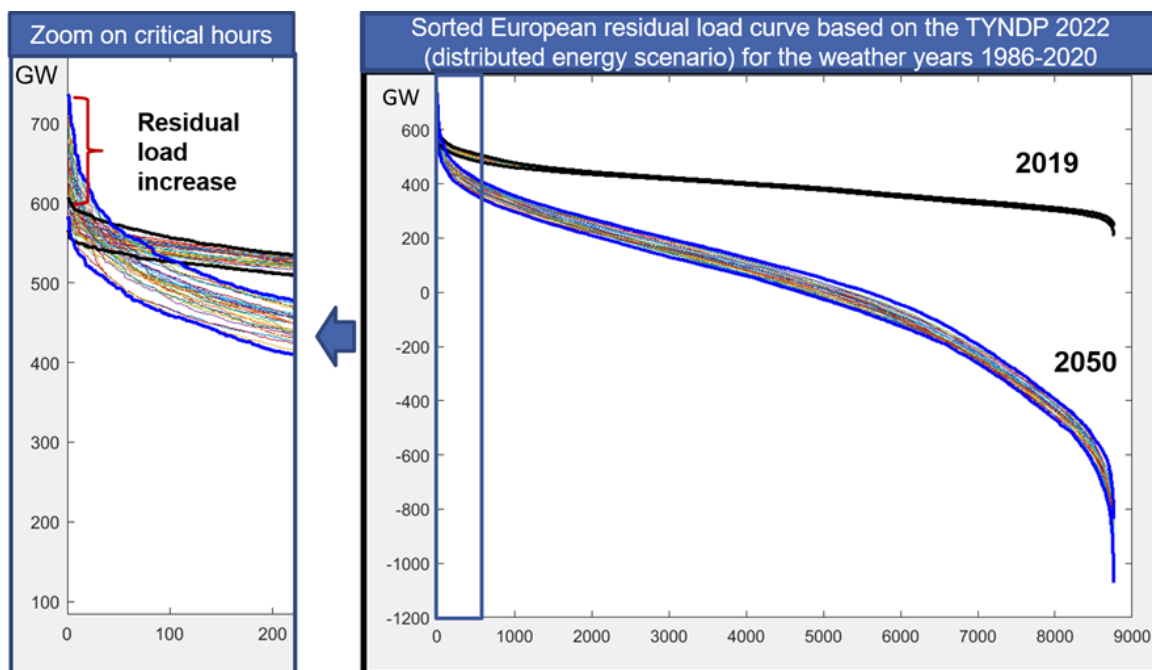


Figure A.22: Analysis of the residual load development in the reference TYNDP 2022 Distributed Energy Scenario for multiple weather years

Country	wind onshore [GW]				wind offshore [GW]				photovoltaic [GW]						
	Final Cap	Add to LB	TYNDP	Delta	Final Cap	Add to LB	TYNDP	Delta	Final Cap	Add to LB	TYNDP	Delta			
ARE	0.01	0.00	-	0.01	0.00	0.00	-	0.00	35.87	31.33	-	35.87			
ARM	-	-	-	-	-	-	-	-	4.96	4.58	-	4.96			
AUT	14.35	0.00	25.31	-	10.96	-	-	-	37.58	2.20	56.75	-	19.17		
AZE	1.06	0.68	-	1.06	0.20	0.00	-	0.20	3.67	3.40	-	3.67			
BEL	6.50	0.00	10.44	-	3.94	7.96	0.00	6.86	1.10	31.64	0.00	46.86	-	15.22	
BGR	6.92	0.00	12.64	-	5.73	0.11	0.00	0.13	-	0.03	17.43	0.47	27.45	-	10.03
BHR	0.00	0.00	-	0.00	0.00	0.00	-	0.00	1.53	1.52	-	1.53			
BLR	30.38	30.29	-	30.38	-	-	-	-	0.20	0.00	-	0.20			
CHE	1.65	0.00	3.03	-	1.37	-	-	-	6.63	0.37	9.88	-	3.26		
CZE	7.87	0.00	15.15	-	7.28	-	-	-	21.76	0.23	36.06	-	14.30		
DEU	111.47	0.50	151.57	-	40.11	59.91	0.40	63.23	-	3.32	230.05	2.26	329.42	-	99.37
DNK	31.99	15.22	10.82	-	21.17	32.56	3.01	33.75	-	1.20	25.51	0.00	46.60	-	21.09
DZA	7.33	2.29	-	7.33	0.00	0.00	-	0.00	19.00	13.60	-	19.00			
EGY	5.19	1.92	-	5.19	0.00	0.00	-	0.00	46.42	43.87	-	46.42			
ESP	93.81	3.25	115.95	-	22.13	3.16	0.00	3.55	-	0.39	134.75	0.04	204.74	-	70.00
FIN	42.64	0.00	69.16	-	26.52	7.37	0.00	7.90	-	0.53	14.47	0.00	20.98	-	6.51
FRA	89.02	18.60	119.44	-	30.42	46.92	0.11	52.37	-	5.44	155.00	3.38	224.57	-	69.57
GBR	103.53	59.66	64.78	-	38.75	95.55	0.02	107.45	-	11.90	88.58	0.01	118.21	-	29.63
GEO	0.32	0.06	-	0.32	-	-	-	-	0.08	0.08	-	0.08			
GRC	33.59	0.80	27.99	-	5.60	2.44	0.00	2.08	0.36	54.59	1.07	48.57	6.02		
HRV	5.38	0.00	10.31	-	4.93	0.00	0.00	-	0.00	5.46	0.17	7.40	-	1.93	
HUN	8.17	0.00	15.74	-	7.56	-	-	-	19.56	0.00	32.78	-	13.22		
IRL	25.42	14.01	16.83	-	8.59	20.37	0.00	23.79	-	3.42	3.14	0.00	4.95	-	1.81
IRN	0.88	0.00	-	0.88	0.00	0.00	-	0.00	15.00	14.55	-	15.00			
IRQ	0.00	0.00	-	0.00	0.00	0.00	-	0.00	13.23	11.73	-	13.23			
ISR	0.06	0.03	-	0.06	-	-	-	-	25.27	22.95	-	25.27			
ITA	32.08	0.89	44.55	-	12.47	12.21	0.00	14.00	-	1.79	166.00	12.40	249.62	-	83.62
JOR	5.13	4.46	-	5.13	-	-	-	-	18.30	16.19	-	18.30			
KAZ	45.71	44.23	-	45.71	0.00	0.00	-	0.00	14.42	11.49	-	14.42			
KWT	11.33	11.31	-	11.33	0.00	0.00	-	0.00	22.62	19.58	-	22.62			
LBN	-	-	-	-	-	-	-	-	0.08	0.00	-	0.08			
LBY	0.85	0.85	-	0.85	0.00	0.00	-	0.00	0.61	0.00	-	0.61			
LTU	2.66	0.00	5.17	-	2.51	1.81	0.00	1.73	0.08	1.98	0.00	3.93	-	1.95	
LVA	2.42	1.06	2.28	-	0.14	1.05	0.00	1.26	-	0.21	1.12	0.00	1.91	-	0.79
MAR	4.96	2.28	-	4.96	0.00	0.00	-	0.00	14.13	0.00	-	14.13			
MKD	0.60	0.00	0.61	-	0.00	-	-	-	6.77	0.00	11.62	-	4.85		
NLD	10.26	0.00	20.00	-	9.74	55.91	2.44	62.00	-	6.09	65.40	0.00	119.47	-	54.07
NOR	18.44	4.42	16.82	-	1.63	1.45	0.01	1.45	-	0.00	0.34	0.00	0.33	-	0.01
OMN	0.05	0.00	-	0.05	0.00	0.00	-	0.00	15.68	0.74	-	15.68			
POL	36.88	1.91	63.19	-	26.31	15.82	0.31	15.65	0.17	30.31	1.72	41.23	-	10.92	
PRT	17.90	0.01	27.95	-	10.05	0.56	0.00	0.67	-	0.10	21.76	0.00	36.97	-	15.20
PSE	0.00	0.00	-	0.00	-	-	-	-	0.48	0.29	-	0.48			
QAT	8.35	8.35	-	8.35	8.02	8.02	-	8.02	20.72	19.90	-	20.72			
ROU	23.15	0.00	40.63	-	17.48	0.09	0.00	0.11	-	0.02	25.85	0.00	43.23	-	17.38
RUS	4.00	1.69	-	4.00	0.06	0.06	0.00	0.06	1.94	0.00	-	1.94			
SAU	26.00	25.59	-	26.00	0.00	0.00	-	0.00	97.81	92.90	-	97.81			
SRB	4.21	0.00	-	4.21	-	-	-	-	1.31	0.00	-	1.31			
SVK	0.26	0.00	0.66	-	0.40	1.92	0.07	2.39	-	0.47	2.39	-	0.47		
SWE	46.77	13.75	43.03	-	3.74	10.51	0.03	10.58	-	0.08	21.23	0.11	32.87	-	11.65
SYR	0.01	0.01	-	0.01	-	-	-	-	0.49	0.00	-	0.49			
TKM	0.00	0.00	-	0.00	0.00	0.00	-	0.00	1.35	1.35	-	1.35			
TUN	7.57	7.17	-	7.57	0.00	0.00	-	0.00	4.10	3.09	-	4.10			
TUR	46.03	13.49	52.49	-	6.46	0.00	0.00	-	0.00	145.94	117.33	48.00	97.94		
UKR	37.15	33.66	-	37.15	0.00	0.00	-	0.00	8.07	0.00	-	8.07			
UZB	3.15	0.64	-	3.15	-	-	-	-	13.58	12.15	-	13.58			
CYP	0.68	0.00	1.12	-	0.43	0.00	0.00	-	0.00	3.74	1.78	3.35	0.40		
MDA	0.06	0.00	-	0.06	-	-	-	-	0.01	0.00	-	0.01			
MLT	0.01	-	0.94	-	0.93	0.14	0.00	0.17	-	0.03	0.71	0.07	0.89	-	0.18
SVN	0.31	0.00	0.53	-	0.21	-	-	0.06	-	0.06	6.33	0.21	9.19	-	2.85
EST	2.92	0.00	4.74	-	1.83	1.12	0.00	0.97	0.15	1.65	0.00	2.51	-	0.87	
ALB	0.83	0.00	1.65	-	0.82	0.00	0.00	-	0.00	1.53	0.25	1.65	-	0.12	
LUX	0.41	0.00	0.56	-	0.15	-	-	-	0.61	0.00	0.80	-	0.19		
TJK	-	-	-	-	-	-	-	-	0.12	0.12	-	0.12			
KGZ	-	-	-	-	-	-	-	-	1.02	1.02	-	1.02			
BIH	7.63	0.00	13.22	-	5.59	-	-	-	2.53	0.06	3.24	-	0.71		
MNE	0.70	0.00	1.21	-	0.51	0.00	0.00	-	0.00	3.26	0.32	5.51	-	2.26	
ISL	1.93	1.91	-	1.93	0.01	0.01	-	0.01	0.01	0.00	-	0.01			
ARG	3.50	0.00	-	3.50	0.00	0.00	-	0.00	-	-	-	-	-		
CHL	4.47	0.66	-	4.47	0.00	0.00	-	0.00	0.11	-	-	0.11			
ESH	1.67	0.00	-	1.67	0.00	0.00	-	0.00	0.11	0.00	-	0.11			

Figure A.23: Installed wind onshore, wind offshore and photovoltaic capacity per country in 2050



Figure A.24: Cumulated wind onshore generation and flows in the AC grid in 2050-focus on Europe

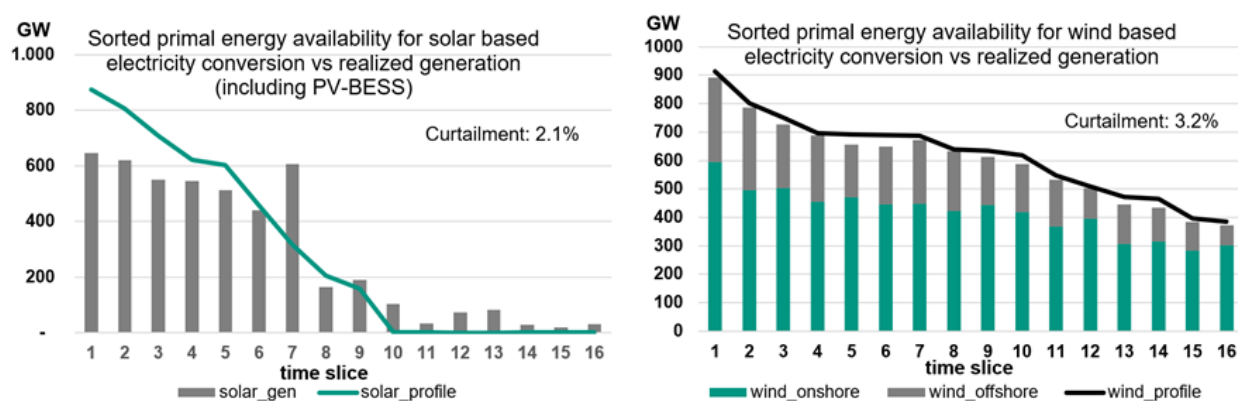


Figure A.25: Comparison of the potential and realized power generation from solar and wind based energy conversion systems (including PV-BESS)

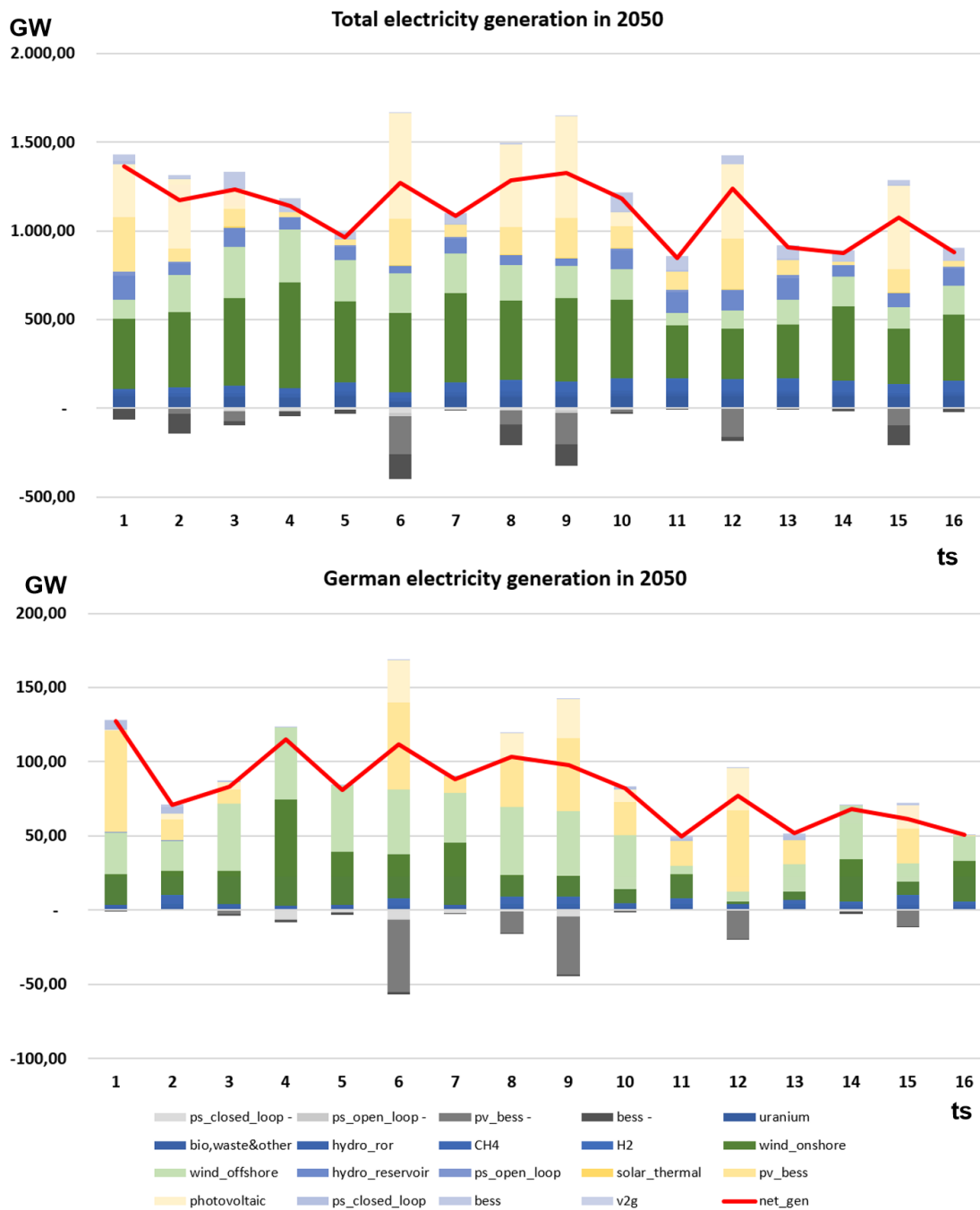


Figure A.26: Comparison of the dispatch of electricity generation units in the complete energy system (top) and in Germany (bottom) in 2050 per time slice



Figure A.27: Comparison of the cumulated dispatch of electrolyzers (bottom right), wind offshore units (top, right), wind onshore units (bottom left) and nuclear power plants (top left) in the English Channel region in 2050

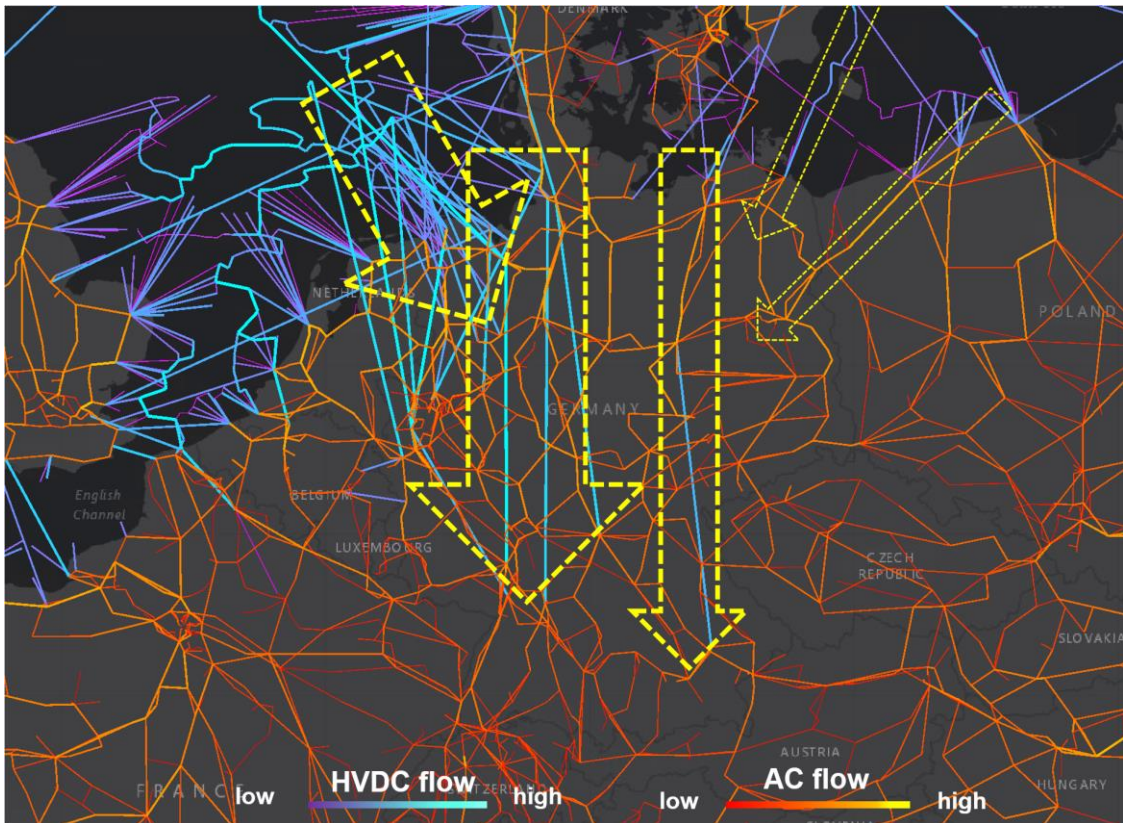


Figure A.288: Cumulated electricity flow in the German grid and neighboring regions in 2050

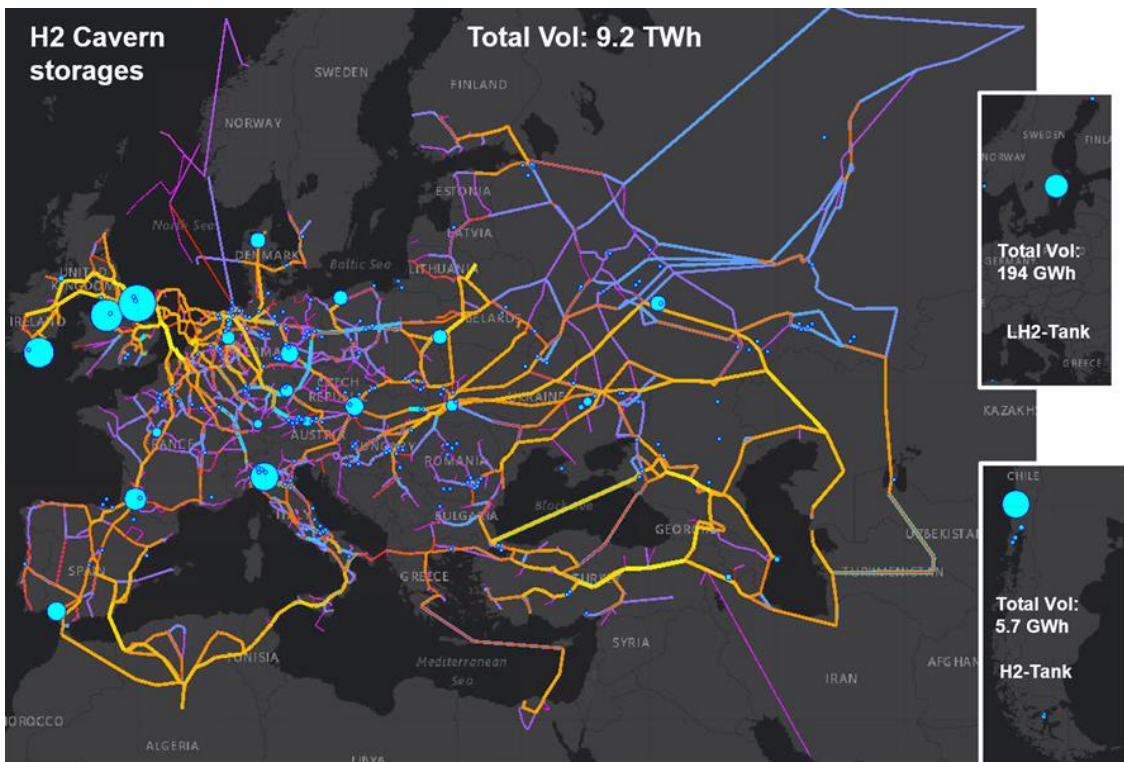


Figure A.29: Volume of hydrogen storages and cumulated hydrogen flows in the gas grid in 2050